Tethered biomimetic phospholipid vesicles: A novel method to study membrane permeation

Williams, Thomas Lloyd

Award date:
2007

Awarding institution:
University of Bath

Tethered Biomimetic Phospholipid Vesicles: A Novel Method To Study Membrane Permeation

THOMAS LLOYD WILLIAMS

A thesis submitted for a degree of Doctor of Philosophy

The University of Bath
Department of Chemistry
October 2007

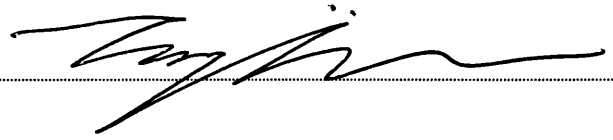

ProQuest LLC
789 East Eisenhower Parkway
P.O. Box 1346
Ann Arbor, MI 48106-1346

Table of Contents

1.0 Introduction

2.0 Theoretical Introduction

3.0 Experimental Methods

5.0 Solid Supported Lipid Bilayer Vesicles: Method to Study Membrane-Bacterial Toxin Interactions

6.0 Solid Supported Lipid Bilayer Vesicles: Method to Study Amyloidosis

Acknowledgements

I would especially like to thank Dr Toby Jenkins for all his help and support over the past three years, and would particularly like to thank him for being patient when teaching me the principles of physical chemistry and surface plasmon resonance.

I would like to thank the National Environmental Research Council and the Engineering and Physical Sciences Research Council for providing funds to carry out the research.

I would like to thank the University of Bath and the Chemistry department for the support they have provided throughout my time in Bath. I would also like to thank Dr Margarida Vareiro for all her help at the start of the PhD and with setting me up with the SPR. I am grateful to Dr Steve Flower for synthesizing the biotin-thiol compound for me. Thank you to Dr Frank Marken for his help devising the dye diffusion coefficient model.

Thank you to the girls of the Raithby group, Teresa and Hazel, for loaning certain chemicals, liquid nitrogen and for the distractions, they were definitely most appreciated. I would also like to thank Claire and Liz for advice, more appreciated distractions and other random friendy things. A big thank you to Sally-Ann and the sparrows for constant amusement and the occasional trip away, (sorry if I led you astray!!).

Finally, I would like to thank my family for all of their support over the past three years. Thank you for the advice, whether it was good or bad, whether I took it or just totally ignored it, it was much appreciated. Thank you one and all.

This thesis is dedicated to Richie Williams

I guess you think you know this story.
You don't. The real one's much more gory.
The phoney one, the one you know,
Was cooked up years and years ago,
And made to sound all soft and sappy
just to keep the children happy.....

Roald Dahl

Abbreviations

ε = absorption coefficient
θ = angle of incidence
ω = frequency
η = refractive index
σ = standard deviation
λ = wavelength
ε_1 = permittivity of metal film
ε_2 = permittivity of dielectric
θ_c = maximum intensity
κET = rate of energy transfer
ω_{max} = maximum frequency
ε_p = permittivity of prism
v_{phase} = phase velocity
κ_Q = bimolecular quencher concentration
(v/v) = volume/volume
(w/v) = weight/volume
$[AB]_t$ = analyte-ligand complex concentration at a specific time
$[B]_0$ = ligand concentration at the starting time
[Q] = quencher concentration
[R] = reflectivity
A = absorbance
A = adsorption
A = analyte
A = area
AA = arachidonic acid
AB = analyte-ligand complex
A_{bulk} = analyte concentration in bulk solution
AC = alternating current
$A_{interface}$ = analyte concentration at the interface
AL = acquired light chain
APP = amyloid precursor protein
ATP = adenosine 5'-triphosphate
ATR = attenuated total reflection
B = ligand
biotin-thiol = 11-mercaptoundecanoic-(8-biotinoylamido-3,6-dioxaoctyl)amide
BLM = bilayer lipid membrane
c = concentration
c = speed of light
cAMP = cyclic adenosine monophosphate
CCD = charged coupled device
cep = core-encoded pilin
CFTR = cystic fibrosis transmembrane conductance regulator
C_{in} = encapsulated dye concentration
$C_{in,0}$ = dye concentration at the start time
$C_{in,t}$ = dye concentration at a specific time
CJD = Creutzfeldt-Jakob disease
CMC = critical micellar concentration
c-PLA_2 = cytosolic phospholipase A_2

cps = counts per second
c_q = quencher concentration
CTP = cytidine triphosphate
CTX = cholera toxin
CTXϕ = Calcutta bacteriophage
D = molecular diffusion coefficient
D^* = apparent dye diffusion coefficient
DC = direct current
DEDA = 7,7 Dimethyl-(5Z,8Z)-eicosadienoic acid
DMPC = 1,2-Dimyristoyl-*sn*-Glycero-3-Phosphotidylcholine
DMPE =1,2-Dimyristoyl-*sn*-Glycero-3-Phosphotidylethanolamine
DMPG = 1,2- Dimyristoyl -*sn*-Glycero-3-[Phospho- *rac*-(1-glycerol)]
DMPS = 1,2-Dimyristoyl-sn-Glycero-3-[Phospho-L-Serine]
DNA = deoxyribonucleic acid
DPPA-biotin = 1,2-Dipalmitoyl-*sn*-Glycero-3-phosphoethanolamine-N-(cap Biotinyl)
DPPC = 1,2-Dipalmitoyl-*sn*-Glycero-3-Phosphotidylcholine
DPPTE = 1,2-Dipalmitoyl-*sn*-Glycero-3-phosphothioethanol
DPPTE = 1,2-Dipalmitoyl-sn-Glycero-3-Phosphothioethanol
DSPC = 1,2-Distearoyl-*sn*-3-Phosphotidylcholine
E = enzyme
E^* = bound enzyme
E^*S = Michaelis complex
Eb^{3+} = erbium (III)
EDTA = ethylenediamine tetraacetic acid
Egg PC = egg phosphatidylcholine
ER = endoplasmic reticulum
ERAD = endoplasmic reticulum associated protein degradation
Eu^{3+} = europium (III)
$EuCl_3$ = europium III chloride
FRET = fluorescence energy transfer
Gd^{3+} = gadolinium (III)
GM1 = monosialoganglioside G_{M1}
GTP = guanosine triphosphate
GUV = giant unilamellar vesicle
hCG = human Chorionic Gonadotrphin
HDL = high density lipoprotein
HeNe laser = Helium Neon laser (5mW, λ = 632.8nm)
HEPES = N-(2-hydroxyethyl)piperazine-N'-(2-ethanesulfonic acid)
HLB = hybrid lipid bilayer
I = reflected and/or refractive light intensity
I_0 = incident light intensity
IAPP = islet amyloid polypeptide
IC_{50} = half maximal inhibitory concentration
IgG = immunoglobulin G
J = flux
K = dye association into the membrane
k = first order rate constant
k = wavelength
K_a = association rate constant
K_A = equilibrium association constant
k_c = mass transfer coefficient

K_D = equilibrium dissociation constant
K_D = Stern-Volmer dynamic quenching constant
kDa = kilodaulton
k_m = mass transfer coefficient
K_m = Michaelis-Menton constant
k_{off} = dissociation rate constant
k_{on} = association rate constant
K_{sv} = Stern-Volmer constant
L = membrane thickness
l = path length
La^{3+} lanthanum (III)
$LaSFN_9$ = high refractive index glass
LB = Langmuir-Blodgett
ld = liquid-disordered phase
LD_{50} = median lethal dose
lo = liquid-ordered phase
LPS = lipopolysaccharide
LT = *Escherichia coli* heat-labile toxin
LUV = large unilamellar vesicle
MHC = major histocompatability complex
mixed-vesicles = 75% DMPC : 20% DMPG : 2.5% DMPS : 2.5% DMPE
MLV = multilamellar vesicle
mRNA = messenger ribonucleic acid
MVV = multivesicular vesicle
MW = molecular weight
NAD = nicotinamide adenine dinucleotide
NIDDM = non-insulin dependant diabetes mellitus
NMDA = N-methyl-D-aspartic acid
OH spacer = 11-mercapto-1-unadecanol
OLV = oligolamellar vesicle
ORS = oral rehydration salts
ORT = oral rehydration therapy
P = product
PD = Parkinson's disease
PLA_2 = phospholipase A_2
PLC = phospholipase C
PLL = poly-L-lysine
PMT = photomultiplier tube
POCT = point-of-care test
r = distance
R = reflectance
R = rotation
R_0 = Föster distance
RDE = radiative decay engineering
R_{eq} = equilibrium response
R_{max} = maximum response
RNA = ribonucleic acid
RPM = revolutions per minute
rRNA = ribosomal ribonucleic acid
S = scattering coefficient
S = substrate

S_0 = ground state
S_1 = relaxed singlet state
S_1' = electronic singlet state
SAM = self-assembled monolayer
SANS = small neutron scattering of x-ray
SAP = serum amyloid P component
SAPP = soluble amyloid precursor protein
SAXS = small angle scattering of x-ray
s-BLM = supported bilayer lipid membrane
SEM = scanning electron microscope
SFL6 = high refractive index glass
SLO = Streptolysin O
so = solid-ordered phase
SPFS = surface plasmon field enhanced fluorescence spectroscopy
s-PLA_2 = secretory phospholipase A_2
SPR = surface plasmon resonance
SPRF = surface plasmon resonance fluoroimmunoassay
SPRS = surface plasmon resonance spectroscopy
SPS = surface plasmon spectroscopy
SUV = small unilamellar vesicle
t = time
Tb^{3+} = terbium (III)
T_c = transition temperature
TIR = total internal reflection
tRNA = transfer ribonucleic acid
TTR = transthyretin
UPS = ubiquitin-protease system
UTP = uridine triphosphate
UV = ultra-violet
V = volume
V_{eq} = equilibrium value
V_L = variable light chain
V_{max} = maximum rate
WHO = World Health Organization
Yt^{3+} = ytterbium (III)
β-PFT = β-pore forming toxin
Δc_A = driving force concentration difference
$\Delta\theta$ = resonance minimum shift
$\Delta\theta/\sigma$ = surface concentration correlation
ε = dielectric permittivity
ε' = electric charge of a material
ε_p = prism dielectric permittivity
τ_D = decay time

Abstract

The cell membrane provides a barrier and maintains the equilibrium between the intracellular and extracellular spaces. It regulate the flux of ions, metabolites and cellular components, and also acts to regulate the communication between the cells. However, any change in the cell membrane, as a result of mechanical, biological or chemical damage, may significantly alter the structure and function of the cell.

Various protein toxins, such as lipolytic enzymes and pore-forming bacterial toxins, have developed means to circumvent this barrier to gain access to resources. The interaction between the toxins and the cell membrane is of interest to understand the mechanisms involved in a range of toxin-related disorders such as cholera, prion diseases, and snake envenomation.

Surface Plasmon Resonance (SPR) provides a technique to simultaneously measure the change in mass density at a surface as a consequence of the adsorption and/or desorption events with a means of exciting fluorescent dye molecules at the surface. The combination of SPR and Surface Plasmon field enhanced Fluorescence Spectroscopy (SPFS) provides a surface sensitive technique with an ability to quantitatively and qualitatively determine small changes in mass and fluorescence in real-time and without the need for labelled molecules, as a result of the toxin-membrane interactions.

Biomimetic membrane phospholipid vesicles were constructed as a model cell membranes and provides a means of monitoring the initial interaction events and the subsequent actions the toxins trigger in relation to the membranes. The biomimetic membranes provide a simple and reliable model to study these events.

Direct membrane lysis, caused by lipolytic enzymes such as phospholipase A_2 (PLA_2) can be observed, and the affinity between the enzyme and the membrane determined. The binding between cholera enterotoxin and the biomimetic membrane can be monitored, and changes in the membrane permeability determined. One of the pathogenic hallmarks of Alzheimer's disease is the accumulation of insoluble β-amyloid deposits on the surface of neurons. The biomimetic membrane system provides a means to monitor the initial stages involved in amyloid aggregation and the subsequent toxic events.

Understanding the mechanisms involved between the analyte-ligand interactions provides insight into possible therapeutic targets against these events. Direct membrane lysis due to PLA_2 activity was shown to be inhibited by manoalide and eicosadienoic acid, whereas cholera toxin and β-amyloid binding were inhibited by lanthanide trivalent compounds. Therefore, the biomimetic membrane system provides a novel method to study toxin antagonists.

1.0 Introduction

Bacterial toxins, neurodegenerative peptides and lipolytic enzymes may be seen to share very little in common. However, as detailed in this thesis, they do consequently share a common connection; their interaction with the cell membrane. The application of optical methodologies, such as Surface Plasmon Resonance and Fluorescence Spectroscopy, allows for the monitoring of the interactions between a constructed artificial model membrane with the membrane binding peptides associated with the diseases and toxins mentioned above.

1.1 The Cell

The cell (Figure 1.1) is the basic structural and functional unit of all living organisms, and was so called because it resembled a small compartment. The term was coined by Robert Hooke in 1667 to describe what he saw when looking at a section of cork under a microscope. He observed it to be "perforated and porous, much like a Honey-comb" and had "very little solid substance, in comparison of the empty cavity that was contained between.....Next, in that these pores, or cells, were not very deep, but consisted of a great many boxes, separated out of one continued long pore, by a certain diaphragm" [1]. This later led to the development of the cell theory in 1839 by Schleiden and Schwann, to conclude that:

- Cells are the basic fundamental unit of structure, physiology and organization of living organisms.
- All living organisms are composed of these fundamental units (cells), either as a single cell, such as a bacterium, or aggregates of cells, such as plants and animals.
- All cells originate from pre-existing cells through cellular division.
- Cells contain the hereditary information, which is passed from generation to generation.
- All cells share a similar chemical composition, and all energy flow (metabolism and biochemistry) occurs within cells.
- Two exceptions exist, viruses are viewed (by some) to be alive but are not composed of cells, and the first cell did not originate from a pre-existing cell.

These observations still remain as the foundations of modern biology.

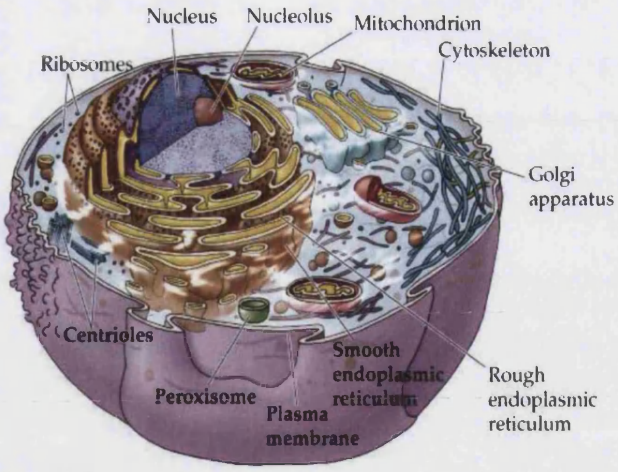

(Picture source *http://www.columbia.edu/cu)*

Figure 1.1 Diagram of a typical eukaryotic cell, consisting of the basic membrane-bound organelles suspended in the cell cytoplasm, self-contained within a plasma membrane.

A living cell is composed of four general classes of macromolecules: nucleic acids, proteins, polysaccharides and lipids. Although subtle differences exist between cell types, they generally contain a comparable proportion of each macromolecule, (Figure 1.2).

Approximate Chemical Composition of a Rapidly Dividing Prokaryotic Cell		
Material	**% Total Wet Weight**	**% Total Dry Weight**
Water	70	-
Proteins	15	50
Nucleic acids	7	23
Polysaccharides	3	10
Lipids	2	7
Others (e.g. inorganic ions)	3	10
Total	**100**	**100**

Figure 1.2 Chemical composition of a unicellular prokaryote, which bares a close similarity to the chemical composition of eukaryotic cell [2, 3].

All the cellular components are bathed in water, which comprises ~70% of the total weight of each cell. The polar properties of water make it an ideal solvent because many cellular molecules are themselves polar, therefore they readily dissolve in water and promote the formation of hydrogen bonds.

1.1.1 Proteins

Proteins are linear amino acid polymers, formed between the carboxyl terminus of one amino acid linked via a peptide bond to the amino group of another amino acid. Each peptide has a unique sequence of amino acids produced from the twenty standard amino

acids. These basic units polymerise into short peptides (Figure 1.3) or into longer polypeptides or proteins. The protein sequence is determined during protein biosynthesis specified within the genetic code of an mRNA molecule.

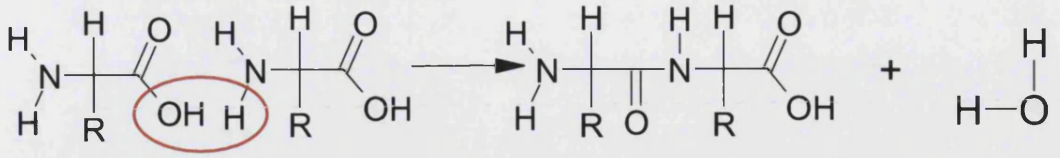

Figure 1.3 The condensation of two generic amino acids into a dipeptide via a peptide bond.

Proteins are hugely diverse, both structurally and functionally, with between 2000-3000 different types of protein molecules in each cell. There are two classes of proteins; globular proteins which are soluble in aqueous solutions and fibrous proteins which are relatively insoluble. Each protein is unique in its participation in processes that characterize the individuality of the containing cells, tissues, organs and organ systems. Many proteins are enzymes that catalyze biochemical reactions vital for metabolism. Other proteins act as transporters or function as messenger molecules, such as hormones. Some act as storage proteins, such as the binding of oxygen by myoglobin in muscle cells, whereas others act as defence proteins in the blood and on the surface of cells as antigens. Proteins can function as structural elements, such as collagen which provide strength and elasticity to skin.

1.1.2 Nucleic acids

The nucleic acids, deoxyribonucleic acid (DNA) and ribonucleic acid (RNA) are nucleotide polymers, which carry the genetic information of the cell and acts as an intermediary molecule to convert the genetic blueprint into a defined amino acid sequence respectively.

Each nucleotide comprises a five-carbon sugar (either deoxyribose in DNA or ribose in RNA), a nitrogen base, and a phosphate group, (Figure 1.4). Nucleic acids are composed of nucleotides covalently linked by a phosphodiester bond to one another via the phosphate from carbon 3 (3') of one nucleotide and the carbon 5 (5') of the adjacent nucleotide, forming the primary sequence of the nucleic acid. The nucleic acids serve an informational

role within the cell, and contain all the necessary information to reproduce an identical copy of the organism.

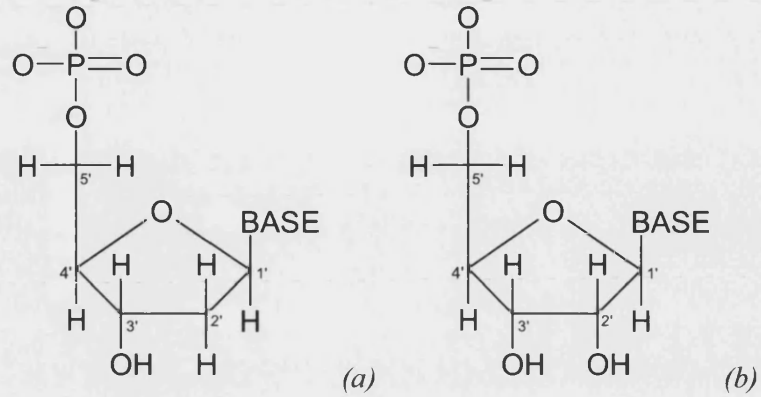

Figure 1.4. Nucleotides. (a) of DNA. (b) of RNA.

Deoxyribonucleic acid (DNA) is a double stranded molecule composed of the nucleotides adenine triphosphate (ATP), guanine triphosphate (GTP), cytosine triphosphate (CTP) and thymine triphosphate (TTP). The two stands associate into a helix conformation by hydrogen bonds, ensuring specific base pairing between adenine and thymine, and between guanine and cytosine. This ensures the two strands are complementary in base sequence.

Ribonucleic acid (RNA) is typically a single stranded molecule, with an ability to fold back on itself in regions where complementary base pairing can occur to form a secondary structure. Three forms of RNA occur within a cell, messenger RNA (mRNA), which contains the genetic information of DNA in a single stranded complementary form, transfer RNA (tRNA), which carries the amino acids to the ribosomes during translation of the mRNA molecule and ribosomal RNA (rRNA), which serve as structural and catalytic components of the ribosome during the initiation and translation.

1.1.3 Polysaccharides

Polysaccharides are polymers of simple sugars containing carbon, hydrogen and oxygen in a ratio of 1:2:1 joined together via glycosidic linkages. The most biologically relevant carbohydrates are those containing between 4-7 carbon atoms, such as pentose (5-carbon sugars) which are the structural backbone of nucleic acids (see 1.1.2), and hexoses (6-carbon sugars), which are the monomeric constituents of cell wall polymers and provide an energy source.

The polymerization of the monosaccharides into carbohydrates can also be combined with other classes of macromolecules, such as proteins and lipids to from complex glycoproteins and glycolipids respectively. These compounds play pivotal roles in cell membranes as cell surface receptors, and glycolipids have additional roles as a major constituent of the cell wall of gram-negative bacteria. Polysaccharides often occur as structural components of cells such as cellulose in the plant cell wall or as storage forms of energy such as glycogen.

1.1.4 Lipids

Fatty acids are the primary constituents of lipids, and show the unusual chemical properties of being soluble in non-polar solvents such as chloroform but are relatively insoluble in water. This is because they contain long hydrocarbon tails which are highly hydrophobic and a head group which is hydrophilic. They serve a wide range of functions within the cell including as energy reserves, hormones, protective barriers and as the major constituent of the cell membrane. They are structurally polymorphic and difficult to define, and are either classified as amphipathic (possessing both polar and non-polar qualities) or as hydrophobic (possessing only non-polar qualities). They are a major class of biomolecule and are a hugely varied group both structurally and functionally (Figure 1.5) adding to their essential nature in all living cells.

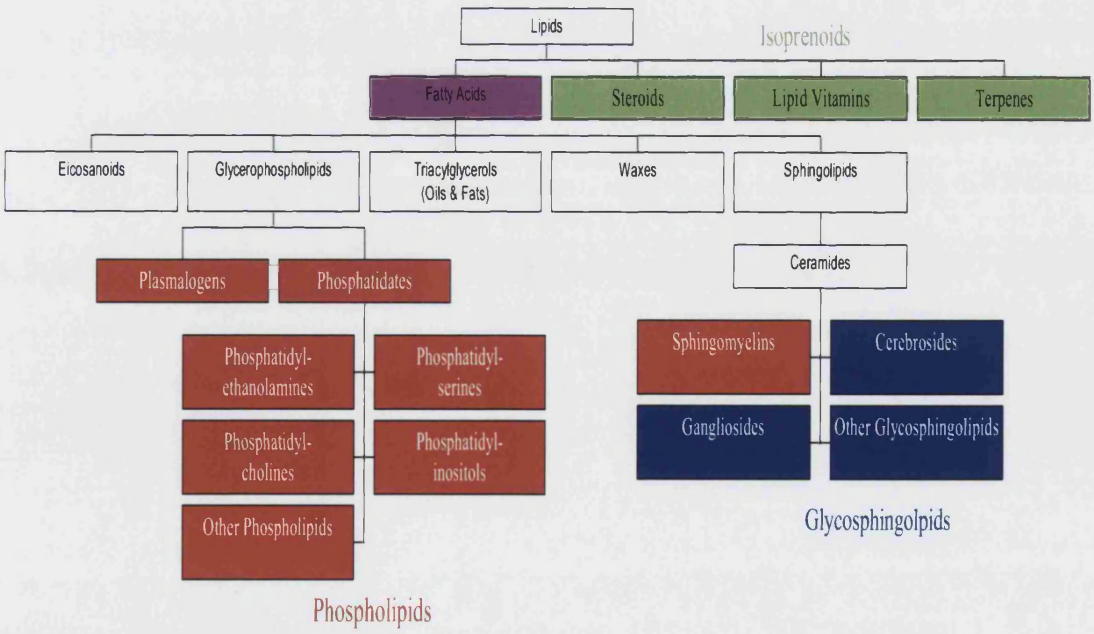

Figure 1.5 Major classes of lipids. Many lipids are composed of the basic units of the fatty acids.[4]

The simplest class of lipid are the fatty acids, which are also the precursors for most other lipid classes, including the sphingolipids, eicosanoids, waxes and the tricylglycerols. They are long-chain hydrocarbons containing a carboxylic acid moiety at one end, which at physiological pH is readily ionized and renders a negative charge onto the fatty acids.

Glyceride-based molecules are the major constituent of biological membranes. These phospholipids contain a glycerol backbone esterified to two fatty acid hydrocarbon chains, and their amphipathic physical nature causes the lipids to spontaneously aggregate so that the hydrophobic portion is shielded from the aqueous environment and the hydrophilic portion aggregate towards the aqueous environment. This compartmentalizes the cell into functional components and maintains the structural integrity of the cell.

The diversity observed among the lipids is the result of the length of the hydrocarbon chain, the degree of hydrocarbon chain unsaturation (mono, di, tri-unsaturation) and the position of unsaturation within the chain. The presence of a double bond within the fatty acid significantly lowers the melting point when compared to a saturated fatty acid, because the double bond causes a pronounced kink in the hydrocarbon chain, therefore, impeding the rotation of the chain and decreases the van der Waals interactions amongst the hydrocarbon chains.

1.1.5 The Origin of the Cell Membrane

Potential membrane components emerged from the polymerisation of simple organic compounds into more complex chemicals and then into macromolecules such as proteins and lipids. An energy source would have been needed for this event to occur, and has been suggested that lightening, volcanic energy, hydrothermal vents and intense UV radiation that penetrated the atmosphere prior to the formation of ozone provided sufficient energy [5]. It has been tentatively demonstrated from fossil records that simple 5-carbon mono-alcohols (terpenoids) were a likely starting point for the evolution of the first membrane. The polymerization of these terpenoids could have anchored to a solid surface through a phosphate group within the polar head group and at a critical chain length and concentration, the polymer peeled off from the solid surface in a manner similar to phase transition [6]. This subsequently enclosed the surrounding materials within its path to form a primitive vesicle [6, 7]. The simple lipids would be highly diluted in the environment, but

a process of condensation caused the concentration of the lipids because of the hydrophobic effect would cause aggregation to shield the hydrophobic portion of the molecule and self assemble either into a basic bilayer, micellar or monolayer system.

1.1.5.1 The Composition of the Cell Membrane

The compartmentalization of cell was first documented by Hooke in Micrographia in 1667. It was stated that cells were "separated out of one continued pore, by certain diaphragms" and that these walls were very thin in comparison to the cells [1]. It was Carl Nägeli in 1885 who introduced the concept and term, plasma membrane, when he observed that the rates of pigment penetration between damaged and undamaged plant cells was different, and this was due to a dense and viscous outer layer distinguishable from the cytoplasm [8]. However, it was not until Groter and Grendel in 1924, that it was determined that these diaphragms consisted of a lipid layer two molecules thick [9]. The thickness of the lipid bilayer was determined to be between 40-50Å by various methods including neutron scattering [10-12]. The lipid bilayer performs many functions, but is primarily a barrier. The lipid membrane is composed of two opposing layers of phospholipids self-assembled so that the hydrocarbon chains face one another, while the polar head groups orientate towards the aqueous environment (Figure 1.6).

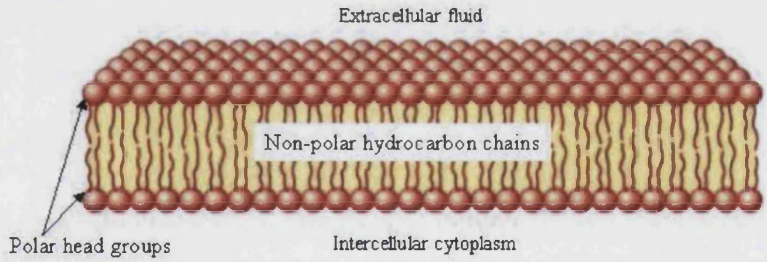

Figure 1.6 Schematic cross section through a lipid bilayer. The polar head groups face the aqueous environment, while shielding the hydrophobic hydrocarbon chains.

The plasma membrane of mammalian cells contains four major phospholipids; phosphatidylcholine, phosphatidylethanolamine, phosphatidylserine, and sphingomyelin. A phospholipid is a class of lipid formed from two fatty acid chains, a glycerol backbone, a negatively-charged phosphate group and an amine group (Figure 1.7). The phospholipids interact mainly be non-covalent interactions. Hydrophobic interactions are responsible for the sequestering of the non-polar hydrocarbon chains away from water, and hydrophilic interactions for the orientation of the polar head groups towards the aqueous environment. Dipole-dipole interactions also contribute to the stabilization of the bilayer structure

between the ion pairs of zwitterionic phospholipids such as phosphatidylcholine. Maximization of these interactions ensures that the system has the lowest free energy possible. Other noncovalant interactions, such as hydrogen bonding and electrostatic attraction, can also contribute to the stabilization of the system. However, these interactions contribute very little to the overall stability of the energy state compared to the hydrophobic and hydrophilic interactions.

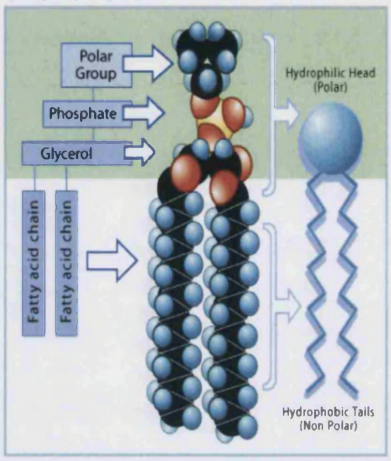

Figure 1.7 Generic phospholipid molecule composed of two fatty acid chains and a phosphate group linked to a glycerol backbone, which in turn is attached to a nitrogen containing head group.

The phase transition temperature (T_c) of a lipid is the temperature at which the lipid changes from the ordered gel phase, where the hydrocarbon chains are fully extended and closely packed, to a disordered liquid crystalline phase, where the hydrocarbon chains are randomly orientated and fluid. In the gel state, the phospholipid hydrocarbon chains are fully extended and in the *trans* conformation with the polar head groups remaining relatively immobile. Above the phase transition temperature for a particular lipid, the polar head group increases in mobility and the hydrocarbon chains change from the *trans* to more unstable *gauche* conformation [13]. The phase transition temperature is directly affected by hydrocarbon length, unsaturation and head group species [14]:

- With increasing hydrocarbon chain length; the phase transition temperature increases.
- With increasing unsaturation of the hydrocarbon chain; the phase transition temperature decreases.

- Position of the unsaturated bound; lower phase transition temperature observed with double bonds situated in the middle of the hydrocarbon chain.
- Nature of the head group; Phosphatidylethanolamine cause the highest phase transition temperature, followed by phosphotidylserine, then phosphatidylcholine, and then phosphotidylglyerol.
- Increasing the pH of the medium lowers the phase transition temperature.

Moreover, high phase transition lipids increase the stability of a membrane system by ensuring the system is in the gel-phase and membrane leakage is reduced. When a membrane system is subjected to an increase in temperature, the rotational freedom of the hydrocarbon chains also increases. So when the system enters phase transition, there is an abrupt decrease in packing density [15].

The two leaflets of the plasma membrane show an asymmetry in phospholipid distribution. The endoplasmic reticulum is the principal site of membrane assembly in eukaryotic cells, and the distribution of asymmetry between the leaflets is maintained and controlled by slow transbilayer diffusion, protein-lipid interactions, and protein-mediated transport. Glycosphingolipids and phosphatidylcholine are concentrated in the exoplasmic leaflet, while aminophospholipids, phosphotidylserine and phosphatidylethanolamine are concentrated on the cytoplasmic face of the lipid bilayer. This asymmetrical transmembrane distribution is not random and has an important role in determining the physical properties of the membrane, as demonstrated by the concentrated distribution of phosphatidylserine in the cytoplasmic leaflet of human erythrocytes, which interacts with the cytoskeleton proteins to maintain membrane integrity [16]. This asymmetry is maintained by spontaneous transbilayer movement, "flip-flop", and is dependant on the charge of the phospholipid head group, as movement of lipids with polar head groups is slower compared to lipids comprising a non-polar head group [17]. The movement of phosphatidylcholine and sphingomyelin from the exoplasmic to the cytoplasmic leaflet is a slow, non-mediated process in comparison to the aminophospholipids, which are rapidly transported from the exoplasmic to the cytoplasmic leaflet by an active ATP dependent and protein mediated process. A thermodynamic barrier exists to prevent rapid spontaneous transbilayer diffusion of phospholipids.

The non-random lipid distribution across the bilayer is important for cell functions. Any significant change in the distribution of phospholipid species generally triggers a physiological event or a signalling event, as shown during the exposure of phosphatidylserine and phosphatidylethanolamine on the exoplasmic leaflet, which signals for the removal of the expressing cells via the apoptotic pathway [18], and this mechanism is phylogenetically conserved [19].

1.1.5.2 The Role of Cholesterol in the Cell Membrane

Sterols are amphipathic lipids, which comprise between 5-30% of the eukaryotic membrane, depending on the cell type. Cholesterol is present in higher concentrations in cells which have more densely-packed membranes, such as the liver, spinal cord and brain cells. However, sterols are absent from the majority of prokaryotic cell membranes, and in its place contain a peptidoglycan to provide structure and support. They are rigid and planar molecules, and share four common rings (Figure 1.9).

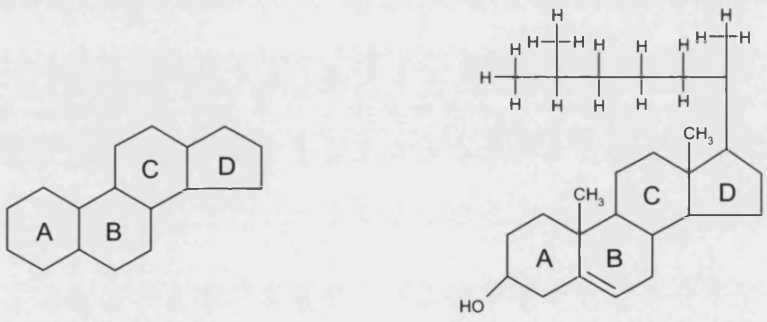

(a) (b)

Figure 1.9 (a) The general structure of a sterol, all containing the same four rings A,B,C and D. (b) The structure of cholesterol.

Cholesterol is abundant in the eukaryotic cell membrane, and ensures the fluidity over a wide range of temperatures and reduces the permeability of membranes to cations. Cholesterol eliminates the sharp thermal transition between the gel and liquid phases [20], therefore, giving the membrane properties intermediate between the two phases. However, the lack of sterols within prokaryotes, the endoplasmic reticulum and the inner mitochondrial membrane suggests they are not solely responsible for membrane integrity. Cholesterol has been demonstrated to inhibit the flow of water through membrane bilayers, and reduces the passive water permeability in direct proportion to the amount of cholesterol in the membrane [21]. This has been speculated to be because the fused ring

domain of the cholesterol molecule orientates between the head group and the carbon-9 of the lipid chains, which presumably squeezes out the water [22]. The constraints placed upon the motion of the hydrocarbon chains suggests that the sterol induces a tight lateral packing between membrane components, as defects due to bad packing make membranes more permeable to ions. The formation of hydrogen bonds between the OH-group of the cholesterol and the carbonyl group of the fatty acyl ester bonds of the phospholipids have been proposed to add to the stability of the membrane [23], but has no effect on the thickness of the membrane [24].

The distribution of cholesterol between the two monolayers of the membrane is experimentally difficult to determine because transbilayer movement of the sterol between leaflets is very rapid in comparison to the "flip-flop" of phospholipids. The preferential distribution of cholesterol in the outer membrane was claimed because the sterol has a preference for saturated and monounsaturated phospholipids compared to polyunsaturated phospholipids [25].

It has been suggested that cholesterol acts as a spacer molecule within the exoplasmic face of the bilayer, aiding the assembly of lipid rafts, which function to segregate and concentrate membrane proteins [26]. Lipid rafts constitute cholesterol and sphingolipids in the exoplasmic leaflet of the plasma membrane, with the cholesterol acting to condense the sphingolipids by occupying the spaces between the saturated hydrocarbon chains. Glycosphingolipids on the exoplasmic leaflet can interdigitate with the cytoplasmic leaflet to couple the two leaflets [27, 28]. These lipid rafts can then incorporate distinct classes of proteins involved in the various cellular functions including signalling and transport.

1.1.6 Self Assembly

Self-assembly is an intrinsic property of certain molecules, which have the capacity to generate structural organizations without input from an external source, thereby maximizing the benefit of the individual [29-31]. Self-assembly is a reversible process in which pre-existing components of a system form patterned structures. The capacity of individual components to self-assemble reflects the information regarding shape, surface properties, charge and mass, coded within these individual components to determine the interactions among them. There must be freedom for the components to move in respect to one another, therefore, the process usually occurs in fluid phases or on smooth surfaces.

The process of self-assembly is reversible as it involves non-covalent or weak covalent interactions, such as van der Waals, electrostatic and hydrophobic interactions [32].

Self-assembly offers some advantages over systems maintained entirely by covalent bonds, including a reduction in structural errors in the final product by rejection of defective subunits during assembly [33]. No system is finite because the assembly is via reversible non-covalent interactions, and results in the formation of an energetically and economically viable structure. If certain systems, such as the cell, were held together by covalent bonds, there would be inherent difficulties associated with this because there would be a need for an excessive amount of time required to effect the synthesis of the end product, and the synthetic steps would proceed with absolute commitment, since one error could risk the functionality of the system [34].

1.1.7 Fluid Mosaic Model

Biological membranes can be viewed as two-dimensional, fluid, asymmetric lipid bilayers, which provides a matrix for transmembrane proteins to act as channels for the transport of molecules from the cytoplasm to the extracellular medium or visa versa. This concept of the fluid mosaic model was established by Singer and Nicolson in 1972, describing the lateral and rotational freedom and random distribution of the molecular components in the membrane [35]. It was named accordingly because of the fluid nature of the phospholipids within the bilayer plane, because the membrane is composed of a heterogeneous array of phospholipids, proteins and glycoproteins give the membrane a mosaic structure (Figure 1.10). The model states that globular proteins alternate with sections of the phospholipid bilayer, therefore, the phospholipids are predominantly arranged as an interrupted bilayer.

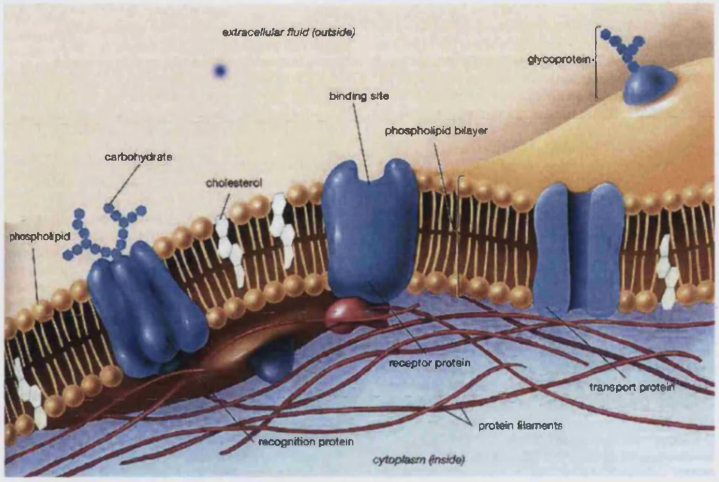

(Picture source www.sun.menloschool.org/~cweaver/cells/c/cell_membrane/)

Figure 1.10 Fluid Mosaic Model of the cytoplasmic membrane. The matrix of the unit membrane is composed of phospholipids, with the hydrophobic hydrocarbon tails directed inwards and the hydrophilic groups towards the aqueous medium. Proteins and carbohydrates are embedded within the matrix.

Moreover, there have been refinements to the fluid mosaic model since its first proposal over the past thirty years, when it became apparent that proteins are not generally floating freely in the lipid matrix even when the lipids are in a liquid state. This is because the hydrocarbon chains of lipids near proteins have different configurations to those in the rest of the bilayer. This is to ensure no void regions are formed (Figure 1.11), therefore, the packing of the hydrocarbon chains adapts to fill voids, usually by causing membrane curvature.

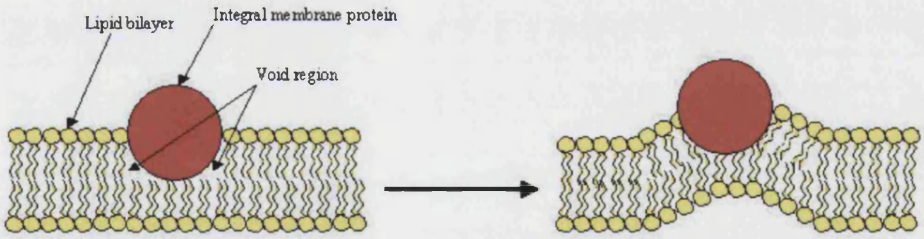

Figure 1.11 Alterations to the original Fluid Mosaic Model suggest proteins are not free floating, since packing constraints impose structural coupling between proteins and neighbouring lipids.

Moreover, the Singer-Nicolson model has been substantially revised to include:

- The mobility of the cell-surface proteins are restricted by lipid-anchored or other lipid domains, with the aim to segregate.
- Membrane proteins may co-localize with each other.

- Membrane proteins may cluster and are accommodated by lipid rafts organized by weak non-covalent interactions.
- Proteins are likely to have an equal importance in determining the constituents, structure, and dynamics of membrane domains.
- Free diffusion can occur within domain boarders where molecular interactions do not hinder.

The Fluid Mosaic Model developed to classify the membrane as a structure that is heavily compartmentalized, quasi-two-dimensional, mosaic and partially fluid [36].

1.2 Poisons, Toxins and Venoms

Living organisms are designed to pass on their hereditary material and reproduce. To do this they must be able to defend themselves from predation and assimilate nutrients for their own survival and growth. Many living organisms have evolved and developed an arsenal of weapons in a bid for survival, whether it be body armour, horns or chemical weapons. Many prokaryotes and eukaryotes produce proteins that have toxic properties that act towards other living organisms either intentionally or inadvertently. The toxicity effects observed from the actions of a particular toxic protein can have an effect on the whole organism or a localized action on a particular substructure such as an organ.

The route of delivery into a system distinguishes poisons, toxins and venoms from each other. A toxin is a poisonous substance that is injected in some way into the system, and venoms are usually defined as biologic toxins that are injected by a bite or sting. Poisons are generically defined as a substance which is ingested or absorbed through epithelial linings such as the skin or gut. The Swiss toxicologist Paracelsus, stated that all things are poisonous if administered at a toxic dose. Toxins are mainly proteins that are capable of producing a detrimental effect on contact or adsorption with cells by interacting with biological macromolecules or cellular receptors. The toxicity of a particular substance varies in their mode of action and their severity depending on dose and tolerance to the toxin. They vary tremendously in structural complexity, from venoms that contain a range of lytic peptides that each target a specific receptor, to relatively simple proteins such as the phospholipase groups.

Biotoxins are substances produced by living organisms, and have two primary functions:

- Predation: snake, spider, scorpion venoms
- Defence: bee, deadly nightshade, poison dart frog venoms

These biotoxins have diverse actions including haemotoxicity that targets red blood cells, necrotoxicity that causes necrosis in all tissue types and neurotoxicity that primarily affects the nervous system. Toxins are believed to increase the chance of survival and/or proliferation and/or spreading of a particular organism in its environment [37]. Naturally occurring toxins are the product of a long term co-evolution of species sharing the same habitat. The evolution of envenomation is believed to have arose in squamates about 200 million years ago [38]. Moreover, these toxins have developed to selectively hit key molecular targets such as the machinery controlling protein synthesis and the cell membrane.

1.2.1 Factors Affecting Toxic Response

The fate of a toxin within a biological system is dependant on the dose-response relationship, which is defined as the change in effect on an organism caused by differing levels of exposure to a particular toxic compound. For a toxin to exert its effects on a system it must gain access and circumvent any host defence systems. The first step in the toxin action cascade (Figure 1.12) is it must come into contact with the biological system. The absorption of the foreign molecule may exert a local effect at the initial site of contact, but must gain entry into the organism to insure a systemic effect. The most common access route for a toxin is via the gastroinstinal tract, the respiratory tract, and to a lesser extent, absorption through the skin. Whatever the initial point of contact for the toxin, it must cross the cell membranes, therefore, for the successful penetration of a biological system there must be physicochemical constraints imposed, such as size/shape of the toxin, structural similarity to endogenous molecules and the charge on the toxin.

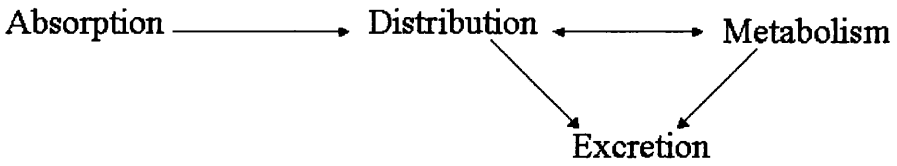

Figure 1.12 Disposition of a toxin molecule in a biological system can be divided into four phases.

1.2.2 Toxic Response to Foreign Compounds

The stages following the exposure of a cell to a toxin can be divided into primary, secondary and tertiary events. Primary events are the result of the initial damage caused by the toxin, such as enzyme inhibition and pore formation. Secondary events result in biochemical and/or structural cellular changes observed following the initial damage, such as changes in membrane structure, nucleic acid damage and stimulation of apoptosis. The final state of toxicity is the observable manifestations, which can include necrosis and apoptosis [39].

1.2.3 Animal Toxins

Toxins produced by animals have evolved for defensive and predatory purposes to ensure their survival and reproduction. A common feature of animal toxins is that most target the systems homeostasis and directed towards cell surface proteins involved in essential cell functions. They tend to be ligands of ion channels which are inactivated upon toxin binding and interfere with neuronal and/or muscular function, ensuring the immobilization of the predator or prey (Figure 1.13). They are targeted towards receptors and ion channels because they are common to the animal kingdom, therefore, the toxins act against a range of animal species. Unlike many of the toxins developed by plant species, animal toxins are designed for rapid effect and action, therefore, they have evolved to act at the cell surface.

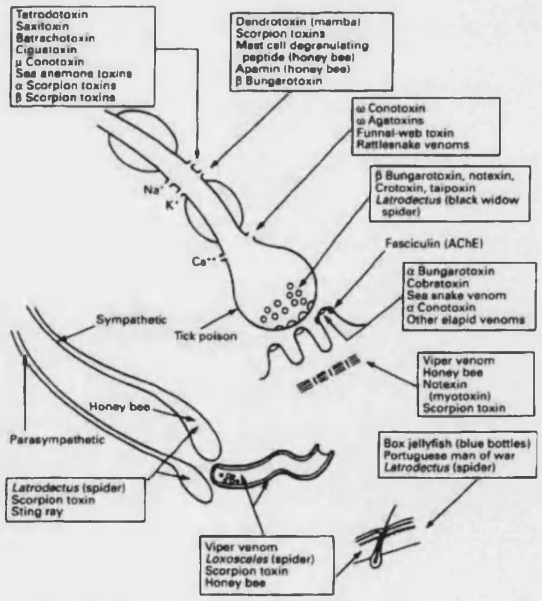

Figure 1.13 Principal sites of action of animal toxins [40].

Venomous animals can be grouped into non-biting/non-stinging and biting/stinging animals depending on their route of venom administration. A range of taxonomic phyla possess venom that is not administered via biting and stinging, including invertebrates, amphibians, and fish.

The injection of venom by means of a sting or a bite are common amongst the reptiles and invertebrate. A bite is described by venom injection via structures associated with the mouth, such as fangs or mandibles, and stings signify the injection of venom via a posterior structure. Venom associated with feeding organs have developed for handling prey and designed to instigate paralysis, tissue destruction and death of the victim. Defensive use of these oral structures are only secondary [41]. Moreover, posterior stings have evolved primarily for defence, and intended to cause immediate pain.

The invertebrates that have developed the means of biting and stinging to deliver venom are widespread. The hymenoptera, which include the honeybee, wasp and hornet, have been shown to administer a venomous sting that include phospholipase A_2, melittin, and a complex range of allergic proteins, active antigens and peptides. These toxins tend to stimulate histamine release from mast cells, causing an inflammatory response, including vasodilatation and lowering of blood pressure. If histamine is released into the skin, it can cause itching and reddening of the area. These localized reactions are self-limiting, and spontaneously resolve within a short time.

Snakes primarily use two methods for prey capture, those that constrict their prey and those that envenomate. Only around 7% of snakes use venom as their means of prey capture [40], and these are taxonomically classified in the families, *Elapids, Viperids, Colubrids* and *Hydrohilldae.* These snakes use modified saliva, delivered through fangs to immobilize or kill its prey (Figure 1.14). Venom serves three primary functions; 1) prey/predator immobilization, 2) initiate digestion, and 3) as a lubricant during swallowing. Moreover, venom has also been suggested to possess antibacterial properties [42] to ensure the upkeep and cleansing of the oral surfaces [43]. The snake venom gland evolved 60-80 million years ago, and has undergone extensive modifications with the development of the front-fanged delivery system [44]. It has been shown that the genes for the various venom constituents have been recruited from a range of sources, including from the pancreas and

from ancestral salivary tissue [45]. It has been proposed, using amino-acid sequences, that the ancestral proteins of snake venoms were phospholipases and ribonucleases [46].

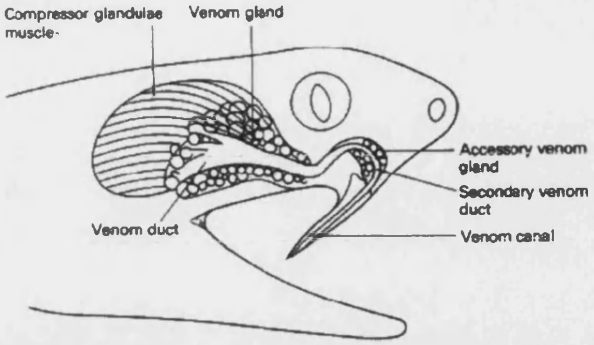

(Picture source:/www.searo.who.int/en/Section10/Section17/Section53/Section1024_3895.htm)

Figure 1.14 Diagrammatic representation of the venom apparatus

The major constituents (>95% of dry weight) of snake venom are polypeptides, which include enzymes, toxins, and small peptides. More than twenty enzymes have been isolated from various species, with 12 common enzymes found in the majority of venoms [40]. Hyaluronidase is present in all snake venoms to facilitate the distribution of the other venom components around the tissues of the predator/prey. Other components present in snake venoms include procoagulant enzymes, that stimulate blood clotting factors and the formation of fibrin, thereby depleting their levels leading to un-clottable blood [47]. Haemorrhagins, such as zinc metalloproteinases, cause damage to the endothelial lining of the blood vessel walls, resulting in haemorrhage. A range of toxins, including necrotic toxins and myolytic toxins cause an increase in membrane permeability and substantial damage to cells respectively. The most potent snake venom known is that from the Inland tipan [48], which causes systemic neurotoxicity that often results in respiratory paralysis. The venom causes the breakdown of skeletal muscle tissues, which leads to acute renal failure [49] and cause the hydrolysis of the cell membranes.

1.2.4 Bacterial Toxins

Animals and plants have developed strategies, through co-evolution with microbes, to attempt to defend and ward off the attack from a pathogen. These defences include simple physical barriers like the dead cell layers of skin, waxy cuticles of plants, mucus-covered epithelia, antimicrobial peptides and the immune response [50]. However, bacterial pathogens have also evolved strategies to circumvent these defences through the development and acquisition of virulence factors. Bacteria have developed a range of

strategies to ensure their survival and modification of the host physiology to promote their multiplication and spread (Figure 1.15). Only around 10% of bacterial species are pathogenic to humans and animals, and not every species in a genus is pathogenic and not every strain of each pathogen causes disease [51]. Some virulence factors employed by certain pathogens include factors that neutralize host defences and factors that cause the destruction of the host cells. Toxins produced by bacteria act differently to those produced by animals, and do not need such a rapid action. Bacterial toxins are not a defensive mechanism employed by bacteria, but are virulence determinants engaged to gain access to environments to sequester nutrients, to multiply, and for transmission to new environments when resources are expended.

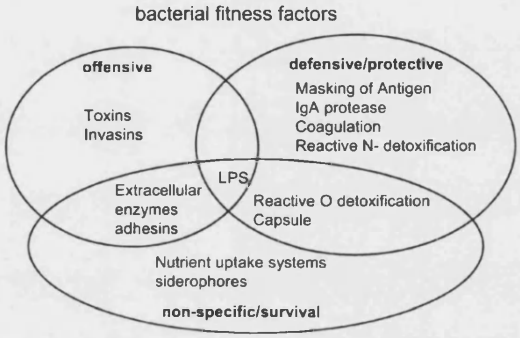

Figure 1.15 Fitness factors found in pathogenic bacteria. (LPS = lipopolysaccharide) [50].

The development of bacterial toxins is believed to have occurred during the co-evolution between bacteria and unicellular eukaryotes during the past 1 billion years. This is supported by the fact that numerous virulence factors attack host cell proteins, molecules and structures present in all eukaryotic cells [50]. Moreover, it is probable that these virulence factors served to paralyze unicellular eukaryotes and were later adopted by pathogenic bacteria. Certain human restricted pathogens, such as *Streptococcus pyogenes*, must have adapted to their hosts in the 1 million years during the emergence of humans. The bacterial genome consists of the core genes that encode fundamental pathways and essential structural features such as cell wall components and ribosomal RNAs. The other part of the bacterial genome is the flexible genetic elements, which encode variable determinants that provide some type of selective advantage under specific conditions, such as infection and growth in specific niches. These housekeeping genes frequently consist of various mobile genetic elements, such as plasmids, bacteriophages, insertion sequence elements and transposons [52] coding for antibiotic resistances and toxins. Horizontal gene transfer allows for the transfer of genetic material between two unrelated organisms and therefore, the exchange of virulence factors between unrelated species.

Bacterial toxins alter the normal metabolism of the host cells with deleterious effects to the host [53], and are often responsible for the symptoms associated with the bacterial infection. Toxins are categorized according to their site of action, and are broadly grouped as exotoxins that modulate intracellular targets and the endotoxins and membrane-damaging toxins that act on the cell surface. However, all bacterial protein toxins must first interact with the cell membranes.

1.2.4.1 Bacterial A-B Subunit Enterotoxins

Enterotoxins are soluble proteins secreted into the surrounding medium by the bacterium, where it circulates around the host and attaches to receptors on the surface of sensitive cells. Bound enterotoxins can become internalized into the host cells where they are capable of modifying the intracellular target through covalent mechanisms. Bacterial enterotoxins vary in specificity, and can either act on a wide range of cells and tissues or only act on specific cells. These toxins share a common structural feature of consisting of two distinct non-identical protein moieties or subunits, the A domain and B domain. The fundamental property of these enterotoxins is for the B domain to bind to the cell membrane and specifically deliver their A subunit into the cytosol of the target cell. The internalization of the toxin occurs by receptor-mediated endocytosis, whereby the B domain binds to the receptor on the cell membrane and utilizes the host cells endocytotic pathway to become enclosed in an endocytic vesicle generated by the invagination of the cell membrane. The internalized toxin within the endocytic vesicle matures and acidifies, causing a conformational change in the B domain, which inserts into the endosome membrane to generate a pore that is involved in the translocation of the A domain into the cytosol [54]. The A domain possesses the enzymatic activity specific for each toxin, causing the modification of the intracellular target (Figure 1.16).

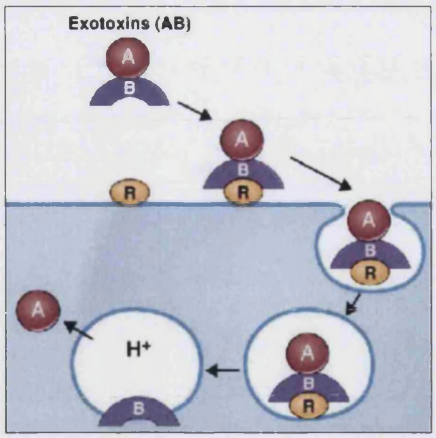

Figure 1.16 Bacterial toxins that modify intracellular host proteins. Exotoxins bind to receptors (R) on the surface of host cells and are endocytozed. After it matures, the endosome acidifies, causing a conformational change in the B domain, which inserts into the endosome membranes to generate a pore for the translocation of the A domain into the cytosol [53].

Many bacterial species have evolved subunit toxins to cause pathogenicity, including *Corynebacterium diphtheriae*, *Pseudomonas aeruginosa* and *Vibrio cholerae* (which will be described in chapter 5).

1.2.4.2 Bacterial Cytolytic & Membrane-Permeating Toxins

Surface-acting toxins exert their actions by binding to the cell membrane and modify the host cell physiology without having to be endocytosed and enter the intracellular space of the host cells. The membrane permeating toxins are largely grouped into two classes: the lipases and the pore-forming toxins. The modulation of the host cell physiology can affect host cell signalling or directly damage the cell membrane. Any non-selective fluxes of ions, fluid and small molecules, disrupts the cells equilibrium and will generally induce cell death. Most of the toxins are produced and stored as an inactive form (protoxins). These protoxins are activated by a chemical modification step, such as the cleavage of a terminal site, and this increases the affinity for the membrane [37].

Pore-forming toxins (PFT) represent more than one third of all bacterial toxins, and are believed to act extracellularly to release nutrients useful for the pathogens growth and reproduction [54]. Toxins that generate defects, channels, or pores in the cell membrane provide a route for the unregulated flux of small solute molecules and fluids. Therefore, the toxins must be amphipathic in nature because the lumen of the channel is in contact with the water, and the other domain is in contact with the non-polar lipid domains. For the

cytotoxicity of a toxin to be satisfied, the toxin must bind to sensitive cells with high affinity. At this stage, conformational changes take place so that the toxin can reoriented and penetrate into the membrane. This is governed by the cell membranes physical properties, and is dependant on phospholipid species, sterol content, and membrane defects. The bound toxin molecules laterally diffuse, oligomerize to ensure that the non-polar domains of the cell membrane are shielded from the medium, and to generate a channel from the extracellular membrane through to the cytoplasmic face of the cell membrane (Figure 1.17). Pore-forming toxins make membranes more permeable to water, and if excessive influx occurs, the cells swell and lyze. If flux is not excessive, cellular damage occurs by perturbation of the permeability barrier that causes the leakage of ions needed for cell viability. This means of non-enzymatic damage uses a mechanism similar to that of the membrane attack complex of the complement system to neutralize the threat from invading pathogenic bacteria during the immune response [53].

Binding to the host cell surface often involves a receptor-toxin association because the toxins are generally secreted at low concentrations into an environment that is rapidly cleared of foreign materials. Therefore, many pore-forming toxins rely on ubiquitous or widely distributed receptors as their targets for binding, such as phosphatidylcholine and cholesterol, both of which are the major constituents of animal cell membranes. Receptor preference ensures toxins bind to host cells and avoid self-interactions by binding to receptors uncommon in their own cell membranes [55]. The small hydrophobic sequence that each toxin monomer contains is not large enough to form a channel. Oligomeric complexes ensure enough hydrophobicity to insert into the target membrane to begin to form a stable structure. Lipid domains, in which the receptors for the binding of the β-PFT monomers facilitates oligomerization by concentrating the receptors in specific areas.

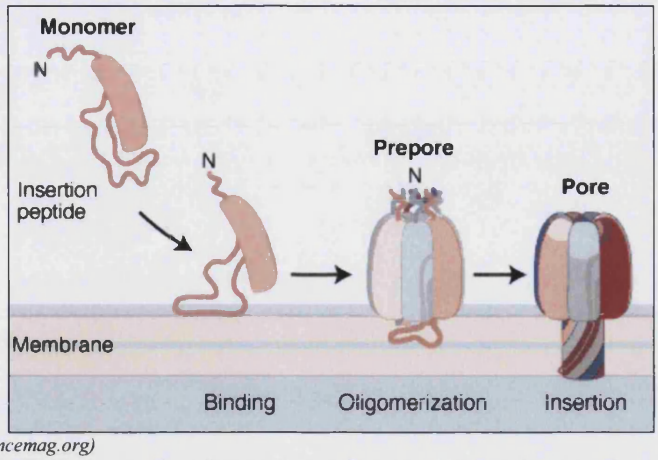

(Picture source: www.sciencemag.org)

Figure 1.17 Steps leading to the formation of a pore by a β-pore forming toxin, such as Staphylococcus aureus α-hemolysin. Soluble monomers bind to the cell membrane and oligomerize on the cell surface forming a non-lytic heptamer. The oligomer inserts the stem into the lipid bilayer, generating a transmembrane channel, allowing the flux of ions and small molecules (~1000 molecular weight).

1.2.5 Endogenous Cytotoxic Peptides and Their Role in Disease

Some proteins and peptides found naturally in the body can cause detrimental effects as a result of improper regulation, misfolding and accumulation to toxic levels. Proteins or peptides which usually perform necessary functions can become toxic if improperly controlled or not recognized as "self".

1.2.5.1 Diseases Caused by the Folding and Misfolding of Proteins

Protein folding is strictly regulated, because abnormal proteins are extremely harmful to cells. Such proteins can originate from mutations, unbalanced subunit synthesis, and damaging conditions such as oxidation. Folding of proteins can take place in the cell cytosol, but the vast majority takes place in the endoplasmic reticulum (ER). This organelle also performs pivotal quality control to ensure proteins are correctly folded, and any misfolded proteins can be re-routed for degradation. The quality control of protein folding is not error free because having some flexibility allows for protein evolution [56].

Other proteins or fragments of proteins can cause toxicity by converting from their normally soluble forms to insoluble fibrils, which accumulate in a variety of organs including the brain, liver and spleen [57]. These insoluble fibrils act as seeds for the formation of amyloid plaques, as misfolded/abnormal proteins aggregate via hydrophobic interactions [58], and causes clinical conditions termed amyloidosis. This group of diseases

include Alzheimer's (as detailed in chapter 6) and Parkinson's disease, Prion diseases such as Creutzfeldt-Jakob disease, and type II diabetes (non-insulin dependant). It has been shown that pancreatic amyloid deposits composed of the islet amyloid polypeptide (IAPP) are found in nearly all type II diabetes patients [59], and their cytotoxic actions are associated with the progression of pancreatic β cells death. It has been suggested that IAPP is normally produced by the islet cells in the pancreas to oppose the actions of insulin in the peripheral tissues [60], but its polymerization into amyloid deposits causes the cytotoxic destruction of the islet cells leading to disrupted glucose and hormone passage from the islet cells.

Protein aggregation is a consistent feature of many neurodegenerative disorders, including Parkinson's, motor neuron, and Creutzfeldt-Jakob diseases. These disorders are characterized by the accumulation of high-ordered insoluble fibrils, and the species of protein aggregate determines which neurones are pathologically affected and what clinical symptoms arise form each protein. It is not known whether protein aggregates are themselves toxic to cells or whether they are the result of an underlying molecular factor. These late-onset, slow-progression disorders result in a gain-of-function associated with abnormally folded forms of the proteins formed under conditions that stabilize a partially folded structure [61]. Progressive neuronal dysfunction is followed by eventual neuronal loss. Protein fibril formation is either believed to be a contributory factor in cell death or is an inseparable epiphenomenon [62]. However, very little information is known regarding what makes certain proteins prone to aggregate. *In vivo*, the cell uses chaperone proteins to assist in protein folding under physiological and stress conditions. Chaperones associate with the nascent polypeptides as they emerge from the ribosome, promoting correct folding [63]. However, protein folding is not error free. Chaperones are also enrolled in the translocation of proteins across the membranes, helping protein complex assembly and disassembly, and suppress protein aggregation [64]. Unfolded or misfolded proteins tend to have exposed hydrophobic domains that render them prone to aggregate, and it is assumed to be the passive process of self-assembly that drives mass-action [63]. Therefore, the cell has developed a mechanism to avoid protein aggregation by ensuring proteins are kept soluble by molecular chaperones or are quickly degraded by the covalent attachment to ubiquitin, which earmarks the abnormal protein for proteolysis by the proteasomes [65]. During the pathological aggregation of proteins, the levels of abnormal proteins is believed to exceed the cells ability to maintain them in soluble form [64]. Protein aggregation

directly impairs the function of the ubiquitin-proteasome system [66], thereby further limiting the cell's ability to dispose of protein aggregates and allowing their continued pathogenicity. The late on-set of diseases associated with protein aggregation suggests that the gradual decrease in the efficiency of the ubiquitin-proteasome system is associated with aging [61]. *In vivo* studies to determine whether protein aggregates are directly pathogenic to cells or the result of an underlying mechanism is unclear, but one study by Bence *et al* reported that protein aggregation directly impairs the function of the ubiquitin-proteasome system (UPS), thus leading to the accumulation of ubiquitin conjugates and cell cycle arrest [66]. The commitment of the proteasome to the ubiquitylated aggregates without being able to unfold or degrade it would ensure the proteasome is unavailable for degrading other abnormal proteins. As a result of a decline in UPS activity, aggregated proteins continue to accumulate, slowly leading to the characteristic progression of many neurodegenerative diseases.

1.2.5.2 Diseases Caused by Inflammation

Inflammation is the non-specific biological response of vascular tissues to any noxious stimulus, such as pathogens, physical damage or chemical irritants. It is a protective response designed to initiate healing by attempting to remove the foreign stimulus from the organism. A single finite event, such as a bee sting, causes a self-limiting and localized response. Whereas, a complex sustained response involving the whole organism is initiated when the foreign stimulus can not be removed, is not recognized as truly foreign, or is perceived as foreign but is in fact "self", such as the development of rheumatoid arthritis. An inflammatory response is a cascade that follows an essentially uniform course of events, with different types of injury and varying degrees of damage leading to variations in the intensity and duration of a particular aspect of the cascade.

Two forms of inflammation exist; acute and chronic inflammation. An accute inflammatory response cascade is triggered involving the local vascular system, the immune system and various cells within the injured tissues (Figure 1.18). The initiation of the inflammatory response by a stimulus causes the blood vessels at the site to exude plasma proteins and leukocytes into the surrounding tissue, causing the characteristic swelling associated with inflammation. The microcirculation responds to the injury by increased blood flow to the site of inflammation, causing reddening and heat. Histamine is the first inflammatory mediator to be released after injury, causing increased vascular

permeability. Polymorphonuclear leukocytes accumulate at the site of inflammation to phagocytoze the stimulus. They also release enzymes that cause damage to the tissues. Down regulation of the inflammatory response is achieved after the injurious stimuli have been removed.

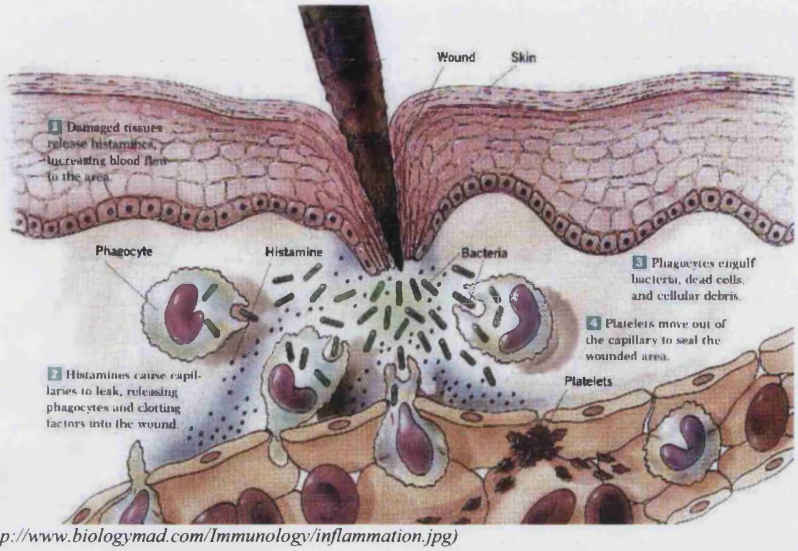

(Picture source http://www.biologymad.com/Immunology/inflammation.jpg)

Figure 1.18 The acute inflammatory cascade, when the stimulus is removed and inflammation response is down regulated.

Chronic inflammation may develop as a progression from acute inflammation if the original stimulus persists or after repeated episodes of acute inflammation. The purpose of chronic inflammation is to clear necrotic debris produced during the acute inflammatory processes, to provide defence against persistent infections, and to heal and repair the damage to the tissues [67]. It is characterized by infiltration of mononuclear immune cells, such as macrophages and lymphocytes, tissue destruction and attempts at healing, which include fibrosis. Chronic inflammation may also occur if the host tissue is modified and new antigenic determinants are produced following the release of lysosomal enzymes by phagocytic cells. This causes the endogenous antigen production, and thereby initiates chronic inflammation and an auto-immune response against self-antigens. The introduction of a foreign antigen initiates a cascade whereby T-lymphocytes begin by recognizing the antigen. The activated T-lymphocyte begins to produce lymphokines to direct the immune system response by signalling between its cells and attracting other immune cells. The monocytes phagocytoze the foreign stimulus and damaged tissues so that new tissue can be generated in the area of inflammation for normal function to resume.

Typically, inflammation is a beneficial response. However, if the inflammatory processes are not stringently regulated or failure to eliminate the noxious stimulus, prolonged local cell injury and trauma occurs. As chronic inflammation proceeds, additional inflammatory cells are recruited to the site of inflammation, resulting in the release of more inflammatory mediators.

Phospholipase A_2 (PLA_2) are lipolytic enzymes which play an extensive role in the cascade of many acute and chronic inflammatory diseases (as discussed in chapter 4). They liberate important precursors of inflammatory mediators, secondary messengers and membrane remodellers [68], from the hydrolysis of phospholipids to free fatty acids and lysophospholipids.

Elevated levels of PLA_2 have been extracted from various tissues suffering from inflammation, including the body fluids of patients suffering from acute pancreatitis and the synovial fluid from arthritic joints [69]. Patients suffering from severe necrotizing acute pancreatitis show increased levels of serum PLA_2-II and highly disturbed renal function [70]. The role of PLA_2 in arthritis has long been established. Considerable PLA_2 catalytic activity has been observed in the synovial fluids that acts to reduce friction between the articular cartilage and other tissues in joints, from patients suffering from rheumatoid arthritis [71]. Rheumatoid arthritis is considered a chronic, inflammatory auto-immune disorder that causes the immune system to attack the joints. It is a disabling and painful inflammatory condition, which can lead to substantial loss of mobility due to pain and joint destruction. Elevated levels of circulating PLA_2-II have been shown to correlate with disease activity in adults and juvenile rheumatoid arthritis [72].

1.3 Monitoring Molecular Interactions

The need to monitor molecular interactions, both quantitatively and qualitatively, between an analyte and a ligand is high priority in both understanding the mechanism of biological interactions and to facilitate the discovery of novel methods and materials for therapeutics and diagnostics. The commercial applications of monitoring molecular interactions extends from health care through to applications in vetinary, agricultural and industrial analysis, and pollution monitoring [73].

The monitoring of biological interactions uses a combination of a recognition step and a transducer step (Figure 1.19). The recognition step involves a biological element, such as an antibody or enzyme receptor, on the surface that can recognize biological or chemical analytes in solution or in the atmosphere. The biological element can either catalyze a chemical reaction, such as an enzyme, or specifically bind the analyte, such as an antibody. It is possible to use various biological components as receptors, therefore providing many different applications. The major types of biological molecules and systems used as receptors include antibodies, enzymes and whole cells [74]. The receptor is connected to or integrated into a transducing element that converts the analyte-receptor reaction into a quantitative electrical or optical signal. Various transducers can be used to construct the receptor-analyte monitor, including optical (fluorescence, absorbance), electrochemical (potentiometric, conductimetric), calorimetric, acoustic, and mechanical [74]. Therefore, with an increasing number of receptor and transducer options, there is increased flexibility in the type of monitor and their applications. The high level of specific biological recognitions between binding partners and a high degree of sensitivity are critical parameters sought-after in the development of these devices. The specificity of the devices is emphasized, and allows it to be used in complex media such as blood, serum, fermentation broths and food, with minimum sample preparation [75].

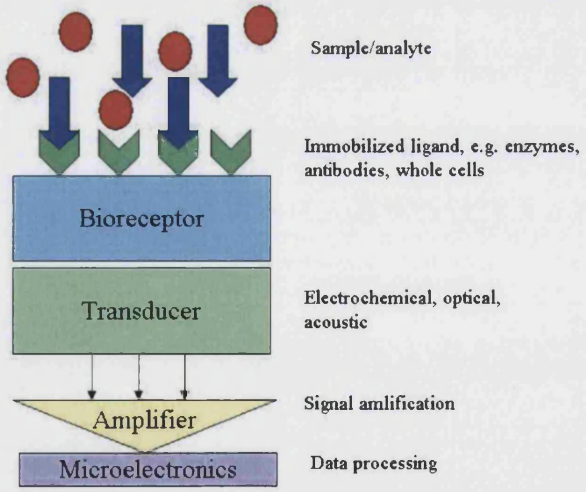

Figure 1.19 Principle of operation of a typical biological spectrometer.

1.3.1 Monitoring Molecular Interactions Using Optical Techniques

Optical spectrometry devices involve determining changes in light absorption or reflection between the reactants and products, or measuring the light output by a luminescent process. This analytical method is becoming increasingly widespread and described in over

4,000 publications (data obtained from SciFinder Scholar 02/05/2007). The use of optics in spectroscopic techniques including, absorption and reflection spectroscopy, chemi- and bio-luminescence, fluorescence spectroscopy and evanescent wave techniques.

The sensitivity of these techniques, relates to the smallest concentration of analyte that can be detected or the degree of discrimination between the desired analyte and potential contaminants [76]. Optics provide a means of constructing a device with high sensitivity, while the specificity is determined by the biochemistry of the receptor/ligand interactions. Therefore, an optical spectroscopic device provides a means of sensitive quantitative analysis of molecular interactions.

1.3.2 Using Evanescent Waves as a Means of Monitoring Molecular Interactions

The use of the evanescent wave in optics allows for monitoring of molecular interactions and events at the surface. An evanescent wave is formed when sine waves are internally reflected off an interface (internal reflection element) at an angle greater than the critical angle, causing total internal reflection (see section 2.1 Surface Plasmon Resonance Spectroscopy). Therefore, receptor-ligand events can be monitored as changes in the light intensity caused by complex formation. The evanescent wave technique can be used to directly monitor the interactions between receptors and their analytes at the surface in real-time. This system is employed in attenuated total reflection (ATR) and surface plasmon resonance spectroscopy. The evanescent wave can also be used to indirectly monitor interactions at the surface by employing the wave to excite fluorescently labelled molecules.

The use of the evanescent wave technique in spectrometry design has become widespread, and has been adapted for various monitoring and sensing needs. This technique has been employed to detect small variations in the sequence of nucleic acids [77], where a capture probe is immobilized on the surface, and the hybridization with a fluorescently-labelled complementary strand can be monitored by fluorescence detection. The commercial significance of this development allows for the detection of point mutations for the diagnosis of genetic diseases and for the detection of specific genomic sequences of an infectious disease. In line with the health-care benefits, the application of the evanescent wave has been used for pesticide detection, where high toxicity of pesticides and their widespread use in agriculture represents a general danger for environmental welfare.

Screening for pesticide residues in drinking water is stringent, and the optical evanescent wave technique allows for the sensitive and specific monitoring of pesticide concentration [78]. The detection of pathogenic bacterial using conventional biochemical diagnostics and molecular screen can be laborious and potentially dangerous to the patient if treatment is not provided quickly. Therefore, the development of a real-time monitor would improve the speed with which the patient can be treated. Moreover, the detection of bacterial toxins could also be beneficial for screening of food-borne toxins such as *Clostridium botulinum* toxin. Fluorescently labelled antibodies specific for *C. botulinum* have been covalently attached to the surface and the botulinum toxin detected in real-time and at concentrations as low as 5ng/ml. The reaction showed high specificity and no response was observed against tetanus toxin [79].

Covering an internal reflection element with a thin metal layer causes the evanescent field wave to excite the quasi-free electron gas in the metal film. Exciting the plasmons in the metal film by a laser causes amplification of the surface wave by ~50 fold compared to ATR. This amplification of the surface wave is dependant on the metal and thickness of the film. The sensitivity of reflectance change decreases when a thick chromium film or a thin gold film is employed, and the linear range becomes narrower as the thickness of the metal films increases. The sensitivity and linear range of the resonance angle shift are not affected by the thickness variation of the metal films [80]. The enhancement field effect increases the sensitivity of the IRE since the angular position of the resonance minimum becomes more sensitive to changes in the refractive index of the metal/dielectric interface. Given that the resonance energy only propagates a few hundred nanometres from the metal surface into the dielectric, it is susceptible to the thickness of the films absorbed on the surface. Therefore, depositing a metal film at an optimal thickness (~50nm) ensures good amplification of the surface wave, good sensitivity to reflectance change, and maximising the penetration depth of the resonance energy into the dielectric. The use of this enhanced evanescent wave technique for quantitative and qualitative observations at the surface has been employed in Surface Plasmon Resonance Spectroscopy (SPS), and its theoretical background is described in chapter 2.

The first optical spectrometer based on Surface Plasmon Resonance (SPR) was described in 1982 [81], to monitor the change in refractive index caused by the adsorption of human γ-globulin IgG on a silver surface and its resultant interactions with the γ-globulin IgG

antiserum in a concentration dependant manner. This led to increased interest in the use of SPR as the basis of biosensors and monitors for analyzing processes occurring at or near the surface. SPS can be used to determine physical parameters including organic vapour concentration gradients to monitor air density and ammonia concentration [82]. The kinetics of adsorption and structure of bio-adhesive films has been monitored using this technique [83], and could be beneficial for determining the efficiency and reliability of bio-adhesives for use in wound healing and tissue repair. An interest in the construction and monitoring of organized organic mono- and bilayers on metal surfaces by self-assembly using SPS have grown considerably. These layers show marked stability to chemical conditions and give uniform, controllable and known thickness dielectric films. Tailoring the surfaces of these devices by processes of self-assembly to form organized systems allows the economical development of sophisticated detection systems and ensuring a native and non-denaturing environment for receptors, proteins and ligands at the surface.

An inherent problem with SPR-based devices is their cost, large dimensions and complexity [84]. Miniaturization using nanotechnology and microelectronics is an attractive objective to produce a portable and cost-effective device. Commercially available portable SPR devices have been developed to detect *Escherichia coli* O157:H7 for use in the food industry [85], *Staphylococcus aureus* enterotoxin [86] and environmental pollutants [87].

1.3.3 Using Evanescent Wave Enhanced Fluorescence as a Means to Monitor Molecular Interactions

One of the key advantages of SPS is it allows for label-free detection of binding events, whereby the presence of bound analyte at the interface generates a change in the optical properties of the surface. However, a major disadvantage of using SPR for bio-analytical applications is that low concentrations of the analyte cannot be detected, with a detectability of approximately 1-10nmol.dm^{-3} for a 20kDa molecule [88, 89]. Sensitivity and detection problems also arise if the analyte has a very low molecular mass. Therefore, the development of strategies for improving the detection limit and sensitivity of SPR must be considered.

The first device to use the evanescent wave to excite a fluorophore was employed in 1975 to determine the concentrations of phenyl arsenic acid and morphine [90]. Totally

internally reflected light was used to excite fluorescein labelled antibodies which had become bound to a hapten-protein conjugate adsorbed on a quartz-plate in an antibody solution. The evanescent field excited fluorescent molecules close to the surface, and this excitation can be enhanced if the fluorescent molecule is placed near to a metal film. The metal causes an enhancement of several orders of magnitude because the local field at the molecule is increased by the dipole field of the resonant plasmon [91]. Metal-enhanced fluorescence is caused by the metal concentrating the local electromagnetic field and subsequently increasing the rate of excitation [92]. Moreover, the nearby metal can increase the intrinsic radiative decay rate of the fluorophore, thereby, modifying the rate at which the fluorophore emits photons [93]. The prospect of combining the best features of the direct SPR device and indirect fluorescence techniques, led to the development of an indirect SPR fluoroimmunoassay (SPRF) technique [94], and its enhanced sensitivity was demonstrated by assaying for human Chorionic Gonadotrophin (hCG) in serum.

The excitation of fluorophores in the evanescent field of the plasmons is distance dependant, and an optimal distance to the metal exists at which maximal fluorescence excitation is observed. The direct interaction between the metal film and an adsorbed dye molecule can result in an enhancement of fluorescence intensity depending upon the metal film thickness, which was determined to be in the range of between 45-70Å depending on the fluorescent species (Figure 1.20). On metal films above 200Å quenching of the fluorophore occurs via energy transfer to the metal surface, and the excitation energy is dissipated in the metal.

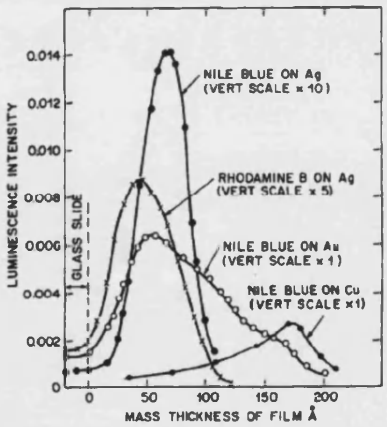

Figure 1.20 Luminescence intensity of various dye molecules on varying thicknesses of silver metal films [91].

The desired situation for fluorescence enhancement is achieved when the chromophores are located close enough to the metal to be excited by the evanescent wave, but are decoupled to ensure no loss of fluorescence intensity by quenching processes is observed.

To ensure bound fluorescent analytes are within the exponentially decaying evanescent fields, it was proposed to develop specific interfacial supamolecular structures to maintain optimal fluorescence enhancement working distances [95]. Self-assembled support layers on the metal surfaces have been used [96] to functionalize the surface.

SPFS has recently been employed to detect various cardiac markers, such as myoglobin, for the early detection of acute myocardial infraction [97]. This immunoassay enabled enhanced fluorescence detection of myoglobin over a range of concentrations from subnormal to elevated levels of the cardiac marker.

The combination of the surface-sensitive technique, SPR and fluorescence detection enables a highly sensitive analytical tool to probe molecular interaction close to the surface.

1.4 Constructing an Artificial Cell Membrane and its Uses

Various strategies have been employed to immobilize biological molecules onto a surface. The direct physisorption encounters inherent problems with lack of orientational control of the adhering molecules, and a decrease in biological activity. Non-specific binding of a protein can become a major problem leading to large background signals. Therefore, more sophisticated strategies using support layers and scaffolds have been used in an attempt to have better control over the immobilization procedures. Poly-L-lysine provides a simple and convenient method for adhering negatively charged macromolecules and biological entities. Poly-L-lysine (PLL) coated surfaces provide a positively charged surface [98], and has been extensively employed in the attachment of mammalian cells to surfaces. It has recently been used for the development of bacterial-based micro-scale medical diagnostic tool [99], whereby, *Escherichia coli* and *Pseudomonas sp.* have been selectively attached to the solid surface using PLL. A direct covalent attachment between proteins and a surface using poly(ethylene glycol) linkers has been reported. It is well-known for its ability to prevent non-specific interactions and also act as hydrophilic spacers minimizing any detrimental interaction between the attached protein and the solid surface [100].

Control over the orientation of the attachment requires two unique and mutually reactive groups on the protein and the support surface. Surface hydrolysis of polyester scaffolds was developed as a convenient technique to promote protein adsorption for improving cell attachment. Hydrolyzed or spontaneously hydrolyzable surfaces display a pronounced fibrous structure, ensuring greater protein absorption compared to the smooth non-hydrolyzed polyester surfaces [101]. Recently, open-pore mesoporous TiO_2-Nafion® film have been shown to provide a surface which allows fast diffusional access into the porous structure and could be employed as a host to study proteins and enzymes [102].

1.4.1 Self-Assembled Monolayers

The use of functionalized Self-Assembled Monolayers (SAM) provides an attractive alternative for the deposition of biological molecules onto surfaces. An organic thin film can be deposited on a solid substrate by various techniques such as thermal evaporation, sputtering, electro-deposition, molecular beam epitaxy, adsorption from solution, Langmuir-Blodgett (LB) technique, and self-assembly. The two most widely used methods for molecular layer deposition on solid surfaces are Langmuir-Blodgett and self-assembly, which both provide a means of producing an ultrathin organic film onto a surface as a support layer.

Certain characteristics are desirable for the adsorption of biological entities to surfaces, and include; a high surface-density of active molecules, the absence of non-specific binding, and stability and durability of the support layer [103]. Langmuir-Blodgett films (LB films) are constructions of high-density monolayers and multilayer transferred from the water-air interface onto a solid surface. LB films produce ultrathin layers of uniform thickness with specific internal structure, and allow for the arrangement of molecules in a fixed configuration which would not spontaneously come about. The process of LB film formation occurs in two distinct steps (Figure 1.21). The initial stage of film formation is the creation of a single layer of molecules, or monolayer, on a water surface. Reduction of the area of the water surface ensures the molecules are forced together to form a densely packed homogenous layer and eliminate any voids. The uniform monolayer is then deposited onto the substrate, which can be repeated any number of times to build up a film of accurately defined thickness, or constructing superlattice structures by depositing monolayers of different materials [104]. A constant surface pressure is maintained on the

film as the glass is raised through the surface, and the surface pressure causes surfactants to transfer from the water and onto the glass [105].

LB films do show drawbacks in their production, including limited high temperature range and a slow rate of deposition which is easily perturbed by small levels of contaminating materials. In spite of their limitations, these films have been extensively used in nano-electronics for the construction of miniaturized components, the construction of artificial cell membranes and in semiconductor devices such as sensors because of their insulating properties [106].

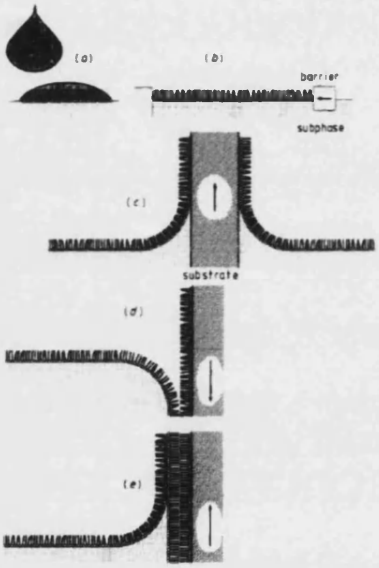

Figure 1.21 Steps in the Langmuir-Blodgett technique: (a) spreading (b) compression (c) transfer of primary monolayer (d) subsequent down stroke (e) subsequent upstroke [104].

SAMs form by the spontaneous and reversible absorption of amphiphilic molecules in an organic solvent onto a substrate [103, 107] forming a 2D arrangement on the surface. The initial driving force for the self-assembly of surfactants is the chemical affinity between the absorbents and the surface. A molecule capable of forming a SAM comprises a head group that ensures the chemisorption of the surfactant onto the substrate surface. The pinning of the head group to a specific site on the surface occurs through a chemical bond resulting in a very strong molecular-substrate interaction. This bond formation can be covalent in nature, such as the Au-S bond in the case between alkanethiols on gold, or ionic in nature, such as between $-CO_2^-Ag^+$ bond between carboxylic acids on AgO/Ag. This chemisorption results in an exothermic interaction, whereby the molecules try to occupy every available binding site on the surface by compacting the existing bound absorbents. This suggests that the amphiphiles retain a level of mobility prior to the final pinning to the surface. The alkyl

chain comprises the second molecular part of the surfactant. The formation of ordered and closely assembled layers occurs, resulting in the formation of van der Waals interactions between the alkyl chains. The tail-to-tail interactions creates lateral interchain interactions causing the alignment of the molecules parallel on the surface and creating a crystalline film. The final molecular part of the surfactant is the terminal functionality (Figure 1.22), and can vary in complexity, such as simple methyl groups, simple hydroxyl groups and complex biotin moieties. The tail group exerts the most direct influence on the interfacial properties of the films, therefore, provides an attractive route for tailoring the structure of the interface by introducing additional steric and electrostatic interactions.

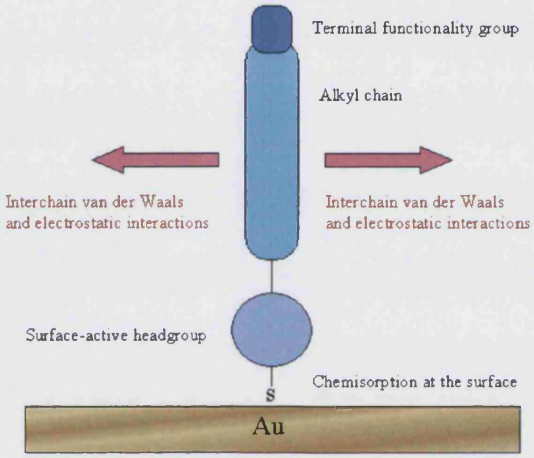

Figure 1.22 Schematic of the constituent parts of a surfactant that forms a self-assembled monolayer, and the forces involved in forming a stable and organised structure.

Commonly paired substrate-absorbents used to generate SAMs include: (*i*) carboxylic acids on aluminium oxide or silver, (*ii*) alcohols, amines, and isonitriles on platinum, (*iii*) alkylsilane derivatives on hydroxylated surfaces, (*iv*) dialkyl sulfides and dialkyl disulfides on gold, and (*v*) alkanethiols on metals such as gold, silver and copper, and non-metals such as gallium arsenide and indium-tin oxide [108]. This provides an attractive system because of the ability to form a flexible structure, with the capacity to incorporate various groups whether in the alkyl chains or in the terminal group, ensuring a variety of surfaces capable of specific interactions. An attractive feature of SAMs are their ease of preparation either from solution or the gas phase, they are precisely orientated, densely pack structures, and show an ability to tune the thickness and surface properties of the films using standard organic synthetic techniques [108].

The most studied system using SAMs is that of an alkanethiolate monolayer on an Au (111) surface, because the gold is particularly chemically inert and permits the formation of reproducibly well defined SAMs. Gold also forms no stable oxides under ambient conditions and can form highly specific interactions with sulphur atoms. Gold is also the standard because it is easy to prepare thin films by physical vapour disposition, sputtering, or electro-deposition. It is also compatible with cells and biological macromolecules without causing any evidence of toxicity. Voltammic studies have shown that thiol groups are de-protonated upon adsorption to the gold surface [109], as depicted in equation 1.1, however, this system is dynamic, therefore, the chemisorption is reversible and must reach an equilibrium to maximise the packing density of the thiols.

$$RSH + Au_{(s)} \rightleftharpoons RS\text{-}Au_{(s)} + e^- + H^+$$

(1.1)

A well packed monolayer of alkanethiols on gold has been reported to allow approximately $8.3x10^{-10}$mol.cm^{-2} total organic material to absorb [110]. The formation of a SAM at temperatures above 25°C improves the kinetics of formation and reduces the number of defects observed in the SAM. The incubation period between the surfactant solution and the surface is typically allowed to proceed until equilibrium is reached. It has been shown that the kinetics of the monolayer formation occur in a relatively short time scale, but the subsequent ordering process is much slower. The initial rapid adsorption is completed within 1 min at thiol concentrations below 1 mmol.dm^{-3} to ensure a 80-90% maximum coverage [111], and is described by diffusion controlled Langmuir adsorption. The effect of temperature has been shown to be particularly relevant during the initial rapid absorption phase to ensure minimum defect formation in the monolayer [112]. The chemisorption of the thiol to the gold surface requires the activation of the S-H bond of the thiol via a dissociative mechanism [113]. The S-Au bond formed is very strong (~40 kcal.mol^{-1}) and has been proposed to occur via oxidative addition [114], followed by a reductive elimination of the hydrogen by the mechanism:

$$R - S - H + Au_n^0 \Rightarrow R - S^- Au^+ \bullet Au_n^0 + \tfrac{1}{2} H_2$$

(1.2)

The sulphur atoms of the bound thiols form a symmetrical hexagonal coverage (Figure 1.23a), whereby the sulphur atoms have a S···S spacing of 4.97Å, and a calculated area of 21.4 Å per molecule [107]. This ensures a central bonding habit between the thiol and the gold to form a $(\sqrt{3}x\sqrt{3})R30°$ overlayer , where R = rotation (Figure 1.23b). The tilt of the

alkyl chains acts to minimize their spacing between neighboring chains, ensuring optimum surface coverage.

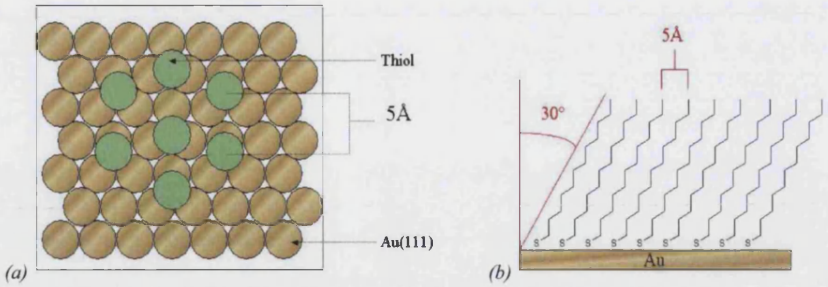

Figure 1.23 (a) Structure of a SAM of thiols on Au(111), arranged in a hexagonal close-packed arrangement with the thiol hexagonal ($\sqrt{3}x\sqrt{3}$)R30° overlayer structure, and (b) side view, where the absorbents are packed 5Å apart with their alkyl chains tilted 30° from the surface normal in a trans-extended conformation.

The subsequent step in SAM formation is the surface crystallization process, where the alkyl chains move from a disordered state to form a two-dimensional crystal. The slower process of additional adsorption and consolidation involves the displacement of contaminants, expulsion of included solvent from the monolayer which alters the interactions between the hydrophobic surface and the surfactant by changing the wetting properties of the surface [115], and lateral diffusion on the surface to reduce defects and enhance packing. The final ordered film is reached within 16 hours [116]. The kinetics of the second step are governed by chain-chain interactions (van der Waals and dipole-dipole) and the surface mobility of the chains. The kinetics of the second step in SAM formation is faster for longer alkyl chains (chain length n>10) because of the increased van der Waals interactions [116]. Moreover, the kinetics of absorption are strongly dependant the introduction of large functional groups within the alkyl chains. Molecules that have their longer alkyl-chain portions above the functional group (i.e., closer to the monolayer-air interface) form monolayers faster than those that have them below [117]. It can therefore be suggested that the length of the upper alkyl chain provides a strong driving force for monolayer formation by maximizing the van der Waals interactions. The defects and variability within a SAM can arise from the presence of contaminants, either absorbed from solution or pre-absorbed onto the substrate, and can influence the absorption kinetics since the thiols must ultimately displace the contaminants to chemisorb [118].

1.4.2 Supported Lipid Bilayers & Hybrid Lipid Bilayers

Phospholipid bilayer vesicles can adsorb on SAMs and yield either supported bilayers (Figure 1.24a) or hybrid bilayers (Figure 1.24b). The determining organization of the adsorbed vesicles depends on the functional groups presented at the exposed surface. SAMs terminated with hydrophilic groups, such as alcohols, promote the formation of bilayers supported by the underlying SAM, while hydrophobic SAMs formed from n-alkanethiols promote the formation of hybrid bilayers [119].

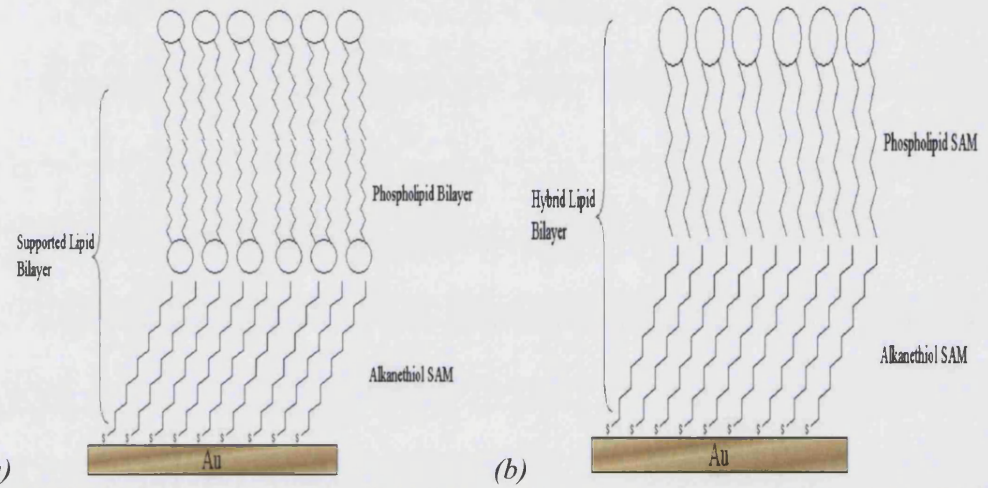

Figure 1.24 (a) Schematic of phospholipid vesicles adsorbed onto a hydrophilic SAM to produce a supported bilayer, and (b) a hybrid bilayer formed due to the hydrophobicity of the SAM layer.

Supported bilayers have been characterized by Atomic Force Microscopy and electrochemistry [120], and have been shown to be complex and contain a number of defects. The formation of supported bilayers is a slow process independent of vesicle concentration, due to the need for vesicle rupture and fusion, however, this process can be accelerated by using fusogenic agents such as polyethylene glycol [121, 122]. The fundamental process of supported bilayer formation is vesicular fusion and their subsequent rupture to from a supported bilayer. Bilayer vesicles introduced to a surface begin to inter-vesicle mix to form larger vesicles. At a critical size, the adsorbed vesicles rupture to form bilayer disks, causing the loss of the vesicle interior content. The adsorbed disks merge to form a continuous bilayer on the SAM support. The early steps of supported bilayer formation were determined using two-colour fluorescence labelled vesicles, and visualized using fluorescence microscopy [123].

The process of hybrid bilayer formation is governed by the effects of interfacial free energy on molecular reorganization at a surface. Phospholipids have a small partition coefficient, therefore in solution, they exist primarily as vesicles. The exposure of lipid vesicles to a hydrophobic SAM causes the spontaneous addition of a single molecular layer to the surface [124]. The driving force for bilayer formation is the free energy of the hydrophobic surface in contact with water. Lowering the free energy of the hydrophobic surface by bilayer formation may be accompanied by a free energy penalty associated with vesicle disruption. The activation energy barrier associated with the delamination of the lipid vesicles, which are thermodynamically stable structures, must be substantial. Hybrid bilayers have shown the ability to be good dielectric barriers with few pinhole defects. The fluidity of hybrid lipid bilayers is less than those seen in supported lipid bilayers, but hybrid bilayers do show improved stability [125]. The decreased fluidity on the bilayer is the result of one of the bilayer leaflets being chemisorbed to the surface, therefore, the fluidity of that particular leaflet is altered, which in turn effects the hybrid leaflet [126]. Hybrid bilayers have significantly more mechanical stability than supported lipid bilayers, because there is hydrophobic coupling between the two leaflets, thereby excluding solvent from the bilayer [127]. The formation of a hybrid bilayer is dependant on the ionic strength of the buffer, and increasing the concentration of Na^+ and Cl^- ions promotes faster absorption and fusion of the phospholipid vesicles to the SAM. The advantages of creating a hybrid lipid bilayer over a supported lipid bilayer is the relatively small amounts of lipid vesicles needed for bilayer formation. The proposed mechanism by which a hybrid bilayer forms from stable vesicles is by a delamination process.

The construction of a mechanically stable bilayer tethered to a surface permits the use of techniques that were not generally applied to biological membranes before. The use of a metal support, such as gold, also allows for the application of electrochemical techniques to examine the insulating capacity of lipid bilayers, and for assessing ion channel activity [128]. The application of surface sensitive techniques, such as Surface Plasmon Resonance, allows for the monitoring of the formation of these biomimetic bilayers and events that occur at the surface of the biomimetic membrane.

1.4.3 Supramolecular Complexes using Biotin-Streptavidin

Bio-specific recognition between biotin and streptavidin is well established, and has become a model system for protein-ligand binding studies. Biotin (vitamin K) is a water soluble B-complex vitamin and is used in cell growth, the production of fatty acids, metabolism of fats and amino acids. Streptavidin is a 60KDalton tetrameric protein secreted from *Streptomyces avidinii*, and has the approximate dimensions 54 x 58 x 48Å [129]. It has been suggested that the production of streptavidin is a defence mechanism of *S.avidinii* to sequester biotinylated enzymes away from competitor bacterial species that require these biotinylated enzymes for growth [130]. Each streptavidin can bind up to four biotin molecules with very high affinity (K_A = $10^{15}mol^{-1}$) [131]. This high affinity interaction has been extensively exploited to improve the sensitivity of immunoassays, immunocytochemical techniques and DNA probe diagnostics.

The multi-valency shown between streptavidin and biotin enables the linkage between two or more biotinylated molecules in a 'bridge' or 'sandwich' mode. The carboxy-terminus of biotin, which is not involved in the binding process to avidin/streptavidin, can be linked to structural elements [132]. Linkage to lipids and thiols allows for the preparation of molecular layer architectures at the water/air interface. This multi-valency can be exploited if streptavidin is bound to a biotinylated thiol or lipid at the air-water interface, causing the molecules to form a two-dimensional crystalline domain [133]. The crystalline functionalized monolayer provides an ordered, planar surface for the ligand binding, thereby producing a functional binding matrix for the construction of self-assembled multilayer films [134].

The mole fraction of the biotinylated-thiol/lipid in the functionalized surface has been shown to influence the streptavidin surface density. High mole fractions of biotin present in the functionalized surface causes steric hindrance and a reduction in streptavidin binding efficiency [135]. SPR has shown that low biotin surface coverage provides optimal accessibility for streptavidin to bind quickly via diffusion controlled adsorption.

1.4.4 Artificial Lipid Bilayers

It was not until 1962 that the first experimental bilayer lipid membrane was pioneered [136] to study their electrical properties and controlled chemical investigations. It was shown that an *in vitro* bilayer lipid membrane (BLM) could be formed from solubilized membrane lipids in the absence of all other cell components and show the cellular function of electrical excitability. Bilayer mixtures of lipids, membrane proteins and glycoproteins have been used by many research groups as an alternative chemically simple model for biological membranes. The cellular lipidome comprises over 1000 different lipids [137], and each of their functionalities is determined by their local concentration, which varies between organelles, between the two leaflets and within the lateral plane of the membrane. Therefore, the non-random mixing of components and compositional heterogeneity reflects the complexity of directly observing and characterizing bio-specific interactions.

The experimental and theoretical difficulties faced when observing the cell membrane makes model BLMs comprised of only simple mixtures of three or four components attractive because it gives the opportunities to monitor these components rigorously. Despite the vast array of lipid species found in cellular membranes, there is an asymmetric distribution of lipid species and predominant lipid components observed [17, 138, 139]. Therefore, by ensuring major membrane components are included in the BLM model a relationship to *in vivo* cell membranes can be ensured.

Artificial bilayer membranes can take numerous forms. Planar BLMs can be formed on various substrates including metal and hydrogels. They show great diversity and versatility and have been used in a number of applications ranging from basic membrane biophysics including transport and microchip studies, the conversion of solar energy via water photolysis, biosensor development using supported bilayer lipid membranes (s-BLMs), and photobiology comprising apoptosis and photodynamic therapy [140]. Spherical BLMs (liposomes) are vesicles which form spontaneously via self-assembly when amphipathic phospholipids are agitated in solution, and were first described in 1965 [141]. Liposomes consist of one or more phospholipid bilayers surrounding an aqueous cavity (Figure 1.25). The bilayer vesicles can range in size and lamellar number; single unilamellar vesicles (SUV) contain a single lipid bilayer with a diameter generally below 100nm, large unilamellar vesicles (LUV) contain a single lipid bilayer with a diameter between 100nm to several microns, oligolamellar vesicles (OLV) contain about five concentric lipid bilayers and a diameter usually below 1000nm, multilamellar vesicles (MLV) generally

contain between five and twenty concentric lipid bilayers and a diameter below 1000nm, and multivesicular vesicles (MVV) contain multi-compartment structures and a diameter in the micrometer range [142].

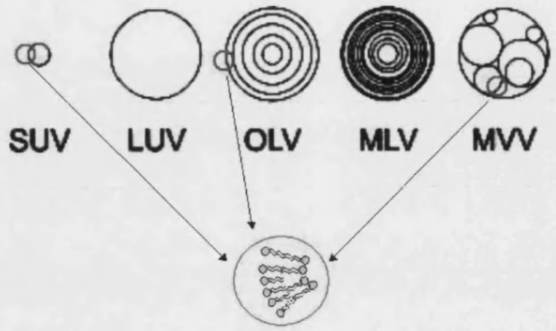

Figure 1.25 Schematic of the five types of liposomes: small unilamellar vesicles (SUV), large unilamellar vesicles (LUV), oligolamellar vesicles (OLV), multilamellar vesicles (MLV) and multivesicular vesicles (MMV) [142].

The composition of the BLMs determine the physical and chemical properties of the vesicles. Altering the composition can result in aggregation, disruption and fusion between the vesicles [15]. The preparation of biomimetic membrane vesicles is generally performed either via replacement of the organic solvent or detergent or via a mechanical method. The amphiphile mixture dissolved in an organic solvent is placed under reduced pressure to remove the solvent, resulting in a dry film. The film is rehydrated by addition of a buffer to yield a heterogeneously sized population of MLVs. The vesicle population can be homogenized by either probe sonication or forced through a polycarbonate membrane via the extrusion method until the required vesicular size is achieved.

The inclusion of a small mole fraction (~1% total lipid concentration) of a biotinylated phospholipid into the vesicles composition has been extensively used to immobilize bilayer membranes to surfaces using a streptavidin-biotin supramolecular architecture to generate high-yield artificial membrane immobilization with good stability [143]. It has been reported that avidin-biotin immobilized SUVs show excellent stability with a low leakage of entrapped reporter molecule after storage at 4°C for seven months, while covalently immobilized SUVs showed poor membrane integrity with 30-50% of the encapsulated reporter molecule diffusing out under the same storage conditions [144]. Non-specifically bound vesicles have been reported not to produce a significant problem during experimental analysis because they are likely to leak their contents by rupturing on the surface and be carried away by diffusion [145].

The rationale design of the supamolecular architecture and the simultaneous monitoring of the surface optical properties and fluorescent signal was subsequently used in this work to optimise the maximal binding capacity of the tethered artificial cell membranes. Prevention of the steric effects of the tethered membranes by engineering the ratio of the anchor molecules in the support layer was performed and SPFS was further employed to develop a surface for interfacial agents of the cell membrane to interact. The determination of binding constants for the receptor-analyte interactions and efficiency of inhibitors of interfacially active agent were performed.

1.5 Bibliography

1. Hooke, R., *Observations XVIII. Of the schematisme or texture of cork, and of the cells and pores of some other such frothy bodies.* Micrographia, 1667: p. 112-121.
2. Watson, J.D., *Molecular Biology of the Gene.* Addison-Wesley, 2004. **5th Edition.**
3. Madigan, M.T., J.M. Martinko, and J. Parker, *Brock Biology of Microorganisms.* Prentice Hall International, Inc, 2000. **9th Edition.**
4. van Holde, K.E., C. Johnson, and P. Shing Ho, *Principles of Biochemistry.* Prentice Hall International, Inc, 2006. **2nd Edition.**
5. Segre, D., et al., *The Lipid World.* Origins of Life and Evolution of the Biosphere, 2001. **31**: p. 119-145.
6. Ourisson, G. and Y. Nakatani, *The terpenoid theory of the origin of cellular life: The evolution of terpenoids to cholesterol.* Chemistry and Biology, 1994. **1**(1): p. 11-23.
7. Maddox, J., *Origin of the first cell membrane?* Nature, 1994. **371**(6493): p. 101.
8. Smith, H.W., *The Plasma Membrane, with Notes on the History of Botany.* Circulation, 1962. **26**(5): p. 987-1012.
9. Gorter, E. and F. Grendel, *ON BIMOLECULAR LAYERS OF LIPOIDS ON THE CHROMOCYTES OF THE BLOOD.* J. Exp. Med., 1925. **41**(4): p. 439-443.
10. Gruhn, T. and R. Lipowsky, *Temperature dependence of vesicle adhesion.* Physical Review E, 2005. **71**(1).
11. Kucerka, N., M.A. Kiselev, and P. Balgavy, *Determination of bilayer thickness and lipid surface area in unilamellar dimyristoylphosphatidylcholine vesicles from small-angle neutron scattering curves: a comparison of evaluation methods.* European Biophysics Journal with Biophysics Letters, 2004. **33**(4): p. 328-334.
12. Ashrafuzzaman, M., et al., *Manipulating lipid bilayer material properties using biologically active amphipathic molecules.* Journal of Physics Condensed Matter, 2006. **18**(28): p. S1235-S1255.
13. Linden, M.V., et al., *Stabilization of phosphatidylcholine coatings in capillary electrophoresis by increase in membrane rigidity.* Journal of Chromatography A, 2004. **1051**(1-2): p. 61-68.
14. Kotyk, A., K. Janacek, and J. Koryta, *Biophysical Chemistry of Membrane Functions.* Whiley-Interscience, 1988. **1**: p. 66-67.
15. Carmona-Ribeiro, A.M., *Synthetic amphiphile vesicles.* Chemical Society Reviews, 1992. **21**(3): p. 209-214.
16. Zachowski, A., *Phospholipids in animal eukaryotic membranes: Transverse asymmetry and movement.* Biochemical Journal, 1993. **294**(1): p. 1-14.
17. Pomorski, T., et al., *Lipid distribution and transport across cellular membranes.* Seminars in Cell and Developmental Biology, 2001. **12**(2): p. 139-148.
18. Fadok, V.A., et al., *A receptor for phosphatidylserine-specific clearance of apoptotic cells.* Nature, 2000. **405**(6782): p. 85-90.
19. Boon, J.M. and B.D. Smith, *Chemical control of phospholipid distribution across bilayer membranes.* Medicinal Research Reviews, 2002. **22**(3): p. 251-281.
20. Brown, D.A. and E. London, *Structure and function of sphingolipid- and cholesterol-rich membrane rafts.* Journal of Biological Chemistry, 2000. **275**(23): p. 17221-17224.
21. Finkelstein, A. and A. Cass, *Effect of cholesterol on the water permeability of thin lipid membranes.* Nature, 1967. **216**(5116): p. 717-718.
22. Haines, T.H., *Do sterols reduce proton and sodium leaks through lipid bilayers?* Progress in Lipid Research, 2001. **40**(4): p. 299-324.

23. Grit, M. and D.J.A. Crommelin, *Chemical stability of liposomes: Implications for their physical stability.* Chemistry and Physics of Lipids, 1993. **64**(1-3): p. 3-18.
24. Mitra, K., et al., *Modulation of the bilayer thickness of exocytic pathway membranes by membrane proteins rather than cholesterol.* Proceedings of the National Academy of Sciences of the United States of America, 2004. **101**(12): p. 4083-4088.
25. Emmelot, P. and R.P. Van Hoeven, *Phospholipid unsaturation and plasma membrane organization.* Chemistry and Physics of Lipids, 1975. **14**(3): p. 236-246.
26. Simons, K. and E. Ikonen, *How cells handle cholesterol.* Science, 2000. **290**(5497): p. 1721-1726.
27. Boggs, J.M. and K.M. Koshy, *Do the long fatty acid chains of sphingolipids interdigitate across the center of a bilayer of shorter chain symmetric phospholipids?* Biochimica et Biophysica Acta - Biomembranes, 1994. **1189**(2): p. 233-241.
28. Simons, K. and D. Toomre, *Lipid rafts and signal transduction.* Nature Reviews Molecular Cell Biology, 2000. **1**(1): p. 31-39.
29. Zhang, S., *Emerging biological materials through molecular self-assembly.* Biotechnology Advances, 2002. **20**(5-6): p. 321-339.
30. Whitesides, G.M. and B. Grzybowski, *Self-Assembly at All Scales.* Science, 2002. **295**(5564): p. 2418-2421.
31. Whitesides, G.M., J.P. Mathias, and C.T. Seto, *Molecular Self-Assembly and Nanochemistry: A Chemical Strategy for the Synthesis of Nanostructures.* Science, 1991. **254**(5036): p. 1312-1319.
32. Perez-Luna, V.H., et al., *Molecular recognition between genetically engineered streptavidin and surface-bound biotin.* Journal of the American Chemical Society, 1999. **121**(27): p. 6469-6478.
33. Sherrington, D.C. and K.A. Taskinen, *Self-assembly in synthetic macromolecular systems via multiple hydrogen bonding interactions.* Chemical Society Reviews, 2001. **30**(2): p. 83-93.
34. Lawrence, D.S., T. Jiang, and M. Levett, *Self-Assembling supramolecular complexes.* Chemical Reviews, 1995. **95**(6): p. 2229-2260.
35. Singer, S.J. and G.L. Nicolson, *The Fluid Mosaic Model of the Structure of Cell Membranes.* Science, 1972. **175**(4023): p. 720-731.
36. Vereb, G., et al., *Dynamic, yet structured: The cell membrane three decades after the Singer-Nicolson model.* PNAS, 2003. **100**(14): p. 8053-8058.
37. Rappuoli, R. and C. Montecucco, *Guidebook to Prtotein Toxins and Their Use in Cell Biology.* Sambrook & Tooze Pulication, 1997.
38. Fry, B.G., et al., *Early evolution of the venom system in lizards and snakes.* Nature, 2006. **439**(7076): p. 584-588.
39. Timbrell, J., *Principles of Biochemical Toxicology.* Taylor & Francis Ltd., 2000. **3rd Edition**.
40. Karalliedde, L., *Animal toxins.* British Journal of Anaesthesia, 1995. **74**: p. 319-327.
41. Vetter, R.S., MS, and P.K. Visscher, *Bites and stings of medically important venomous arthropods.* International Journal of Dermatology, 1998. **37**(7): p. 481-496.
42. Jansen, D.W., *A Possible Function of the Secretion of Duvernoy's Gland.* Copeia, 1983. **1983**(1): p. 262-264.
43. Harris, J.B., *Natural Toxins: Animal, Plant and Microbial.* Clarendon Press, 1986.

44. Fry, B.G. and W. Wuster, *Assembling an Arsenal: Origin and Evolution of the Snake Venom Proteome Inferred from Phylogenetic Analysis of Toxin Sequences.* Mol Biol Evol, 2004. **21**(5): p. 870-883.
45. Fry, B.G., *From genome to "venome": Molecular origin and evolution of the snake venom proteome inferred from phylogenetic analysis of toxin sequences and related body proteins.* Genome Res., 2005. **15**(3): p. 403-420.
46. Strydom, D.J., *Snake-Venom Toxins - Structure-Function Relationships and Phylogenetics.* Comparative Biochemistry and Physiology, 1973. **44**(1B): p. 269-281.
47. Billing, W.M., *THE ACTION OF THE TOXIN OF CROTALUS ADAMANTEUS ON BLOOD CLOTTING.* J Pharmacol Exp Ther, 1930. **38**(2): p. 173-196.
48. Crachi, M.T., L.W. Hammer, and W.C. Hodgson, *The effects of antivenom on the in vitro neurotoxicity of venoms from the taipans Oxyuranus scutellatus, Oxyuranus microlepidotus and Oxyuranus scutellatus canni.* Toxicon, 1999. **37**(12): p. 1771-1778.
49. Morrison, J., et al., *Studies on the Venom of Oxyuranus-Microlepidotus.* Journal of Toxicology-Clinical Toxicology, 1984. **21**(3): p. 373-385.
50. Brussow, H., C. Canchaya, and W.-D. Hardt, *Phages and the Evolution of Bacterial Pathogens: from Genomic Rearrangements to Lysogenic Conversion.* Microbiol. Mol. Biol. Rev., 2004. **68**(3): p. 560-602.
51. Stephen, J. and R.A. Pietrowski, *Aspects of Microbiology: Bacterial Toxins.* Nelson, 1981. **1st Ed.**
52. Hacker, J., et al., *Pathogenomics of mobile genetic elements of toxigenic bacteria.* International Journal of Medical Microbiology, 2004. **293**(7-8): p. 453-461.
53. Engelberg, N.C., V. DiRita, and T.S. Dermody, *Schaechter's Mechanisms of Microbial Disease.* Lippincott Williams & Wilkins, 2007. **4th Ed.**
54. Geny, B. and M.R. Popoff, *Bacterial protein toxins and lipids: pore formation or toxin entry into cells.* Biology of the Cell, 2006. **98**(11): p. 667-678.
55. Tucker, A.N. and D.C. White, *Heterogeneity of Phospholipid Composition in Bacterial Membrane.* Journal of Bacteriology, 1970. **102**(2): p. 508-&.
56. Sitia, R. and I. Braakman, *Quality control in the endoplasmic reticulum protein factory.* 2003. **426**(6968): p. 891-894.
57. Dobson, C.M., *Protein misfolding, evolution and disease.* Trends in Biochemical Sciences, 1999. **24**(9): p. 329-332.
58. Agorogiannis, E.I., et al., *Protein misfolding in neurodegenerative diseases.* Neuropathology and Applied Neurobiology, 2004. **30**(3): p. 215-224.
59. Gazit, E., *Arrest of Amyloid Fibril Formation Associated to Type II Diabetes: Structural and Functional Links to the Mechanism of Alzheimers beta- Amyloid Fibrillization.* Drug Design Reviews - Online, 2005. **2**: p. 115-119.
60. Johnson, K., et al., *Islet amyloid, islet-amyloid polypeptide, and diabetes mellitus.* N Engl J Med, 1989. **321**(8): p. 513-518.
61. Lansbury, P.T., Jr., *Evolution of amyloid: What normal protein folding may tell us about fibrillogenesis and disease.* PNAS, 1999. **96**(7): p. 3342-3344.
62. Koo, E.H., P.T. Lansbury, Jr., and J.W. Kelly, *Amyloid diseases: Abnormal protein aggregation in neurodegeneration.* PNAS, 1999. **96**(18): p. 9989-9990.
63. Taylor, J.P., J. Hardy, and K.H. Fischbeck, *Toxic Proteins in Neurodegenerative Disease.* Science, 2002. **296**(5575): p. 1991-1995.
64. Giffard, R.G., et al., *Chaperones, protein aggregation, and brain protection from hypoxic/ischemic injury.* J Exp Biol, 2004. **207**(18): p. 3213-3220.
65. Hershko, A. and A. Ciechanover, *THE UBIQUITIN SYSTEM.* Annual Review of Biochemistry, 1998. **67**(1): p. 425-479.

66. Bence, N.F., R.M. Sampat, and R.R. Kopito, *Impairment of the Ubiquitin-Proteasome System by Protein Aggregation.* Science, 2001. **292**(5521): p. 1552-1555.
67. Thacker, E.L., *Lung inflammatory responses.* Vetinary Research, 2006. **37**: p. 469-486.
68. Six, D.A. and E.A. Dennis, *The expanding superfamily of phospholipase A2 enzymes: classification and characterization.* Biochimica et Biophysica Acta (BBA) - Molecular and Cell Biology of Lipids, 2000. **1488**(1-2): p. 1-19.
69. Nevalainen, T.J., M.M. Haapamaki, and J.M. Gronroos, *Roles of secretory phospholipases A2 in inflammatory diseases and trauma.* Biochimica et Biophysica Acta (BBA) - Molecular and Cell Biology of Lipids, 2000. **1488**(1-2): p. 83-90.
70. Nevalainen, T., *Serum phospholipases A2 in inflammatory diseases.* Clin Chem, 1993. **39**(12): p. 2453-2459.
71. Thwin, M.M., et al., *Effect of phospholipase A(2) inhibitory peptide on inflammatory arthritis in a TNF transgenic mouse model: a time-course ultrastructural study.* Arthritis Research & Therapy, 2004. **6**(3): p. R282-R294.
72. Lin, M.K.S., et al., *Induction of secretory phospholipase A(2) confirms the systemic inflammatory nature of adjuvant arthritis.* Inflammation, 1998. **22**(2): p. 161-173.
73. Foulds, N.C. and C.R. Lowe, *What's new: Biosensors: Current applications and future potential.* BioEssays, 1985. **3**(3): p. 129-132.
74. Byfield, M.P. and R.A. Abuknesha, *Biochemical aspects of biosensors.* Biosensors and Bioelectronics, 1994. **9**(4-5): p. 373-399.
75. Alvarezicaza, M. and U. Bilitewski, *Mass-Production of Biosensors.* Analytical Chemistry, 1993. **65**(11): p. A525-A533.
76. Sadana, A., *Engineering Biosensors:Kinetics and Design Applications.* Academic Press, 2002.
77. Abel, A.P., et al., *Fiber-Optic Evanescent Wave Biosensor for the Detection of Oligonucleotides.* Anal. Chem., 1996. **68**(17): p. 2905-2912.
78. Ksenevich, T.I., et al., *Study of biochemical reactions in thin organic films by means of evanescent optical wave.* Applied Surface Science, 1996. **92**: p. 426-430.
79. Ogert, R.A., et al., *Detection of Clostridium botulinum toxin A using a fiber optic-based biosensor.* Analytical Biochemistry, 1992. **205**(2): p. 306-312.
80. Ekgasit, S., et al., *Influence of the Metal Film Thickness on the Sensitivity of Surface Plasmon Resonance Biosensors.* Applied Spectroscopy, 2005. **59**: p. 661-667.
81. Liedberg, B., C. Nylander, and I. Lundstrom, *Surface-Plasmon Resonance for Gas-Detection and Biosensing.* Sensors and Actuators, 1983. **4**(2): p. 299-304.
82. Kim, Y.-C., et al., *Fiber-optic surface plasmon resonance for vapor phase analyses.* The Analyst, 2005. **130**(6): p. 838-843.
83. Berglin, M., et al., *Use of Surface-Sensitive Methods for the Study of Adsorption and Cross-Linking of Marine Bioadhesives.* The Journal of Adhesion, 2005. **81**(7): p. 805 - 822.
84. Service, R.F., *TECHNOLOGY: Versatile Chemical Sensors Take Two Steps Forward.* Science, 1997. **278**(5339): p. 806-.
85. Meeusen, C.A., E.C. Alocilja, and W.N. Osburn, *Detection of E-coli O157 : H7 using a miniaturized surface plasmon resonance biosensor.* Transactions of the ASAE, 2005. **48**(6): p. 2409-2416.
86. Naimushin, A.N., et al., *Detection of Staphylococcus aureus enterotoxin B at femtomolar levels with a miniature integrated two-channel surface plasmon resonance (SPR) sensor.* Biosensors and Bioelectronics, 2002. **17**(6-7): p. 573-584.

87. Soelberg, S., et al., *A portable surface plasmon resonance sensor system for real-time monitoring of small to large analytes.* Journal of Industrial Microbiology and Biotechnology, 2005. **32**(11): p. 669-674.
88. Fontana, E., R. Pantell, H,, and S. Strober, *Surface plasmon immunoassay.* Applied Optics, 1990. **29**(31): p. 4694-4704.
89. Wink, T., et al., *Liposome-mediated enhancement of the sensitivity in immunoassays of proteins and peptides in surface plasmon resonance spectrometry.* Analytical Chemistry, 1998. **70**(5): p. 827-832.
90. Kronick, M.N. and W.A. Little, *A new immunoassay based on fluorescence excitation by internal reflection spectroscopy.* Journal of Immunological Methods, 1975. **8**(3): p. 235-240.
91. Glass, A., M,, et al., *Interaction of metal particles with absorbed dye molecules:absorption and luminescence.* Optics Letters, 1980. **5**(9): p. 368-370.
92. Sokolov, K., G. Chumanov, and T.M. Cotton, *Enhancement of molecular fluorescence near the surface of colloidal metal films.* Analytical Chemistry, 1998. **70**(18): p. 3898-3905.
93. Geddes, C.D. and J.R. Lakowicz, *Metal-Enhanced Fluorescence.* Journal of Fluorescence, 2002. **12**(2): p. 121-129.
94. Attridge, J.W., et al., *Sensitivity enhancement of optical immunosensors by the use of a surface plasmon resonance fluoroimmunoassay.* Biosensors and Bioelectronics, 1991. **6**(3): p. 201-214.
95. Liebermann, T. and W. Knoll, *Surface-plasmon field-enhanced fluorescence spectroscopy.* Colloids and Surfaces a-Physicochemical and Engineering Aspects, 2000. **171**(1-3): p. 115-130.
96. Liebermann, T., et al., *Complement hybridization from solution to surface-attached probe-oligonucleotides observed by surface-plasmon-field-eahanced fluorescence spectroscopy.* Colloids and Surfaces a-Physicochemical and Engineering Aspects, 2000. **169**(1-3): p. 337-350.
97. Matveeva, E., et al., *Myoglobin Immunoassay Utilizing Directional Surface Plasmon-Coupled Emission.* Anal. Chem., 2004. **76**(21): p. 6287-6292.
98. Jacobson, B., S, and D. Branton, *Plasma Membrane: Rapid Isolation and Exposure of the Cytoplasmic Surface by Use of Positively Charged Beads.* Science, 1977. **195**(4275): p. 302-304.
99. Cowan, S., E,, D. Liepmann, and J. Keasling, D, *Development of engineered biofilms on poly- L-lysine patterned surfaces.* Biotechnology Letters, 2001. **23**: p. 1235-1241.
100. Camarero, J.A., Y. Kwon, and M.A. Coleman, *Chemoselective Attachment of Biologically Active Proteins to Surfaces by Expressed Protein Ligation and Its Application for "Protein Chip" Fabrication.* Journal of the American Chemical Society, 2004. **126**(45): p. 14730-14731.
101. Atthoff, B. and J. Hilborn, *Protein adsorption onto polyester surfaces: Is there a need for surface activation?* Journal of Biomedical Materials Research Part B: Applied Biomaterials, 2007. **80B**(1): p. 121-130.
102. Milsom, E., et al., *Layer-by-layer deposition of open-pore mesoporous TiO2-NafionÂ® film electrodes.* Journal of Solid State Electrochemistry, 2007. **11**(8): p. 1109-1117.
103. Ulman, A., *An Introduction to Ultrathin Organic Films: From Langmuir-Blodgett to Self-Assembly.* Academic Press, 1991. **1st Edition**.
104. Peterson, I.R., *Langmuir-Blodgett films.* Journal of Physics D: Applied Physics, 1990. **23**(4): p. 379.

105. Blodgett, K.B., *Films Built by Depositing Successive Monomolecular Layers on a Solid Surface.* J. Am. Chem. Soc., 1935. **57**(6): p. 1007-1022.
106. Roberts, G.G., *An applied science perspective of Langmuir-Blodgett films.* Advances in Physics, 1985. **34**(4): p. 475 - 512.
107. Bigelow, W.C., D.L. Pickett, and W.A. Zisman, *Oleophobic monolayers : I. Films adsorbed from solution in non-polar liquids.* Journal of Colloid Science, 1946. **1**(6): p. 513-538.
108. Colorado, J., R. and T.R. Lee, *Thiol-based Self-assembled Monolayers: Formation and Organization.* Encyclopedia of Materials: Science and Technology, 2001: p. 9332-9344.
109. Widrig, C.A., C. Chung, and M.D. Porter, *The electrochemical desorption of n-alkanethiol monolayers from polycrystalline Au and Ag electrodes.* Journal of Electroanalytical Chemistry, 1991. **310**(1-2): p. 335-359.
110. Flink, S., F. van Veggel, and D.N. Reinhoudt, *Sensor functionalities in self-assembled monolayers.* Advanced Materials, 2000. **12**(18): p. 1315-1328.
111. Kawasaki, M., et al., *Rapid self-assembly of alkanethiol monolayers on sputter-grown Au(111).* Langmuir, 2000. **16**(4): p. 1719-1728.
112. Yamada, R., H. Wano, and K. Uosaki, *Effect of temperature on structure of the self-assembled monolayer of decanethiol on Au(111) surface.* Langmuir, 2000. **16**(13): p. 5523-5525.
113. Nuzzo, R.G., B.R. Zegarski, and L.H. Dubois, *Fundamental-Studies of the Chemisorption of Organosulfur Compounds on Au(111) - Implications for Molecular Self-Assembly on Gold Surfaces.* Journal of the American Chemical Society, 1987. **109**(3): p. 733-740.
114. Ulman, A., *Formation and structure of self-assembled monolayers.* Chemical Reviews, 1996. **96**(4): p. 1533-1554.
115. Kokkoli, E. and C.F. Zukoski, *Effect of Solvents on Interactions between Hydrophobic Self-Assembled Monolayers.* Journal of Colloid and Interface Science, 1999. **209**(1): p. 60-65.
116. Bain, C.D., et al., *Formation of Monolayer Films by the Spontaneous Assembly of Organic Thiols from Solution onto Gold.* Journal of the American Chemical Society, 1989. **111**(1): p. 321-335.
117. Evans, S.D., et al., *Self-assembled monolayers of alkanethiols containing a polar aromatic group: effects of the dipole position on molecular packing, orientation, and surface wetting properties.* J. Am. Chem. Soc., 1991. **113**(11): p. 4121-4131.
118. Schreiber, F., *Structure and growth of self-assembling monolayers.* Progress in Surface Science, 2000. **65**(5-8): p. 151-256.
119. Kalb, E., S. Frey, and L.K. Tamm, *Formation of Supported Planar Bilayers by Fusion of Vesicles to Supported Phospholipid Monolayers.* Biochimica Et Biophysica Acta, 1992. **1103**(2): p. 307-316.
120. Jenkins, A.T.A., et al., *Lipid vesicle fusion on mu CP patterned self-assembled monolayers: Effect of pattern geometry on bilayer formation.* Langmuir, 2002. **18**(8): p. 3176-3180.
121. Proux-Delrouyre, V., et al., *Formation of Tethered and Streptavidin-Supported Lipid Bilayers on a Microporous Electrode for the Reconstitution of Membranes of Large Surface Area.* Langmuir, 2002. **18**(8): p. 3263-3272.
122. Berquand, A., et al., *Two-Step Formation of Streptavidin-Supported Lipid Bilayers by PEG-Triggered Vesicle Fusion. Fluorescence and Atomic Force Microscopy Characterization.* Langmuir, 2003. **19**(5): p. 1700-1707.
123. Johnson, J.M., et al., *Early steps of supported bilayer formation probed by single vesicle fluorescence assays.* Biophysical Journal, 2002. **83**(6): p. 3371-3379.

124. Hubbard, J.B., V. Silin, and A.L. Plant, *Self assembly driven by hydrophobic interactions at alkanethiol monolayers: mechanism of formation of hybrid bilayer membranes.* Biophysical Chemistry, 1998. **75**(3): p. 163-176.
125. Twardowski, M. and R.G. Nuzzo, *Molecular Recognition at Model Organic Interfaces: Electrochemical Discrimination Using Self-Assembled Monolayers (SAMs) Modified via the Fusion of Phospholipid Vesicles.* Langmuir, 2003. **19**(23): p. 9781-9791.
126. Favero, G., et al., *Mixed hybrid bilayer lipid membrane incorporating valinomycin: improvements in preparation and functioning.* Microchemical Journal, 2003. **74**(2): p. 141-148.
127. Florin, E.-L. and H.E. Gaub, *Painted supported lipid membranes.* Biophysical Journal, 1993. **64**(2): p. 375-383.
128. Plant, A.L., *Self-Assembled Phospholipid Alkanethiol Biomimetic Bilayers on Gold.* Langmuir, 1993. **9**(11): p. 2764-2767.
129. Hendrickson, W.A., et al., *Crystal Structure of Core Streptavidin Determined from Multiwavelength Anomalous Diffraction of Synchrotron Radiation.* PNAS, 1989. **86**(7): p. 2190-2194.
130. Diamandis, E.P. and T.K. Christopoulos, *The Biotin (Strept)Avidin System - Principles and Applications in Biotechnology.* Clinical Chemistry, 1991. **37**(5): p. 625-636.
131. Chaiet, L. and F.J. Wolf, *The properties of streptavidin, a biotin-binding protein produced by Streptomycetes.* Archives of Biochemistry and Biophysics, 1964. **106**: p. 1-5.
132. Knoll, W., et al., *Streptavidin arrays as supramolecular architectures in surface-plasmon optical sensor formats.* Colloids and Surfaces a-Physicochemical and Engineering Aspects, 2000. **161**(1): p. 115-137.
133. Darst, S.A., et al., *Two-dimensional crystals of streptavidin on biotinylated lipid layers and their interactions with biotinylated macromolecules.* Biophysical Journal, 1991. **59**(2): p. 387-396.
134. Ahlers, M., et al., *Specific Interactions of Proteins with Functional Lipid Monolayers - Ways of Simulating Biomembrane Processes.* Angewandte Chemie-International Edition in English, 1990. **29**(11): p. 1269-1285.
135. Haussling, L., et al., *Biotin-Functionalized Self-Assembled Monolayers on Gold - Surface-Plasmon Optical Studies of Specific Recognition Reactions.* Langmuir, 1991. **7**(9): p. 1837-1840.
136. MUELLER, P., et al., *Reconstitution of Cell Membrane Structure in vitro and its Transformation into an Excitable System.* 1962. **194**(4832): p. 979-980.
137. van Meer, G., *Cellular lipidomics.* EMBO, 2005. **24**: p. 3159-3165.
138. Boon, J., M, and B. Smith, D., *Chemical Control of Phospholipid Distribution Across Bilayer Membranes.* Medicinal Research Reviews, 2002. **22**(3): p. 251-281.
139. Daleke, D.L., *Regulation of transbilayer plasma membrane phospholipid asymmetry.* Journal of Lipid Research, 2003. **44**(2): p. 233-242.
140. Tien, H.T. and A.L. Ottova, *The lipid bilayer concept and its experimental realization: from soap bubbles, kitchen sink, to bilayer lipid membranes.* Journal of Membrane Science, 2001. **189**(1): p. 83-117.
141. Bangham, A.D., M. Standish, M,, and J. Watkins, C., *Diffusion of univalent ions across the lamellae of swollen phospholipids.* Journal of Molecular Biology, 1965. **13**(1): p. 238-252.
142. Rongen, H.A.H., A. Bult, and W.P. van Bennekom, *Liposomes and immunoassays.* Journal of Immunological Methods, 1997. **204**(2): p. 105-133.

143. Yang, Q., et al., *Avidin-biotin immobilization of unilamellar liposomes in gel beads for chromatographic analysis of drug-membrane partitioning.* Journal of Chromatography B: Biomedical Applications, 1998. **707**(1-2): p. 131-141.
144. Liu, X.Y., et al., *Avidin-biotin-immobilized liposome column for chromatographic fluorescence on-line analysis of solute-membrane interactions.* Journal of Chromatography B, 2001. **750**(1): p. 51-60.
145. Boukobza, E., A. Sonnenfeld, and G. Haran, *Immobilization in surface-tethered lipid vesicles as a new tool for single biomolecule spectroscopy.* Journal of Physical Chemistry B, 2001. **105**(48): p. 12165-12170.

2.0 Theoretical Introduction

This chapter details the theoretical background associated with the experimental methodologies employed in this thesis. An introduction to the theory behind Surface Plasmon Resonance (SPR), and its applications in monitoring the changes in refractive index associated with adsorption and desorption events at the surface will be described. The employment of this technique will be detailed along with the background relating to the modification of the spectrometer to include for fluorescence detection using Surface Plasmon field enhanced Fluorescence Spectrometry (SPFS). The concept of molecular adsorption at the surface will also be described in relation to the Langmuir isotherm model and mass transfer effects.

2.1 Surface Plasmon Resonance Spectroscopy

Surface Plasmon Resonance (SPR) is a phenomenon which occurs in thin metal films at the interface between two media of different refractive indices. At a critical angle, incident light travelling through the medium of higher refractive index is totally internally reflected at the interface with the medium of lower refractive index. The electromagnetic field component of the incident light penetrates into the medium of lower refractive index and creates an exponentially decaying evanescent field wave. Surface Plasmon Resonance Spectroscopy (SPS) measures changes in reflectivity as a result of changes in the refractive index at the air/dielectric interface. This subsequently equates to monitoring changes as a result of the adsorption and/or desorption of analytes at the interface.

2.1.1 Refractive index

The refractive index (η) of a material is the factor by which the rate of the electromagnetic radiation phase velocity is slowed compared to its velocity in a vacuum. It is dependant on the wavelength of light, and to some extent, the temperature and pressure at which the refractive index is measured. The refractive index of a material is defined as:

$$\eta \equiv \frac{c}{v_{phase}} \tag{2.1}$$

Where c is the speed of light, and v_{phase} is phase velocity.

A material with a high refractive index means light passes through more slowly compared to a material with a lower refractive index. The refractive index can be used to determine the identity of an unknown material (Figure 2.1), and can also be used to determine purity or concentration, *i.e.* determining the glucose concentration in bodily fluid.

Material	**Refractive index *(n)*** **at λ = 589.3 nm**
Vacuum	1
Air (at standard temperature and pressure)	1.00029
Water (20°C)	1.33
Ethanol	1.36
Teflon	1.35 - 1.38
Cytoplasm	1.37 [1]
Planar Lipid Bilayer	1.45 [2]
Cell membrane	1.45 [1]
Lipid	1.48 [3]
Crown glass (Quartz)	1.50 - 1.54 [4]
Flint glass (High refractive index glass)	1.60 - 1.62
LaSFN9 glass	1.85

Figure 2.1 Refractive index for various materials

2.1.2 Surface Plasmons

A plasmon is a quasiparticle (a quantum of energy) assembled from an electron plasma and a photon to produce collective oscillations. The plasma is a dense gas of charged particles, which is formed from mobile delocalized valence electrons in the metal. Surface plasmons are electromagnetic transversal waves that propagate along the surface of a conductor or semi-conductor, and possesses both longitudinal and transverse wave components. Surface plasmons interact strongly with light, and are confined to the surface of the interface between the negative dielectric (conductor) and the positive dielectric (Figure 2.2). The incident electromagnetic radiation passing through the optically dense material reflects off the boundary between the optically dense medium and the metallic film. This causes the evanescent field to extend from this interface and propels the electrons, causing the production of a surface plasmon.

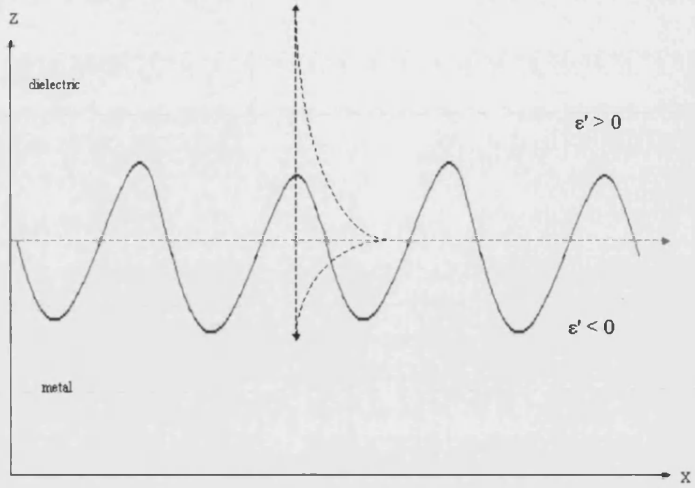

Figure 2.2 Schematic of the propagating plasmon wave along the surface of the dielectric/metal interface in the x direction, and the decaying evanescent wave (----)

An evanescent wave exhibits exponential decay away from the metal/dielectric interface, and is produced when sine waves are reflected off the dielectric/metal interface at an angle greater than the critical angle, therefore, causing total internal reflection.

Plasmons give rise to some of the physical and optical properties associated with metals. Light of a frequency below that of the plasma wave frequency is reflected because the electrons in the metal shield the electric field from the light. Conversely, light of a frequency above that of the plasma wave frequency is transmitted, because the electrons in the metal cannot shield the electric field rapidly enough. Surface plasmons have been employed in a range of applications including in electrochemistry [5], biosensing [6], and in surface plasmon resonance spectroscopy [7].

2.1.3 Excitation of Surface Plasmons

Incident transversal magnetic light, which has an electric field component perpendicular to the magnetic field, causes the excitation of surface plasmons. The frequency of the photon propagating in the dielectric material must be smaller than the frequency of the surface plasmon propagating along the metal/dielectic interface for the excitation of a surface plasmon to occur. The dispersion relation (relation between the energy of a system and its corresponding momentum) for an electromagnetic wave shows that the energy is proportional to the frequency of the wave and the momentum to the wavenumber (Figure 2.3). The dispersion relation for surface plasmons is not linear, and reaches a maximum frequency (ω_{max}), because it has a lower energy compared to the incident light. Therefore,

the surface plasmon wave vector propagating along the metal/dielectric interface is greater than the wave vector of the free photon in the dielectric [8]. This means that incident light in a vacuum can not directly excited surface plasmons, as there is no intersect between the incident light wavevector (*a)* and the surface plasmon wavevector (*P1+2)* (Figure 2.3).

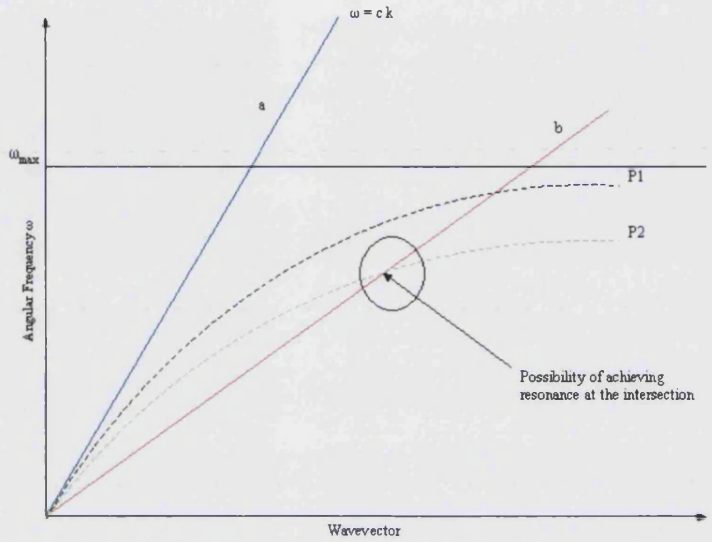

Figure 2.3 Dispersion relation of free photons in a dielectric(a), free photons propagating in a coupling prism (b). With the dispersion relation for surface plasmons at the metal/dielectric interface before(P1) and after adsorption of an additional dielectric layer (P2). Where ω= frequency, c= speed of light and k= wavevector.

To excite the surface plasmons at the metal/dielectric interface, the wavevector of the incident light must be adapted to match the wavevector of the plasmons. This can be achieved by increasing the wavevector by passing the incident light though a material with a higher refractive index compared to the dielectric, such as a prism. This causes attenuated total reflection (ATR), and is known as prism coupling. Altering the incident light wavevector can also be achieved using grating couplers, whereby the metal/dielectric interface is periodically distorted. The incident wave is diffracted causing a series of beams to be directed away from the interface at a variety of angles, and if the diffracted wavevector is equal to the surface plasmon wavevector then coupling occurs [9].

Prism coupling is achieved by reflecting the incident light on to the base plane of a high refractive index prism, either in the Otto or Kretschmann configurations (Figure 2.4). In the Otto configuration, the incident light passes through the high refractive index prism, and at a critical angle, total internal reflection is achieved, resulting in the creation of an evanescent field. This evanescent field propagates into the air dielectric, to a penetration

depth of around 200nm. However, this setup is not experimentally preferred, due to its challenging nature and contamination of the air space by dust particles, etcetera.

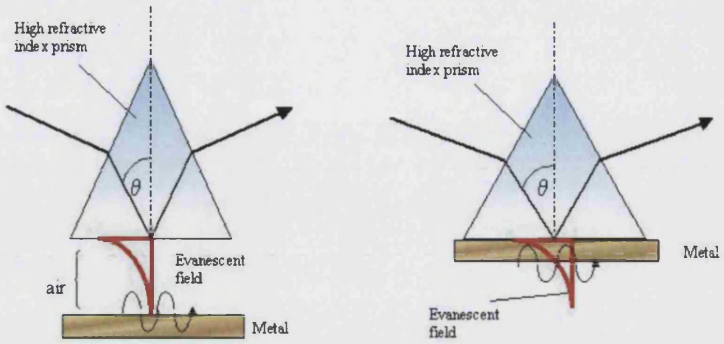

Figure 2.4 Schematic of the Otto configuration and Kretschmann configuration respectively, used to achieve photon excitation of the surface plasmons in the metal film.

Experimentally, the Kretschmann configuration is the preferred method of prism coupling, whereby, a thin metal film (~50nm) is either evaporated directly onto the base plane of the prism or onto a high refractive index glass slide that is optically matched to the prism. The metal film has a limiting thickness, since thick films cause damping of the evanescent field and prevents the excitation of the plasmons on the opposite side of the film. Moreover, metal films that are too thin cause a loss in the excited plasmon field because the field reaches back into the prism. Therefore, the optimum thickness is in the range of 50nm for a gold film, when excited with a Helium-Neon (HeNe) laser at 632.8nm [10].

The excitation of the surface plasmons is only possible when the system enters resonance. This is achieved when the plasmon wavevector and incident photon wavevector couple. This situation occurs at the intersection shown in Figure 2.3, where the resonance coupling happens at a given combination of defined frequency and incident angles. Once resonance is achieved, the surface plasmons are excited by the energy of incident light, resulting in a decrease of the reflected intensity because part of the incident energy is coupled into a surface plasmon wave. Therefore, this loss of energy is observed as a resonance minimum when reflected light intensity is plotted against incident light angle (Figure 2.5)

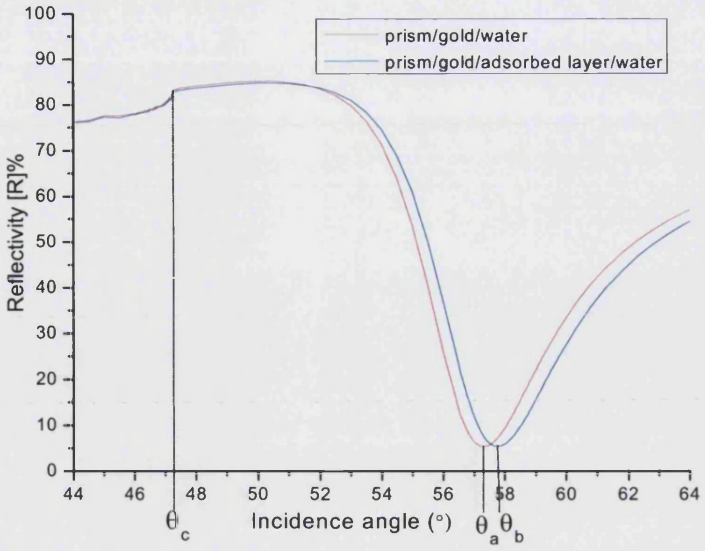

Figure 2.5 Resonance curve obtained during the adsorption of an analyte to the metal surface using the Kretschmann configuration.

If the reflectivity is monitored, a maximum intensity is observed, θ_c, which can be determined as follows:

$$\sin\theta_c = \frac{n_2}{n_1} \tag{2.2}$$

This is determined according to the laws of total internal reflection (TIR), whereby, the incident light passing through a material with refractive index, n_1, will be reflected when passing through to a material with a lower refractive index, n_2.

In accordance with Snell's law (**2.3**), increasing the angle of incidence, θ_1, causes the transmission angle θ_2 to increase until a maximum value of $\theta_2 = 90°$ is reached. Therefore, θ_1 is called the critical angle θ_c, as given in **2.2**.

$$n_1.\sin\theta_1 = n_2.\sin\theta_2 \tag{2.3}$$

Increasing the incidence angle θ_1 further, can not change the transmission angle θ_2 passed 90°, since transmitted light can not enter back into the optically dense material (Figure 2.6). Since all incident light is reflected at angles greater than the critical angle θ_c, the reflectivity reaches 100 [R]% and is referred to as the total reflection edge.

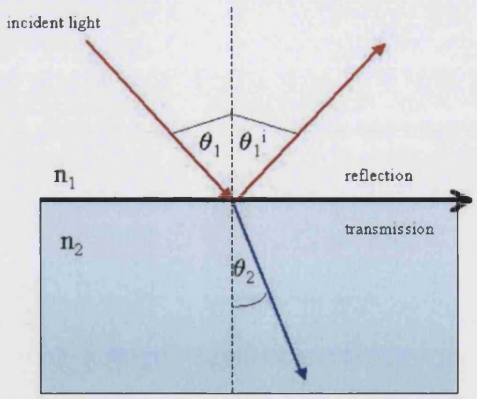

Figure 2.6 Schematic representation of the reflected and transmitted light at an interface between two optical media of different refractive index (n_1 and n_2). The reflection angle equals the incident angle, and the transmission angle is determined by Snell's law.

Above the critical angle, resonance is achieved, resulting in a decrease in the measured reflectivity to a minimum value of θ_a (Figure 2.5). This is the resonance angle at which maximal energy transfer occurs, and is determined as follows:

$$\theta_i = \arcsin \sqrt{\frac{\varepsilon_1 \varepsilon_2}{\varepsilon_p(\varepsilon_1 + \varepsilon_2)}} \qquad \textbf{(2.4)}$$

Where ε_1 = *permittivity of metal film*
ε_2 = *permittivity of dielectric*
ε_p = *permittivity of prism*

2.1.4 Sensitivity of Surface Plasmons to Optical Changes

Biomolecular interactions taking place in the immediate proximity of the evanescent field causes a change in the optical properties of the wave by altering the conditions at which the excitation of the surface plasmons occurs. Adsorption or desorption of a dielectric layer at the interface can be observed by the excited plasmon field and monitored as a result of the change in the angle of resonance for minimum energy transfer (resonance minimum).

The addition of subsequent layers to the prism/gold/dielectric interface causes the refractive index to change in the area within the evanescent field. This results in the dispersion relation of the new surface plasmons to shift towards a higher wave vector (Figure 2.3).

2.1.5 Surface Plasmon Field Distribution

The evanescent field decays away from the interface exponentially, resulting in a certain penetration depth into the dielectric medium. However, the electromagnetic field of a surface plasmon wave is distributed in an asymmetrical manner, and the majority of the field is concentrated in the dielectric. This penetration depth is a function of the wavelength used to excite the surface plasmons. Moreover, it is influenced by the choice of metal used at the interface, and therefore, determines the detection sensitivity of changes in refractive index at the surface (Figure 2.7).

Gold is used to increase the field enhancement of the evanescent wave by a factor of sixteen compared to the intensity of the incident electromagnetic field. In comparison, silver causes the field enhancement of the evanescent wave to increase by a factor of ~fifty, and gives a narrower resonance minimum compared to gold. This is because evaporated gold causes surface roughness, which broadens the resonance curve [11]. The greater field enhancement seen at the silver/dielectric interface compared to that of the gold/dielectric is the result of less attenuation of the evanescent signal and higher localization of the evanescent field in the dielectric. This is due to an energy loss through enhanced scattering at the gold interface because of the roughness of the gold surface [12]. Moreover, silver shows increased field enhancement because coupling of the incident light with the surface plasmons in the silver film is achieved via a two photon process, whereas, a three photon process is required to cause the coupling of the incident light with the surface plasmons in gold, aluminium and copper films [13]. A two photon process is a photophysical event triggered by a two photon excitation.

Metal Layer Supporting Surface Plasmon Waves	**Silver**		**Gold**	
Wavelength	*λ=630nm*	*λ=850nm*	*λ=630nm*	*λ=850nm*
Propagation length (μm)	19	57	3	24
Penetration depth into metal (nm)	24	23	29	25
Penetration depth into dielectric (nm)	219	443	162	440

Figure 2.7 Major characteristics of surface plasmon waves at the metal/dielectric interface (optical constants taken from [14]).

2.2 Fluorescence

Fluorescence is an included term under the heading of luminescence, which describes any process in which energy is emitted from a material at a different wavelength from that at which it is absorbed.

2.2.1 Excitation of Fluorophore

Fluorescence occurs when photons of light are absorbed by a fluorophore, fluorochrome or fluorescent probe when in its ground electronic state. The molecule is elevated to an excited state due to the transfer of the electron to a higher energy orbit. The excess energy is dissipated when the electron returns to the original electronic ground state, and thereby releasing a quantum of light [15]. This fluorescence emission has a lifetime of approximately 10^{-8} seconds, and was first described by Sir David Brewster in 1838. However, the term was not coined until 1852 by Stokes, who stated that the refrangibility of light is always lowered by internal dispersion [16]. Stokes also dispelled the idea that the colour dependence seen was not because of coloured particles in suspension as suggested by Brewster nor because of the colour of the incident light, but was the direct result of the refrangibility.

A fluorophore is the functional group of a molecule, usually a polyaromatic hydrocarbon or heterocyclic group, that absorbs energy at a specific wavelength and re-emits energy at a specific yet different wavelength. There are many natural and synthetic compounds that exhibit fluorescence and they have been used in various applications, such as fluorescent strip lights which employ mercury atoms to emit light in the ultraviolet range of the spectrum. But the field of immunoassays and diagnostics employs the greatest range of fluorescent probes and fluorophores. Automated sequencing of DNA uses labelled fluorescent tags to identify the DNA sequence and antibodies can be modified to include a fluorescent functional group to observe analyte binding quantitatively in immunoassays.

The process of fluorescence is a three stage process, as diagrammatized by Jablonski (Figure 2.8) to describe the adsorption and emission of light.

Stage 1: Excitation

A photon of energy supplied by an external source such as a laser is absorbed by the fluorophore. This causes the electrons in the ground state ($\mathbf{S_0}$) to become excited and move

to one of the many higher electronic singlet states (S_1'). This occurs within approximately 10^{-15} seconds.

Stage 2: Excited State Lifetime

The excited state is maintained for a finite period of time, and the fluorophore undergoes conformational changes and may also interact with its molecular environment. This causes the partial dissipation of some of the energy it possesses as the electron moves from the higher electronic singlet state (S_1') to a relaxed singlet state (S_1), by a process of internal conversion. This takes approximately 10^{-12} seconds. Some of the excited molecules do not return to the original ground state (S_0) by fluorescence emission, but rather by other processes such as collisional quenching and fluorescence energy transfer (FRET).

Stage 3: Fluorescence Emission

A photon of energy is emitted as the excited molecule in the relaxed singlet state (S_1) returns to the ground state (S_0), taking approximately 10^{-8} seconds. However, due to the dissipation of some of the energy, the energy of the photon is lower, therefore, of a longer wavelength than the excitation photon. The energy difference between the excitation photon and the emission photon is the Stokes shift.

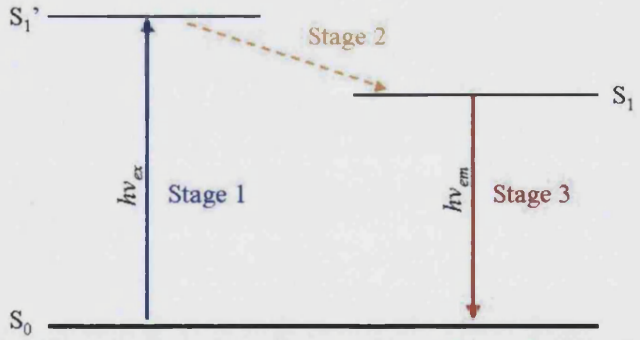

Figure 2.8 Jablonski diagram depicting the excitation (Stage 1) of a fluorophore from its ground singlet state (S_0) to the excited electronic state (S_1') by a specific photon (hv_{ex}), and subsequent emission of fluorescence (Stage 3) by the dissipation of energy (hv_{em}) from the relaxed singlet state (S_1) back to the ground state (S_0).

The process of fluorescence is cyclic, therefore, the fluorophores can be repeatedly excited, unless the fluorophore is irreversibly inactivated by photobleaching. The fact that each fluorophore can be continually excited provides a highly desirable property of sensitivity. Molecules with short excited state lifetimes permit the greatest sensitivity since multiple excitations can be achieved if the molecule is quickly returned from the excited state to the

ground state [15]. Fluorophores demonstrate environmental sensitivity to exogenous factors such as solvent polarity and the pH of the aqueous medium, therefore, the choice of fluorophore for each application must be carefully considered.

The recording of an emission spectrum for a particular molecule is achieved by detecting the fluorescence intensity over a range of emission wavelengths at a constant excitation wavelength. The fluorescence excitation spectrum of a single fluorophore species is generally identical to its adsorption spectrum. For fluorescence detection to be possible, four basic elements are required; an excitation source, the fluorophore, wavelength filters to isolate the emission photons from the excitation photons and a detector to register the output.

2.2.2 Fluorescence Quenching

The fluorescence intensity of a fluorescent molecule can be decreased by a variety of processes, and requires the molecular contact between the fluorophore and the quencher. This contact can be due to diffusive encounters (dynamic quenching) or through complex formation (static quenching). In dynamic quenching, the fluorophore comes into contact with the quenching species during the excited fluorescence lifetime and causes the excited molecule to return to the ground state without emitting a photon. Collisional quenching provides a nonradiative pathway from the excited state back to the ground state. In static quenching, the formation of a complex between the fluorophore and the quencher is non-fluorescent. The process of quenching is sensitive to the molecular environment that affects the rate and probability of the fluorophore coming into contact with the quencher, such as steric shielding and charge-charge interactions [17].

The decrease in fluorescence intensity caused by dynamic quenching can be described by the Stern-Volmer equation:

$$\frac{I_0}{I} = 1 + \kappa_Q \tau_0 [Q] = 1 + K_D [Q] \qquad \textbf{(2.5)}$$

Where I_0 and I are the fluorescence intensities in the absence and presence of a quencher respectively. κ_Q is the bimolecular quenching constant, τ_0 is the unquenched lifetime, K_D is the Stern-Volmer dynamic quenching constant, and [Q] is the quencher concentration. The Stern-Volmer plot of I_0/I verses quencher concentration should be linear, and any deviation

from linearity often indicates multiple populations of fluorophore, which may not be accessible to the quencher. In the collisional quenching of fluorophores, the quantum yield (the fraction of the excited fluorophores that decay by emission relative to the total decay) and the lifetime are reduced because of the additional rate process which depopulates the excited state. Fluorophores with longer lifetimes are quenched more than those with shorter lifetimes [18].

Static quenching, caused by complex formation between the quencher and the fluorophore, is described by:

$$\frac{I_0}{I} = 1 + K_s[Q] \tag{2.6}$$

Where K_s is the association constant for the complex formation between the quencher and the fluorophore.

The combination of the static and dynamic quenching equations for the same fluorophore can be produced as the modified Stern-Volmer equation:

$$\frac{I_0}{I} = (1 + K_S[Q])(1 + K_D[Q]) \tag{2.7}$$

2.2.3 Resonant Energy Transfer

Fluorescence resonance energy transfer (FRET) describes the transfer of energy between two fluorescent molecules over a range of 1-10nm [19]. Through long range dipole-dipole coupling, the energy from an excited fluorescent molecule is nonradiatively transferred to an acceptor fluorescent molecule. The donor molecule returns to the ground singlet state without the emission of a photon, which provides a non-radiative pathway back to the ground state, while the acceptor molecule is excited to a higher singlet state and then subsequently emits a photon.

The rate of energy transfer between the donor and the acceptor molecule is given by:

$$K_{ET} = \frac{1}{\tau_D}\left(\frac{R_0}{r}\right)^6 \tag{2.8}$$

Where τ_D is the decay time of the donor molecule in the absence of the acceptor molecule, and r is the distance between the donor and the acceptor molecule. R_0 is the Förster distance, at which half of the donor molecules decay via resonant energy transfer and the other half decay via radiative and nonradiative means. The Förster distance depends on the overlap of the donor emission spectrum with the acceptor absorption spectrum and their mutual molecular orientation.

The efficiency of the transfer of energy between a donor and acceptor fluorophore is dependant on whether the rate of transfer is faster than the rate of decay, if this is so, then the transfer of energy will be feasible and efficient. If not, then little transfer of energy between the donor and acceptor molecules will occur during the excited state lifetime.

The efficiency of the resonant energy transfer between two molecules is given by:

$$E = \frac{k_T}{\tau_D^{-1} + k_T} = \frac{R_0^6}{R_0^6 + r^6} \tag{2.9}$$

The FRET efficiency verses the donor-acceptor distance can be plotted (Figure 2.9), from which the Förster distance can be determined from 50% energy transfer efficiency.

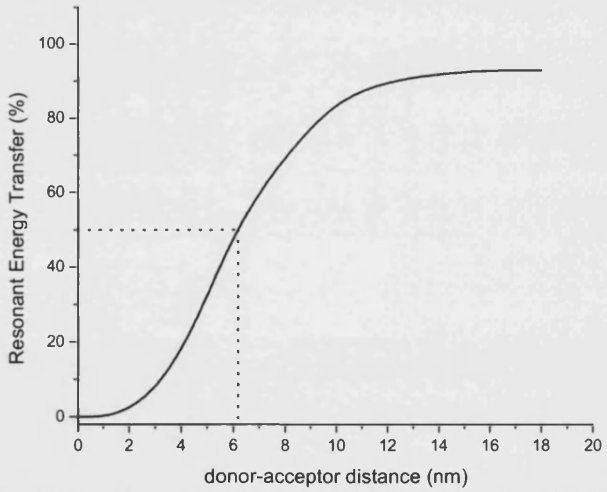

Figure 2.9 Simulation of the fluorescence resonant energy transfer (FRET) efficiency for the energy transfer between a donor molecule and an acceptor molecule. From which, the Förster distance can be calculated from 50% resonant energy transfer (……)

It has been shown that quenching of fluorophores by resonant energy transfer results in increased photostability because the fluorophore spends less time in the excited state, therefore decreasing its opportunity to partake in photochemical reactions [19].

The most common application of FRET is to measure the distanced between two sites on a macromolecule, such as between two sites on a protein. The macromolecule is covalently labelled with a donor and acceptor, and from this, the distance can be determined from the efficiency of energy transfer from the extent of donor quenching due to the acceptor [17]. In fluorescence microscopy, fluorescence confocal laser scanning microscopy and molecular biology, FRET is used to quantify molecular dynamics such as protein-protein interactions and conformational changes.

2.3 Surface Plasmon Field Enhanced Fluorescence

It has been extensively documented that fluorophores are excited resonantly by the plasmon field enhancement effect observed at metal surfaces. This technique has been exploited in various applications including, monitor the interfacial binding between oligonucliotide probes and their complementary target strands [20] and observing the lateral mobility of lipid molecules in model membrane systems [21]. Increasingly, Surface Plasmon field enhanced Fluorescence Spectroscopy (SPFS) is being used for sensing and monitoring purposes, such as the detection of the pregnancy hormone, human Chorionic Gonadotrophin (hCG) [22].

Surface Plasmon Resonance Spectroscopy (SPS) is renowned for showing a lack of sensitivity towards detecting low molecular weight analytes or small numbers of molecules, because of the small shift in resonance minimum and refractive index. However, the simultaneous measurement of surface plasmon resonance and fluorescence provides an improvement in sensitivity. The inclusion of a thin metal film in the Kretschmann configuration for SPS also provides a means of exciting the fluorophores. The coupling of the surface plasmons in the metal film and incident light produces the evanescent field that is capable of exciting the fluorophores present in the dielectric. However, the fluorescence intensity observed for any given fluorophore is highly dependant on the proximity to the metal surface, as both collisional quenching and FRET provide a nonradiative pathway to the ground state. Quenching and FRET have no significant effect on the spontaneous rate at which a fluorophore emits photons (radiative decay) [23]. Moreover, an opportunity arises to control the radiative rates of a fluorophore from its interactions with nearby metal surfaces, which has been termed Radiative Decay Engineering (RDE) by Lakowicz, who described this phenomenon in 2001. Metal surfaces

in close proximity to oscillating fluorophores can modify the rate of emission and spatial distribution of the radiated energy of the fluorophore [23]. Excited fluorophores close to a metal surface, 20nm or less, are almost all quenched, because the fluorescence dipole is coupled to the surface plasmons causing the damping of this dipole.

Enhancements in fluorescence can be observed of up to 1000 times, depending on the distance and the geometry at which the fluorophore and metal surface are orientated [24, 25]. This enhancement occurs at distances up to 200Å, and is partly due to the amplification of the evanescent field, which penetrates into the dielectric and causes an increase in the local excitation intensity of the fluorophore by increasing the intrinsic radiative decay rate [26]. Fluorophores with high radiative decay rates have high quantum yields and short lifetimes, and fluorophores in close proximity to the metal surface increase their quantum yields. Therefore, this causes the increase in the radiative decay rate and intensity of fluorescence. This is because the fluorophore returns to the ground state quicker, shortening the fluorescent lifetime and resulting in an increased number of photons observed per fluorophore. Moreover, since the fluorophores spend less time in the excited state, the extent of photobleaching is also decreased because the fluorophores spend less time in the higher singlet states. The combination of increased quantum yield through shortened lifetime and decreased photobleaching through shorter excitation times results in a substantially increased numbers of detectable photons per fluorophore.

At metal/fluorophore distances greater than 200nm, little fluorescence is observed because the fluorophores move beyond the evanescent field. Therefore, they can not be excited and are too far from the metal surface to experience any enhancement effects. However, this does prove advantageous in some experimental circumstances. By ensuring the supamolecular architecture of the surface is specifically designed, it is possible to provide binding sites for biorecognition events in the proximity of the fluorescence detection field, while excluding the fluorescent probe in the bulk solution that could significantly contribute to the fluorescence signal, and cause over reporting.

2.4 Mass Transfer

The physical process involved is the diffusive and convective transport of molecules within a system is termed mass transfer, and is caused by the difference in concentration between two areas. This causes the random net movement of molecules from a region of high concentration to a region of low concentration. The mass transfer coefficient is a diffusion rate constant, defined by:

$$k_c = \frac{k_m}{A\Delta c_A} \tag{2.10}$$

Where k_m is the mass transfer coefficient, A is the effective mass transfer area, and Δc_A is the driving force concentration difference. This coefficient can be used to quantify the mass transfer between phases, such as the analyte in the bulk phase of a solution and the surface.

With low mass transfer, the diffusion of molecules from the bulk to the surface is slower than the rate of binding of the analyte to the ligand, creating a deficit of analyte at the surface.

The mass transfer coefficient is small if the flow rates at which the analyte approaches the ligand is low or the molecular weight of the diffusing molecule is very high, causing the diffusion layer to be large. Therefore, by controlling the flow rate, mass transfer can also be controlled. A high flow rate increases the association and dissociation rate constants, bringing the analyte from the bulk to the surface faster and avoids the deficit of analyte at the surface created by slow diffusion of the analytes.

2.5 Langmuir Adsorption

The adsorption of an analyte in the gaseous phase or in solution to an immobilised receptor provides a convenient methodology for monitoring the interaction between the analyte-ligand complex. This diffusion-limited reaction can be characterised and modelled using the Langmuir adsorption isotherm, and was originally developed by Irving Langmuir in 1916 to model the adsorption of gases on a plane crystal surface. The theory stated that adsorption of gases onto the surface was the result of a time lag between the gas molecules impinging on the surface and the time taken for the condensation of the gas, leading to an

accumulation of these molecules in the surface layer [27]. It was also said that if a gas molecule strikes a portion of the surface already covered, it evaporates so quickly that it is equivalent to a reflection.

This model was later expanded for the adsorption of liquids to solids. It stated that if the liquid molecules contained active groups, it will orientate and pack into the surface layer in a way that is dependant upon the number of atoms exposed in the surface of the solid [28].

The assumptions made for this model are that: 1) the adsorption of molecules on the surface produces only a homogenous monolayer, 2) all binding sites are equivalent and there is no bias between the molecule and any of the binding sites, and 3) all occupied sites do not interfere with the binding of neighbouring binding sites. The adsorption of molecules is limited by the number of available binding sites, until complete surface saturation is met and all binding sites are occupied.

The interactions which take place at the surface are expressed by the k_{on} rate constant ($mol^{-1}Ls^{-1}$) for the processes of association between the analyte (A) and the ligand (B) to form the complex (AB), and the k_{off} rate constant (s^{-1}) for the disassociation of the analyte and ligand complex.

$$A + B \underset{k_{off}}{\overset{k_{on}}{\rightleftharpoons}} AB$$

(2.11)

The rates of association and disassociation between the ligand and analyte will become equal in time. When equilibrium is achieved, the concentrations of analyte, ligand and complex will be constant, therefore:

$$k_{on}[A][B] = k_{off}[AB]$$

(2.12)

From this, the dissociation equilibrium constant (K_D $mol.dm^{-3}$) and the association equilibrium constant (K_A $mol.dm^{-3}$) can be resolved:

$$\frac{[A][B]}{[AB]} = \frac{k_{off}}{k_{on}} = K_D \quad \text{and} \quad \frac{1}{K_D} = K_A$$

(2.13)

This simple example interaction between two reactants (Figure 2.10), is not under the influence of exogenous factors such mass transfer. However, in experimental situations these have to be taken in to consideration. The movement of the analyte from the bulk solution into the proximity of the ligand to initiate association is most influential, and is determined by the mass transfer rate constant. Therefore;

$$A_{bulk} \underset{k_m}{\overset{k_m}{\rightleftharpoons}} A_{interface} + B \underset{k_{off}}{\overset{k_{on}}{\rightleftharpoons}} AB$$

(2.14)

Where A_{bulk} is the concentration of the analyte in the bulk solution, $A_{interface}$ is the concentration of the analyte at the interface of the ligand and k_m is the mass transport coefficient.

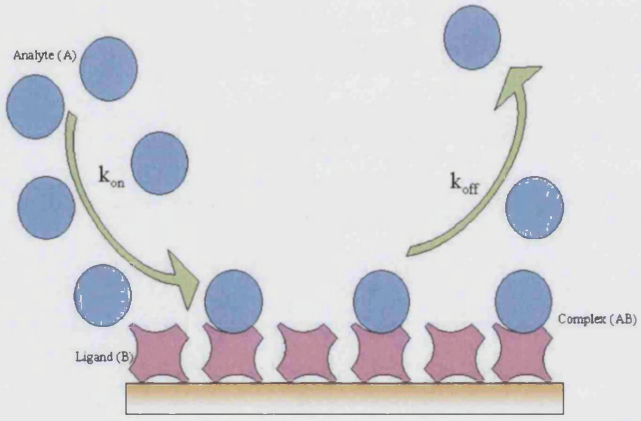

Figure 2.10 Schematic depiction of the adsorption and desorption process between the analyte (A) and ligand (B). The surface coverage is dependant on the rate constants k_{on} and k_{off}.

The rate of complex formation between the analyte and the ligand at the surface is equal to:

$$\frac{d[AB]}{dt} = k_{on}[A]_{interface}[B] - k_{off}[AB]$$

(2.15)

However, the number of free ligand sites (B) will decrease over time as the analyte binds to the receptor sites, therefore,

$$[A]_t = [B]_o - [AB]_t$$

(2.16)

Where $[AB]_t$ is the concentration of the bound complex at time t, and $[B]_0$ is the ligand concentration at the starting time. This can be integrated with **2.15** to give:

$$\frac{d[AB]_t}{dt} = k_{on}([B]_o[A]_t - [A]_t[AB]_t) - k_{off}[AB]_t$$

(2.17)

Which in turn can be simplified to:

$$\frac{d[AB]_t}{dt} = k_{on}[A]_t([B]_o - [AB]_t) - k_{off}[AB]_t$$

(2.18)

The formation of the AB complex provides the signal response, which in SPS and SPFS, is the reflectivity and fluorescence respectively. The maximum response/signal, R_{max}, is equivalent to $[B]_0$, because all binding sites are occupied, therefore:

$$\frac{dR_t}{dt} = k_{on}[A](R_{max} - R_t) - k_{off}R_t$$

(2.19)

When the system is in equilibrium, it is possible to determine the equilibrium constant, R_{eq}, for the binding between the analyte and the ligand at various analyte concentrations:

$$R_{eq} = \frac{R_{max}[A]}{k_{off}/k_{on}[A]}$$

(2.20)

Therefore,

$$R_{eq} = \frac{R_{max}[A]}{K_D + [A]}$$

(2.21)

The graphical plot of R_{eq} against the free analyte concentration produces the Langmuir adsorption curve (Figure 2.11), where the concentration required to saturate 50% of the available ligand sites is $R_{max}/2$, therefore, the dissociation equilibrium constant, K_D, can be determined:

$$R_{max}/2 = \frac{[A]R_{max}}{[A] + K_D}$$

(2.22)

Therefore,

$$[A] = K_D \text{ at equilibrium.}$$

(2.23)

So, K_D is the analyte concentration to cover half the ligand surface sites.

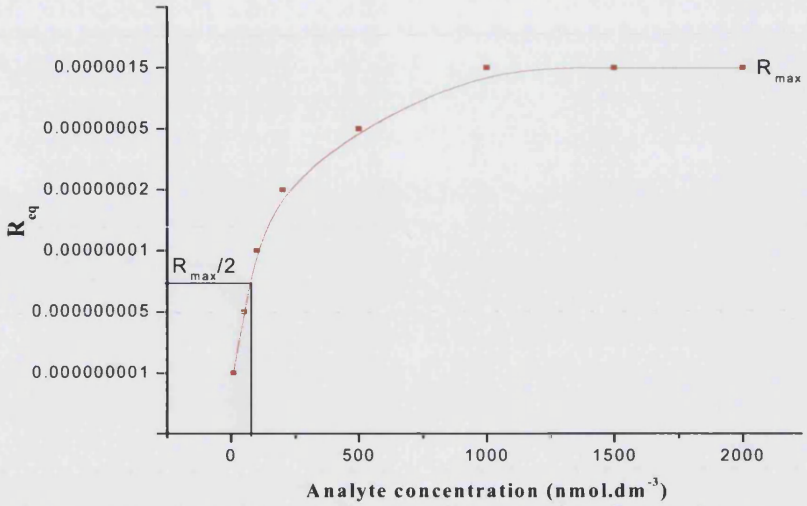

Figure 2.11 Langmuir adsorption isotherm, allowing the direct determination of the equilibrium constants (75 nmol.dm^{-3} for the above representation).

The Langmuir simulation was used in the subsequent work to calculate the kinetic and equilibrium constants.

2.6 Bibliography

1. Smithpeter, C., et al., *Near real time confocal microscopy of cultured amelanotic cells: Sources of signal, contrast agents and limits of contrast.* Journal of Biomedical Optics, 1998. **3**(4): p. 429-436.
2. Popplewell, J., et al., *Quantification of the effects of melittin on liposome structure.* Biochemical Society Transactions, 2005. **33**(5): p. 931-933.
3. Bochert, R., et al., *Contribution to comprehension of image formation in confocal microscopy of cornea with Rostock cornea module.* Br J Ophthalmol, 2005. **89**(10): p. 1351-1355.
4. Ghosh, G., *Dispersion-equation coefficients for the refractive index and birefringence of calcite and quartz crystals.* Optics Communications, 1999. **163**(1): p. 95-102.
5. Knoll, W., *Interfaces and thin films as seen by bound electromagnetic waves.* Annual Review of Physical Chemistry, 1998. **49**(1): p. 569-638.
6. Malmqvist, M., *Biospecific interaction analysis using biosensor technology.* Nature, 1993. **361**(6408): p. 186-187.
7. Schuck, P., *Use of surface plasmon resonance to probe the equilibrium and dynamic aspects of interactions between biological macromolecules.* Annual Review of Biophysics and Biomolecular Structure, 1997. **26**: p. 541-566.
8. Eagen, C.F. and W.H. Weber, *Modulated Surface-Plasmon Resonance for Adsorption Studies.* Physical Review B, 1979. **19**(10): p. 5068-5082.
9. Homola, J., S.S. Yee, and G. Gauglitz, *Surface plasmon resonance sensors: review.* Sensors and Actuators B-Chemical, 1999. **54**(1-2): p. 3-15.
10. Giannattasio, A., I.R. Hooper, and W.L. Barnes, *Transmission of light through thin silver films via surface plasmon-polaritons.* Optics Express, 2004. **12**(24): p. 5881-5886.
11. de Bruijn, H.E., R.P.H. Kooyman, and J. Greve, *Choice of metal and wavelength for surface-plasmon resonance sensors: some considerations.* Applied Optics, 1992. **31**(4): p. 440-442.
12. Wakamatsu, T. and K. Aizawa, *Penetration-depth characteristics of evanescent fields at metal attenuated total reflection.* Japanese Journal of Applied Physics, Part 1: Regular Papers and Short Notes and Review Papers, 2005. **44**(6 A): p. 4272-4274.
13. Tsang, T., T. Srinivasan-Rao, and J. Fischer, *Surface-plasmon field-enhanced multiphoton photoelectric emission from metal films.* Physical Review B, 1991. **43**(11): p. 8870 LP - 8878.
14. Ordal, M.A., et al., *Optical Properties of the Metals Al, Co, Cu, Au, Fe, Pb, Ni, Pd, Pt, Ag, Ti, and W in the Infrared and Far Infrared.* Applied Optics, 1983. **22**(7): p. 1099-1119.
15. Mason, W.T., *Fluorescent and luminescent probes for biological activity: A practical guide to technology for quantatative Real-Time analysis.* Academic Press, 1999(2nd Edition).
16. Stokes, G.G., *On the Change of Refrangibility of Light.* Abstracts of the Papers Communicated to the Royal Society of London, 1850. **6**: p. 195-200.
17. Lakowicz, J.R., *Principles of Fluorescence Spectroscopy.* Kluwer Academic, 1999(2nd Edition).
18. Geddes, C.D. and J.R. Lakowicz, *Metal-Enhanced Fluorescence.* Journal of Fluorescence, 2002. **12**(2): p. 121-129.
19. Kirsch, M., et al., *Fluorescence resonance energy transfer detected by scanning near-field optical microscopy.* Journal of Microscopy, 1999. **194**(2-3): p. 448-454.

20. Neumann, T., et al., *Surface-Plasmon Fluorescence Spectroscopy.* Advanced Functional Materials, 2002. **12**(9): p. 575-586.
21. Tawa, K. and K. Morigaki, *Substrate-Supported Phospholipid Membranes Studied by Surface Plasmon Resonance and Surface Plasmon Fluorescence Spectroscopy.* Biophysical Journal, 2005. **89**: p. 2750-2758.
22. Vareiro, M.M.L.M., et al., *Surface plasmon fluorescence measurements of human chorionic gonadotrophin: Role of antibody orientation in obtaining enhanced sensitivity and limit of detection.* Analytical Chemistry, 2005. **77**(8): p. 2426-2431.
23. Lakowicz, J.R., *Radiative decay engineering: Biophysical and biomedical applications.* Analytical Biochemistry, 2001. **298**(1): p. 1-24.
24. Glass, A.M., et al., *nteraction of metal particles with adsorbed dye molecules: absorption and luminescence.* Optics Letters, 1980. **5**(9): p. 368-370.
25. Sokolov, K., G. Chumanov, and T.M. Cotton, *Enhancement of Molecular Fluorescence near the Surface of Colloidal Metal Films.* Analytical Chemistry, 1998. **70**(18): p. 3898-3905.
26. Lakowicz, J.R., et al., *Radiative decay engineering: 2. Effects of silver island films on fluorescence intensity, lifetimes, and resonance energy transfer.* Analytical Biochemistry, 2002. **301**(2): p. 261-277.
27. Langmuir, I., *THE CONSTITUTION AND FUNDAMENTAL PROPERTIES OF SOLIDS AND LIQUIDS. PART I. SOLIDS.* J. Am. Chem. Soc., 1916. **38**(11): p. 2221-2295.
28. Langmuir, I., *THE CONSTITUTION AND FUNDAMENTAL PROPERTIES OF SOLIDS AND LIQUIDS. II. LIQUIDS.* J. Am. Chem. Soc., 1917. **39**(9): p. 1848-1906.

3.0 Experimental Methods

This chapter details the experimental set-ups and methodologies followed during this study. The optical instrumentation setup is described with reference to Surface Plasmon Resonance (SPR) and Surface Plasmon field enhanced Fluorescence Spectroscopy (SPFS) as detailed in chapter 2. The construction of the supamolecular surface is laid out along with the preparation of all solutions, bilayer vesicles and membrane binding/permeablizing agents.

3.1 Optical Setup & Methodology

The technique of SPR was applied here to qualitatively and quantitatively study the construction of the supamolecular surface and the absorption and desorption of analytes to that surface in real time and without the need to label molecules. Moreover, simultaneous detection of fluorescence using SPFS facilitated the detection of low molecular weight analytes and small numbers of analytes. This provides a highly sensitive analytical tool for observing small changes in mass at the metal/dielectric interface.

3.1.1 Experimental Instrumentation Set-up

The home built spectrometer used in this work is of a common geometrical design in the Kretschmann configuration [1], with the modification to include a facility to detect fluorescence. As depicted in Figure 3.1, the Surface Plasmon Spectrometer (SPS) consists of a Helium-Neon (HeNe) laser (JDS Uniphase, Co, Output power = 5mW, λ = 632.8nm) that is focused onto the metal/dielectric interface at the base plan of the prism. The laser beam passes a fixed frequency precision light chopper (Perkin Elmer, Inc), which cuts the incident light at a constant frequency, and the information regarding chopping frequencies is fed to the lock-in amplifier (Perkin Elmer, Inc). Light passing through the chopper subsequently passes through two polarizers (Melles-Griot, Inc) causing the light to be p-polarized. The light is focused onto the back of the thin metal film via a prism. The reflected light is detected by a photodiode and amplified by a low power battery amplifier. The signal is fed to the lock-in amplifier, which subtracts the received signal when the light is chopped (blocked) from that when the light passes through the chopper. Moreover, this cleans up the signal by removing any extraneous light, such as that from the laboratory.

The polarised light is focused on to the base plane of the high refractive index (n = 1.84489) $LaSFN_9$ prism (Schott UK, Ltd), which is optically matched to the substrate using refractive index liquid (Serie B n = 1.70, Cargille-Sacher Laboratories Inc). The reflected light is focused by a lens (f = 25mm, Ovis) towards the photodiode, which monitors the intensity of the reflected light. As with the chopper, the photo-detector is connected to the lock-in amplifier to ensure all the frequencies of light not regulated by the chopper are filtered.

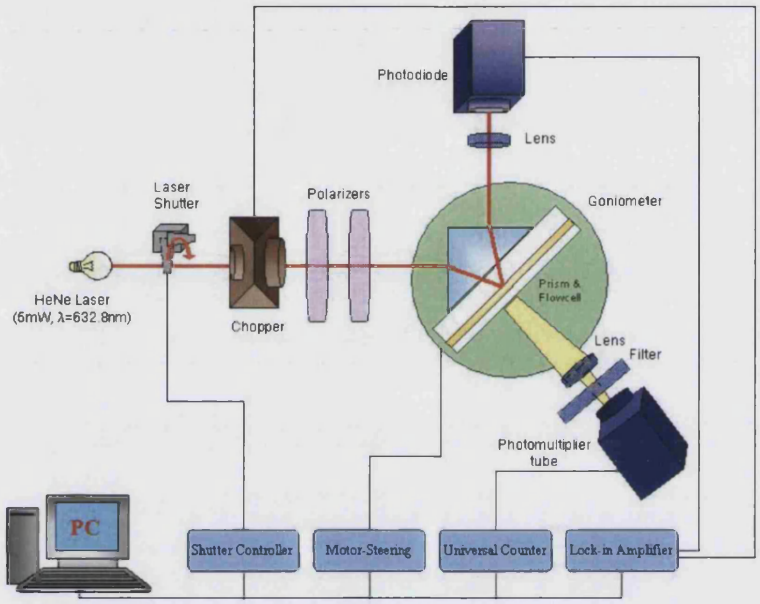

Figure 3.1 Surface Plasmon field enhanced Fluorescence Spectroscopy set-up. With an ability to concurrently measure reflectivity and fluorescence.

The addition of a photomultiplier tube (PMT) (Hamamatsu Photonics UK Ltd) onto the goniometer to the rear of the mounted sample allows for the detection of light emitted by the sample as fluorescence. The emitted fluorescent light is focused by a lens (f = 50mm, Ovis), and then passes through an interference filter, which controls the spectral transmission of the incident light by reflecting one or more spectral bands and transmitting others. The filtered incident light strikes the PMT, which is a sensitive device for measuring photon count that also amplifies the signal produced by the incident light. The PMT is enclosed in a home built protection unit, provided by the Max-Planck Institute, to reduce exposure from extrinsic light. A computerized shutter, positioned in front of the HeNe laser beam, cuts the incident light at timed intervals to minimise the exposure of the fluorophore to photobleaching. The PMT is also connected to a photon counter that has an automatic shut-off if the irradiation exceeds a predefined level, preventing damage to the fluorescence detection equipment.

The prism is mounted onto a motorized 2-phase goniometer (Huber GmbH & Co), which allows the sample to be rotated to a precise angular position at 0.005° steps in the *x* and *y* direction. Two *x* and *y* tables and two tilting tables allow for optimum control of movement of the mounted sample. The instrumentation is controlled by a personal computer using Windows-plasmon Steuresoftware (Wasplas™) version 2.60 developed by Scheller [2].

The spectrometer is isolated from the external environment by means of a cushioned optical breadboard (Melles Griot, Inc), which aims to minimise interference due to vibrations, and a Faraday box to prohibit light infiltration and fluctuations in temperature (Figure 3.2).

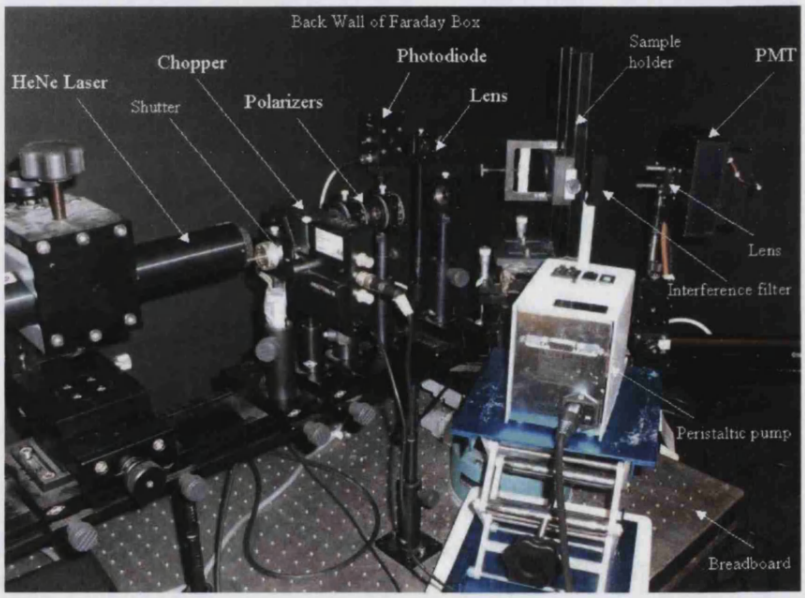

Figure 3.2 SPR Kretschmann configuration housed within a Faraday box to exclude environmental interference.

3.1.2 Flow Cell Set-up

The conventional geometric set-up of the flow cell used during SPR measurements is schematically depicted in Figure 3.3. Initially, a quartz glass flow cell (Herasil, Schott) is used in part of the thesis. However, due to the fragility of the glass and general wear over time, a Teflon flow cell constructed by the Mechanical Engineering Department of the University of Bath replaced the quartz flow cell. The Teflon cell is placed onto a quartz glass slide of low florescence (n = 1.46, Schott UK Ltd), with a viton O-ring to seal the contact between them. Another O-ring is placed into the rivet on top of the flow cell, were

the gold coated high refractive index glass slide (SFL6, n = 1.799, UQG Optics Ltd) is placed on top, with the gold layer facing the flow cell. A high refractive index prism ($LaSFN_9$, n = 1.845) is optically matched to the base plane of gold coated slide with Series B refractive index liquid (n = 1.70, Cargille Labs, Ltd). Optical matching between the base plane of the prism and the gold substrate is pivotal to allow unperturbed coupling (Figure 3.3)

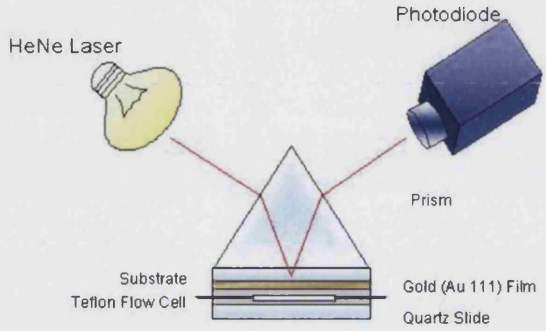

Figure 3.3 Schematic of the flow cell set-up

The flow cell is equipped with an inlet and outlet valve, to which Tygon™ tubing (Cole Parmer, UK) with an internal diameter of 0.76mm is attached (Figure 3.4). The flow cell circuit is connected to a peristaltic pump (Rego Analog, Istmatec SA) to ensure the even delivery of the sample. A hypodermic needle (19G 2", Becton Dickinson UK, Ltd) was removed from the luer lock and attached to the each ends of the tygon tubing. The needle ends of the tygon tubing are inserted into the Eppendorf containing the sample for injection into the flow cell. The circulating volume around the flow cell circuit is approximately 500µl, which circulates at 1.8ml.min^{-1} (50 RPM, tubing internal diameter = 0.76mm), for optimised analyte delivery, while minimising the mass transport effect and the shear force on the bilayer vesicles.

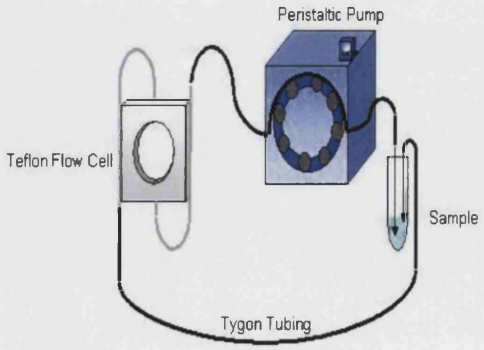

Figure 3.4 Schematic of the flow cell circuit.

3.1.3 Instrumentation Alignment

The alignment of the spectrometer is critical for the accuracy of the measurements performed, and must be done before any experimental procedure to ensure the incident laser beam is aligned with the centre of the flow cell. Moreover, the reflected laser beam must be aligned with the centre of the photodiode, and the emitted fluorescence must be aligned with the photomultiplier tube to ensure optimum fluorescence detection.

3.1.3.1 Alignment of the Surface Plasmon Spectrometer

The alignment of the spectrometer is performed using two iris diaphragm apertures (25mm diameter, Ovis). One diaphragm is mounted after the polarizers; to align the incident light. With a second diaphragm positioned before the photodiode to align the reflected light.

The detector motor is moved to 180° and the orientation and height of the photodiode is adjusted to optimize the position of the reflected light beam into the centre of the photodiode. The sample is mounted securely into the holder on the goniometer and the sample motor is moved to 45°, while the detector motor moved to 90° (Figure 3.5). In accordance with the Laws of Reflection, part of the incident light is reflected as the laser strikes the base plane of the prism, and is reflected towards the photodiode through iris diaphragm 2 (Figure 3.5). To ensure the incident light and reflected light beams are aligned with the centre of the sample flow cell and the photodiode respectively, both iris diaphragms 1 and 2 are closed so that only a weak beam of light penetrates the iris'. The two tilting tables are manually adjusted to align the height of the reflected laser beam into the centre of the iris diaphragms. The tilting table that controls the height of the reflected laser beam is aligned to the centre of iris 2 initially. Then, the back reflected beam is aligned with iris 1 because the tilting table that controls the height of the reflected beam also affects the height of the back reflected beam.

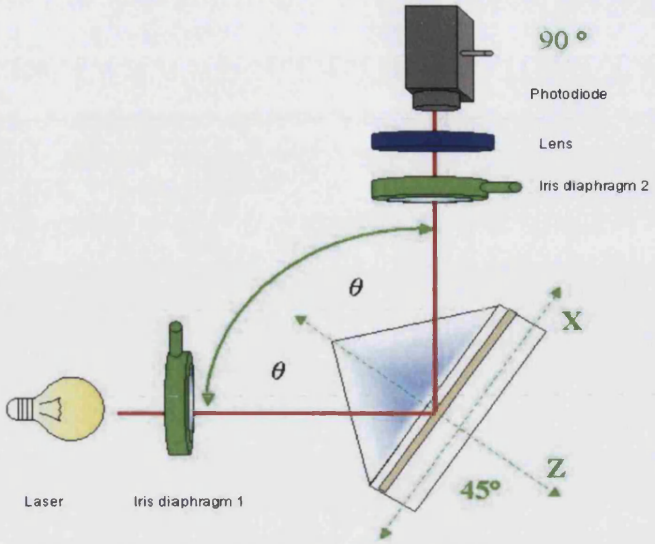

Figure 3.5 Schematic of the practical alignment of the spectrometer in accordance of the laws of reflection.

For the accurate alignment of the system, the incident light at the base plane of the prism and the reflected light at the iris diaphragm 2 should be fixed irrespective of changes in angle of incidence. The goniometer is adjusted in the z direction until the incident beam seen at the base plane of the prism is fix. The beam can then be adjusted in the *x* direction into the centre of the sample. The iris apertures are opened when the alignment is completed and the measurements are to be started.

3.1.3.2 Alignment of the Surface Plasmon field enhanced Fluorescence Spectrometer

In cases where simultaneous detection of reflectivity and fluorescence are desired, the spectrometer must be aligned accordingly. Where dual detection is required, the alignment of the SPS is followed as previously reported in section 3.1.3.1, with the additional alignment of the photomultiplier tube (PMT). The photosensitive device consists a photoemissive cathode, which directs the emitted electrons to the photomultiplier. The multiplied electrons are collected at the anode as an output signal (Figure 3.6).

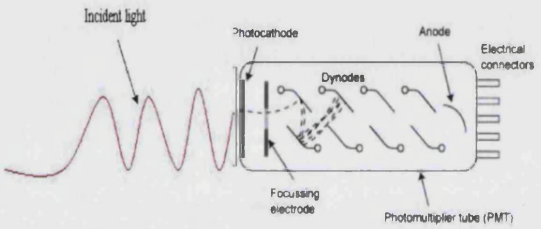

Figure 3.6 Schematic of the photomultiplier tube
(www.wikipedia.org/wiki/Photomultiplier_tube)

The PMT is attached to the backend of the goniometer and can be adjusted in height (y) and in the x plane to adjust the orientation and alignment (Figure 3.7). The fluorescence collection lens is position in between the sample holder and the PMT. It is placed near to the sample to maximize the fluorescence collection area. The centre of the lens is positioned at the same height as the incident laser beam. The optimisation of the fluorescence detection unit is achieved by adjusting the position of the PMT in the x and z directions, and performing a fluorescence measurement. The adjustments are repeated until a maximum fluorescence value is achieved.

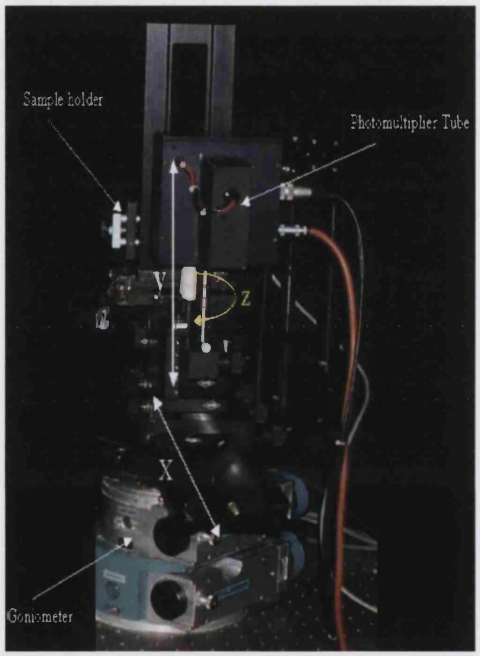

Figure 3.7 Photograph of the Photomultiplier Tube (Hamamatsu) attached to the goniometer behind the sample holder.

3.1.4 Measurement Procedure

The measurements performed are recorded as scan curves and resonance kinetic plots. After the alignment of the spectrometer and the loading of the sample onto the goniometer, a resonance scan curve is carried out.

3.1.4.1 Surface Plasmon Resonance Spectroscopy Measurement Procedure

The incident light beam focused on to the base plane of the prism and the reflected light is monitored at the photodiode, while varying the angle of incidence. Therefore, the intensity of the reflected light detected will also vary. This scan curve is a plot of the normalized

reflected light intensity verses the incident angle (Figure 3.8). The adsorption of analyte to the surface causes a change in the optical properties of the metal interface resulting in a shift in the resonance scan curve along the *x* axis (as depicted in Figure 3.8) A scan curve is taken after each addition of a sample and at the start and end of each experiment.

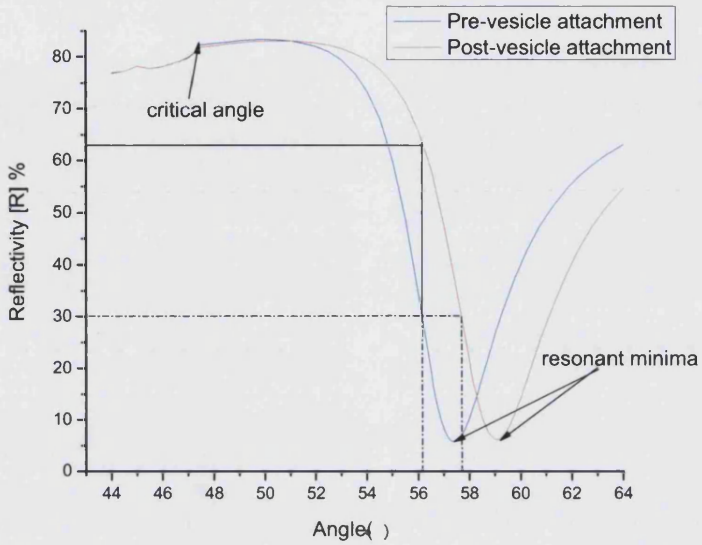

Figure 3.8 Example of a resonant scan curve, pre- (blue curve) and post- (red curve) analyte binding.

The experiments are followed and monitored by recording the change in reflected light intensity detected at the photodiode, and any change in the optical properties of the functionalized surface caused by the adsorption or desorption of analytes can be visualized in real-time. The change in intensity of reflected light is achieved by maintaining a fixed angle, at around 1.5° lower than the initial angle of minimum on the scan curve (usually, 30% Reflectivity), such that the change in the angle of resonance gives a linear change in the measured reflectivity.

As the optical properties of the functionalized surface change, either through adsorption or desorption of analytes, the reflectivity at the fixed incidence angle also increases or decreases respectively (Figure 3.9). In the example in Figures 3.8 and 3.9, the adsorption of the analyte to the surface causes an increase in reflectivity from 30 % to ~ 63% at the fixed angle of incidence, as shown with the shift in scan curves (Figure 3.8) and as monitored in real-time in the resonance kinetic plot (Figure 3.9).

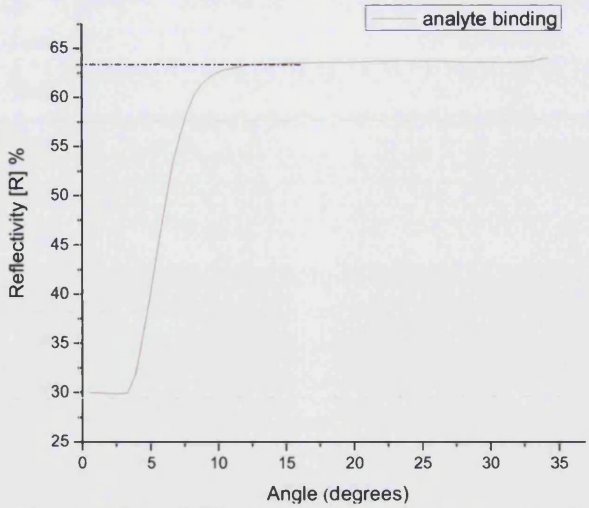

Figure 3.9 Resonance kinetic plot of adsorption of analyte to the surface. Measured at a fix angle of incidence, the adsorption of analyte to the surface is visualized as an increase in reflectivity [R]%.

3.1.4.2 Surface Plasmon field enhanced Fluorescence Spectroscopy Measurement Procedure

The inclusion of fluorescence measurements along with the standard resonance measurements is performed to increase the sensitivity of detection of low molecular weight analytes or small numbers of analytes, when little or no change is observed with surface plasmon resonance spectroscopy. Therefore, this optimizes the signal sensitivity by dual detection of reflectivity and fluorescence.

Much in the same way as with resonance scan curves, measurements of the intensity of the reflected light at varying angles of incidence is performed, as well as photon count produced by the fluorescent sample detected by the PMT and lock-in amplifier (Figure 3.10). A background fluorescence of ~5000 counts per second (cps) is detected at angles below the critical angle because of the intrinsic fluorescent properties of the prism. At angles above the critical angle, when total internal reflection occurs, the strong evanescent field excites the fluorescent molecules which are then detected.

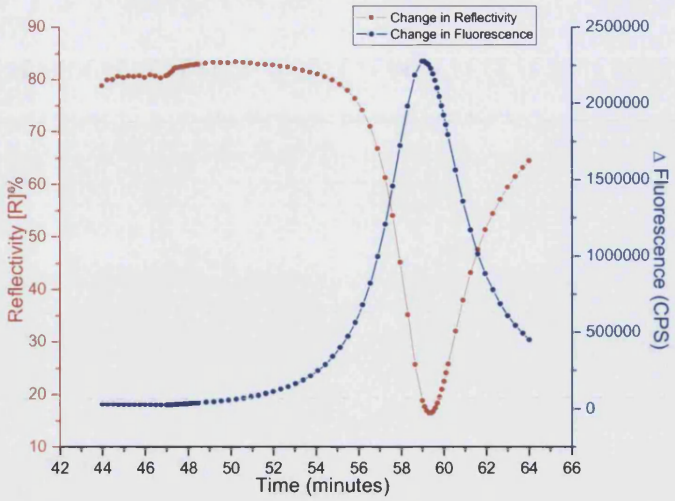

Figure 3.10 Dual Resonance scan curve, showing the change in reflectivity with varying angle of incidence (Red plot), and the change in photon count with varying angle of incidence (Blue plot).

The fluorescence kinetics measurement is performed at a fixed angle of incidence (~30% reflectivity), within the linear range of the reflectivity scan curve. This is in order for the fluorophores to be under constant excitation conditions and any change in fluorescence is due to adsorption or desorption of the molecule and not changes in the angle of incidence. Kinetics measurements involving fluorescence are executed under non-continuous light illumination to prevent the photo-bleaching of the fluorophore. Fluorescence is used in this study to provide a means of observing small changes at the surface that are not easily visualized using conventional Surface Plasmon Spectroscopy (Figure 3.11), and shows the sensitivity of this methodology.

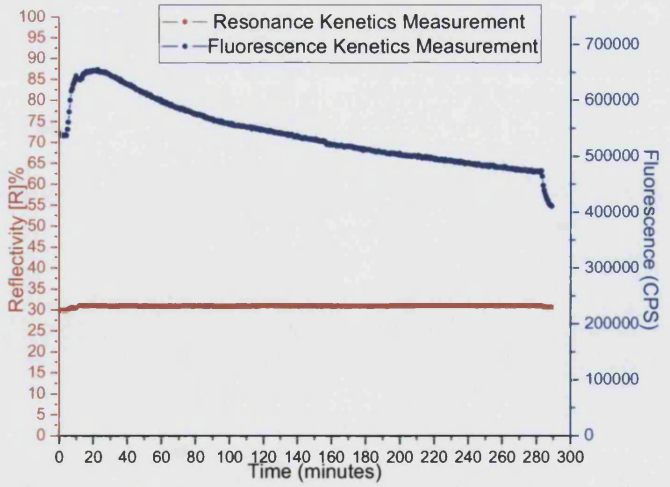

Figure 3.11 Fluorescence Kinetics Measurements, showing an observable change in fluorescence over time as a result of membrane-pore formation (Blue plot), but little observable change in reflectivity (Red plot).

3.1.4.3 Measurement Sequence

The generalized sequence for the measurement of adsorption and desorption remains fairly consistent, however, the reagents, experimental conditions and analytes usually vary between experiments.

The functionalized surface is constructed and monitored with the adsorption of each layer being followed by SPR. The analyte components of each layer are dissolved and injected into the flow cell after a stable baseline is observed. Running buffer is passed across the surface between the addition of each layer to remove any unbound or non-specifically adsorbed analytes.

After the adsorption of each layer, a scan curve is performed. The adsorption of the bilayer vesicles marks the complete construction of the functionalized surface, and any non-encapsulated fluorophore can be rinsed away from the flow cell with buffer. Following the construction and rinsing of the surface, a fluorescence scan curve is performed to quantify the fluorescence intensity.

The monitoring of the adsorption or desorption to/from the model cell membrane (bilayer vesicles) is performed either using SPR or combined SPR/SPFS. After the adsorption or desorption process, the flow cell is rinsed with buffer, and another scan curve is performed, which can be used as a comparison with the previous scan curve to monitor any change in the optical properties of the surface, and therefore, any changes in thickness, reflectivity and fluorescence.

The sequence of events is repeated for each experimental procedure, unless otherwise stated.

3.2 Surface Preparation & Modification Procedure

In the following section, the preparation and modification techniques used throughout this work are explained and described, from the initial cleaning procedure of the glass up to the self assembly of the monolayers ready for the tethering of bilayer vesicles.

3.2.1 Substrate Preparation

High refractive index glass (SFL6, n = 1.7988, UQG Optics Ltd) is used as the substrate, onto which the gold is thermally evaporated and the subsequent supramolecular layers are attached. Before any modification of the substrate, it is carefully cleaned to remove any contaminants. The glass is sonicated in a 2% Hellmanex® II solution (Hellma GmbH & Co.KG) for fifteen minutes, and then repeatly washed ten times with Milli-Q® ultrapure water (Millipore UK, Ltd) to remove any trace of detergent and contaminants. The glass wafers are then sonicated twice for fifteen minutes in absolute ethanol (Fisher Scientific UK). The cleaned glass slides are then dried in a stream of nitrogen and immediately placed into the UV TipCleaner (BioForce Nanosciences, Inc) for ten minutes, which removes debris and organic contaminants by a combination of UV and ozone. The clean wafers are then placed immediately into the evaporator for further processing.

When used gold substrates are to be cleaned, the metal films are removed by sonicating the gold-glass wavers in a potassium iodide/iodine solution (0.6mmol.dm^{-3} KI and 0.098mmol.dm^{-3} I_2, Sigma Aldrich) for fifteen minutes. The glass wavers are then repeatedly rinsed ten times with Milli-Q® water, and then cleaned as above.

3.2.2 Thermal Evaporation of Metal onto Clean Substrate

Clean glass wavers (25mm x 25mm) are placed onto the carrier in the thermal evaporator (K975x Turbo Evaporator, Emitech Ltd) and centred over the tungsten basket. Approximately 125mg (±1mg) of gold 99.99% (Advent Research Materials Ltd) is rinsed with absolute ethanol and placed into the tungsten basket. The evaporator is brought down to a vacuum of 3x10^{-6} mbar, and then a current of 3-4 amps is passed through the tungsten element for ten minutes to evaporate the gold onto the glass wavers below. The resulting layer of 50nm thermally evaporated gold on high refractive index glass is annealed in a furnace at 500°C for ninety seconds, and then allowed to cool to room temperature before storing in a holder in a nitrogen atmosphere at +5°C.

3.2.3 Self-Assembly Procedure for Construction of Hybrid Lipid Bilayer

As mentioned in section 1.4.1, self-assembly is based on the spontaneous formation of ordered films from solution directly onto a substrate, in this case, gold. This process provides a means of producing highly structured systems, with functional group flexibility which are easy to produce and analyze.

The foundation layer of the Hybrid Lipid Bilayer (HLB) is produced from the chemisorption of a sulphur bearing thiol to the substrate. The gold slides are immersed in a 1mmol.dm^{-3} solution of 1,2-Dipalmitoyl-*sn*-Glycero-3-phosphothioethanol (DPPTE, Avanti Polar Lipid, Inc) (See Figure 3.12) in chloroform for over 16hours at room temperature, to ensure the formation of a densely packed and highly ordered monolayer. The strong specific interaction between the sulphur-bearing thiol and the gold induces spontaneous assembly at the interface. Experimentally, it has been shown that the monolayer reaches its equilibrium at around 1000minutes [3].

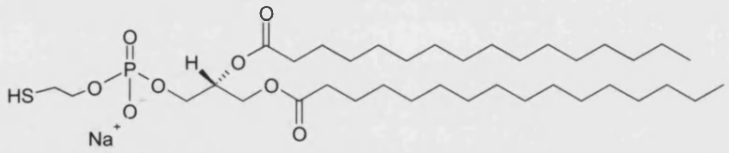

Figure 3.12 Schematic of DPPTE (16:0), which chemisorbs to the gold substrate

The monolayer coated slides are rinsed with absolute ethanol to remove any non-specifically adsorbed thiol molecules and then dried under a stream of nitrogen before being assembled into the flow cell set-up (Figure 3.3), and mounted into the spectrometer to follow the subsequent layer formations.

The upper leaflet of the HLB is composed of a biotinylated lipid mixed with a natural lecithin. 0.4mg.mL^{-1} egg lecithin Grade I (Egg PC, Avanti Polar Lipid, Inc) dissolved in 2:1 (v/v) chloroform:methanol is mixed with 1%mol 1,2-Dipalmitoyl-*sn*-Glycero-3-phosphoethanolamine-N-(cap Biotinyl) (DPPE-biotin, Avanti Polar Lipid, Inc). The solvent is removed from the dissolved lipid mixture with a stream of nitrogen, and put under vacuum over night to ensure all traces of solvent have been evaporated and to prevent oxidative damage to the phospholipids. After removal of the solvent, the lipid film is rehydrated in HEPES pH7.4 buffer (10 mmol.dm^{-3} HEPES 99%, 150 mmol.dm^{-3} sodium chloride 99.5%, 2 mmol.dm^{-3} calcium chloride dihydrate 99%, all reagents from Sigma

Aldrich, in MilliQ water), to give a final Egg PC concentration of 0.4mg.mL^{-1}. The hydrated suspension is vortexed vigorously for 10 minutes to produce multilamellar vesicles. These vesicles are extruded eleven times using a manual LiposoFast extruder (Avestin Europe GmbH) and a 100nm pore diameter polycarbonate membrane to shape the multilamellar vesicles into uniformly spherical small unilamellar vesicles (SUV) of 100nm diameter. The vesicles are then allowed to sit for thirty minutes before use to allow the vesicles to stabilize. The Egg PC vesicles are introduced into the flow cell and the binding of the vesicles is monitored with SPS overnight to allow the binding, fusion and reorientation of the vesicles to the foundation monolayer (Figure 3.13). This ensures that the head groups are orientated towards the aqueous environment. The flow cell is subsequently rinsed with fresh buffer to displace any non-specifically bound analyte from the surface.

The self assembled hybrid bilayer can then be used to tether bilayer vesicles via biotin/streptavidin conjugation.

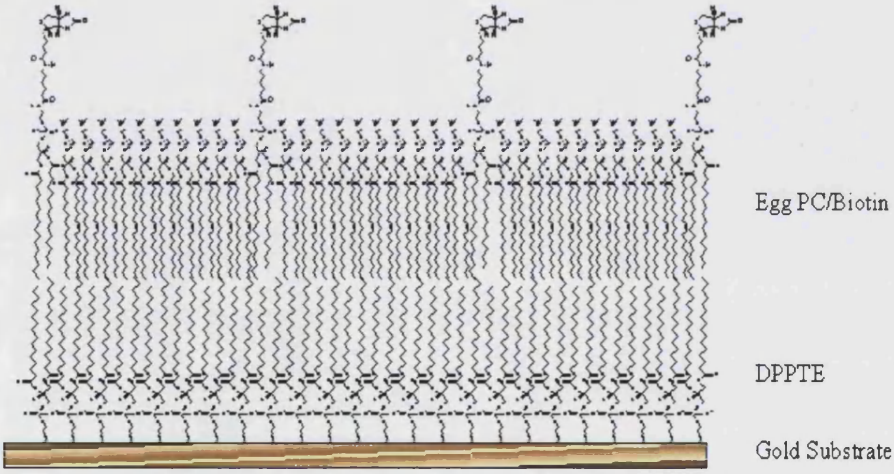

Figure 3.13 Schematic of the Hybrid Lipid Bilayer (HLB) attached to the gold substrate, in preparation for the attachment of bilayer vesicles via biotin/streptavidin conjugation.

3.2.4 Self-Assembly Procedure for Construction of Biotinylated-Thiol:Thiol-Alcohol Monolayer

The second procedure for the modification of the gold substrate for the tethering of bilayer vesicles is the construction of a biotinylated-thiol SAM. 11-mercaptoundecanoic-(8-biotinoylamido-3,6-dioxaoctyl)amide (Figure 3.14), known throughout this thesis as biotin-thiol, is custom synthesized at the University of Bath, using a modification of the procedure published by Bushby *et al* [4].

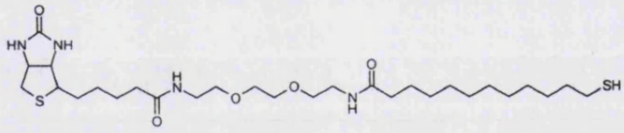

Figure 3.14 11-mercaptoundecanoic-(8-biotinoylamido-3,6-dioxaoctyl)amide

The biotin-thiol is dissolved in absolute ethanol to a 1mmol.dm^{-3} stock solution, where it is stored at -20°C until use. A 1mmol.dm^{-3} stock solution of 11-mercapto-1-unadecanol (Figure 3.15) in absolute ethanol is also prepared and store at -20°C until use.

Figure 3.15 Hydroxyl spacer, 11-mercapto-1-unadecanol, used to control the proportion of biotin-thiol linker molecule expressed on the surface of the gold substrate.

The gold slides are immersed in a mixed ethanolic solution of 0.05mmol.dm^{-3} biotin-thiol and 0.95mmol.dm^{-3} 11-mercapto-1-unadecanol, and allowed to self-assemble onto the gold substrate for over 16 hours to ensure maximum surface coverage and optimum orientation of the thiols (Figure 3.16). The excess thiols and non-specifically adsorbed thiols are rinsed away with absolute ethanol and dried under nitrogen before being assembled as part of the flow cell.

The self assembled thiol monolayer can then be used to tether bilayer vesicles via biotin/streptavidin conjugation

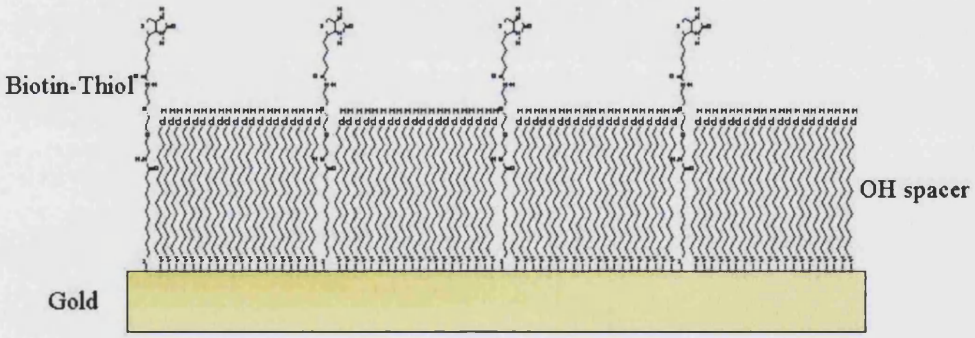

Figure 3.16 Schematic of the self-assembly of 0.05mmol.dm^{-3} 11-mercaptoundecanoic-(8-biotinoylamido-3,6-dioxaoctyl)amide and 0.95mmol.dm^{-3} 11-mercapto-1-unadecanol hydroxyl spacer.

3.3 Preparation of Bilayer Vesicles

The use of bilayer vesicles as model membrane systems provides an attractive model system because they allow a means of stringently controlling the composition of the bilayer vesicles and the extrinsic environment used to study their behaviour. They can have a very simple composition to study specific events or can be more complex to mimic the composition of cell membranes. Small unilamellar vesicles are usually produced in one of two ways: either by sonication or extrusion of the phospholipid suspension.

3.3.1 Preparation of 1,2-Dimyristoyl-sn-Glycero-3-Phosphocholine vesicles

A 4mg.mL^{-1} stock solution of 1,2-Dimyristoyl-sn-Glycero-3-Phosphocholine (DMPC, Avanti Polar Lipid, Inc) dissolved in 2:1 (v/v) chloroform:methanol is prepared, and kept at -20°C until use. 100µL of the 4mg.mL^{-1} DMPC stock solution is mixed with 1%mol 1,2-Dipalmitoyl-*sn*-Glycero-3-phosphoethanolamine-N-(cap Biotinyl) (DPPE-biotin, Avanti Polar Lipid, Inc) in a glass vial, and vortexed briefly. The solvent is removed from the dissolved lipid mixture with a stream of nitrogen, and put under vacuum over night to ensure all traces of solvent have been removed and to prevent the oxidative damage of the phospholipids. After removal of the solvent, the lipid film is rehydrated in HEPES pH7.4 buffer (10mmol.dm^{-3} HEPES 99%, 150mmol.dm^{-3} sodium chloride 99.5%, 2mmol.dm^{-3} calcium chloride dihydrate 99%, all reagents from Sigma Aldrich, in MilliQ water), to give a final DMPC concentration of 0.4mg.mL^{-1}. The hydrated suspension is vortexed vigorously for 10minutes to produce multilamellar vesicles. These vesicles are extruded eleven times using a manual LiposoFast extruder (Avestin Europe GmbH) and a 100nm pore diameter polycarbonate membrane to shape the multilamellar vesicles into uniformly spherical small unilamellar vesicles (SUV) of 100nm diameter. The vesicles are then allowed to stand at room temperature for thirty minutes before use to allow the vesicles to stabilize.

3.3.2 Preparation of 1,2-Dimyristoyl-sn-Glycero-3-Phosphocholine: Cholesterol vesicles

A 4mg.mL^{-1} stock solution of cholesterol (95%, Sigma Aldrich) in 2:1(v/v) chloroform:methanol is prepared and kept at -20°C until use. The DMPC vesicles are prepared as above in section 3.3.1, with the addition of 30mol% cholesterol to the glass vial before the removal of the solvent. The inclusion of 30mol% cholesterol into the bilayer vesicles is determined experimentally in results section 4.7.3.1.

3.3.3 Preparation of High Transition Phospholipid Bilayer Vesicles

DMPC has a phase transition temperature of 23°C, meaning the physical state of the lipid is in the disordered liquid crystalline phase at room temperature (20-25°C). Therefore, the hydrocarbon chains are randomly oriented and fluid. 1,2-Dipalmitoyl-*sn*-glcero-3-phosphocholine (DPPC, 99%, Sigma Aldrich) has a phase transition temperature of 41°C, therefore, will be in the ordered gel state at room temperature where the hydrocarbon chains are closely packed.

The phospholipid 1,2-Distearoyl-*sn*-glycero-3-Phosphocholine (DSPC, 99%, Sigma Aldrich) has a phase transition temperature of 45°C, therefore, is also in the ordered gel phase at room temperature. Stock solutions of 4mg.mL^{-1} DPPC and DSPC dissolved in 2:1(v/v) chloroform:methanol are prepared and stored at -20°C until use. In a 2mL glass vial, 0.4mg.mL^{-1} (100µL) of either DSPC or DPPC stock solution is pipetted, with 1mol% biotin. The solution is vortexed briefly, and the solvent removed using a stream of nitrogen. The vial is then placed under vacuum for around 16 hours to remove all traces of solvent. The lipid film is rehydrated in HEPES pH7.4 buffer to give a final lipid concentration of 0.4mg.mL^{-1}. The hydrated suspension is vortexed vigorously for 10minutes to produce multilamellar vesicles. The vesicles are extruded eleven times using a manual LiposoFast extruder (Avestin Europe GmbH) and a 100nm pore diameter polycarbonate membrane. The vesicles are then allowed to stand at room temperature for thirty minutes before use to allow the vesicles to stabilize.

High phase transition temperature vesicles with 48mol% cholesterol are prepared by the addition of 0.192mg.mL^{-1} of either DSPC or DPPC stock solution into a glass vial with 0.192mg.mL^{-1} cholesterol stock solution and 0.04mg.mL^{-1} biotin stock solution. The solution is vortexed briefly, and the solvent removed using a stream of nitrogen. The vial is then placed under vacuum for around 16 hours to remove all traces of solvent. The lipid film was then hydrated and processed as above.

3.3.4 Preparation of Ganglioside (GM1) Bilayer Vesicles

Gangliosides such as GM1 (Figure 3.17) are cell membrane glycosphingolipids, which modulate cell signal transduction events, and are involved in neuronal plasticity and cell membrane repair mechanisms. However, the GM1 cell surface receptor has also been exploited by adventitious prokaryotic species such as *Vibrio cholerae* and *Escherichia coli* as a point of entry for the internalization of their toxins into the cytosol of the eukaryotic cell.

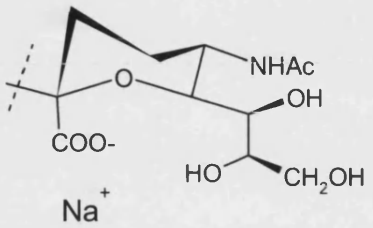

Figure 3.17 Monosialoganglioside GM1.

A stock solution of 4mg.mL^{-1} GM1 ammonium salt from ovine brain (Avanti Polar Lipid, Inc) is prepared in 2:1 (v/v) chloroform:methanol, and stored at -20°C until use. A mixed solution of 2mol% GM1, 1mol% Biotin, 30mol% Cholesterol and 67mol% DMPC is pipetted from the 4mg.mL^{-1} stock solutions into a 2mL glass vial and vortexed briefly. The solvent is evaporated off using a stream of nitrogen and place under vacuum for over 16 hours to remove any residual solvent. The lipid film is hydrated with HEPES buffer pH 7.4 to a final lipid concentration of 0.4mg.mL^{-1} and extruded as detailed previously, and stored at room temperature for thirty minutes before use.

3.3.5 Preparation of Mixed Phospholipid Bilayer Vesicles

A 4mg.ml^{-1} stock solution of 1,2-Dimyristoyl-*sn*-Glycero-3-Phosphotidylcholine (DMPC), 1,2-Dimyristoyl-*sn*-Glycero-3-Phosphotidylethanolamine (DMPE), 1,2- Dimyristoyl -*sn*-Glycero-3-[Phospho- *rac*-(1-glycerol)] (DMPG) and 1,2-Dimyristoyl-sn-Glycero-3-[Phospho-L-Serine] (DMPS) (All from Avanti Polar Lipid, Inc) are dissolved in 2:1(v/v) chloroform:methanol, and kept at -20°C until use. A mixed lipid solution is prepared from the phospholipid stock solutions in the proportions 75% (DMPC) + 20% (DMPE) + 2.5% (DMPG) + 2.5% (DMPS). The lipids are vortexed to ensure a homogenous mixture. In a small glass vial, the mixed phospholipids are mixed with 1mol% biotin, 30mol% cholesterol, and 2mol% GM1 ganglioside. The mixture is vortexed briefly, then prepared as in section 3.3.1.

3.4 Preparation of Protein Solutions and Membrane Binding Agents

All protein solutions are prepared in 10mmol.dm^{-3} HEPES (99%), 150mmol.dm^{-3} sodium chloride (99.5%), 2mmol.dm^{-3} calcium chloride dihydrate (99%) in MilliQ water adjusted to pH 7.4, and referred to HEPES 7.4, unless otherwise stated. HEPES is a zwitterionic buffer, used for many biological studies because it has been shown to be relatively free from side effects [5] and it does not collate metal ions [6]. HEPES has also been shown to protect lipids against peroxidation [7]. The incorporation of sodium chloride into the buffer aids with vesicle stability, but also promotes the adsorption and fusion of the hybrid lipid bilayer [8]. The inclusion of $CaCl_2$ into the buffer promotes tethered vesicle stability, and has been suggested to prevent tethered vesicles from fusing [8].

3.4.1 Streptavidin

A 5μmol.dm^{-3} stock solution of streptavidin from *Streptomyces avidinii* is prepared in HEPES 7.4 and stored at +5°C until use. A 500nmol.dm^{-3} solution is prepared and injected onto the functionalized surface, which binds with great affinity to the biotinylated layer.

3.4.2 Phospholipase A_2

A 3.3x10^{-9}mol.dm^{-3} (39Units/mL - one Unit liberates 1μmol of acid from soybean lecithin per minute at 25°, pH8.9) stock solution of phospholipase A_2 from *Crotalus adamanteus* (PLA_2, Worthington Biochemical. Co) is prepared in HEPES 7.4 and stored at +5°C until use. Dilutions of PLA_2 are made from the stock solution to give final concentrations in the range of 3.3x10^{-8}mol.dm^{-3} to 3.3x10^{-9}mol.dm^{-3} in HEPES 7.4.

3.4.3 Crotalus adamanteus venom

Crotalus adamanteus (Eastern Diamondback Rattle snake, Sigma Aldrich) venom is dissolved in HEPES 7.4 by sonication at a stock solution of 1mg.mL^{-1} and stored at +5°C until use.

3.4.4 Cholera toxin

A 5.745nmol.dm^{-3} stock solution of Cholera αβ-toxin (95%, Sigma Aldrich) from *Vibrio cholerae* in HEPES 7.4 is prepared, and stored at –20°C until use. Working solutions ranging between 0.01149pmol.dm^{-3} to 1.149nmol.dm^{-3} are prepared from the stock solution in HEPES 7.4.

A 21nmol.dm^{-3} stock solution of Cholera β-subunit (95%, Sigma Aldrich) from *Vibrio cholerae* in HEPES 7.4 is prepared and stored at –20°C until use. Working solutions ranging between 42pmol.dm^{-3} - 4.2nmol.dm^{-3} are prepared from the stock solution in HEPES 7.4.

3.4.5 β-amyloid 1-42

A 2mmol.dm^{-3} stock solution of β-amyloid 1-42 (Ultra pure, TFA, rPeptide) in DMSO is prepared, sonicated for thirty minutes and stored at –20°C until use. Working concentrations ranging between 0.1-10μmol.dm^{-3} are prepared from the stock solution in HEPES 7.4

3.5 Preparation of fluorophores

Fluorophores are highly photosensitive and prone to photobleaching, therefore, prepared fluorophores are kept at –20°C in the dark.

3.5.1 BODIPY 650/665-X STP ester

A 1 mmol.dm^{-3} stock solution of 6-(((4,4-difluoro- 5-(2-pyrrolyl) -4-bora-3a,4a- diaza-s-indacene- 3-yl)styryloxy) acetyl) aminohexanoic acid, sulfotetrafluorophenyl ester, sodium salt (Molecular Probes, Invitrogen, Co) is prepared in HEPES 7.4 buffer, and stored at –20°C in the dark until use. Preliminary experiments use a working fluorophore concentration of 100nM, but is subsequently revised to 5μmol.dm^{-3}.

3.6 Preparation of inhibitors

Phospholipase A_2 inhibitors and cholera toxin antagonists are prepared and stored as follows.

3.6.1 Eicosadienoic acid (DEDA)

A 3mmol.dm^{-3} stock solution of 7,7 Dimethyl-(5Z,8Z)-eicosadienoic acid (95%, Sigma Aldrich) in chloroform is prepared and stored at –20°C until use. Working concentrations of the inhibitor are prepared between 3mmol.dm^{-3} and 0.3mmol.dm^{-3}. Experiments using DEDA (Figure 3.18) as a potential antagonist to PLA_2 are prepared by aliquoting the inhibitor into a glass vial and removing the chloroform using a stream of nitrogen. The film is resuspended to the desired concentration in HEPES 7.4. Experiments using the inhibitor as a competitive inhibitor to PLA_2 are prepared by aliquoting the inhibitor into the vesicle/solvent suspension and removing the solvent using a stream of nitrogen. The film is place under vacuum for over 16 hours to remove all the residual solvent. The lipid film is resuspended in HEPES 7.4 to give a final lipid concentration of 0.4mg.mL^{-1} with the desired concentration of DEDA. The suspension is vortex vigorously for 10 minutes to produce multilamellar vesicles, which is subsequently extruded as describe previously in section 3.2.3 to produce small unilamellar vesicles with DEDA incorporated into the vesicle bilayer.

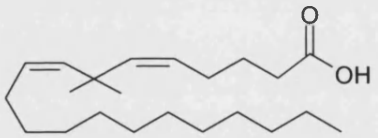

Figure 3.18 Schematic of 7,7-Dimethyl-(5Z,8Z)-eicosadienoic acid

3.6.2 Manoalide

A 6x10^{-8}mol.dm^{-3} stock solution of 4-[3,6-Dihydro-6-hydroxy-5-[4-methyl-6-(2,6,6-trimethyl-1-cyclohexen-1-yl)-3-hexenyl] -2H-pyran-2-yl]- 5-hydroxy-2- (5H) - furanone (Manoalide, 75%, Sigma Aldrich) is dissolved in ethanol and stored at –20°C until use. The PLA_2 inhibitor, manoalide (Figure 3.19) is aliquoted into glass vials to prepare the working concentrations of 6 x 10^{-8}mol.dm^{-3} to 2.4x10^{-9}mol.dm^{-3}. The solvent is removed using a stream of nitrogen and resuspended to the desired working concentration in HEPES 7.4.

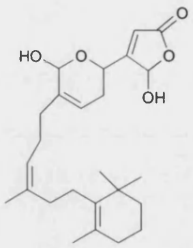

Figure 3.19 Schematic of Manoalide

3.6.3 Europium III chloride

A 100μmol.dm^{-3} solution of europium III chloride anhydrous (99.99%, Sigma Aldrich) in HEPES 7.4 is prepared and stored at +5°C until use. Working solutions of 0.1μmol.dm^{-3} to 100 μmol.dm^{-3} europium III chloride ($EuCl_3$) are prepared in HEPES 7.4 from the stock solution.

3.6.4 Other lanthanide trivalent compounds

100μmol.dm^{-3} solutions of lanthanum III nitrate, terbium III chloride, erbium III chloride, gadolinium III chloride and ytterbium III chloride (99.99%, Sigma Aldrich) in HEPES 7.4 are prepared and stored at +5°C until use. Working solutions of 10μmol.dm^{-3} the lanthanide trivalent compounds are prepared in HEPES 7.4 from the stock solution.

3.7 Preparation of tethered biomimetic membrane vesicle slides for electron microscopy

Lipid vesicle films are rehydrated in HEPES 7.4 to the desired concentration and extruded as mentioned previously in this chapter. The unilamellar vesicles are tethered to the solid support, and after adsorption, the gold coated substrate is removed from the flow cell set-up for fixing and staining for examination under the electron microscope. The tethered vesicle substrates are immersed in a 2% glutaraldehyde solution (25% EM grade, Agar Scientific Ltd) for 30 minutes to fix the specimen. The fixed lipid vesicles are then immersed in a 1% osmium tetraoxide solution (2% solution, Agar Scientific Ltd) for 20 minutes, which acts both as a biological fixative and a stain. After immersion, the substrates are rinsed carefully with HEPE 7.4 and then air dried before examination under the scanning electron microscope.

3.8 Bibliography

1. Rothenhausler, B., C. Duschl, and W. Knoll, *Plasmon Surface Polariton Fields for the Characterization of Thin-Films.* Thin Solid Films, 1988. **159**: p. 323-330.
2. Scheller, A., *Windows-plasmon Steuresoftware version 2.60, Max-Planck-Institut fur Polymerforshung: Mainz.* 2003.
3. Bain, C.D., et al., *Formation of Monolayer Films by the Spontaneous Assembly of Organic Thiols from Solution onto Gold.* Journal of the American Chemical Society, 1989. **111**(1): p. 321-335.
4. Booth, C., et al., *Synthesis of novel biotin anchors.* Tetrahedron, 2001. **57**(49): p. 9859-9866.
5. Stoll, V.S. and J.S. Blanchard, *Buffers - Principles and Practice.* Methods in Enzymology, 1990. **182**: p. 24-38.
6. Vasconcelos, M.T.S.D., M.A.G.O. Azenha, and O.M. Lage, *Electrochemical Evidence of Surfactant Activity of the Hepes pH Buffer Which May Have Implications on Trace Metal Availability to Culturesin Vitro.* Analytical Biochemistry, 1996. **241**(2): p. 248-253.
7. Grit, M. and D.J.A. Crommelin, *Chemical stability of liposomes: Implications for their physical stability.* Chemistry and Physics of Lipids, 1993. **64**(1-3): p. 3-18.
8. Kalb, E., S. Frey, and L.K. Tamm, *Formation of Supported Planar Bilayers by Fusion of Vesicles to Supported Phospholipid Monolayers.* Biochimica Et Biophysica Acta, 1992. **1103**(2): p. 307-316.

4.0 Solid Supported Lipid Bilayer Vesicles: Method to Study Membrane Permeation & Lysis

The immobilization of cell membrane models to a surface provides a means of studying simple ligand-analyte interactions involving the cell surfaces using a range of surface sensitive techniques that would otherwise be unavailable for their characterization and observation. A detailed description of the functionalized surface and its application in studying membrane permeation processes caused by lipases is presented. The binding constants for the construction of the surface and membrane permeation processes are also detailed.

Chapter Synopsis

Biological membranes are very diverse and contain a huge assortment of macromolecules. However, it can be difficult to study these membranes and/or events that occur at these surfaces in detail. Therefore, a simple and reliable artificial cell membrane model has been developed. Preliminary measurements regarding the construction of these biomimetic membranes will be discussed. Attention will be focused on the effects that snake venom and phospholipase A_2 has on these biomimetic membrane models and the determination of binding constants. Optimization of the biomimetic membrane vesicles will be performed to ensure a stable system to monitor these binding events, and includes the development of a simple theoretical model to determine the diffusion constant for the movement of solutes from the cytoplasmic face to the extracellular face of the membrane. Finally, the inhibition of these lipolytic toxins will be detailed.

4.1 Construction of the Hybrid Lipid Bilayer Surface

1,2-Dipalmitoyl-*sn*-Glycero-3-Phosphothioethanol (DPPTE) was self-assembled from solution onto a thin metal-film. The assembly of this layer was not followed spectroscopically because self-assembled monolayer (SAM) coated slides must be rinsed and dried thoroughly before the addition of the subsequent biological layers. A small amount of solvent can cause defects in the SAM. Therefore, the most reliable method was to form the SAM outside of the spectrometry setup and assemble the flow-cell after the thorough rinsing and drying of the substrate.

The formation of a monolayer is influenced by a number of factors, including temperature, solvent, concentration and chain length of the adsorbent, and the cleanliness of the

substrate. The use of absolute ethanol as the solvent was preferred because of its high purity, low cost, low toxicity and it has a low tendency to incorporate into the monolayer [1]. It has been reported that the initial formation of a monolayer is rapid, and a clean gold substrate immersed in a $1mmol.dm^{-3}$ long-chain alkanethiol solution in ethanol is autophobic, whereby the solvent peels away to leave a dry surface when the substrate is removed from the solvent [1]. Using ellipsometry, it has been proposed that 80-90% of the maximum SAM thickness is reached within the initial few minutes. However, it is followed by a slower period which lasts several hours, and promotes the formation of an organized, well-defined film. The slower phase of additional adsorption and consolidation is believed to involve the displacement of contaminants, expulsion of solvent from the monolayer, and lateral diffusion on the surface to minimize defects [2]. The limiting properties of an alkanethiol SAM are typically reached within 1000 minutes, therefore, the SAM was allowed to reach its limiting properties at room temperature. The shift in the resonance minimum observed after the chemisorption of the SAM to a bare gold-coated substrate (Figure 4.1) was proportional to the layer optical thickness. Providing the refractive index of the adsorbent is know, it was possible to determine the thickness of the adsorbed material. It was shown that the SPR signal correlates to the absolute surface concentration, and a surface concentration correlation ($\Delta\theta/\sigma$) for this SPR system was equal to 0.1868^{o} $(ng.mm^{-2})^{-1}$ [3]. Moreover, the adsorption of biological molecules can then be determined from the empirical relationship between the shift in resonance minimum, $\Delta\theta$, and the surface concentration correlation, $\Delta\theta/\sigma$:

$$Adsorption(A) = \frac{\Delta\theta}{\Delta\theta/\sigma}(ng.mm^{-2}) \qquad \textbf{4.1}$$

The correlation applies for commonly used biological molecules, since they have similar refractive indices and do not differ considerably with respect to their SPR response [4]. The SAM was quantitatively determined from the shift in resonance angle after the adsorption of the monolayer to the bare gold substrate (Figure 4.1).

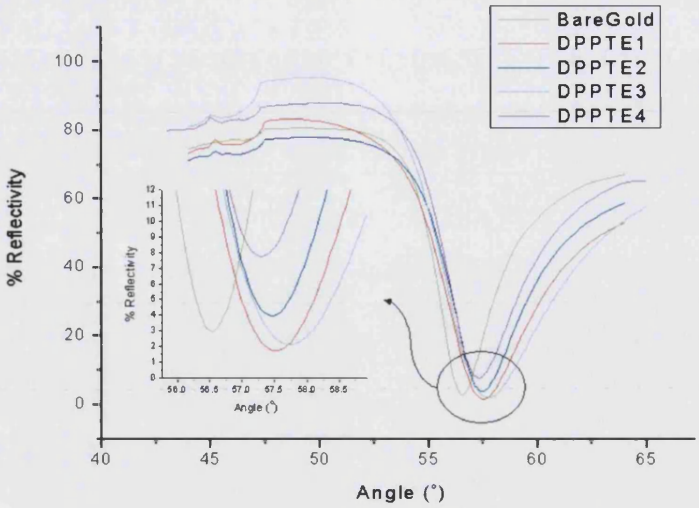

Figure 4.1 Scan curves for the formation of several DPPTE SAM on thin gold-coated substrates.

A 0.94° shift in resonance minimum was observed upon the adsorption of an average DPPTE monolayer on the gold substrate, which equated to the adsorption of 5.04ng.mm^{-2} (*standard deviation* ±0.8) mass to the surface. The subsequent formation of the supramolecular layers was followed spectroscopically using SPR.

5x10^{-4}mol.dm^{3} egg phosphatidylcholine (egg PC) + 1mol% biotin vesicles were added to the DPPTE SAM layer and allowed to bind, rupture and fuse for 1000minutes to form a biotinylated hybrid lipid bilayer (HLB) (Figure 4.2) This resulted in the production of a biological matrix to which biomimetic membrane vesicles were tethered.

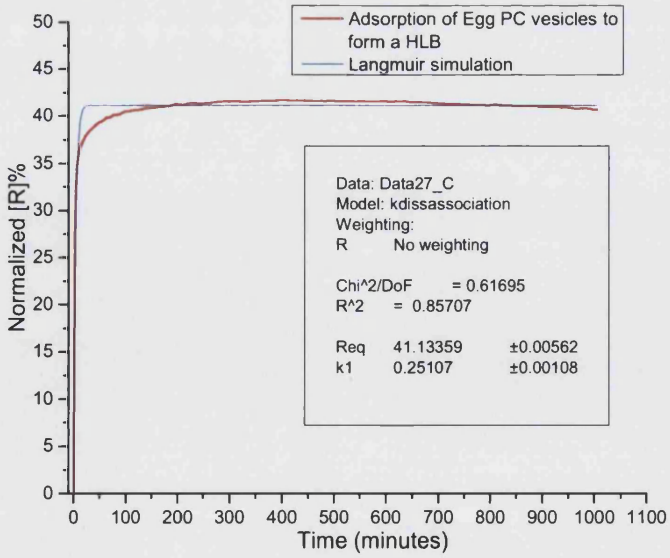

Figure 4.2 The binding kinetics of Egg PC vesicles, forming the upper leaflet of the HLB on the gold-coated substrate. The Langmuir simulation is highlighted.

The hydrophobic residues that terminate the DPPTE SAM causes a single egg PC monolayer to form via the delamination of the egg PC bilayer vesicles (as discussed in chapter 1.4.2). The formation of the egg PC SAM followed a typical Langmuir isotherm. Here, the upper leaflet formed via a two-step mechanism, with around 90% of the total mass adsorbed during the initial fast step. The remaining adsorption occurred during the subsequent slower step, where further lipids adsorb and laterally diffuse to create a well-packed upper leaflet. There was an observable overshoot in egg PC binding as the system attempts to reach equilibrium. During this time, there was more adsorbent bound to the surface than there was at equilibrium because there was a time delay before desorption commenced to reach a state of equilibrium [5]. The association rate constant, k_{on}, and the dissociation rate constant, k_{off}, were 345.66mol^{-1}.Ls^{-1} and 0.07827s^{-1} respectively for the addition of the egg PC vesicles. Further analysis enabled the quantitative determination of the equilibrium binding constant, K_D, to be 2.26x10^{-4}mol.dm^{-3}, which was relatively weak compared to many biological analyte-ligand interactions.

The adsorption of the egg PC monolayer to the DPPTE lower SAM leaflet showed a typical increase in mass at the surface of around 13.65 ng.mm^2, as a result of a 2.55° shift in the resonance minimum (Figure 4.3).

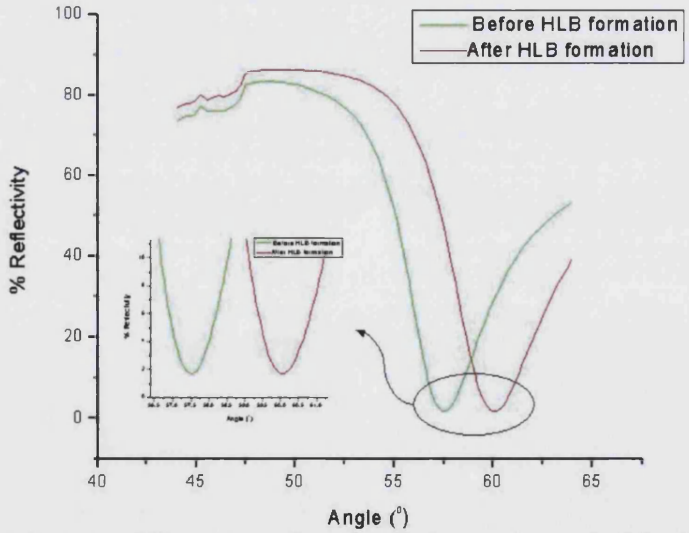

Figure 4.3 Resonance shift upon the formation of a standard HLB of egg phosphatidylcholine on a DPPTE SAM.

The formation of the biotinylated support layer allowed for streptavidin-biotin conjugation chemistry to be employed to act as a capture for biotinylated biomimetic membrane vesicles. The high affinity between streptavidin and biotin ensured a quick and tight

association. The complex formation between the streptavidin and biotin occurs though a series of non-covalent interactions. The high affinity interaction is the result of multiple van der Waals and hydrogen bonds which causes the ordering of surface polypeptide loops to bury the biotin into the streptavidin interior [6]. The mass adsorption of streptavidin to the functionalized surface was calculated to be in the region of 2.94ng.mm^{-2} (Figure 4.4). This was in good agreement with work carried out by Vareiro, who observed a streptavidin adsorption of 2.54ng.mm^{-2} to a mixed thiol SAM [7]. The number of streptavidin molecules bound to the biotinylated support system was estimated assuming a mass of one streptavidin molecules was equal to 9.97x10^{-20}grams (i.e. 60000 MW/6.02 x 10^{23}), therefore, the number of streptavidin molecules bound to the surface was 2.95x10^{19}mm^{-2} (*i.e.* 2.94ng.mm^{-2}/9.97 x10^{-20} grams).

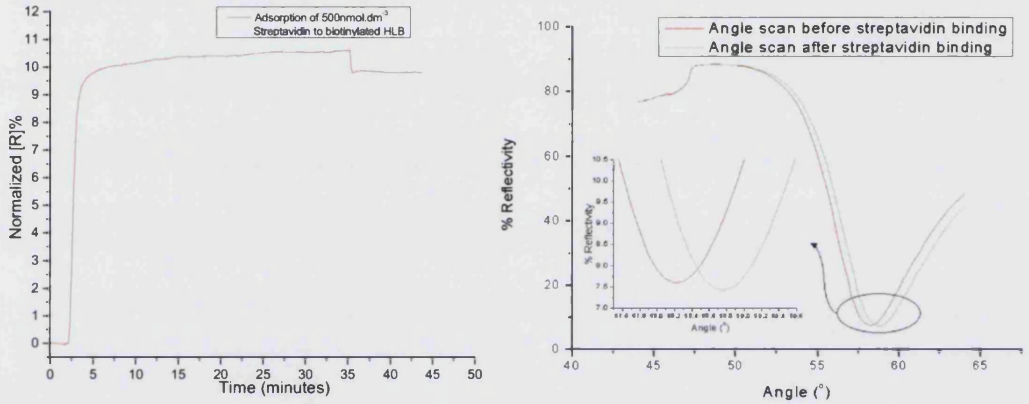

Figure 4.4 Adsorption of 500nmol.dm^{-3} streptavidin to the biotinylated HLB, and scan curves before and after streptavidin adsorption.

Biomimetic membrane vesicles, comprising 1% biotin and 99% DMPC were prepared and adsorbed to the functionalized surface. The tethering of the vesicles to the substrate surface occurred through the biotin-streptavidin coupling, and was monitored as a change in the resonance minimum (Figure 4.5).

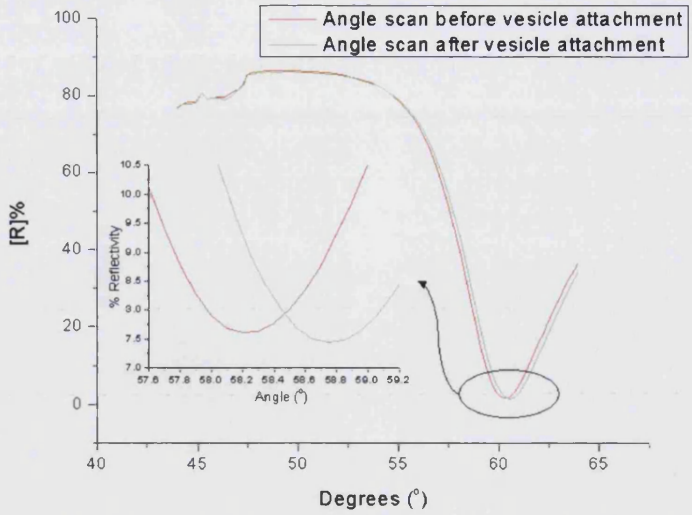

Figure 4.5 Shift in resonance minimum upon biomimetic membrane vesicle adsorption to the functionalized surfaces.

The shift in resonance minimum resulted in a 1.07ng.mm^{-2} increase in mass at the surface. The attachment of the bilayer lipid vesicles completed the construction of the functionalized surface, and is schematized in Figure 4.6. The binding of specific adlayers was quantitatively determined, along with the maximum expected response.

The tethered vesicles were produced by a physical preparatory method that ensured the homogeneity of the vesicle population. Therefore, the dimensions of the vesicle were; outer diameter =100nm (determined by the polycarbonate membrane pore diameter), internal diameter =90nm, and membrane thickness =5nm [8]. Moreover, it was possible to determine the total number of lipids comprising a single vesicle, 95000 lipids.vesicle^{-1}. The weight of a single vesicle was 1.07x10^{-16}g. The maximum theoretical response for vesicle attachment would be 2.95x10^{20} mm^{-2} (*i.e.* the number of streptavidin molecules bound to the biotinylated support system). However, because the vesicles were 100nm in diameter, it was only possible for a maximum of 1x10^{8}vesicles.mm^{-2} to attach. The observed resonance shift for the attachment of the bilayer vesicles was 0.5°, which equated to the adsorption of 1.07ng.mm^{-2} mass at the surface. Therefore, the observed number of vesicles which bound to the surface was around 1x10^{7} vesicles.mm^{-2}.

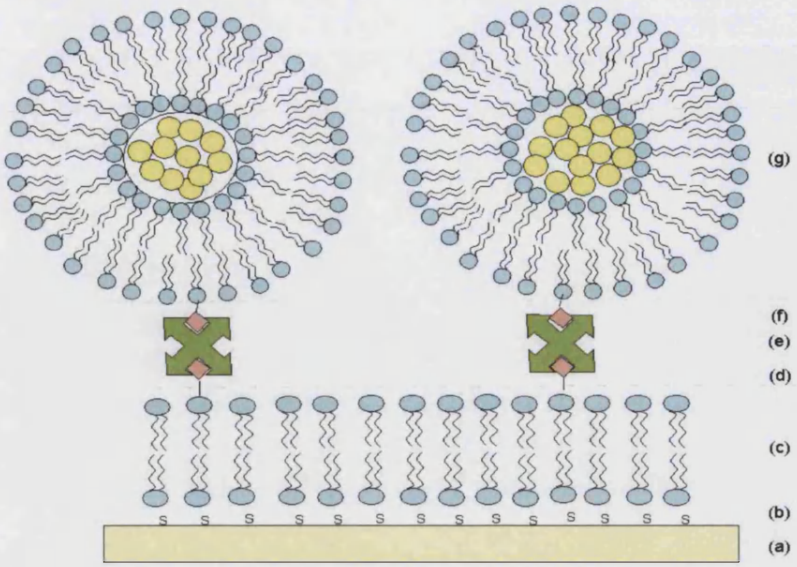

Figure 4.6 Schematic representation of the HLB solid supported model cell membrane vesicles. (a) 50nm thin metal film-coated substrate, (b) 1,2-dipalmitoyl-sn-glycero-3-phosphothioethanol (DPPTE) thiol chemisorbed SAM, (c) egg-phosphatidylcholine mixed with (d) 1 mol% dipalmitoyl-phosphoethanolamine-N-biotinyl (DPPE-biotin) SAM forming the HLB, (e) Streptavidin, (f) 1 mol% DPPE-biotin incorporated into (g) 1,2-dimyristoyl-phosphtidylcholine(DMPC) artificial cell membranes.

The results obtained for the binding of the biological adlayers to the gold substrate are summarized in Figure 4.7.

Adlayer	*Resonance angle shift ($\Delta\theta$)*	*Mass adsorption ($ng.mm^{-2}$)*	*Number of molecules adsorbed (mm^{-2})*
DPPTE	0.94 °	5.04	4.17×10^{12} DPPTE molecules
Egg PC	2.55 °	13.65	1.14×10^{8} vesicles
Streptavidin	0.55 °	2.94	2.95×10^{20} streptavidins
Vesicles	0.2 °	1.07	1×10^{7} vesicles

Figure 4.7 Mass adsorption of the adlayers; DPPTE, Egg PC, streptavidin and biomimetic membrane vesicle attachment, with the corresponding number of single molecules/vesicles adsorbed to the surface.

4.2 Scanning Electron Microscopy of the HLB-Tethered Biomimetic Membrane Vesicles

Scanning electron microscopic measurements of the tethered vesicles were made to ensure the vesicles remained intact and to image the lateral spacing of the vesicles on the surface. Measurements were made on a JEOL JSM6480LV scanning electron microscope (SEM), at the Centre for Optical Studies, University of Bath. The HLB solid supported bilayer

vesicles were fixed with 2% glutaraldehyde, followed by staining with 1% osmium tetraoxide, and viewed under low vacuum (Figure 4.8).

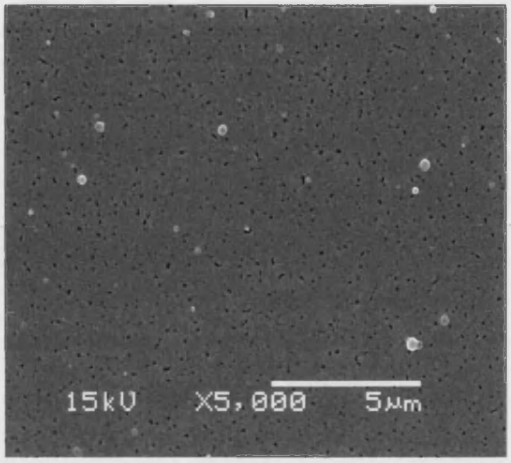

Figure 4.8 Electron micrograph of the HLB-tethered biomimetic membrane vesicles (bright white/grey circles), under low vacuum (magnification = x5,000).

It can be observed that the bilayer vesicles tethered to solid supports using coupling chemistry (vesicles can be seen as lighter spheres on the darker backdrop). The visualization of the tethered vesicles showed intact vesicles on the solid substrate. Decoupling the biotinylated lipid vesicles from the solid surface using the biotin-streptavidin anchors ensured the vesicles did not come into direct contact with the solid surface, and therefore rupture. Observed in the micrograph, are small areas of black colouration in the solid surface (Figure 4.8). These are pin-hole defects caused during the thermal evaporation and annealing of the gold to the glass substrate.

4.3 Preliminary Measurements of the Permeation of Tethered Vesicles Using Surface Plasmon Resonance Spectroscopy

The HLB tethered vesicles system allowed for the real-time monitoring of biological interactions between a crude lipolytic enzyme and the membrane surface using SPR.

4.3.1 Real-time Monitoring of Biomimetic Membrane Vesicle Hydrolysis by Lipolytic Toxins

The production of the stable cell membrane mimic allowed for the real-time monitoring of membrane hydrolysis as a result of toxin-membrane interactions. To ensure permeation was observable using SPR, the constructed surface was immediately followed by the addition of 1mg.ml^{-1} *Crotalus adamanteus* (Eastern Diamondback Rattlesnake) venom (Figure 4.9).

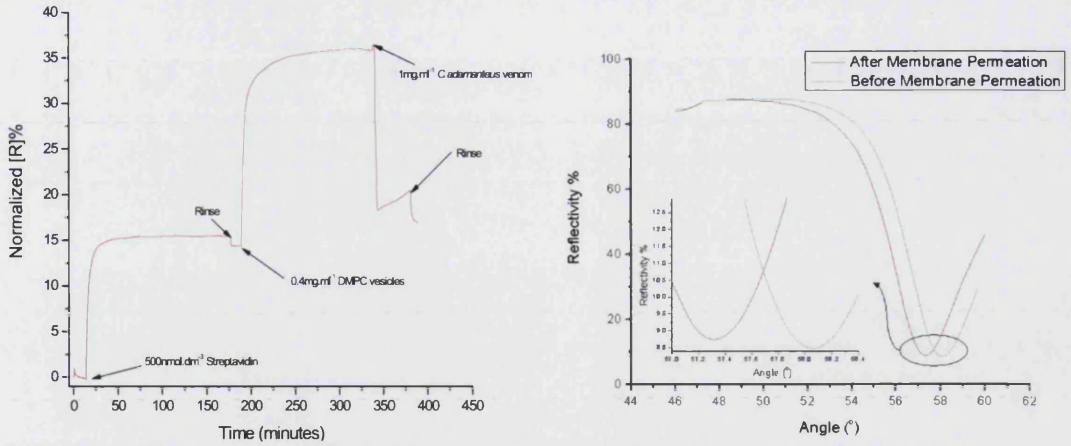

Figure 4.9 Construction of the functionalized surface, and the subsequent lysis of the biomimetic membranes using a lytic peptide (C.adamanteus venom), and the resonance minimum shift for the desorption of mass from the surface as a result of membrane lysis.

The desorption of mass from the surface, as a result of the lytic toxin, caused a 0.75° shift in the resonance minimum, which equated to a 4.0ng.mm^{-2} mass desorption. Therefore, it shows the proof-of-principle that permeation processes were directly observable.

4.3.2 Monitoring Permeation Processes Using SPR and SPFS

The evanescent wave can be used to excite fluorescent molecules within the depth of its field (typically within 200nm of the surface), at the metal/dielectric interface. Therefore, if a fluorescently excitable molecule is present at the interface it can be excited by the energy wave, and an intense fluorescent signal can be observed. Moreover, both reflected light intensity and fluorescence can then be measured simultaneously.

A method to detect permeation processes, as a result of lytic peptides and toxins, using fluorescence was implemented to monitor the flux of dye molecules from the interior aqueous space of the bilayer vesicles into the bulk solution. The aqueous space of the vesicles were loaded with 5μmol.dm^{-3} BODIPY dye, and using the biotin-streptavidin supramolecular support surface, were tethered within the evanescent energy field. As a result of permeation processes, the dye molecules were released from the aqueous space of the biomimetic membranes and diffuse into solution and out of the path of the energy field. Therefore, any dye molecules released as a result of permeation are followed in real-time. The HLB support acts to decouple the fluorescent dye molecules from the surface, because gold is an efficient fluorescence quencher via Fluorescence Resonance Energy Transfer

(FRET). Since FRET is distance dependant, decoupling the dye molecules from the gold surface ensures spatial separation [9].

The biotinylated-SAM-streptavidin matrix was employed to exert spatial control over the fluorophore distance from the surface (*z* direction) and vesicle density (*x-y* direction).

The introduction of the lipolytic venom to the tethered vesicles was followed as a change in mass density at the surface caused by the hydrolysis of the phospholipids, and as a change in fluorescence (Figure 4.10).

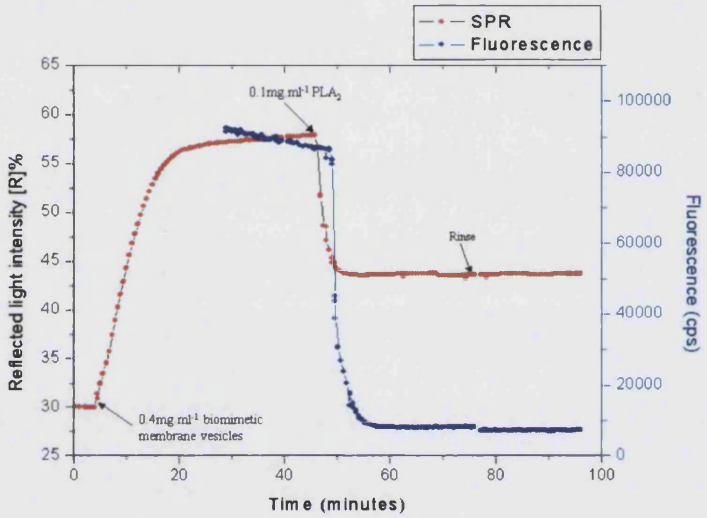

Figure 4.10 Simultaneous monitoring of the change in reflected light intensity (SPR) and the change in fluorescence (SPFS) on the addition of crude PLA_2 (C.adamanteus venom) to the solid supported biomimetic membrane vesicles.

The injection of the lipolytic venom at 45 minutes showed a decrease in detected light intensity as a result of a decrease in mass at the membrane surface. This was subsequently followed, three minutes after the start of vesicle hydrolysis, by a 90.7% decrease in fluorescence over a 10 minute period, which was observed as a 78704 counts per second (cps) decrease in measured fluorescence.

4.4 Measuring the Dose-Response of Lipolytic Peptides on Biomimetic Membrane Vesicles

Direct membrane lysis can be induced by a range of lytic peptides and toxins. This lipolysis can be provoked by purified phospholipase A_2 and crude PLA_2 which is found in various venoms.

4.4.1 Phospholipase A_2

PLA_2 is a lipolytic enzyme that specifically hydrolyzes the *sn*-2 acyl ester bond of phospholipids (Figure 4.11). This hydrolysis liberates a lysophospholipid, causing a change in the membrane fluidity and permeability. However, it can also be converted to a platelet-activating factor which is involved in signalling pathways. The hydrolysis of the phospholipid also liberates a free fatty acid (arachidonate), which modulates ion channels and is a precursor for the production of eicosanoids [10]. Both eicosanoids and platelet-activating factors are key mediators of inflammation. The proposed hydrolytic mechanism primarily involves the polar part of the substrate, *i.e.* the carbonyl oxygen of the ester bond, and occurs through a nucleophilic attack [11].

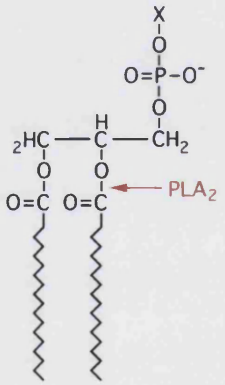

Figure 4.11 The hydrolysis of a phospholipid at the sn-2 acyl ester bond to liberate a lysophospholipid and a free fatty acid

Phospholipases are found in a variety of forms and in a range of biological systems. These enzymes share a common role in the metabolism of phospholipids. At present, there are fourteen different groups of phospholipases (Figure 4.12) characterized according to their structure, molecular weight and substrate preference [12]. Their locations are either grouped as secretory or cytosolic. Type I PLA_2 have a physiological and pathological role in mammals, and have been shown to be present in pancreatic juice for the digestion of phospholipids in food [13]. Moreover, type I pancreatic enzymes contribute to the pathogenic pathway in acute pancreatitis, where it combines with bile salts and contributes

to the development of parenchymal necrosis [14]. The other form of type I PLA_2 is found in snake venoms. The type II PLA_2 have been shown to be constitutively expressed in several tissues, including the spleen, intestine, liver and thymus. This group has been linked to organ related inflammatory responses. Group II PLA_2 have recently been proposed to have a central role in the development of severe acute inflammatory diseases, and its levels have been shown to increase in patients suffering from bacterial infections, sepsis and multiple organ failure [15]. However, this group of PLA_2 has marked antimicrobial properties, and is believed to have a possible role in the innate immune response against pathogens such as *Staphylococcus aureus* [15]. Group II PLA_2 enzymes are distributed in trace amounts in various mammalian tissues naturally, but are found in high levels in inflamed tissues, such as in patients suffering from rheumatoid arthritis and septic shock. There is also a significantly higher tissue level of membrane-associated PLA_2 in breast cancers compared to benign breast tumours or normal breast tissue [16]. The 85kDa group IV and the 14 kDa group II secretory PLA_2 are involved in inflammatory diseases through the metabolism of intracellular arachidonic acid. Group IV PLA_2 are also involved in the development of the allergic reactions and parturitation [17].

Group	Subgroup	Common Source	Size (kDa)	Location	Ca^{2+} requirement
I	A	Cobra, kraits venom	13-15	secreted	$mmol.dm^{-3}$
	B	Porcine/human pancreas	13-15	secreted	$mmol.dm^{-3}$
II	A	Rattlesnake, viper venoms, human synovia, platelets.	13-15	secreted	$mmol.dm^{-3}$
	B	Gaboon viper	13-15	secreted	$mmol.dm^{-3}$
	C	Rat/mice testes	15	secreted	$mmol.dm^{-3}$
III	D, E, F	Mouse, human cells, bee, lizards, scorpions	14-18	secreted	$mmol.dm^{-3}$
IV	A	Human U937 cells, rat kidney	85	cytosolic	$\mu mol.dm^{-3}$
	B	Human pancreas, liver, heart, brain	100	cytosolic	$\mu mol.dm^{-3}$
	C	Human heart, skeletal muscles	65	secreted	none
V		Mammal heart, lung, mast cells, macrophages	14	secreted	$mmol.dm^{-3}$
VI	A-1	$P338D_1$ macrophages, CHO cells	84-85	cytosolic	none
	A-2	Human B-lymphocytes, testis	88-90	cytosolic	none
	B	Human heart, skeletal muscles	88	cytosolic	none
VII	A	Human plasma	45	secreted	none
	B	Bovine brain	40	cytosolic	none
VIII	A	Human brain	26	cytosolic	none
	B	Human brain	26	cytosolic	none
IX		Snail venom	14	secreted	$mmol.dm^{-3}$
X*					
XI	A	Green rice shoots	12.4	cytosolic	none
	B	Green rice shoots	12.9	cytosolic	none
XII*					
XIII*					
XIV*					

** Not sufficiently characterized.*

Figure 4.12 Classification of phospholipase A_2 [18, 19].

PLA_2 has been shown to regulate certain functions in the brain, and modulates the levels of secondary messengers, such as arachidonate, eicosanoids and the platelet-activating factor. It has been postulated that the enzyme plays a role in neurotransmitter release, long-term potentiation (increase in the strength of a chemical synapse), membrane repair, neurodegeneration, apoptosis and ethanol tolerance [20]. PLA_2 role in membrane repair involves the removal of peroxidized phospholipids by reduction and re-esterification, because peroxidized lipids may introduce defects in the membrane and lead to alterations in membrane permeability. However, this repair mechanism may also cause areas of neuronal degradation, because removal of phospholipids from the neurons may lead to loss of essential membrane phospholipids and cause the accumulation of harmful by-products such as free fatty acids. In chronic neurodegenerative disorders, such as Alzheimer's disease, there is abnormal phospholipid metabolism accompanied by elevated activity of PLA_2 [21].

Another major source of PLA_2 enzymes are the venoms of various insects and snakes. As mentioned in section 1.2, these venoms are typically complex mixtures of toxins and peptides that exert an array of deleterious effects including neurotoxicity, myotoxicity, cardiotoxicity and inflammation. They directly lyze the membranes and cause significant necrosis, inflammation and tissue destruction (Figure 4.13). These toxins are typically produced as offensive and defensive mechanisms for the capture of prey, to defend against predation and to initiate digestion.

(Picture source: http://sidewinder78.tripod.com/thesidewinderranchenglish/index.html)

Figure 4.13 Tissue damage, necrosis and inflammation of the leg and foot caused by the envenomation by the Naja kaouthia (Thai cobra) and in the arm caused by the envenomation by the Crotalus atox (Western diamondback rattlesnake) respectively.

Two basic secretory-PLA_2 (s-PLA_2) from *Vipera russelli* and *Trimeresurus flavoviridis* show similar binding affinities and homologies, however, they attack different organs and induce different symptoms [22]. This apparent target specificity observed between the

enzymes and the membrane is better perceived as a specificity for particular phospholipid domains compared to actual membrane targets. It has been shown that these enzymes have a preference for certain phospholipid species; phosphatidylcholine > phosphatidylserine > phosphatidylethanolamine [23]. This preference to phosphatidylcholine probably arose because the extracellular face of membranes are typically rich in this lipid species [24], compared to the cytoplasmic face of the membranes which are richer in aminophospholipids, phosphatidylserine and phosphatidylethanolamine. The specificity results from head group preferences due to the difference in their ability to bind to the lipid interface [25].

Typical peptides found in snake venoms include proteolytic enzymes, collagenase, hyaluronidase, phospholipases, RNase, DNase, phosphodiesterase and acetylcholinesterase [26]. The components of the venoms work synergistically with each other, thereby increasing the potency of the whole venom compared to the individual fractions. These snake venoms tend to be highly stable and resistant to temperature changes, drying and drugs. The snake venom s-PLA_2 are grouped as type I PLA_2 from the *Elapidae* and *Hydrophidae* groups, and type II PLA_2 from *Crotalidae* and *Viperidae* group. The s-PLA_2 all have a similar molecular mass in the range of 14 kDa, and have a similar requirement for millimolar concentrations of Ca^{2+} for the effective hydrolysis of the membranes at an optimum pH of 8.0-9.0 [27]. The levels of PLA_2 in the venoms of the elapine, viprine and crotaline subfamilies has been shown to be statistically indistinguishable, but demonstrate a difference in enzymatic activity [28]. The *Crotalinae* (pit vipers), which include the rattlesnakes, contain venom that causes increased permeability of the capillary membranes, and results in the extravasations of electrolytes, albumin and red cells into the envenomed site. Altered permeability of the red-cell membranes may lead to haemolysis and the necrosis of skeletal muscle fibres.

The requirement for Ca^{2+} as a co-factor has been proposed to mediate the enzymatic reactions at the lipid-aqueous interface and the binding of the substrate [29]. The ion provides two ligation positions, one to lower the activation barrier for hydrolysis and the second to aid substrate binding and correct orientation [30]. The calcium ion orientates and polarizes the carbonyl group of the phospholipid, resulting in a more positive charge on the phospholipids, which favours a nucleophilic attack by the PLA_2 enzyme. The enzymes are capable of hydrolyzing monomeric, micellar and bilayer phase phospholipids, however,

their catalytic activity is significantly increased (up to 10,000-fold) during aggregate hydrolysis [31]. As the substrate of the enzyme reaches its critical micellar concentration (CMC = the surfactant concentration at which micelles form) the enzymatic activity is enhanced (Figure 4.14).

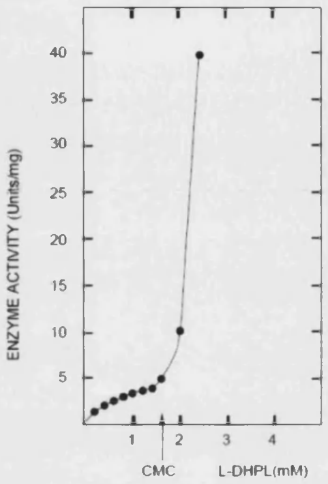

Figure 4.14 Interfacial activation of PLA_2 as a function of phospholipid concentration. Increase in activity upon reaching and exceeding the Critical Micellar Concentration (CMC) [32].

Various models have been proposed concerning the interfacial activation properties of the enzyme. These models include the possibility that the enzyme is held at the interface and the phospholipids diffuse laterally, increasing the rate of hydrolysis [33]. Another suggested model results from the substrate being confined to a preferential conformation, compared to monomeric phospholipids which possess additional conformational and rotational freedom [34]. It has also been suggested that the phospholipids alter conformation at/above the CMC, and 'kinks' appear in the fatty acid chains of the phospholipids [35]. This could cause defects in the bilayers and allow for increased PLA_2 enzymatic activity. Many of these models have be developed using a range of approaches including the application of molecular dynamics [36] to simulate the behaviour of the enzyme with phospholipids in different states of aggregation (Figure 4.15).

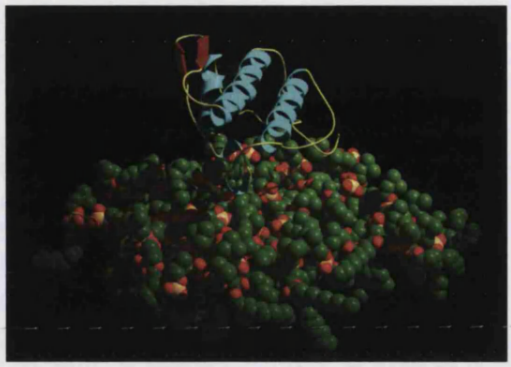

Figure 4.15 Molecular dynamic simulation of the phospholipase A_2 enzyme binding to a disordered lipid bilayer [36].

4.4.2 Crotalus adamanteus venom

There are around 8000 venomous snake bites a year in the USA, which lead to around 10-15 death per annum, and the rattlesnakes causing around two-thirds of these bites [37]. The *C.adamanteus* is the largest rattlesnake, and is reputed to be the most venomous snake in the United States, injecting between 370-720 mg of venom per envenomation [38]. The venom of this snake is particularly toxic, with a calculated lethal dose of LD_{50} =100-150 mg for humans [39]. If an envenomed bite remains untreated there is a 10-20% lethality rate. Localized effects include pain, severe swelling, bruising and blistering. These are typically accompanied by moderate to severe necrosis, myotoxicity and coagulopathy [40]. The venom alters blood fibrinogen, causing an anti-coagulating action, and has a marked proteolytic and lipolytic action. The lipolytic actions of PLA_2 causes an inhibition of blood coagulation because phospholipids typically accelerate clot formation by providing a surface on which the clotting factors interact [41]. The proteolytic and lipolytic enzymes facilitates the digestion of prey, assists the entry of the snake's digestive secretions into the prey, inhibits bacterial activity and therefore reduces the putrefaction of the prey before it can be digested [42].

4.4.3 Catalysis of the Substrate by Phospholipase A_2

The catalytic actions exhibited by the lipolytic enzyme occurs at the lipid-aqueous interface, and is dependant on the chemical structure of the phospholipids and the physical structure of the aggregate formed. It has been observed that most s-PLA_2 can not readily hydrolyze densely packed monolayers and bilayers of zwitterionic phospholipids, because they tend to contain few defects and the fatty acid chains tend to be well aligned and packed. Therefore, it is difficult for the enzyme to gain access to the *sn-2* acyl bonds of the

phospholipids for hydrolysis. The kinetics for substrate hydrolysis typically contains a lag phase (Figure 4.16). The latency period and the slow activation of the enzyme is the period needed for the enzyme to penetrate the aggregate phospholipids and initiate hydrolysis.

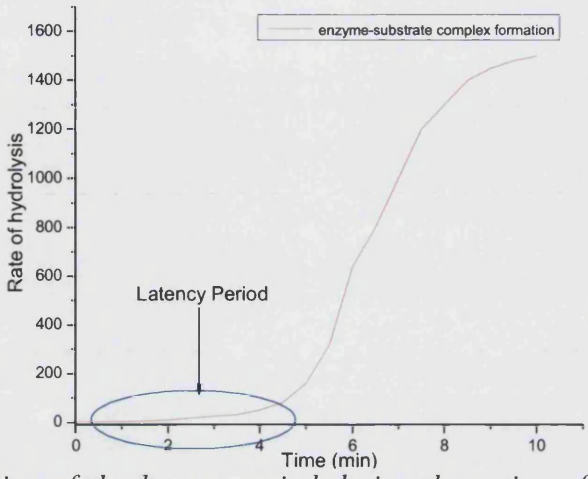

Figure 4.16 Simulation of the latency period during the action of PLA_2 on aggregate phospholipids.

The period of low enzymatic activity is followed by a burst in activity, which is believed to be caused by the accumulation of hydrolysis products (free fatty acid and lysophospholipid) [43]. This causes an alteration in the susceptibility of the phospholipids to degeneration. The duration of the latency period is determined by a number of factors, including substrate concentration, calcium concentration, and the accumulation of hydrolytic products. Defects in the aggregated phospholipids, lipids in the liquid phase, and phospholipids with unequal chain lengths, all promote hydrolysis, and will ultimately decrease the latency period. The initial interfacial binding step is represented as:

$$E + S \underset{\leftarrow}{\rightarrow} E^*S \underset{\leftarrow}{\rightarrow} E^*P \underset{\leftarrow}{\rightarrow} E + P \qquad \textbf{4.2}$$

Where E is the PLA_2 enzyme, S is the substrate, P is the product and E^* is the bound enzyme at the interface. The enzyme in the aqueous phase binds to the phospholipid interface to form a Michaelis complex (E^*S). This undergoes catalytic changes to release the hydrolytic products and follows the dissociation of the enzyme from the interface.

4.4.4 Dose-Response of Lipolysis Induced by Purified-PLA_2

Phospholipase A_2 hydrolyzed the phospholipid vesicles in a concentration dependant manner, and this response can be monitored using SPR. PLA_2 was added to the tethered membrane system and observed for changes in reflectivity and fluorescence (Figure 4.17).

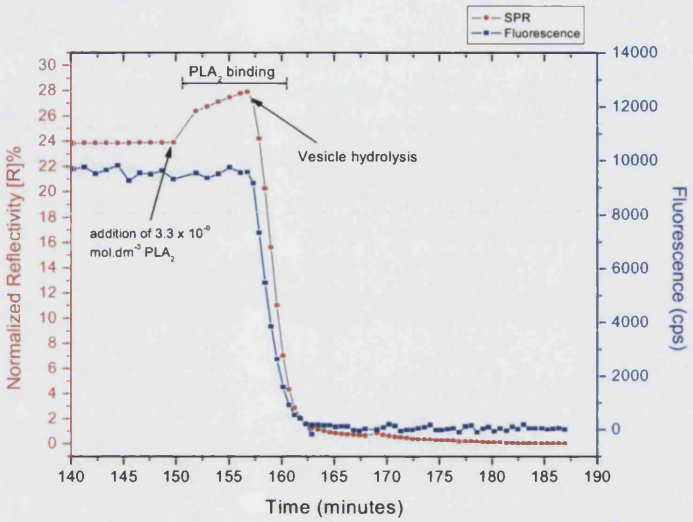

Figure 4.17 Monitoring the change in reflectivity [R]% and fluorescence upon the addition of 3.3 x 10^{-9} mol.dm^{-3} PLA_2. Initial binding of the enzyme is observed before lysis of the vesicle membranes.

The addition of PLA_2 at 150 minutes, showed an initial increase in reflectivity of 3.98 [R]%. This increase in reflectivity equated to the approximate adsorption of 0.7ng.mm^{-2} mass to the membrane surface which was the adsorption of the enzyme to the membrane surface. There was a circa 7 minute latency period from initial enzyme binding to the commencement of vesicle hydrolysis. This was in good agreement with other measurements of vesicle hydrolysis. The Sanchez group observed a circa 8 minute lag period before the accelerated phospholipid hydrolysis [44]. They were also able to visualize the shrinkage of giant unilamellar vesicles (GUVs) as a result of the phospholipid hydrolysis by s-PLA_2 from *Crotalus atrox* (Western diamondback rattlesnake) (Figure 4.18).

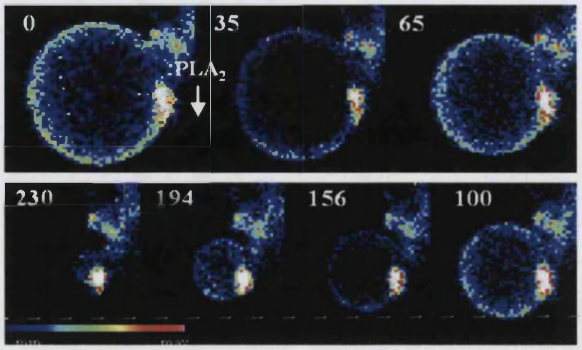

Figure 4.18 PLA_2-dependent shrinking of a DPPC GUV at 53°C, where fluorescence intensity images of LAURDAN-containing vesicles were collected upon the addition of C. atrox $sPLA_2$ [44].

The hydrolysis of the phospholipid vesicles was observed at 157 minutes, where there was a huge rise in membrane hydrolysis, leading to a circa 27.9 [R]% decrease in reflectivity (Figure 4.17). The change in mass density at the surface was observed as a shift in the resonance minima (Figure 4.19) upon the injection of 3.3 x 10^{-9} mol.dm^{-3} PLA_2.

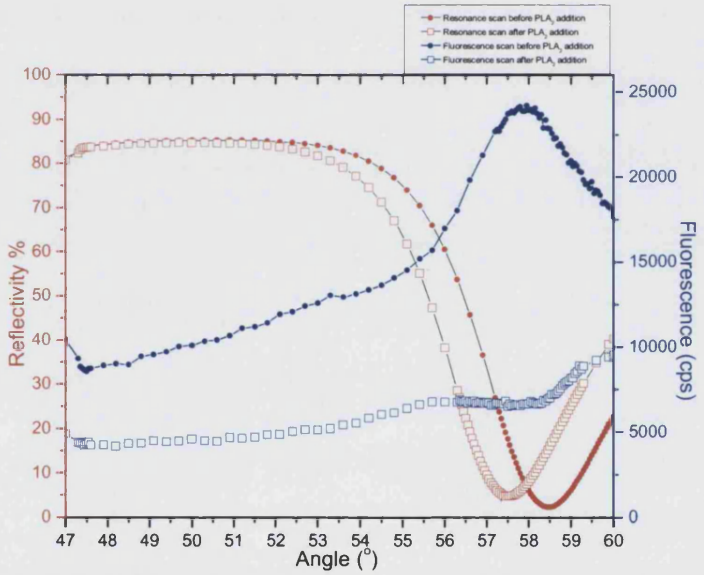

Figure 4.19 Resonance shift and fluorescence intensity of the tethered vesicle system before and after the injection of 3.3 x 10^{-9} mol.dm^{-3} PLA_2.

The 0.95° resonance minimum shift equated to the loss of 5.09ng.mm^{-2} mass from the surface. However, the adsorption of biomimetic vesicles to the support matrix only yielded a 3.0ng.mm^{-2} adsorption of mass to the surface. Therefore, there was a circa 2ng.mm^{-2} mass density deficit in desorbed material, suggesting there was partial hydrolysis of the support matrix. This will be discussed further in section 4.5. The simultaneous monitoring of the fluorescence intensity showed a 73% reduction in fluorescence, with a total decrease

of 17738 counts.second^{-1} over the course of vesicular hydrolysis. The remaining fluorescent signal was background signal.

The hydrolysis of the artificial membrane vesicles showed dose dependency. The dose response for the PLA_2 on the vesicles was performed at varying concentrations between $1.67x10^{-11}$ and $3.3x10^{-9}$ mol.dm^{-3}. The hydrolysis was allowed to reach equilibrium and the normalized change in resonance shift was plotted as a function of enzyme concentration (Figure 4.20).

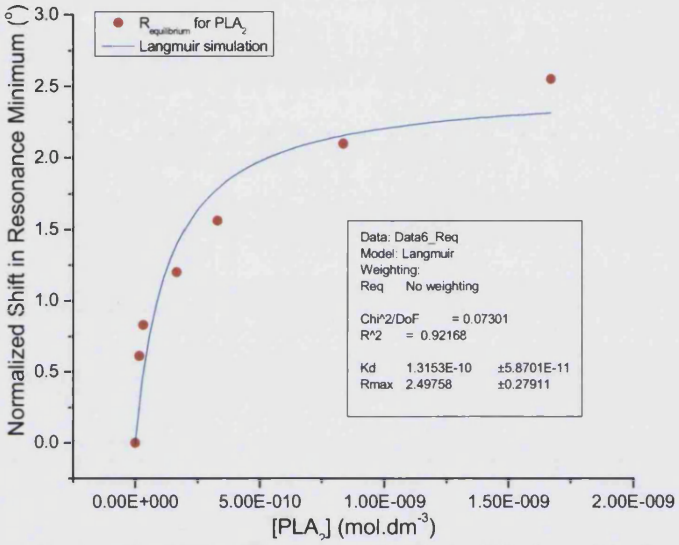

Figure 4.20 Langmuir isotherm for the normalized equilibrium for the resultant loss of mass from the surface as a function of enzyme concentration.

The plot followed a standard Langmuir equilibrium isotherm, where the maximum rate of hydrolysis occurred, R_{max}. Langmuir makes several assumptions:

- All surface sites have the same adsorption energy for the adsorbent.
- Adsorption at one site does not affect the availability of the next site to adsorb.
- Adsorption at one site doesn't affect the energy of adsorption of the neighbouring sites.
- The activity of the adsorbent is directly proportional to its concentration.

The equilibrium dissociation constant, K_D, is an indication of the strength of binding between a ligand and receptor in terms of the ease it takes to separate the complex. K_D is an inverse measure of the affinity of binding between the ligand and its receptor (lower K_D = greater affinity between substrate and ligand). The K_D can be determined as followed:

$$R_{eq} = \frac{R_{max}[P]_{eq}}{K_D + [P]_{eq}} \quad \textbf{(4.3)}$$

Where R_{eq} is the equilibrium value for each reaction, $[P]_{eq}$ is the analyte concentration and R_{max} is the maximum equilibrium response. However, it can be calculated directly from the Langmuir equilibrium plot, because when $R_{eq}=R_{max}/2$, then $[P]_{eq}=K_D$. Therefore, K_D can be directly established from the plot. The calculated K_D was 1.31×10^{-10}mol.dm^{-3}.

4.4.5 Dose-Response of Lipolysis Induced by Crude-PLA$_2$ from Crotalus adamanteus

The secretory PLA$_2$ found in *C.adamanteus* venom works in synergy with a range of other toxic peptides, lytic peptides, co-factors and digestive enzymes. The PLA$_2$ enzyme helps to cause substantial tissue damage and direct membrane lysis to ensure the rapid effect of the venom. Unlike the significant observable binding of the pure-PLA$_2$ to the membrane surface that occurred in Figure 4.18, there was very little increase in reflectivity observed upon the addition of the crude-PLA$_2$ (*C.adamanteus* venom) to the biomimetic membrane vesicles (Figure 4.21).

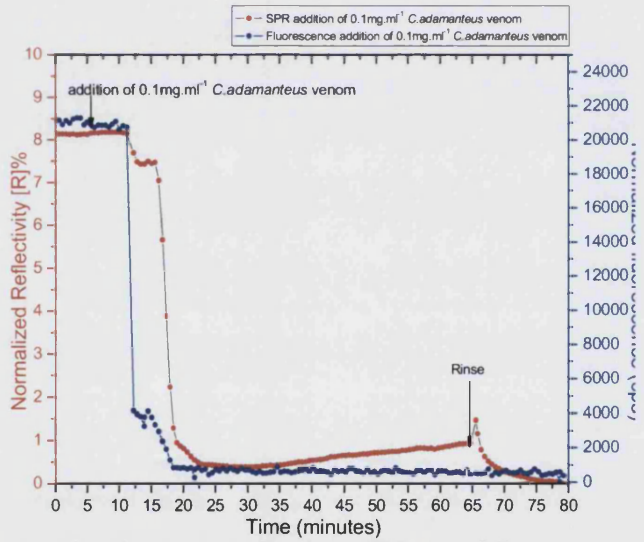

Figure 4.21 Monitoring the change in reflectivity [R]% and fluorescence upon the addition of 0.1mg.ml^{-1} C.adamanteus venom (crude-PLA$_2$). Initial binding of the enzyme is minimal before lysis of the vesicle membranes.

There was a circa 5-6 minute latency period between the addition of the snake venom and an observable change in the mass density and fluorescence intensity at the membrane surface. There was a very small increase in mass density upon addition of the venom to the membrane surface (Δ Reflectivity [R]%=0.05), which equated to a 0.0082ng.mm^{-2} increase in mass. This was a significantly lower increase in adsorption at the membrane surface

compared to that of the purified-PLA_2, which showed a 0.7ng.mm^{-2} adsorption (Figure 4.17).

Hydrolysis was observed at 10 minutes, where there was a circa 8.12 [R]% decrease in reflectivity (Figure 4.21). The change in mass density at the surface was observed as a shift in the resonance minima (Figure 4.22) upon the injection of 0.1mg.ml^{-1} *C.adamanteus* venom.

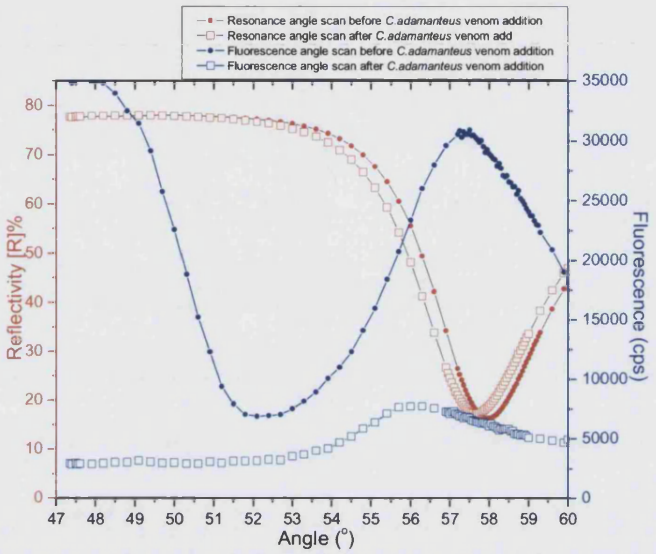

Figure 4.22 Resonance minimum shift and fluorescence intensity of the tethered vesicle system before and after the injection of 0.1mg.ml^{-1} C.adamanteus venom.

The addition of the *C.adamanteus* venom caused a 0.25° shift in resonance minimum. The shift equated to a 1.338ng.mm^{-2} loss of mass from the surface. Moreover, the adsorption of biomimetic vesicles to the support matrix yielded a 0.2° shift in the resonance minimum, equating to the adsorption of 1.07ng.mm^{-2} of mass to the surface. Therefore, there was a 0.27ng.mm^{-2} mass density deficit in desorbed material, suggesting there was partial removal of the support matrix as observed with purified- PLA_2.

The monitoring of fluorescence intensity showed a 75% reduction in fluorescence, with a total decrease of 23175counts.second^{-1} over the course of vesicular hydrolysis. The remaining fluorescence signal was background fluorescence.

The hydrolysis of the artificial membrane vesicles by the crude snake venom showed dose dependency. The dose response for the venom was performed at varying concentrations between 0.1ng.ml^{-1} to 0.1mg.ml^{-1}. The hydrolysis was allowed to reach equilibrium and the

normalized change in resonance minimum was plotted as a function of venom concentration to produce an equilibrium Langmuir plot (Figure 4.23)

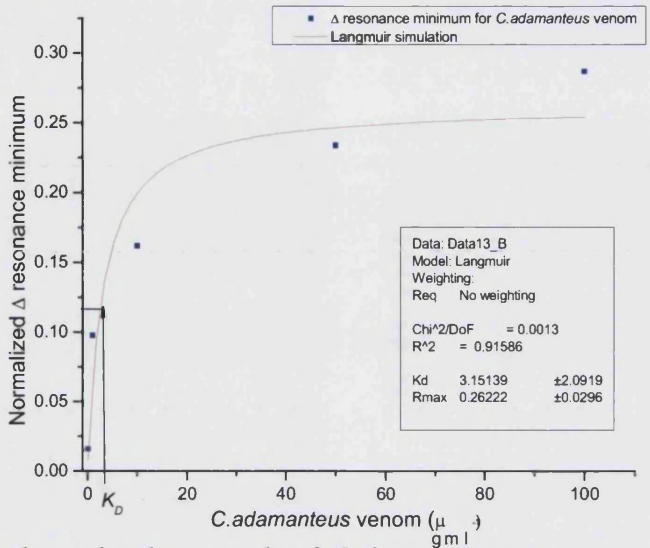

4.23 Langmuir isotherm for the normalized shift in resonance minimum as a function of C.adamanteus venom concentration.

The equilibrium dissociation constant, K_D, for the hydrolysis of the biomimetic membrane vesicles by *C.adamanteus* venom was determined directly from the plot to be 3.15μg.ml^{-1}.

4.5 Optimization of the Supramolecular Surface: Using a Simplified Thiol SAM as the Solid Support System

The desorption deficit observed during the lysis of the tethered biomimetic membrane vesicles (section 4.4.4 and 4.4.5) resulted from the partial hydrolysis of the HLB support. Therefore, an alternative support system was devised to ensure that no hydrolysis of the support occurred.

The partially hydrolyzed HLB support was caused by the presence of *sn-2* ester bonds in the DPPTE self-assembled lower leaflet (Figure 4.24a) and in the egg PC upper leaflet (Figure 4.24b) of the HLB.

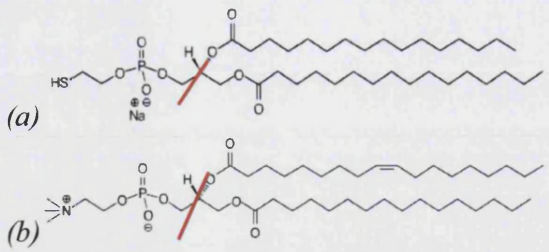

Figure 4.24 (a) Schematic of DPPTE, which chemisorbs to the gold substrate to form the lower leaflet, and (b) egg PC, which self-assembled as a single monolayer to form the upper leaflet of the hybrid lipid bilayer support. (The site of hydrolysis is marked with a red line).

The addition of $3.3x10^{-9}$mol.dm^{-3} PLA_2 to the biotinylated HLB (no biomimetic membrane vesicles attached), showed direct enzyme attachment to the support matrix (Figure 4.25), directly followed by the hydrolysis of the HLB.

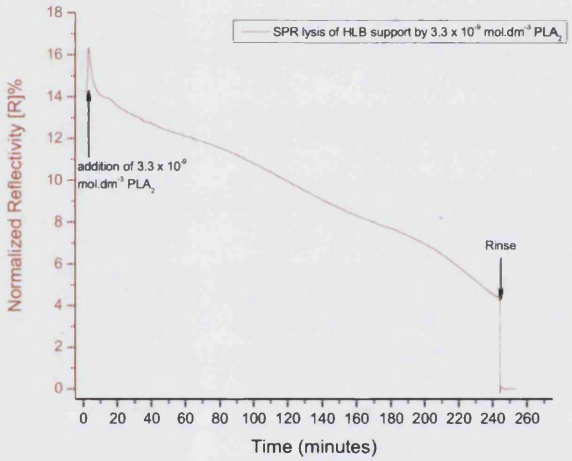

Figure 4.25 Monitoring the change in reflectivity [R]% upon addition of $3.3x10^{-9}$ mol.dm^{-3} PLA_2. Initial binding of the enzyme is observed before hydrolysis of the HLB support matrix.

On addition of the lipolytic enzyme, there was an observable increase of 2.07 [R]% in reflectivity at the membrane surface (Figure 4.25). This equated to a mass increase of 0.62ng.mm^{-2}. Hydrolysis of the supramolecular architecture occurred after a three minute time lag, during which time the enzyme bound to the support system and penetrated the bilayer to gain access to the *sn-2* ester bonds of the lipids. The hydrolysis of the support system did not show the typical membrane lysis of the biomimetic vesicles (Figure 4.10), instead, there was a slower rate of hydrolysis over a much longer period. The lipolysis of the support matrix was quantified by observing the shift in the resonance minimum (Figure 4.26).

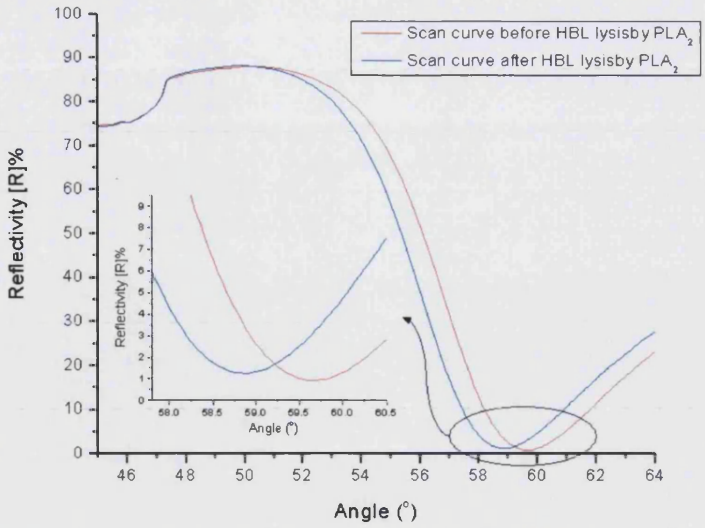

Figure 4.26 Resonance scan curves of the supramolecular HLB support system before and after the injection of 3.3 x 10^{-9} mol.dm^{-3} PLA_2.

There was a 0.8° decrease in the resonance minimum after the addition of the PLA_2 to the supramolecular support matrix, which equated to the desorption of 4.28ng.mm^{-2} mass at the surface. The ability of the PLA_2 enzyme to hydrolyze the supramolecular architecture explains the mass density deficit observed between the adsorption of vesicles and their hydrolysis. The atypical hydrolysis kinetics observed (Figure 4.25), suggests that the HLB is densely packed and relatively defect free, and the ability of the lipolytic enzyme to penetrate thought the densely packed head-groups of the phospholipids was significantly reduced. The slow hydrolysis suggests the enzyme faces a strong barrier against accessing the *sn-2* ester bonds of the HLB support.

4.5.1 Formation of an Alkanethiol Mixed SAM as an Alternative Support Matrix

The phospholipids containing *sn-2* ester linkages were replaced with alkanethiols. Various groups have used biotinylated thiol systems as anchor systems for forming multilayer films [7, 45, 46]. Long-chain thiols form well-packed, pseudo-crystalline, oriented monolayers on gold, in which all the hydrocarbon chains are in the *trans* conformation and at a 30° tilt from the normal to the surface [1]. However, inclusion of high densities of the anchor thiol causes steric hindrance and also causes the biotinylated vesicles to tether to close together causing inter-vesicle fusion. A homogenous monolayer of a single thiol typically only produces a limited range of properties, however, a greater control over the structure of the monolayer can be established by the co-adsorption of two or more thiols that differ in the nature of the tail group or length of the hydrocarbon chains [47, 48].

Hydroxyalkanethiols can be utilized as dilution reagents to control the density of reactive groups on the surface and to prevent non-specific binding of analytes to the surface. These packing molecules provide hydrophilic regions in between the reactive thiol groups, thereby, maintaining the hydrophilic nature of the surface [49]. The distance from the hydroxyl group of the packing molecule to the terminus of the reactive thiol can be adjusted and optimized to ensure space in the *x, y* and *z* planes for either the inclusion of integral proteins, receptors or large biological entities. The utilization of SAMs has found many applications, including for electrochemical sensing, where deprotonatable adsorbents are self-assembled to form a pH sensor [50]. Another benefit of using alkanethiols is that they interact strongly with the gold surface and form well packed, complete and rugged monolayers. In comparison, lipid monolayers tend to weakly associate with the surface, causing potential variations [51]. Co-adsorption of mixed thiols from solution typically favours the adsorption of thiols with longer chain length, and the monolayer is enriched with the longer chain thiols [52]. The composition of the mixed monolayer on gold parallels, but does not equal the solution composition [53]. Co-adsorption is not random and favours certain thiols, but there is no evidence for the formation of discrete domains of specific thiol clusters [53].

Mixed monolayers of biotin-terminated thiol and 11-mercapto-1-undecanol on gold have been shown to resist non-specific binding. 11-mercaptoundecanoic-(8-biotinoylamido-3,6-dioxaoctyl) amide (Figure 4.27a) does not contain any *sn-2* ester bonds within its chain, therefore, resists PLA_2 induced hydrolysis. 11-mercapto-1-undecanol (Figure 4.27b) was used as a spacer molecule to dilute the concentration of the biotin anchor on the gold substrate surface.

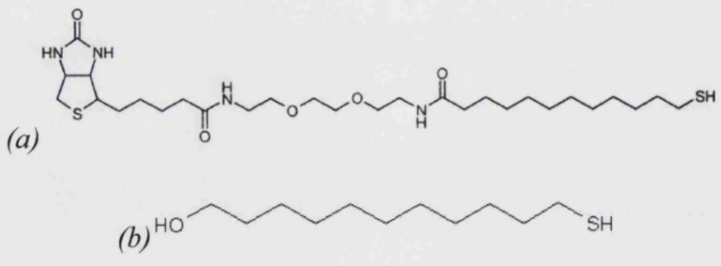

Figure 4.27 (a) Schematic of 11-mercaptoundecanoic-(8-biotinoylamido-3,6-dioxaoctyl) amide, and (b) 11-mercapto-1-undecanol, which acts as a diluent to ensure the capture anchor is optimally spaced.

1mmol.dm^{-3} stock solutions of 11-mercaptoundecanoic-(8-biotinoylamido-3,6-dioxaoctyl) amide, from here known as biotin-thiol, and 11-mercapto-1-undecanol, from here know as OH spacer, were dissolved in an appropriate solvent. Absolute ethanol was used as it dissolves most thiols and can be obtained at high purity in large quantities. The self-assembly of the mixed thiols on gold ensures a non-lipolyzed support for the tethering of the biomimetic membrane vesicles. To ensure the biotin-thiol support matrix did not succumb to hydrolysis, the support system was exposed to PLA_2, and the interaction was monitored by SPR (Figure 4.28a).

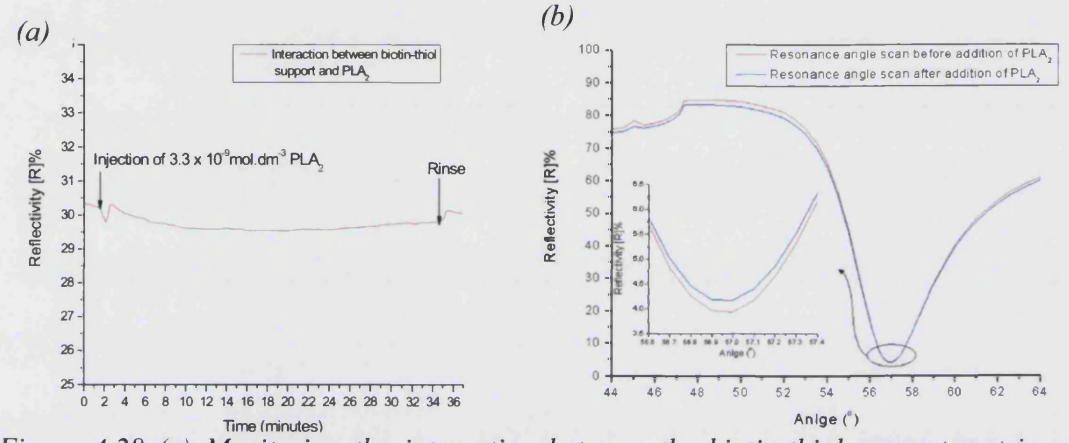

Figure 4.28 (a) Monitoring the interaction between the biotin-thiol support matrix and phospholipase A_2 enzyme. (b) Resonance minimum shift upon addition of PLA_2 to the biotin-thiol support.

It can be observed that hydrolysis of the biotin-thiol support matrix did not occur. Moreover, there was no adsorption of the PLA_2 to the membrane surface, as observed between PLA_2 and the HLB (Figure 4.25). This was because the thiol molecules did not contain ester linkages, therefore, could not be hydrolyzed by the lipolytic peptides. This was confirmed by the shift in resonance minimum (Figure 4.28b). No shift was observed, therefore, the biotinylated support layer provided an inert support in terms of resistance to hydrolysis, and is schematized in Figure 4.29.

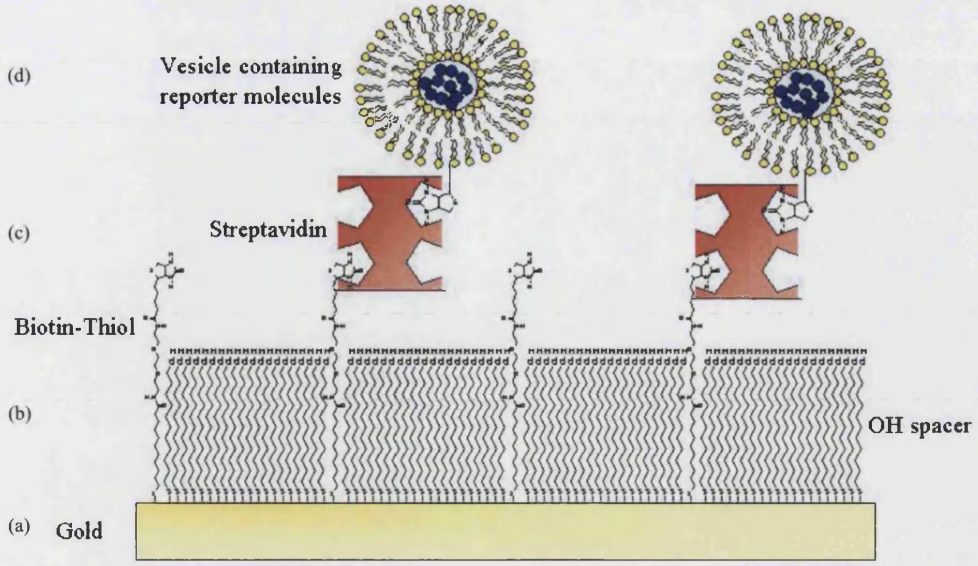

Figure 4.29 Schematic representation of the Biotin-Thiol: OH spacer SAM solid supported model cell membrane vesicles. (a) 50nm thin metal film-coated substrate, (b) 11-mercaptoundecanoic-(8-biotinoylamido-3,6-dioxaoctyl) amide and 11-mercapto-1-undecanol chemisorbed mixed-SAM, (c) Streptavidin, (d) 1 mol% DPPE-biotin incorporated into (DMPC artificial cell membranes.

4.5.2 Optimization of the Reactive Alkanethiol Concentration on Gold

The optimization of the alkanethiol concentration was performed to ensure the maximal binding of the subsequent supramolecular layers. Various concentrations of the reactive biotin-thiol (0.005 - 0.5mmol.dm^{-3}) were diluted with the lateral OH-spacer determinant (0.995 – 0.5mmol.dm^{-3}) and allowed to self-assemble on a clean gold substrate for over 16 hours to ensure a well packed and dense thiol monolayer. The SAM-gold substrate was assembled into the flow-cell for further processing of the multilayers. Streptavidin (500nmol.dm^{-3}) was added to the flow cell and allowed to bind to the biotin-thiol. Using the biotin-streptavidin coupling chemistry, the biomimetic membrane vesicles were attached to the solid support. These successive steps were monitored and the shift in resonance minimum determined, as summarized for streptavidin (Figure 4.30a) and the biomimetic vesicles (Figure 4.30b).

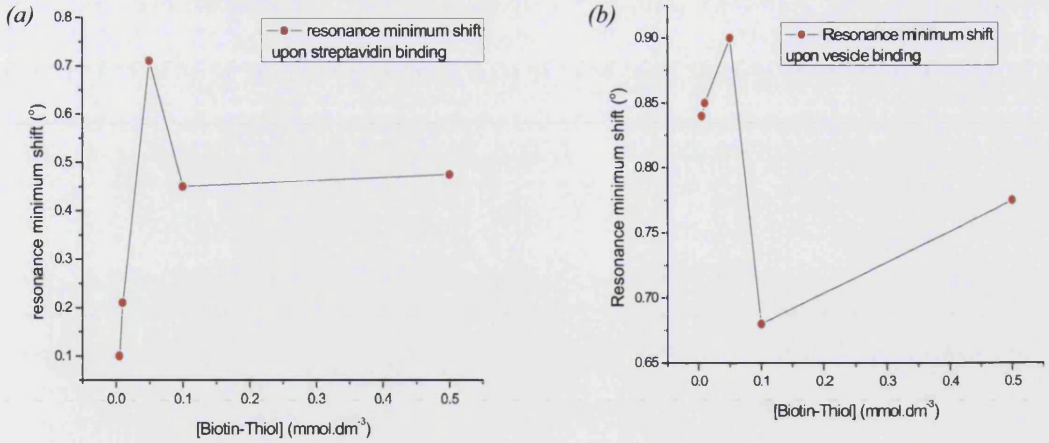

Figure 4.30(a) Correlation between the mole fraction of Biotin-Thiol:OH-spacer and the change in the resonance minimum upon adsorption of 500nmol.dm^{-3} streptavidin and (b) the correlation between the mole fraction of Biotin-Thiol:OH-spacer and the change in the resonance minimum upon adsorption of 0.4mg.ml^{-1} biomimetic vesicles.

At low mole fractions of biotin-thiol (0.005-0.01mmol.dm^{-3}) there was little adsorption of streptavidin to the biotinylated-SAM, however, there was good subsequent vesicle adsorption. The optimum mole fraction of biotin-thiol was 0.05mmol.dm^{-3} diluted in 0.995mmol.dm^{-3} OH-spacer, which ensured maximal streptavidin adsorption and maximal vesicle attachment to the support matrix. At higher biotin-thiol mole fractions (0.1-0.5mmol.dm^{-3}), a decrease in streptavidin binding was observed in comparison to the 0.05mmol.dm^{-3} biotin-thiol SAM. Moreover, there was also a significant reduction in the adsorption of the biomimetic vesicles to the support surface. The decreased tethering capacity was the result of an inaccessibility of the biotin groups caused by steric hindrance and over-crowding of the SAM with the reactive species. High densities of the biotin-thiol caused the vesicles to become too close to one another and vie for space. Tethered vesicles shielded some vacant streptavidin moieties and rendered them inaccessible to other vesicles. The adsorption of the streptavidin and biomimetic membrane vesicles to varying mole fractions of reactive biotin-thiol is summarized in Figure 4.31.

[Biotin-Thiol] ($mmol.dm^{-3}$)	*[OH-spacer] ($mmol.dm^{-3}$)*	*Streptavidin*		*Biomimetic vesicles*	
		Minimum shift (°)	*Mass adsorption ($ng.mm^{-2}$)*	*Minimum shift (°)*	*Mass adsorption ($ng.mm^{-2}$)*
0.5	0.5	0.47	2.54	0.78	4.15
0.1	0.9	0.45	2.4	0.68	3.64
0.05	**0.95**	**0.70**	**3.80**	**0.90**	**4.82**
0.01	0.99	0.21	1.12	0.85	4.55
0.005	0.995	0.22	1.20	0.84	4.50

Figure 4.31 Comparing the resonance shift and equating adsorbed mass of streptavidin and biomimetic vesicle layers onto varying proportions of the biotin-thiol:OH-spacer self-assembled monolayer.

The greatest increase in mass density was observed with the 0.05 mol% anchor molecule. A resonance shift of 0.71° equated to an absorption of 3.80ng.mm^{-2} streptavidin to the surface, and therefore equated to 3.8x10^{19} streptavidin.mm^{-2} (3.80ng.mm^{-2}/9.97 x 10^{-20}). The resonance minimum shift of 0.9° equated to an increase in mass of 4.82ng.mm^{-2} for the adsorption of the biomimetic vesicles. Therefore, there were 4.5x10^{7} vesicles.mm^{-2} attached to the support matrix (molecular weight of a single vesicle ~ 1.07x10^{-16}g).

4.5.3 Gold Surface Oxidative Pre-treatment

The formation of a SAM-gold substrate has advantages over other commonly used metals such as silver and copper, because gold possesses a high degree of chemical inertness. Gold also resists oxidation under ambient conditions, unlike other metals including platinum, titanium and copper, where oxygen chemisorbs by forming O^{2-} ions by electrons donated from the *s* and *p* bands of the metal [54]. Gold contains unusually tightly bound s-valence electrons, therefore, does not readily donate electrons. However, organic molecules can chemisorb to the gold, causing a lowering of the high surface energy characteristic of the metal surface [55]. Moreover, it is consequently vital for the gold substrate to be of high quality and thoroughly cleaned. Contamination of the gold substrate results in poor film quality and may include defects and pinholes.

Common cleaning procedures include exposure to powerful oxidizing agents such as oxygen plasma [56], a mixture of concentrated sulphuric acid and hydrogen peroxide [57], and UV/o-zone[58]. These cleaning procedures have been proven to be efficient in removing organic contaminants, however, they tend to oxidize the gold surface [59]. UV/o-zone cleaned gold films are hydrophilic, while freshly evaporated films tend to be

hydrophobic [60]. Optimum UV/o-zone cleaning of the gold surface is limited to the first 10 minutes of exposure because extended exposure results in CH-, CO-, carbonyl and carboxyl groups contaminating the gold surface [61]. The oxidation of the gold forms thermodynamically unstable compounds which decompose in ambient conditions. If the self-assembly of alkanethiols is carried out on peroxidized gold, the SAM forms a densely packed monolayer which encapsulates the oxide underneath [62]. This gold oxide can be reduced by ethanol [63] prior to formation of the SAM.

The production of a contaminant free gold surface for the self-assembly of alkanethiols occurs by:

$$2Au + 3H_2O - 6e^- \rightarrow Au_2O_3 + 6H^+ \quad \textbf{(4.4)}$$

The reduction of the gold oxide to metallic gold by ethanol occurs by:

$$Au_2O_3 + CH_3CH_2OH \rightarrow 2Au(0) + 3CH_3CH0 + 3H_2O \quad \textbf{(4.5)}$$

Scanning Tunnel Microscopy has been used to examine the gold substrates before pre-treatment and after pre-treatment with o-zone and ethanol. The freshly annealed gold exhibits atomically flat terraces approximately 100nm in diameter. Exposure to the pre-treatment regime, caused a high density of small depressions on the gold surface [64], thereby effectively removing oxidized material from the surface.

The freshly evaporated gold film and the pre-treated gold (o-zone oxidation and ethanol reduction) were observed under the electron microscope (Figure 4.32).

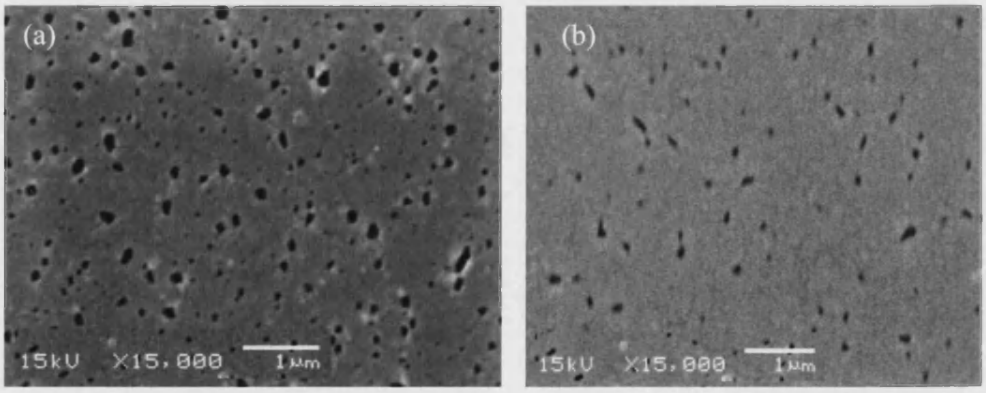

Figure 4.32 (a) Scanning electron micrograph of the freshly evaporated gold film on a clean glass substrate, and (b) an electron micrograph of the o-zone oxidized, ethanol reduced pre-treated gold substrate.

From the electron micrographs, there were fewer contaminants, debris and pinholes in the pre-treated gold substrate (Figure 4.32b) compared to the freshly evaporated gold (Figure 4.32a). The o-zone and ethanol treatment assisted in the removal of contaminants, producing a more homogenous gold surface for subsequent self-assembly.

All subsequent experiments were carried out on 10 minute o-zone cleaned, 20 minute ethanol reduced metallic gold films, onto which a SAM consisting of 5% Biotin-Thiol anchor and 95% OH-spacer were chemisorbed.

4.6 Scanning Electron Microscopy of the SAM-Tethered Biomimetic Membrane Vesicles

The Biotin-Thiol:OH spacer SAM solid supported bilayer vesicles were observed under the same condition as previously mentioned in section 4.2. The tethered vesicles were fixed with 2% glutaraldehyde, followed by staining with 1% osmium tetraoxide, and viewed under low vacuum.

Vesicles tethered to a 5% mole fraction biotin-thiol monolayer (0.05mmol.dm^{-3} biotin-thiol + 0.995mmol.dm^{-3} OH-spacer) were examined using an electron microscope (Figure 4.33).

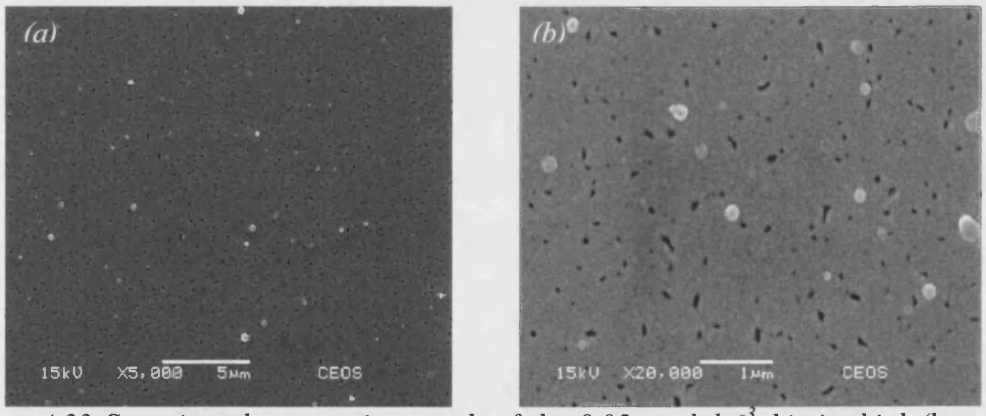

Figure 4.33 Scanning electron micrograph of the 0.05mmol.dm^{-3} biotin-thiol (low mole fraction) tethered vesicles.

The vesicles showed a homogeneity in size and there was a reduction in vesicle-vesicle fusion and vesicle distortion. Maintaining a lower mole fraction of the anchor molecule ensured the biomimetic vesicles did not come into close proximity to one another and reduce the probability of vesicles fusing and/or rupturing. Therefore, a more homogenous population of biomimetic membrane vesicles were tethered for permeation studies.

4.7 Optimization of the Biomimetic Vesicles: A View to Enhancing Encapsulated Dye Retention

The stability of biomimetic lipid vesicles is governed by a number of physical and chemical factors. The vesicular environment is critical to their overall longevity both *in vivo* and *in vitro*. Phospholipid vesicles have a limited shelf-life because of their oxidation and their susceptibility to hydrolytic degradation. Unsaturated phospholipids are the primary target for oxidation, but saturated fatty acid vesicles are also susceptible to oxidation at high temperatures. Oxidation tends to occur via a free radical chain mechanism in the absence of specific oxidants [65]. The use of high grade phospholipids, storage at low temperatures, and protection from light and oxygen can minimize their degradation [66]. It has also been shown that the choice of buffer is significant in the determination of vesicle stability. HEPES has been found to be the most effective, and a 10mmol.dm^{-3} concentration provides 70% protection after 30 minutes sonication [67], because the buffer sequesters the hydroxyl radicals.

The physical stability of lipid vesicles concerns their ability to retain their average vesicle size due to vesicle aggregation and fusion, and the loss of encapsulated molecules due to leakage. Their physical stability characteristics are strongly influenced by the phospholipid composition, medium composition and pH [68]. Lipid vesicles which carry a charge tend to reduce the vesicles tendencies to aggregate and fuse. Leakage of the encapsulated aqueous environment is also highly dependant of the vesicle composition.

4.7.1 Modelling the Dye Diffusion through the Biomimetic Membrane Vesicles

Membrane permeabilization is an important characteristic of natural cell membranes, as it is essential for the movement of water, ions and small molecules into and out of the cell. The rate of diffusion through a lipid bilayer is dependant of the physical state of the membrane, and altering the membrane components can dramatically change the rate of diffusion through the bilayer. The nature of spontaneous leakage of the encapsulated aqueous environment from the lipid vesicles is important for drug delivery [69], but in the context of this thesis, it is important for maintaining good fluorescence signal sensitivity.

Various models have been devised to simulate dye leakage through membranes, including the 'sphere-of-action' model and the 'weak-association' model [70, 71]. Described here, is

a simple passive diffusion model derived from Fick's law. The model has been adapted to take into account the physical dimensions of the lipid vesicles and leads to the determination of the dye flux through the lipid bilayer over time.

Fick's first law states that, for steady-state diffusion: the diffusion flux is proportional to the concentration gradient, and this concentration gradient drives diffusion *i.e.* a high gradient means high flux. The apparent diffusion of the dye through the membrane is given by:

$$J = \frac{KDC_{in}}{L} \tag{4.6}$$

Where J is the flux of the dye through the membrane ($mol.s^{-1}.m^{-2}$), K relates to the association of the dye into the membrane ($K = [dye]_{membrane}/[dye]_{vesicle}$), C_{in} is the concentration of dye encapsulated within the vesicle aqueous space, and L is the thickness of the membrane which the dye must diffuse through (Figure 4.34).

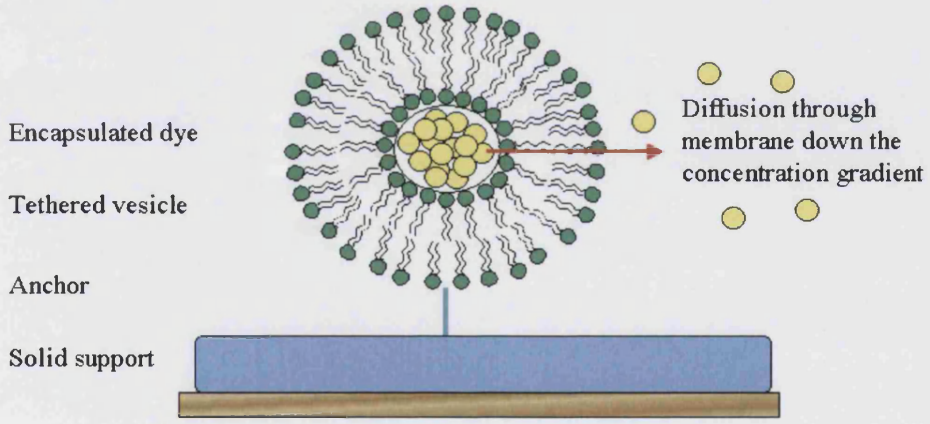

Vesicle volume, V, dye concentration, C_{in}, membrane thickness, L and vesicle surface area, A.

Figure 4.34 Schematic of the dye diffusion through the biomimetic membrane vesicles, governed by Fick's first law.

The change in dye concentration in the vesicle aqueous space over time is defined as:

$$\frac{dC_{in}}{dt} = \frac{AJ}{V} = \frac{AKDC_{in}}{VL} \tag{4.7}$$

Where A is the surface area of the vesicle, V is the volume of the vesicle and D is the molecular diffusion coefficient

Therefore, the rate of diffusion of the dye through the vesicle membrane is defined by:

$$D^* = KD \tag{4.8}$$

Where, D^* is the apparent diffusion coefficient, which is dependant on the size of the diffusing molecule and the viscosity through what it is moving.

The rate of dye diffusion as a result of time (mol.s^{-1}), can then be further simplified to give:

$$\frac{dC_{in}}{dt} = \frac{AC_{in}D^*}{VL} \tag{4.9}$$

The diffusion through the membrane follows a first order kinetics pathway, as the reaction only depends on the concentration of one reactant (*i.e.* the concentration of the dye), therefore:

$$\frac{dC_{in}}{dt} = -kC_{in} \tag{4.10}$$

Where k is the first order rate constant, and is equal to:

$$k = \frac{AD^*}{VL} \tag{4.11}$$

Linearizing the dye diffusion through the membrane is defined by:

$$lnC_{in,t} = lnC_{in,t=0} - kt \tag{4.12}$$

Where $C_{in,t}$ is the dye concentration at a particular time and $C_{in,t=0}$ is the dye concentration at time zero.

Therefore, plotting the log of dye concentration (mol.m^{-3}) against time (seconds) gives a linear plot, where the gradient of the line is the first order rate constant, k (s^{-1}). Then the apparent diffusion coefficient, D^* (m^2.s^{-1}), can be calculated using the first order rate constant, k, the vesicle surface area, A (m^2), the vesicle volume, V (m^3) and the membrane thickness, L (m), as follows:

$$D^* = \frac{kVL}{A} \tag{4.13}$$

This gives the apparent diffusion coefficient for the dye molecule through the lipid bilayer of the membrane vesicles. A commonly used approach to evaluate membrane leakage and/or membrane fusion is to monitor the dye change of the lipid vesicles after the properties of the vesicles have been altered. The natural diffusion of the dye can then be modelled and a quantitative analysis concerning the porosity of the biomimetic membranes can be performed.

4.7.2 Altering the Phase Transition Temperature of the Biomimetic Membrane Vesicles by Varying the Fatty Acid Chain Length

Phosphotidylcholines are the most abundant phospholipid class in mammalian membranes and are a major component in eukaryotic organisms. They are also the most widely used model membrane lipid in studies. However, the cellular membranes are highly diverse, and contain a huge range of different phospholipid species found at different frequencies depending on the function of the membrane in question. Phospholipids undergo a transition from the crystalline gel state through intermediates and into the liquid phase upon heating. The phase transition temperature is the temperature required to induce the change from the gel phase (hydrocarbon chains are closely packed and ordered), to a disordered liquid phase (hydrocarbons are randomly orientated and fluid). There are numerous factors that govern the phase transition temperature including hydrocarbon length, unsaturation, charge, and head-group species. It has been shown that the lipid alkyl chain length influences the encapsulation efficiency of the dye/drug molecules and the release rate. Studies using ibuprofen, showed its incorporation efficiency increased with increasing lipid chain length, and was believed to be attributed to the increased hydrophobic area within the vesicle bilayer [72]. It was also demonstrated that increasing chain length also caused an increased capacity to retain the ibuprofen.

Production of biomimetic membrane vesicles from phospholipids with varying chain length alters the physical properties of the vesicles, in particular, the temperature at which the vesicles transition from the ordered gel phase to the liquid disordered phase. DMPC (Figure 4.35a), which contains two hydrocarbon chains of 14 carbons in length, phase transitions at 23°C, DPPC (Figure 4.35b) contains two hydrocarbon chains of 16 carbons in length, phase transitions at 41 °C, and DSPC (Figure 4.35c) contains two hydrocarbon chains of 18 carbons in length, phase transitions at 55°C.

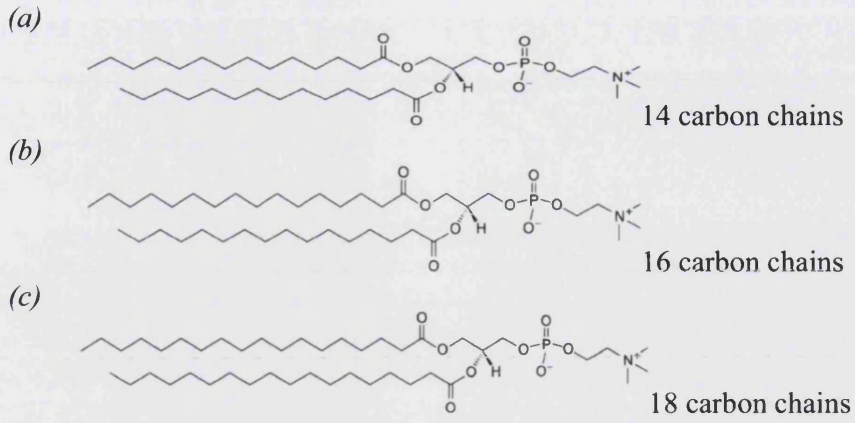

Figure 4.35 (a) Structure of 1,2-Dimyristoyl-sn-Glycero-3-Phosphocholine (DMPC), (b) Structure of 1,2-Dipalmitoyl-sn-Glycero-3-Phosphocholine (DPPC) and (c) Structure of 1,2-Distearoyl-sn-Glycero-3-Phosphocholine (DSPC).

Tethered vesicles containing either DMPC, DPPC, or DSPC were produced and monitored using SPR/SPFS for changes in relative fluorescence over time due to the intrinsic porosity of the vesicle bilayer. The natural leakage of the fluorescent dye from the vesicle aqueous space into the bulk solution was monitored over 120 minutes (Figure 4.36).

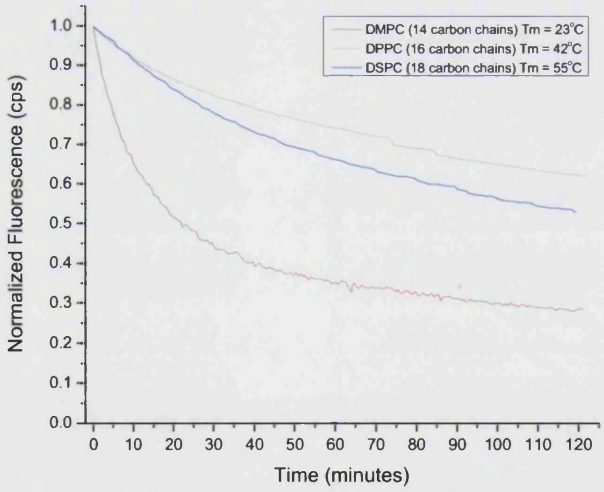

Figure 4.36 Monitoring the change in relative fluorescence of three phospholipid vesicle systems (DMPC, DPPC and DSPC), with various phase transition temperatures over a 120 minute time period.

The retention of the encapsulated BODIPY dye within the vesicle aqueous space was seen to be directly influenced by the lipid species comprising the bilayer. Over the observed 120 minutes, the vesicles comprising the shorter hydrocarbon chain phospholipid (DMPC), showed the poorest retention capacity of the three systems tested. The two vesicle systems

comprising the longer hydrocarbon chain phospholipids (DPPC and DSPC), showed a marked improvement in their capacity to retain the encapsulated dye molecules. This retention capacity was the direct influence of the hydrocarbon chain length.

A natural log plot of the decrease in fluorophore concentration ($\mu mol.m^{-3}$) as a function of time (seconds) was plotted (Figure 4.37). It was assumed that at time= 0minutes, the fluorophore concentration was $5\mu mol.dm^{-3}$, which was the encapsulation concentration of the dye at vesicle extrusion. Using the passive diffusion model detailed in section 4.7.1, the apparent diffusion coefficient for the three phospholipid vesicle systems was determined.

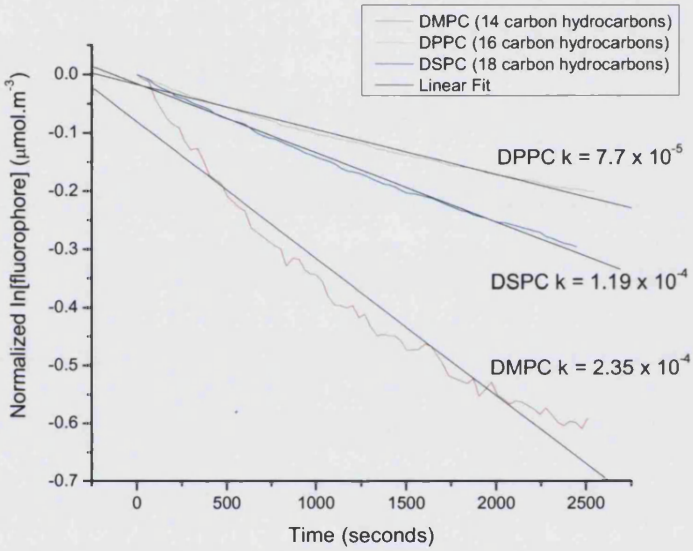

Figure 4.37 Plot of the normalized ln fluorescence concentration ($\mu mol.m^{-3}$) as a function of time (seconds) for the three vesicle systems containing either DMPC, DPPC or DSPC.

The monitoring of the dye leakage through the membrane bilayer of the DMPC tethered vesicles offered the lowest resistance to dye permeation. The calculate apparent diffusion coefficient (D*), was $1.76x10^{-14}cm^2.s^{-1}$. The DMPC lipid was in the liquid phase at room temperature (23°C), therefore, the hydrocarbon chains were disordered and offer a weak barrier to the diffusion of the dye into the bulk solution. Moreover, the lipids with longer hydrocarbon chains, DPPC and DSPC, which were in the gel phase at room temperature, 42°C and 55°C respectively, ensured that their hydrocarbon chains were ordered and fully extended and offered a greater barrier to the diffusion of the dye through the bilayer. DSPC had a calculated apparent diffusion coefficient of, $D^* = 8.9x10^{-15}cm^2.s^{-1}$, while DPPC had a calculated apparent diffusion coefficient of, $D^* = 5.76x10^{-15}cm^2.s^{-1}$. Therefore, lipids in the

gel phase offered a higher barrier to dye diffusion than phospholipids in the disordered liquid phase.

The increased barrier against porosity observed by increasing hydrocarbon length has been attributed to inter-chain bonding. A vesicles capacity to retain the entrapped aqueous environment was the result of increasing van der Waals interactions between the neighbouring chains, because longer hydrocarbon chains induce stronger bonding. This in turn requires more energy to disrupt the ordered packing, therefore, the phase transition temperature increases [72]. Vesicles at or near their phase transition temperature show increased rates of dye movement due to packing defects in the phase boundaries between the coexisting liquid phases and the gel phases [73].

4.7.3 The Effect of Sterols in the Bilayer of the Biomimetic Membrane Vesicles

Sterols comprise a major constituent of the eukaryotic cell membranes, and cholesterol has a flat, rigid fused ring structure, which is able to form stable stacked aggregates that other lipid components tend not to form [74]. Human erythrocytes typically contain 20% cholesterol but can be higher in certain membranes [75]. At 20-50% cholesterol content, the sterol dissolves into the bilayer, where the hydroxyl group hydrogen bonds to water. The sterol acts as a spacer between the hydrocarbon chains of the phospholipids and functions as a 'cement' to keep the assembly together and to fill in any voids between the hydrocarbon chains.

4.7.3.1 The Effect of Cholesterol on Pure DMPC Bilayer Vesicles

Cholesterol-phospholipid interactions dramatically alter the integrity and functionality of the phospholipid bilayer. A substantial body of work has determined the thermodynamic effects of varying the proportion of cholesterol within the phospholipid bilayer at a range of temperatures (Figure 4.38). From the phase diagram, the thermodynamics observed for a large proportion of cholesterol in DMPC promotes the formation of a liquid-ordered phase. However, at low concentrations of cholesterol, it is the gel-phase.

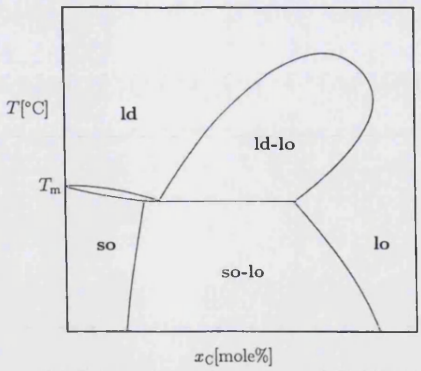

Figure 4.38 Schematic phase diagram for mixtures of DMPC and cholesterol. T_m = main phase transition temperature of pure DMPC, ***so*** *= solid-ordered (gel phase),* ***ld*** *= liquid-disordered (fluid phase), and* ***lo*** *= liquid-ordered [76].*

Cholesterol also has a pronounced effect on biomimetic lipid vesicles, and has been fundamental in the evolution of drug-encapsulating liposomes for therapeutic uses. The *in vivo* and *in vitro* stability of the biomimetic vesicles is not only influenced by the environment which they come into contact, but also their structural characteristics and the characteristics of the encapsulated aqueous environment. Inclusion of cholesterol into the bilayer of the biomimetic vesicles significantly affects the diffusion of the encapsulated aqueous material into the bulk solution.

Various mole percent (0-70 mol%) of cholesterol was included in DMPC vesicles, and monitored for dye leakage through the vesicle bilayer (Figure 4.39a). This allowed for the determination of the apparent dye diffusion coefficients for each of the cholesterol/DMPC systems (Figure 4.39b).

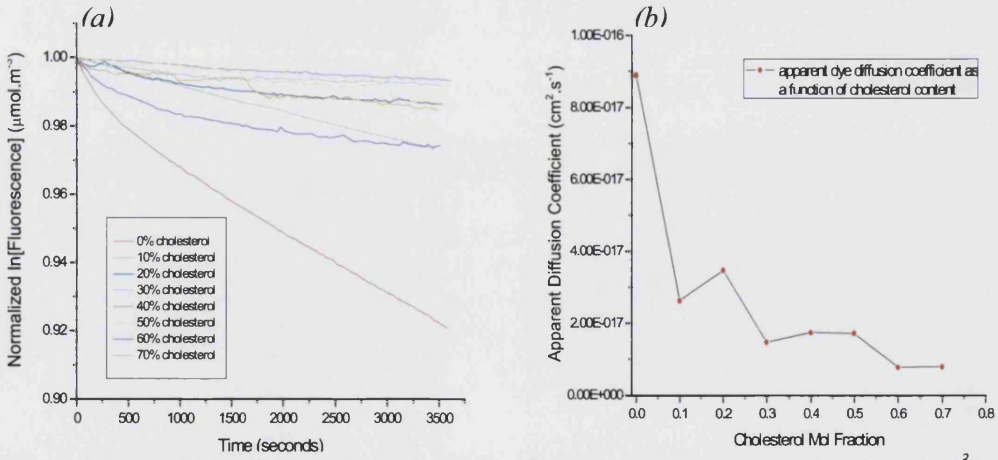

Figure 4.39 (a) Plot of the normalized ln fluorescence concentration(µmol.m^{-3}) as a function of time (seconds) for each of the cholesterol/DMPC vesicle systems. (b) Plot of the apparent dye diffusion coefficient (cm^2.s^{-1}) as a function of cholesterol content of the DMPC vesicles.

As mentioned in this section, natural biological membranes contain varying proportions of sterols, and are typically found in the range 5-30%. As shown in Figure 4.39, the inclusion of cholesterol in this range, substantially decreased the leakage of encapsulated dye. The cholesterol altered the phase transition temperature of the pure DMPC vesicles, changing its physical characteristics at room temperature from its typical disordered liquid phase into an intermediate condensed ordered gel phase. Moreover, the cholesterol reduced the mobility of the fatty acyl chains [77], thereby altering the permeability of the bilayer. A comparison of the apparent dye diffusion coefficients of the DMPC/cholesterol vesicle systems is summarized in Figure 4.40.

Mole Percentage of Cholesterol Included in Vesicles (%)	**Apparent Dye Diffusion Coefficient ($cm^2.s^{-1}$)**
0	8.9×10^{-14}
10	2.63×10^{-14}
20	3.47×10^{-14}
30	1.47×10^{-14}
40	1.74×10^{-14}
50	1.72×10^{-14}
60	7.78×10^{-15}
70	7.93×10^{-15}

Figure 4.40 Summary of the apparent dye diffusion coefficients for the various DMPC/cholesterol vesicle systems.

The inclusion of sterols in the vesicle bilayer showed a decrease in the apparent dye diffusion coefficient compared to the pure DMPC vesicle system. At low cholesterol concentrations (10%) there was a >3-fold improvement in the ability of the biomimetic vesicles to retain their fluorescent content compared to the system with no cholesterol present. At higher concentrations of cholesterol (20-50%), there was around >5-fold improvement in fluorophore retention compared to the control system containing no sterols. Moreover, an >11-fold improvement in dye retention was observed at high cholesterol concentrations (60-70%).

4.7.3.2 The Effect of Cholesterol on High Phase Transition Temperature Phospholipid Bilayer Vesicles

Sterols, such as cholesterol, stabilize phospholipid vesicles by broadening the main phase transition of the phospholipid species. It has been shown that cholesterol causes the thermal fluctuations of the phospholipids to decrease at the main phase transition but to increase in the wings of the transition [78]. Thermal fluctuations of lipids are the physical properties of the system, such as thermodynamic stability, self-assembly, elasticity, interaction potentials, and phase transitions. Therefore, cholesterol acts to decrease the phase boundary between the liquid and gel phases, but also acts to broaden the 'wings' of the phase transition between the liquid and gel phases. Cholesterol has also been shown to cause larger fluctuations at the phase temperature of phospholipids with longer chain lengths. High concentrations of cholesterol has been shown to suppress the permeability of the phospholipid bilayer, and that relative permeability increases with decreasing chain length.

Inclusion of cholesterol in the bilayer of high phase transition temperature lipids, DPPC and DSPC, were tethered to the solid support system and the permeability was monitored and compared to the lower phase transition temperature (DMPC) vesicle system (Figure 4.41).

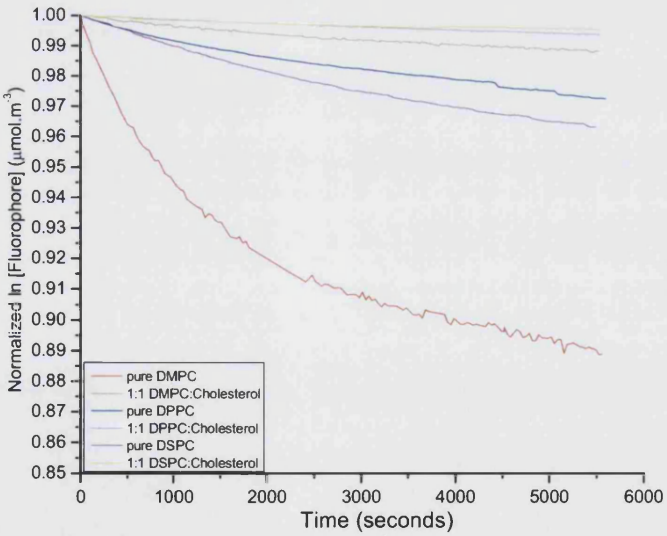

Figure 4.41 Plot of the permeability ($\mu mol.m^{-3}$) of the high phase transition bilayer vesicles, DPPC and DSPC, compared to the lower phase transition vesicle system, DMPC, as a function of time (seconds).

Inclusion of sterols in the bilayer of the tethered vesicles significantly increased the retention of the BODIPY dye, for all phase transition lipid systems tested. Monitoring the

permeability of the vesicles allowed for the calculation of the first order rate constant, *k*, for each of the vesicle systems. The apparent dye diffusion coefficients, D*, were calculated and summarized in Figure 4.42.

The pure-DMPC vesicles offered the lowest resistance to dye diffusion, $D^* = 1.20 \times 10^{-15} cm^2.s^{-1}$, while 1:1 DSPC:cholesterol vesicles offered the highest resistance to dye diffusion through the membrane, $D^* = 5.7 \times 10^{-17} cm^2.s^{-1}$. The three mixed vesicle systems all showed significantly higher permeability barriers against dye diffusion than their pure-lipid counterparts. The sterol:lipid vesicles offered a higher permeability barrier because the cholesterol caused a change in the physical properties of the vesicles, placing them in the intermediate phase of liquid-ordered state. There was around an 8-fold improvement in dye retention in both the sterol containing DMPC and DSPC systems compared to pure-lipid forms, and around a 4-fold improvement in the retention of dye in the DPPC:sterol system compared to its pure lipid form. The highest barrier to dye permeability was offered by the phospholipids with the longer acyl chains, DSPC>DPPC>DMPC, and increasing chain length caused an increase in the temperature at which phase transition occurred. Therefore, the lipids with the higher phase transition temperature ensured the phospholipid membranes were ordered, and the acyl chains were fully extended and rigid. This helped to block the passage of the dye molecules though the bilayer. Cholesterol altered the phase transition properties of the phospholipid vesicle systems by introducing conformational order and broadening the main phase transition [78]. This caused the phospholipids to increase their packing density [79] and filling in defects and gaps in the bilayer. The acyl chains of the phospholipids showed reduced mobility when in the presence of cholesterol, therefore, the vesicle systems demonstrate reduced permeability [77]. Higher levels of cholesterol in biological membranes imparts the membrane with mechanical coherence, resistance to mechanical fatigue, and stabilization of the permeability barrier [80, 81]. The inclusion of a small faction of cholesterol in phospholipid bilayers resulted in the formation of lipid domains, which enhances the dynamic membrane heterogeneity. Moreover, this was because the low concentration of cholesterol is unable to fully break the ordered structure when the lipids are in the gel-ordered phase and is unable to fully induce order of the acyl chains in the fluid phase. Therefore, cholesterol at low concentrations produces a phase intermediate between the gel and fluid phases [82].

Vesicle system	Apparent dye diffusion coefficient ($cm^2.s^{-1}$)
Pure DMPC	1.20×10^{-15}
1:1 DMPC:Cholesterol	1.50×10^{-16}
Pure DPPC	3.38×10^{-16}
1:1 DPPC:Cholesterol	8.45×10^{-17}
Pure DSPC	4.94×10^{-16}
1:1 DSPC:Cholesterol	5.70×10^{-17}

Figure 4.42 Summary of the apparent dye diffusion coefficient for pure-DMPC vesicles (Tm = 23°C), pure-DPPC vesicles (Tm = 41°C) and pure-DSPC vesicles (Tm = 55°C), compared to the calculated apparent dye diffusion coefficients of the 1:1 phospohlipid:cholesterol vesicle systems.

The inclusion of the cholesterol into the vesicle bilayer stabilized the membrane vesicles by inducing conformational order in the phospholipid acyl chains and acting as a filler to seal defects in the bilayer. However, sterol content of subsequent experiments was kept at 30 mol% to ensure the cholesterol content mimic that of biological membranes.

4.8 Monitoring the Permeation Processes using Phospholipase A_2

As mentioned previously in this chapter, the production of a stable cell mimic allows for the real-time monitoring of permeation processes as a result of toxin-membrane interactions. The adapted support system provides a reliable and simple support layer for the attachment of biomimetic membrane vesicles, and can be prepared more efficiently compared to the laborious HLB support system used in section 4.1.

Vesicles were tethered to the biotin-thiol SAM, and $3.3 \times 10^{-9} mol.dm^{-3}$ PLA_2 was injected into the system, with the subsequent events being monitored using combined SPR and SPFS (Figure 4.43a).

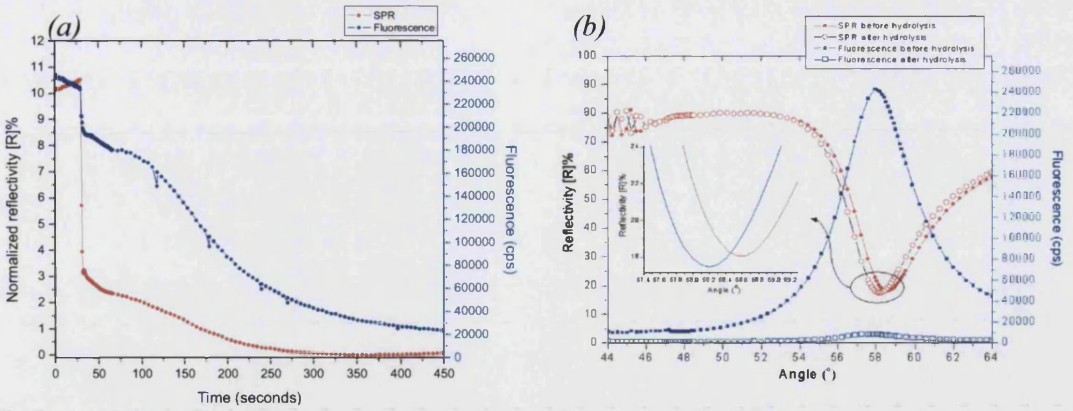

Figure 4.43 (a) Simultaneous measurement of SPR and SPFS for the monitoring of the events during the injection of 3.3 x 10^{-9}mol.dm^{-3} PLA_2 into the biotin-thiol tethered biomimetic vesicles. (b) Shift in resonance minimum upon vesicle hydrolysis with 3.3 x 10^{-9}mol.dm^{-3} PLA_2

The hydrolysis of the biomimetic membranes occurred rapidly after injection of the lipolytic enzyme at 30 seconds. The hydrolysis of the vesicles proceeded rapidly until 45 seconds, when there was a reduction in the rate of hydrolysis. The hydrolysis of the vesicles caused a 0.35° resonance shift in the minimum (Figure 4.43b). This equated to the desorption of 1.87ng.mm^2 of mass from the surface. Moreover, the vesicle adsorption to the surface caused a resonance minimum shift of 1.0°, which equated to the adsorption of 5.35ng.mm^{-2} mass at the surface. Therefore, vesicle hydrolysis did not proceed to completion, and the reduction in hydrolysis rate was the time required to penetrate the densely packed vesicle.

The monitoring of the fluorescence during the hydrolysis of the tethered vesicles showed an initial decrease in fluorescence as the vesicles were hydrolyzed, followed by a slower subsequent leakage of the dye into solution. This suggests that the kinetics of the lipolytic enzyme are reduced because of the time needed to penetrate the optimized DMPC/cholesterol vesicles. The inclusion of sterols into the vesicle bilayer renders them less prone to hydrolysis by the PLA_2, because the enzyme preferentially hydrolyzed defective bilayers as it improves their accessibility to the ester bond of the phospholipids.

The biotin-thiol support and the optimized biomimetic membrane vesicles provided a stable system with reduced natural permeability of the bilayer for the study of membrane-protein interactions.

4.9 Inhibition of Lipolysis in Relation to the Effects of Eicosadienoic acid and Manoalide on Phospholipase A_2

A means of altering phospholipase A_2 activity towards a biological system is an attractive route to modifying the inflammatory cascade and the associated medical conditions, such as arthritis, asthma, and venomous bites. Therefore, potential PLA_2 inhibitors were monitored for their ability to prevent vesicle lysis.

The initiation of the inflammatory response is mediated by the biosynthesis of eicosanoids from arachidonic acid (a product of the lipolysis of phospholipids). Therefore, the actions of lipolytic enzymes such as PLA_2 and snake venoms cause the hydrolysis of lipid to produce lysophospholipids and a free fatty acid. The liberation of arachidonic acid from the *sn-2* position provides the substrate for the biosynthesis of eicosanoids. Hence, compounds that inhibit PLA_2 activity are potential therapeutic agents for treatment of inflammation and the diseases with which they are associated.

4.9.1 Effect of Eicosadienoic acid on PLA_2 Induced Lipolysis

7,7-Dimethyl-(5Z,8Z)-eicosadienoic acid (Figure 4.44), is an analogue of arachidonic acid, and inhibits the biosynthesis of the Slow Reacting Substance of Anaphylaxis (SRS-A) group of leukotrienes, that are the mediators of bronchoconstriction, hypersensitivity and other allergic reactions [83]. 7,7-Dimethyl-(5Z,8Z)-eicosadienoic acid's (DEDA) mode of action is to inhibit PLA_2 via a non-selective mode of action, as it is capable of blocking the activities of both $cPLA_2$ and $sPLA_2$ [84]. As DEDA is an analogue of arachidonic acid, it is capable of interfering with the biosynthesis of the prostaglandins and leukotrienes, which in turn alters the steps in the inflammatory cascade or inhibit it altogether.

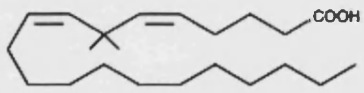

Figure 4.44 Structure of 7,7-Dimethyl-(5Z,8Z)-eicosadienoic acid, a know PLA_2 inhibitor.

DEDA is an unsaturated fatty acid and is an analogue of a natural fatty acid (arachidonic acid). However, the analogue contains two cis-bonds, therefore, it cannot match the alignment and conformation of other fatty acid hydrocarbons. This causes the DEDA to have a larger area/head-group at the membrane interface compared to the other phospholipids [85]. This increased surface area causes an increase its accessibility, thereby

making it a good competitive inhibitor. Little is known about the mechanism with which PLA_2 is inhibited by DEDA, but the fatty acid analogue appears to act as a pseudo-substrate.

The inclusion of 0.3mmol.dm^{-3} DEDA in the circulating buffer did not prevent the permeation and lysis of the tethered biomimetic membrane vesicles upon injection of 3.3x10^{-9}mol.dm^{-3} PLA_2 (Figure 4.45).

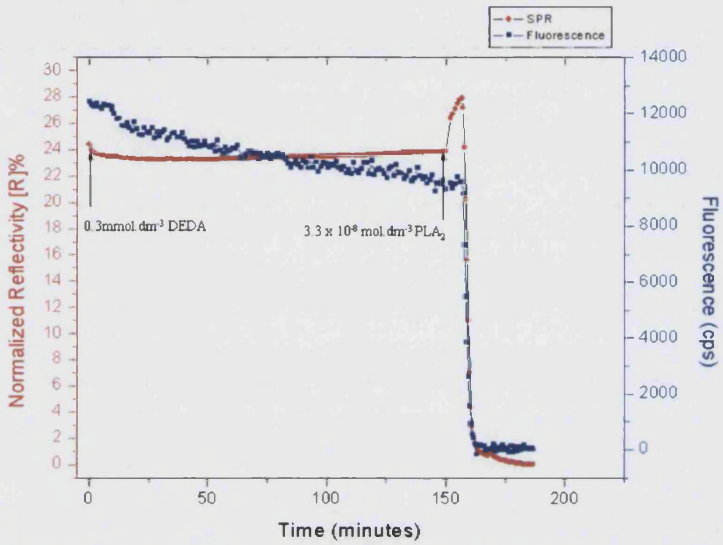

Figure 4.45 Circulation of 0.3 mmol.dm^{-3} DEDA around the tethered biomimetic membrane vesicles for ~150 minutes before the addition of 3.3x10^{-9}mol.dm^{-3} PLA_2 into the system.

DEDA did not sequester the PLA_2 from the tethered vesicles, and inclusion of the arachidonic acid analogue in solution did not prevent the lysis of the biomimetic membrane vesicles. Direct injection of the lipolytic enzyme into the circulating buffer containing the DEDA showed the enzyme binding to the tethered vesicles, which was subsequently followed by the hydrolysis of the phospholipid aggregates.

The inclusion of the DEDA into the bilayer of the biomimetic membrane vesicles provided an effective means of preventing the hydrolysis of the phospholipids, and thereby maintaining the integrity of the vesicles (Figure 4.46a). A suspension of DMPC, cholesterol and biotin was prepared in chloroform to which 1mol% DEDA was added. This suspension was mixed and the solvent removed. The lipid film was then processed according to the procedure outlined in section 3.6.1. This methodology ensured that the DEDA was incorporated into the phospholipid bilayer and not in the aqueous space or free in the bulk solution.

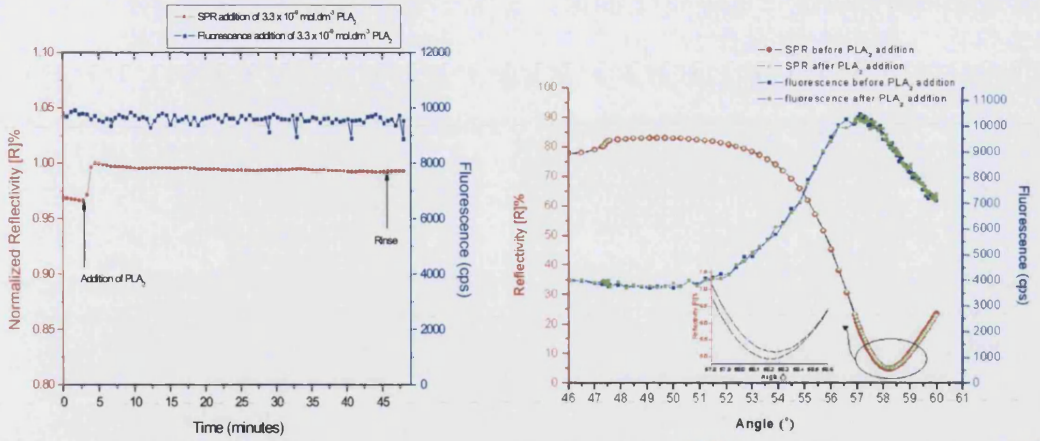

Figure 4.46 (a) Simultaneous measurement of reflectivity (SPR) and Fluorescence (SPFS) upon the addition of 3.3 x 10^{-9} mol.dm^{-3} PLA_2 to the tethered vesicle system containing 1mol% DEDA within the vesicle bilayer. (b) Resonance angle scans before and after the addition of PLA_2 to the DEDA-containing vesicles.

The addition of PLA_2 to the DEDA-tethered vesicles showed an adsorption of mass at the surface, and the increase in mass was confirmed by the shift in resonance minimum (Figure 4.46b). The 0.05° shift in resonance minimum equated to the adsorption of 0.27ng.mm^{-2} of mass to the surface. The adsorption of the enzyme to the surface was mediated by the increased head-group area of the DEDA. Therefore, the PLA_2 preferentially bound to the arachidonic acid analogue. This attachment of the enzyme to the analogue prevented the lysis of the phospholipids and maintained the membranes structural integrity. This was because the analogue did not contain the *sn-2* ester bond necessary for hydrolysis. The integrity of the vesicles was confirmed by the simultaneous monitoring of the fluorescence, which demonstrated that there was no rapid efflux of dye from the vesicle aqueous space.

The addition of varying concentration of the PLA_2 to the DEDA-containing tethered vesicles allowed for the monitoring of the binding of the enzyme to the biomimetic membranes (Figure 4.47).

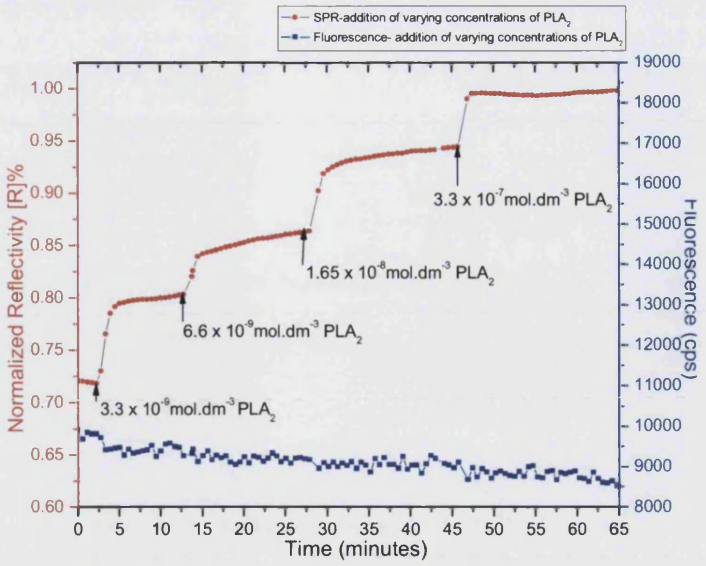

Figure 4.47 Simultaneous monitoring of the adsorption of mass at the surface (SPR) and change in fluorescence (SPFS) upon addition of varying concentrations of PLA_2.

Increasing the concentration of PLA_2 from $3.3x10^{-8}$ $mol.dm^{-3}$ to $3.3x10^{-9}$ $mol.dm^{-3}$ followed a concentration dependant relationship. Plotting the change in reflectivity with increasing enzyme concentration produced a Langmuir isotherm (Figure 4.48) from which it was possible to directly determine the equilibrium dissociation constant, K_D.

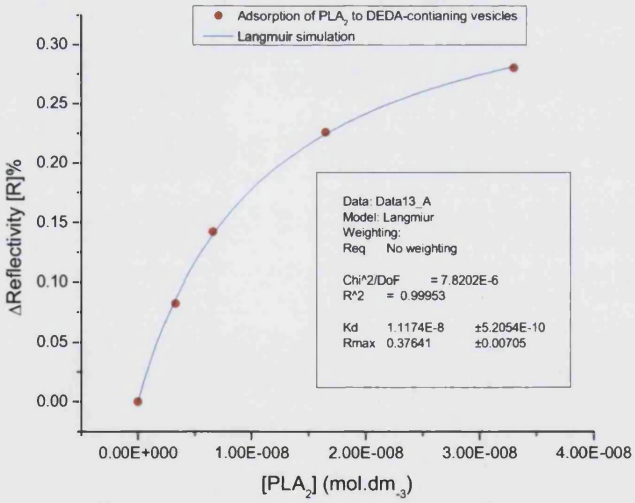

Figure 4.48 Langmuir plot of change in reflectivity with increasing PLA_2 concentration from 3.3×10^{-9} $mol.dm^{-3}$ to 3.3×10^{-8} $mol.dm^{-3}$.

Using the Langmuir plot the K_D was calculated to be $1.12x10^{-8}$ $mol.dm^{-3}$.

The incorporation of DEDA into biomimetic membrane vesicles provided a protection against lipolysis by PLA_2, because the analogue prevented the hydrolysis of the *sn-2* ester bonds of the phospholipids via a competitive inhibitory mechanism. The inclusion of the DEDA allowed for the determination of the equilibrium constants between the membrane vesicles and the lipolytic enzyme. Preventing the lysis of the phospholipids is a major step in understanding the mechanisms and improved therapeutic agents against disorders associated with the introduction of high levels of PLA_2, including arthritis, asthma, chronic inflammatory diseases and venomous bites.

4.9.2 Effect of Manoalide on PLA_2 Induced Lipolysis

Secondary metabolites, such as antibiotics, are organic compounds produced by a living organism, which are involved in the long-term survival of the producer. These compounds are not directly involved in the normal growth, development or reproduction of the organism. The secondary metabolites have been exploited for a variety of purposes including in the food, fragrance, pigment, insecticidal and medicinal industries. Around 40% of today's pharmaceutical sales are derived from terrestrial microbial and plant products, however, the diversity of the marine environment, which remains largely untapped, exceeds their terrestrial counterparts. The marine environment is a reservoir for bioactive natural products, many of which exhibit structural features and chemical properties not found in terrestrial natural products [86]. Various groups of marine organisms produce secondary metabolites including bacteria, algae, seaweeds and molluscs. The marine sponges are the simplest multicellular organisms, which contain no true tissues or organs. These organisms synthesize a variety of natural products, and have been found to be a rich source of anti-PLA_2 compounds. Many of these anti-PLA_2 molecules show a high degree of selectivity for secretory-PLA_2s compared to cytosolic-PLA_2s.

The non-steroidal sesterterpenoid, manoalide (Figure 4.49), was first isolated from the *Luffariella variabilis* sea sponge in 1980 [87], and shows antibacterial properties. The molecule was shown not to inhibit arachidonic acid induced inflammation, but inhibited the inflammatory cascade prior to the release of the arachidonic acid [88]. Manoalide has been shown to irreversibly inactivate both bee and cobra venom PLA_2, with an IC_{50} of 0.05 and 2.0$\mu mol.dm^{-3}$ respectively [89-91]. The inhibitor is believed to cause the covalent modification of the lysine residues of the PLA_2 enzyme mediated by a neucleophilic attack.

Manoalide shows analgesic activity and inhibition of non-arachidonic acid induced inflammation. It has been shown to inhibit the hydrolysis of phosphatidylcholine but fails to inhibit the hydrolysis of phosphatidylethanolamine [92], suggesting it does not cause the modification of the PLA_2 at the catalytic site of the enzyme, but interferes with the binding of the enzyme to the phospholipid interface.

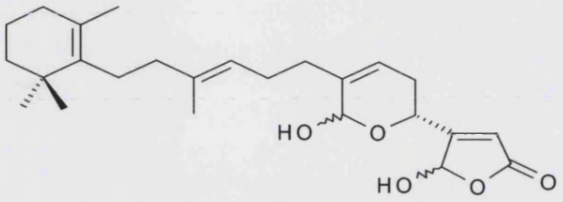

Figure 4.49 Structure of manoalide, isolated from the Laffariella variabilis sea sponge.

As manoalide is an antagonist of PLA_2 and not an analogue of the enzymes substrate, like DEDA, manoalide was not incorporated into the membrane bilayer, but was added to the PLA_2 5 minutes prior to injection into the tethered vesicle system. Various concentrations of manoalide were added to 3.3 x 10^{-9}mol.dm^{-3} PLA_2, which was subsequently injected into the tethered vesicle system (Figure 4.50).

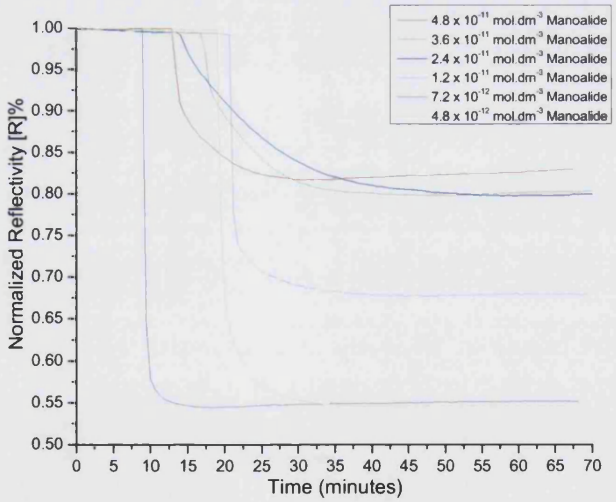

Figure 4.50 Change in reflectivity as a result of adding various concentrations of manoalide to 3.3 x 10^{-9}mol.dm^{-3} PLA_2.

From the results, it can be seen that by increasing the concentration of manoalide there was a decrease in the change in reflectivity upon addition of the PLA_2. Therefore, it was possible to observe the inhibitory effects of manoalide on PLA_2. The addition of $4.8x10^{-11}$

mol.dm^{-3} manoalide into the tethered vesicle system significantly decreased the desorption of mass from the surface upon addition of PLA_2.

Increasing the concentration of manoalide from $4.8x10^{-12}$ mol.dm^{-3} to $4.8x10^{-11}$mol.dm^{-3} followed a concentration dependant relationship. Plotting the shift in resonance minimum with increasing inhibitor concentration produced a dosage dependant plot (Figure 4.51).

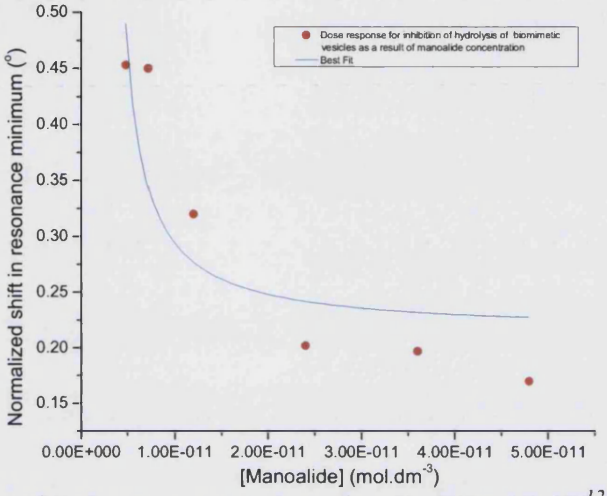

Figure 4.52 Addition of various concentration of manoalide, $4.8x10^{-12}$ mol.dm^{-3}- $4.8x10^{-11}$ mol.dm^{-3}, with $3.3 x10^{-9}$mol.dm^{-3} PLA_2 to the tethered vesicles.

The addition of manoalide to the tethered biomimetic membrane system significantly reduced the desorption of mass from the surface, showing its ability to prevent the hydrolysis of the phospholipids caused by PLA_2. The inactivation of PLA_2 by manoalide caused the membrane vesicles to remain intact, signifying prevention of the production of eicosanoids and thereby inhibiting the steps of the inflammatory cascade. Prevention of the actions of PLA_2 by manoalide has been reported to inhibit the catabolism of cartilage in the arthritic joints of rabbits [93].

However, DEDA prevented the hydrolysis of the tethered membrane vesicles by PLA_2 to a greater extent compared to manoalide. DEDA did not prevent the adsorption of the PLA_2 to the membrane surface but prevented the hydrolysis of the *sn-2* ester bonds of the phospholipids. Moreover, manoalide reduced the effects of PLA_2 on the membrane vesicles but did not completely inhibit the hydrolysis of the phospholipids.

4.10 Conclusions

The functionalization of a substrate was employed to tether intact biomimetic lipid vesicles to a surface. The phospholipid vesicles act as a cell membrane mimic, and are designed to control the physical properties of the permeability barrier. The modification of the phospholipid bilayer properties allowed the control over the intrinsic porosity and leakiness of the membrane, thereby allowing for the encapsulation and retention of hydrophilic molecules within the aqueous space of the phospholipid vesicles. The natural permeability of the phospholipid barrier was modelled upon Fick's law to determine the apparent diffusion coefficient of the encapsulated reporter molecules during its diffusion from the aqueous space of the vesicles into the bulk solution. Using the basic diffusion model it was possible to maximize the retention capacity of the tethered membrane mimics, ensuring an optimum sensitivity for the detection of membrane permeation events.

The generation of a functionalized surface was achieved by the constructing a biotinylated-HLB, to which intact phospholipid vesicles were tethered using biotin-streptavidin coupling chemistry. The functionalized surface evolved to a simpler, more reliable and less time-consuming support system, by substituting the HLB for a thiol SAM. Maximal binding of the phospholipid vesicles was achieved using a surface with $\chi = 0.05$ density of the biotin-thiol molecule in a mixed SAM with an hydroxyl-terminated lateral spacer. The lower surface density of the reactive thiol ensured spatial separation between the biomimetic lipid membranes, preventing their fusion with one another and reducing the steric interaction between the lipid vesicles on the solid substrate.

Surface Plasmon Resonance (SPR) and Surface Plasmon field enhanced Fluorescence Spectroscopy (SPFS) were employed to monitor and quantify the construction of the tethered vesicle system. The techniques were also employed to monitor the effects of membrane hydrolysis as a result of lipolytic toxins from *Crotalus adamanteus* venom and purified phospholipase A_2. Direct membrane hydrolysis was observed for both whole snake venom and purified PLA_2 peptide.

The manipulation of the membrane hydrolysis was achieved by the inhibition of the lipolytic peptides and venom. Eicosadienoic acid, an analogue of arachidonic acid, was incorporated into the bilayer of the biomimetic membrane vesicles. This analogue of AA had a larger surface area compared to the phospholipids, therefore, acted as a competitive inhibitor. Manoalide, a natural compound isolated from a marine sponge, was shown to

reduce the hydrolysis of the biomimetic lipid vesicles in a dose dependant manner. The inhibitor acted by covalently bond to the lysine residues within the phospholipase A_2, thereby preventing the hydrolysis of the phospholipid ester bonds.

A study of the affinity binding constants of the enzymes to the biomimetic membrane vesicles was performed. The equilibrium titration method was used to observe the effects of the lytic peptides, which followed a Langmuir isotherm. This allowed the determination of the equilibrium affinity constants between the toxins and the model membranes.

4.11 Bibliography

1. Bain, C.D., et al., *Formation of Monolayer Films by the Spontaneous Assembly of Organic Thiols from Solution onto Gold.* Journal of the American Chemical Society, 1989. **111**(1): p. 321-335.
2. Bewig, K.W. and W.A. Zisman, *Investigation of Solution Adsorption on Platinum of Pure and Mixed Films of Fatty Amines by Contact Potentials.* American Journal of Physical Chemistry, 1963. **67**(1): p. 130-135.
3. Yu, F., *Surface Plasmon Fluorescence Spectroscopy and Surface Plasmon Diffraction in Biomolecular Interaction Studies*, in *Max-Plank-Institut fur Polymerforschung*. 2004, University of Mainz: Mainz. p. 1-138.
4. Stenberg, E., et al., *Quantitative determination of surface concentration of protein with surface plasmon resonance using radiolabeled proteins.* Journal of Colloid and Interface Science, 1991. **143**(2): p. 513-526.
5. Filippov, L.K. and N.L. Filippova, *Overshoots of Adsorption Kinetics.* Journal of Colloid and Interface Science, 1996. **178**(2): p. 571-580.
6. Weber, P.C., et al., *Structural Origins of High-Affinity Biotin Binding to Streptavidin.* Science, 1989. **243**(4887): p. 85-88.
7. Vareiro, M.M.L.M., *Antigen-Antibody Interactions Measurements Using Surface Plasmon Fluorescence Spectroscopy*, in *Department of Chemistry*. 2006, University of Bath: Bath. p. 1-196.
8. Kucerka, N., M.A. Kiselev, and P. Balgavy, *Determination of bilayer thickness and lipid surface area in unilamellar dimyristoylphosphatidylcholine vesicles from small-angle neutron scattering curves: a comparison of evaluation methods.* European Biophysics Journal with Biophysics Letters, 2004. **33**(4): p. 328-334.
9. Neumann, T., et al., *Surface-Plasmon Fluorescence Spectroscopy.* Advanced Functional Materials, 2002. **12**(9): p. 575-586.
10. Balsinde, J., M.V. Winstead, and E.A. Dennis, *Phospholipase A(2) regulation of arachidonic acid mobilization.* Febs Letters, 2002. **531**(1): p. 2-6.
11. Wells, M.A., *Kinetic Study of Phospholipase A2 (Crotalus-Adamanteus) Catalyzed-Hydrolysis of 1,2-Dibutyrl-Sn-Glycero-3-Phosphorylcholine.* Biochemistry, 1972. **11**(6): p. 1030-&.
12. Balsinde, J., et al., *Regulation and inhibition of phospholipase A(2).* Annual Review of Pharmacology and Toxicology, 1999. **39**: p. 175-189.
13. de Haas, G.H., et al., *Purification and properties of phospholipase a from porcine pancreas.* Biochimica et Biophysica Acta (BBA) - Enzymology, 1968. **159**(1): p. 103-117.
14. Hatao, M., *On the etiology and pathophysiology of acute pancreatitis, with special reference to participation of phospholipase A.* Nippon Geka Hokan, 1969. **38**(1): p. 76-106.
15. Laine, V.J.O., D.A. Grass, and T.J. Nevalainen, *Protection by group II phospholipase A(2) against Staphylococcus aureus.* Journal of Immunology, 1999. **162**(12): p. 7402-7408.
16. Yamashita, S., et al., *Increased Expression of Membrane-Associated Phospholipase-A2 Shows Malignant Potential of Human Breast-Cancer Cells.* Cancer, 1993. **71**(10): p. 3058-3064.
17. Uozumi, N., et al., *Role of cytosolic phospholipase A(2) in allergic response and parturition.* Nature, 1997. **390**(6660): p. 618-622.
18. Six, D., A, and A. Dennis E, *The expanding superfamily of phospholipase A2 enzymes: classification and characterization.* Biochimica et Biophysica Acta (BBA)/Molecular and Cell Biology of Lipids. **1488**: p. 1-19.

19. Jaross, W., R. Eckey, and M. Menschikowski, *Biological effects of secretory phospholipase A(2) group IIA on lipoproteins and in atherogenesis.* European Journal of Clinical Investigation, 2002. **32**(6): p. 383-393.
20. Farooqui, A.A., et al., *Phospholipase A(2) and its role in brain tissue.* Journal of Neurochemistry, 1997. **69**(3): p. 889-901.
21. Stephenson, D.T., et al., *Cytosolic phospholipase A(2) (cPLA(2)) immunoreactivity is elevated in Alzheimer's disease brain.* Neurobiology of Disease, 1996. **3**(1): p. 51-63.
22. Kim, S.J., et al., *I-PLA(2) activation during apoptosis promotes the exposure of membrane lysophosphatidylcholine leading to binding by natural immunoglobulin m antibodies and complement activation.* Journal of Experimental Medicine, 2002. **196**(5): p. 655-665.
23. Fletcher, J.E., et al., *Relationship between Catalysis and Toxicological Properties of 3 Phospholipases-A2 from Elapid Snake-Venoms.* Toxicology and Applied Pharmacology, 1981. **59**(2): p. 375-388.
24. Pomorski, T., et al., *Lipid distribution and transport across cellular membranes.* Seminars in Cell and Developmental Biology, 2001. **12**(2): p. 139-148.
25. Murakami, M. and I. Kudo, *Secretory phospholipase A(2).* Biological & Pharmaceutical Bulletin, 2004. **27**(8): p. 1158-1164.
26. Gold, B.S., R.C. Dart, and R.A. Barish, *Bites of venomous snakes.* New England Journal of Medicine, 2002. **347**(5): p. 347-356.
27. Murakami, M., et al., *Regulatory functions of phospholipase A(2).* Critical Reviews in Immunology, 1997. **17**(3-4): p. 225-283.
28. McCue, M.D., *Enzyme activities and biological functions of snake venoms.* Applied Herpetology, 2005. **2**: p. 109-123.
29. Scott, D.L., et al., *Interfacial Catalysis - the Mechanism of Phospholipase-A2.* Science, 1990. **250**(4987): p. 1541-1546.
30. Kuipers, O.P., et al., *Evidence for the Involvement of Tyrosine-69 in the Control of Stereospecificity of Porcine Pancreatic Phospholipase-A2.* Protein Engineering, 1989. **2**(6): p. 467-471.
31. Verger, R., M.C.E. Mieras, and G.H. Dehaas, *Action of Phospholipase a at Interfaces.* Journal of Biological Chemistry, 1973. **248**(11): p. 4023-4034.
32. Pieterso, W., et al., *Zymogen-Catalyzed Hydrolysis of Monomeric Substrates and Presence of a Recognition Site for Lipid-Water Interfaces in Phospholipase-A2.* Biochemistry, 1974. **13**(7): p. 1455-1460.
33. Wells, M.A., *The mechanism of interfacial activation of phospholipase A2.* Biochemistry, 1974. **13**(11): p. 2248-57.
34. Gupta, S.P. and G. Govil, *Molecular orbital studies on the conformation of phospholipids EHT calculations on the polar end.* FEBS Letters, 1972. **27**(1): p. 68-70.
35. Thuren, T., *A model for the molecular mechanism of interfacial activation of phospholipase A2 supporting the substrate theory.* FEBS Letters, 1988. **229**(1): p. 95-99.
36. Meulenhoff, P., J,, *Interfacial action of phospholipase A2 : a molecular dynamics study*, in *The Molecular Dynamics Group*. 1999, Univeristy of Groningen: Groningen. p. 1-132.
37. McNamee, D., *Tackling venomous snake bites worldwide.* Lancet, 2001. **357**(9269): p. 1680.
38. Moore, G., M., *Poisonous Snakes of the World: Manual for Use by United States Amphibious Forces*. 1968: Defense Dept., Navy, Bureau of Medicine and Surgery. 220.

39. Norris, R., L, *Venom poisoning by North American reptiles.* Venomous Reptiles of the Western Hemisphere, ed. J. Campbell, A, and W. Lamar, W. 2004, New York: Cornell University Press. 683-708.
40. Toxinology, *Clinical Toxinology Resources*, in *Children, Youth & Women's Health Service*, J. White, Editor. 2007: Adelaide.
41. Hemker, H., C. and M. Kahn, J, P., *Reaction Sequence of Blood Coagulation.* 1967. **215**(5106): p. 1201-1202.
42. Thomas, R.G. and F.H. Pough, *The effect of rattlesnake venom on digestion of prey.* Toxicon, 1979. **17**(3): p. 221-228.
43. Apitzcastro, R., M.K. Jain, and G.H. Dehaas, *Origin of the Latency Phase During the Action of Phospholipase-A2 on Unmodified Phosphatidylcholine Vesicles.* Biochimica Et Biophysica Acta, 1982. **688**(2): p. 349-356.
44. Sanchez, S.A., et al., *A two-photon view of an enzyme at work: Crotalus atrox venom PLA(2) interaction with single-lipid and mixed-lipid giant unilamellar vesicles.* Biophysical Journal, 2002. **82**(4): p. 2232-2243.
45. Booth, C., et al., *Synthesis of novel biotin anchors.* Tetrahedron, 2001. **57**(49): p. 9859-9866.
46. Knoll, W., et al., *Functional tethered lipid bilayers.* Reviews in Molecular Biotechnology, 2000. **74**(3): p. 137-158.
47. Bain, C.D. and G.M. Whitesides, *Formation of Monolayers by the Coadsorption of Thiols on Gold - Variation in the Length of the Alkyl Chain.* Journal of the American Chemical Society, 1989. **111**(18): p. 7164-7175.
48. Bain, C.D., J. Evall, and G.M. Whitesides, *Formation of Monolayers by the Coadsorption of Thiols on Gold - Variation in the Head Group, Tail Group, and Solvent.* Journal of the American Chemical Society, 1989. **111**(18): p. 7155-7164.
49. Cheng, Y., et al., *Discrete membrane arrays.* Reviews in Molecular Biotechnology, 2000. **74**(3): p. 159-174.
50. Flink, S., F. van Veggel, and D.N. Reinhoudt, *Sensor functionalities in self-assembled monolayers.* Advanced Materials, 2000. **12**(18): p. 1315-1328.
51. Hubbard, J.B., V. Silin, and A.L. Plant, *Self assembly driven by hydrophobic interactions at alkanethiol monolayers: mechanism of formation of hybrid bilayer membranes.* Biophysical Chemistry, 1998. **75**(3): p. 163-176.
52. Love, J.C., et al., *Self-assembled monolayers of thiolates on metals as a form of nanotechnology.* Chemical Reviews, 2005. **105**(4): p. 1103-1169.
53. Laibinis, P.E., et al., *Comparisons of self-assembled monolayers on silver and gold: mixed monolayers derived from HS(CH2)21X and HS(CH2)10Y (X, Y = CH3, CH2OH) have similar properties.* Langmuir, 1991. **7**(12): p. 3167-3173.
54. Trapnell, B.M.W., *The Activities of Evaporated Metal Films in Gas Chemisorption.* Proceedings of the Royal Society of London. Series A, Mathematical and Physical Sciences, 1953. **218**(1135): p. 566-577.
55. Ron, H. and I. Rubinstein, *Alkanethiol monolayers on preoxidized gold. Encapsulation of gold oxide under an organic monolayer.* Langmuir, 1994. **10**(12): p. 4566-4573.
56. Sabatani, E., et al., *Organized Self-Assembling Monolayers on Electrodes .1. Octadecyl Derivatives on Gold.* Journal of Electroanalytical Chemistry, 1987. **219**(1-2): p. 365-371.
57. Evans, S.D., R. Sharma, and A. Ulman, *Contact-Angle Stability - Reorganization of Monolayer Surfaces.* Langmuir, 1991. **7**(1): p. 156-161.
58. Sondaghuethorst, J.A.M. and L.G.J. Fokkink, *Potential-Dependent Wetting of Octadecanethiol-Modified Polycrystalline Gold Electrodes.* Langmuir, 1992. **8**(10): p. 2560-2566.

59. Bolon, D.A. and C.O. Kunz, *Ultraviolet Depolymerization of Photoresist Polymers.* Polymer Engineering and Science, 1972. **12**(2): p. 109-&.
60. King, D.E., *Oxidation of Gold by Ultraviolet-Light and Ozone at 25-Degrees-C.* Journal of Vacuum Science & Technology a-Vacuum Surfaces and Films, 1995. **13**(3): p. 1247-1253.
61. McIntyre, N.S., et al., *Uses of Ultraviolet Ozone for Hydrocarbon Removal - Applications to Surfaces of Complex Composition or Geometry.* Journal of Vacuum Science & Technology a-Vacuum Surfaces and Films, 1991. **9**(3): p. 1355-1359.
62. Ron, H. and I. Rubinstein, *Self-assembled monolayers on oxidized metals. 3. Alkylthiol and dialkyl disulfide assembly on gold under electrochemical conditions.* Journal of the American Chemical Society, 1998. **120**(51): p. 13444-13452.
63. Ron, H. and I. Rubinstein, *Alkanethiol Monolayers on Preoxidized Gold - Encapsulation of Gold Oxide under an Organic Monolayer.* Langmuir, 1994. **10**(12): p. 4566-4573.
64. Ron, H., S. Matlis, and I. Rubinstein, *Self-assembled monolayers on oxidized metals. 2. Gold surface oxidative pretreatment, monolayer properties, and depression formation.* Langmuir, 1998. **14**(5): p. 1116-1121.
65. Klein, R.A., *Detection of Oxidation in Liposome Preparations.* Biochimica Et Biophysica Acta, 1970. **210**(3): p. 486-&.
66. Grit, M. and D.J.A. Crommelin, *Chemical stability of liposomes: Implications for their physical stability.* Chemistry and Physics of Lipids, 1993. **64**(1-3): p. 3-18.
67. Fiorentini, D., et al., *Buffers Can Modulate the Effect of Sonication on Egg Lecithin Liposomes.* Free Radical Research Communications, 1989. **6**(4): p. 243-250.
68. Lichtenberg, D. and Y. Barenholz, *Liposomes - Preparation, Characterization, and Preservation.* Methods of Biochemical Analysis, 1988. **33**: p. 337-462.
69. Weinstein, J.N., et al., *Liposome-Cell Interaction - Transfer and Intracellular Release of a Trapped Fluorescent Marker.* Science, 1977. **195**(4277): p. 489-492.
70. Eftink, M.R. and C.A. Ghiron, *Fluorescence Quenching Studies with Proteins.* Analytical Biochemistry, 1981. **114**(2): p. 199-227.
71. Vaugham, W.M. and G. Weber, *Oxygen Quenching of Pyrenebutyric Acid Fluorescence in Water . A Dynamic Probe of Microenvironment.* Biochemistry, 1970. **9**(3): p. 464-&.
72. Mohammed, A.R., et al., *Liposome formulation of poorly water soluble drugs: optimisation of drug loading and ESEM analysis of stability.* International Journal of Pharmaceutics, 2004. **285**(1-2): p. 23-34.
73. Clerc, S.G. and T.E. Thompson, *Permeability of dimyristoyl phosphatidylcholine/dipalmitoyl phosphatidylcholine bilayer membranes with coexisting gel and liquid-crystalline phases.* Biophys. J., 1995. **68**(6): p. 2333-2341.
74. Epand, R.M., R.F. Epand, and S. Maekawa, *The arrangement of cholesterol in membranes and binding of NAP-22.* Chemistry and Physics of Lipids, 2003. **122**(1-2): p. 33-39.
75. Spector, A. and M. Yorek, *Membrane lipid composition and cellular function.* J. Lipid Res., 1985. **26**(9): p. 1015-1035.
76. Ipsen, J.H., et al., *Phase equilibria in the phosphatidylcholine-cholesterol system.* Biochim Biophys Acta, 1987. **905**(1): p. 162-72.
77. Demel, R.A. and B. De Kruyff, *The function of sterols in membranes.* Biochimica et Biophysica Acta, 1976. **457**(2): p. 109-132.
78. Corvera, E., et al., *The permeability and the effect of acyl-chain length for phospholipid bilayers containing cholesterol: Theory and experiment.* Biochimica et Biophysica Acta - Biomembranes, 1992. **1107**(2): p. 261-270.

79. Kirby, C., J. Clarke, and G. Gregoriadis, *Effect of the Cholesterol Content of Small Unilamellar Liposomes on Their Stability Invivo and Invitro.* Biochemical Journal, 1980. **186**(2): p. 591-598.
80. Bloom, M., E. Evans, and O.G. Mouritsen, *Physical-Properties of the Fluid Lipid-Bilayer Component of Cell-Membranes - a Perspective.* Quarterly Reviews of Biophysics, 1991. **24**(3): p. 293-397.
81. Needham, D. and R.S. Nunn, *Cohesive Properties (Elastic-Deformation and Failure) of Lipid Bilayers Containing Cholesterol.* Biophysical Journal, 1990. **57**(2): p. A219-A219.
82. Cruzeirohansson, L., J.H. Ipsen, and O.G. Mouritsen, *Intrinsic Molecules in Lipid-Membranes Change the Lipid-Domain Interfacial Area - Cholesterol at Domain Interfaces.* Biochimica Et Biophysica Acta, 1989. **979**(2): p. 166-176.
83. Cohen, N., et al., *Analogs of arachidonic acid methylated at C-7 and C-10 as inhibitors of leukotriene biosynthesis.* Prostaglandins, 1984. **27**(4): p. 553-62.
84. Li, Q. and M.K. Cathcart, *Selective Inhibition of Cytosolic Phospholipase A2 in Activated Human Monocytes. REGULATION OF SUPEROXIDE ANION PRODUCTION AND LOW DENSITY LIPOPROTEIN OXIDATION.* Journal of Biological Chemistry, 1997. **272**(4): p. 2404-2411.
85. Lister, M.D., et al., *Inhibition Studies on the Membrane-Associated Phospholipase-A2 Invitro and Prostaglandin-E2 Production Invivo of the Macrophage-Like P388d1 Cell - Effects of Manoalide, 7,7-Dimethyl-5,8-Eicosadienoic Acid, and P-Bromophenacyl Bromide.* Journal of Biological Chemistry, 1989. **264**(15): p. 8520-8528.
86. Ireland, C., M,, et al., *Uniqueness of the marine environmnet: categories of marine natural products from invertebrates.* Biomedical Importance of Marine Organisms, ed. F. DG. 1988, San Francisco: Californica Academy of Science.
87. de Silva, D., E. and P.J. Scheuer, *Manoalide, an Antibiotic Sesterterpenoid from the Marine Sponge Luffariella-Variabilis (Polejaeff).* Tetrahedron Letters, 1980. **21**(17): p. 1611-1614.
88. Potts, B.C.M. and D.J. Faulkner, *Phospholipase-A2 Inhibitors from Marine Organisms.* Journal of Natural Products, 1992. **55**(12): p. 1701-1717.
89. Lombardo, D. and E.A. Dennis, *Cobra Venom Phospholipase-A2 Inhibition by Manoalide - a Novel Type of Phospholipase Inhibitor.* Journal of Biological Chemistry, 1985. **260**(12): p. 7234-7240.
90. Glaser, K.B. and R.S. Jacobs, *Molecular Pharmacology of Manoalide - Inactivation of Bee Venom Phospholipase-A2.* Biochemical Pharmacology, 1986. **35**(3): p. 449-453.
91. Gomez-Paloma, L., et al., *Chemistry and biology of anti-inflammatory marine natural products. Phospholipase A(2) inhibitors.* Current Organic Chemistry, 2005. **9**(14): p. 1419-1427.
92. Fujii, S., et al., *Chemical Modification and Inactivation of Phospholipases a(2) by a Manoalide Analog.* Biochemical Journal, 1995. **308**: p. 297-304.
93. Schrier, D.J., et al., *The effects of the phospholipase A(2) inhibitor, manoalide, on cartilage degradation, stromelysin expression, and synovial fluid cell count induced by intraarticular injection of human recombinant interleukin-1 alpha in the rabbit.* Arthritis and Rheumatism, 1996. **39**(8): p. 1292-1299.

5.0 Solid Supported Lipid Bilayer Vesicles: Method to Study Membrane-Bacterial Toxin Interactions

Pathogenic bacteria have acquired the ability to produce a range of toxins that act as an offensive mechanism against host organisms. These toxins must be secreted from the producing organism to cause their detrimental effects, however, they must also circumvent the host defences and gain access to the intracellular environment for purposes of multiplication, transmission and to sequester nutrients. The cell membrane acts as a barrier to block the passage and the actions of these toxins. The interaction between the toxins and the cell membrane provides an insight into the mechanism of toxin action and into possible therapeutic areas to combat these diseases. Using a biotin-thiol supramolecular architecture to tether the biomimetic membrane vesicles to the solid substrate, it is possible to observe the interaction between bacterial toxins and the model membranes.

Chapter Synopsis

Cholera is particularly prevalent in areas with poor sanitation, and causes significant loses of life each year. The history of cholera disease, and the associated microbe will be reviewed. Preliminary measurements concerning the interaction between the whole toxin with DMPC-GM1-cholesterol vesicles and between β-subunit toxin with DMPC-GM1-cholesterol vesicles will then be detailed. The influence GM1 and cholesterol on toxin binding will also be discussed. Additional measurements showing the relationship between the toxin concentration and the amount of toxin binding will be detailed and binding constants determined. Finally, a novel therapeutic for the inhibition of cholera toxin binding to GM1 receptors will be detailed, and potential applications of the compound will be discussed.

5.1 *Vibrio cholerae*, its toxin and the associated disease

The Gram-negative bacterium, *Vibrio cholerae* (Figure 5.1), is a facultative aerobic curved rod. The *Vibrio* group are typically polarly flagellated, which aids the movement of the bacterium. Most vibrios are aquatic microbes, either in freshwater or marine habitats. One species, *Vibrio cholerae*, is pathogenic to humans, and it does not usually infect other host species. The bacteria adhere to and colonize the small bowel, where they secrete a potent enterotoxin.

(picture source: www.mit.edu/people/tprester/dtm2001/about_cholera.htm)

Figure 5.1 Electron micrograph of a Vibrio cholerae bacterium

V.cholerae causes cholera disease, which is an acute intestinal infection, with an incubation period from less than one day to five days. Infections begin with the ingestion of contaminated food or water containing the bacteria. After passage through the acid barrier of the stomach, the organism colonizes the epithelium of the small intestine. Cholera enterotoxin produced by the adherent bacteria causes the disease-associated symptoms (Figure 5.2). Secretory diarrhoea is abruptly induced following the incubation period. The loss of several litres of water as a result of the watery diarrhoea may lead to hypovolemic shock and severe dehydration. Vomiting tends to accompany the diarrhoeal episodes leading to further dehydration. Muscle cramps are common when water and electrolytes are lost from the body tissue, also causing a loss in skin turgor and a drop in heart rate. The disease tends to run its course within 2 to 7 days, and the outcome depends on the extent of fluid and electrolyte loss and the method of treatment. Death can result from hypovolemic shock, metabolic acidosis, and acute renal failure.

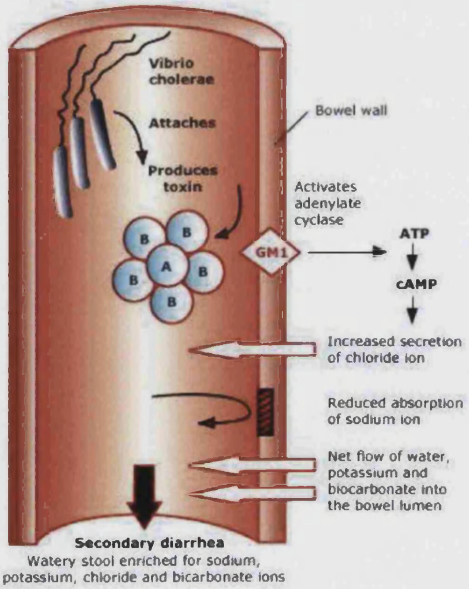

Figure 5.2 Schematic representations of the mechanism involved in diarrhoea production by Vibrio cholerae [1].

Treatment of cholera typically consists of replacing the essential fluid and electrolytes which are lost as a result of the watery diarrhoea and vomiting. This is the standard treatment procedure, but may be supplemented with antibiotics, such as tetracycline, to shorten the period of infection. The oral rehydration solution contains various salts to restore the fluid and electrolyte balance and sugars as an energy source. The addition of rice powder into the solution can reduce stool output and the duration of diarrhoea [2, 3]. Without proper treatment, the case-fatality rate for severe cholera is around 50%, however, treatment is typically effective (mortality rate reduced to <1% with proper treatment) [4, 5]. *V.cholerae* is transmitted via the faecal-oral route, therefore, the disease is especially prevalent in areas where sanitation is poor, drinking water is contaminated and areas which experience man-made and natural disasters. These outbreaks tend to occur sporadically. The disease can spread very quickly, and the rate of transmission is intensified by close confined conditions, such as those found in refuge camps.

Historically, cholera was originally endemic to the Indian subcontinent in the early 1800s, and the Ganges River was believed to serve as the contaminated reservoir which harboured the disease. Prior to this, little was known about cholera. However, it soon spread across many parts of Asia, and the first documented case in England occurring in 1848 when a sailor arrived from Hamburg where the disease was prevalent. He left the ship and sought a room to rent, where he died a few hours later. The next case was a man who subsequently rented the same room after the sailors death [6]. There have been seven sporadic pandemics of cholera between 1800 and 1970. But it was in 1854 that cholera was first described, and was later isolated in pure culture by Robert Koch in 1884. However, a milestone in cholera research was the work by John Snow, who determined that the disease was water-borne rather than spread via the aerosol route as originally thought. Moreover, during the 1854 cholera epidemic in London, Snow isolated the source of contamination as the Broad Street water pump that had become contaminated with sewage, and all the people who had contracted the disease had used that pump to collect their water [6, 7].

Cholera is still particularly prevalent in areas of Africa and Asia (Figure 5.3). The last cholera outbreak occurred in Angola, on the western coast of Africa between February 2006 and May 2007 (correct at time of submission). The country reported over 82000 cases, resulting in around 3100 deaths. The peak of the outbreak was reached at the end of April 2006 where a daily incidence of 950 cases were reported [8]. There has been a sharp

increase in the number of cholera cases reported to the World Health Organization, and in 2005, a total of 131 943 cases of the disease were reported, including 2272 deaths, notified from 52 countries. This was an increase of 30% compared to numbers reported from the previous year [9]. Outbreaks still pose a considerable public health risk, causing soci-economic disruption as well as loss of life. These disruptions are also believed to result in the under-reporting of cholera cases for fear of further trouble in the economy, unjustified travel restrictions and trade-related sanctions. Epidemiological studies show that cholera tends to follow a pronounced seasonality, and peaks in the warm seasons aiding the growth of the vibrios [4].

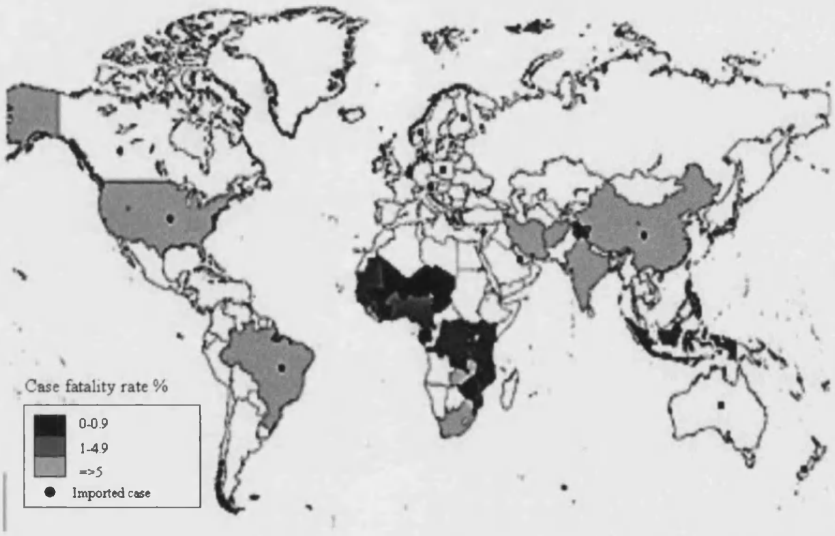

Figure 5.3 Countries reporting cases of cholera in 2005 [9].

The prevalence of cholera ensures continued interest in its mode of action, physiology, and therapeutic possibilities.

5.1.1 Cholera toxin

Vibrio cholerae has been well characterized biochemically and genetically, however, this species is not homogeneous in terms of pathogenicity. There is variation in the production of its enterotoxin, serogroup and its ability to spread epidemically. Two serogroups are associated with epidemic spread, *Vibrio cholerae* O1 and O139. However, there are strains of these serogroups which do not have the capacity to produce the enterotoxin and therefore, do not produce cholera epidemics (Figure 5.3).

Serotype	Toxin production (%)	Epidemic spread
O1	>95% positive	Yes
O139	>95% positive	Yes
O2-O138	>95% negative	No

Figure 5.3 Classification of the major Vibrio cholerae serotypes, and their capacity to produce the enterotoxin and ability to cause epidemics.

Bacterial virulence factors such as toxins, adhesion factors and the ability to assimilate unusual substrates, are often encoded on accessory genetic element (bacteriophages, plasmids, pathogenicity islands and transposons). Pathogenic strains of *V.cholerae* differ in their expression of virulence factors, and possess two gene clusters that provide normally aquatic bacteria with the ability to colonize the human intestine and secrete potent toxins. The gene encoding the cholera toxin was acquired from a filamentous bacteriophage (CTXΦ), where it replicates as a plasmid [10]. The core of the CTX element carries six known gene, including *ctxAB* (encoding the α and β subunits of cholera toxin), *ace* (accessory cholera enterotoxin) and *cep* (core-encoded pilin). The *V.cholerae* virulence cluster also contains the *tcp* gene cluster, which regulates the pilus structure essential for colonization and also acts as a receptor for CTXΦ transposition [11].

The toxin produced by pathogenic *V.cholerae* is a secreted hexameric AB_5 enterotoxin (choleragen), composed of structurally independent α (enzymatic) and β (targeting) subunits (Figure 5.4). The crystalline structure of the toxin closely resembles that described for the heat-labile enterotoxin from *Escherichia coli* (LT) with which it shares 80% sequence homology. The wedge-shaped α subunit (molecular weight 27,500 Da) is loosely held high above the plane of the pentameric β subunits (molecular weight 11,800 Da each) by the tethering A_2 chain [12]. The enzymatic activity of the toxin is solely located in the A_1 peptide of the α-subunit, however, the A_1 peptide has little effect on its own, and it is proposed the remaining toxin components are needed to aid with the insertion of the enzymatic peptide though the membrane [13]. The toxin arranges into a toroidal ring of five β subunits to which the α-subunit associates. All the subunits associate non-covalently [12], with the adjacent β subunits interacting directly via multiple hydrogen bonds. The β subunits form a pore, 30Å long, with a diameter ranging from ~11Å near the surface at which the α-subunit is positioned ~15Å on the lower surface [5]. The β subunits are lectins capable of binding carbohydrates which are highly specific for their sugar moieties. The β

subunits are able to form the pentamer in the absence of the α-subunit, however, for a toxic effect to ensure, the whole αβ toxin is required.

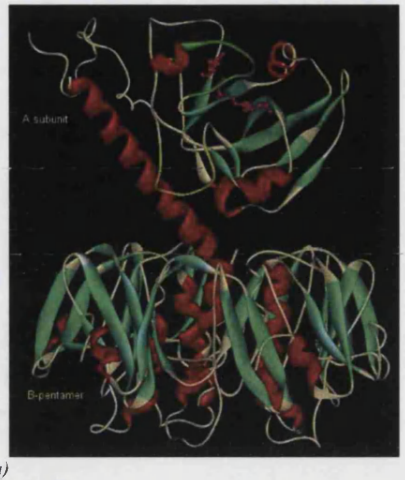

(Picture source www.bmsc.washington.edu)

Figure 5.4 Crystal structure of the cholera heterohexameric (AB5) protein toxin secreted by pathogenic strains of Vibrio cholerae.

Cholera toxin (*Ctx*) exerts its diarrheagenic action by subverting the normal physiological processes of gut epithelial cells, here, it must bind to and enter the cells of the gut epithelium.

5.1.2 Toxin-Membrane Interactions

To induce the symptoms associated with the disease, *Ctx* released into the intestinal lumen must enter the intestinal epithelial cells. *V.cholerae* does not invade the intestinal mucosa but it directly assists the delivery of the toxin into the cytosol of the cell. Therefore, the ability to enter the cells cytoplasm is entirely within the structure of the fully assembled and folded protein toxin.

For the toxin to gain entry into the cytosol of the sensitized cell, it must first circumvent the cell membrane that acts as a barrier to the toxin. The β subunits must bind to cell surface receptors to ensure the translocation of the toxin from the extracellular environment into the cytosol. The principal receptor for *Ctx* is the GM1 ganglioside (Figure 5.5). The primary event is the tight and rapid binding of the toxin to the receptors on the cell surface. There is a high affinity shown by the *Ctx* for the cell surface receptors and the equilibrium association constant has been shown to be approximately $K_A = 1 \times 10^9$ mol^{-1} [14]. It is possible for a single toxin molecule to bind up to five GM1 molecules [15],

which was confirmed by *in vitro* fixation studies showing each β subunit binds to one GM1 molecule. The interaction between the GM1 receptor and the cholera toxin shows both specificity and stability, and this dictates toxin function because it affects the toxin trafficking into the cell. The initial binding of the β-subunit to the cell surface receptors is reversible. The GM1 receptor contains two long hydrophobic acyl chains, which partition into the lipid bilayer, and a hydrophilic pentasaccharide head group, which is responsible for the recognition of the *Ctx*. The toxin binds to the cell surface to ensure that the A_1 chain of the α-subunit is facing away from the membrane [16]. This ensures that the whole toxin is internalized [17] rather than if the A_1 subunit faced towards the membrane which promotes the direct penetration of the A_1 chain through the membrane [18].

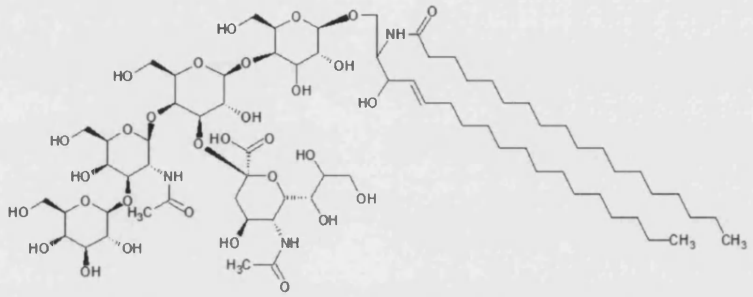

Figure 5.5 GM1 ganglioside, a glycosphingolipid found ubiquitously on the surface of eukaryotic cells. Cholera toxin exploits the receptors exclusivity to gain access into the cells cytosol.

The toxin hijacks the cells trafficking machinery to directly enter the cell using a retrograde trafficking pathway from the cell membrane into the cell. The tethered toxin associates with lipid rafts in the plasma membrane, which are rich in cholesterol. The sterol has been shown to play an important role in the assembly of the toxin oligomer [19]. The toxin is internalized by clatherin-dependant and –independent mechanisms [20], causing the endocytosis of the toxin from the extracellular environment into the cell cytosol within an endosome. Upon endocytosis, the encapsulated toxin is transported retrogradly to the Golgi apparatus. The acidic conditions found within the aqueous space of the endosome causes a conformational change within the *Ctx*. This causes the dissociation of the α- from the β-subunits. The β subunits form a pore in the endosome to allow the translocation of the α-subunit into the Golgi. The α-subunit continues on to the endoplasmic reticulum (ER), which is mediated by the KDEL motif (an ER-targeting motif) present in the α-subunit [21]. The released β subunit can then recycle from the Golgi into late endosomes and lysosomes [22]. In the ER, the α-subunit commandeers the machinery necessary for

retro-translocation of misfolded proteins to enter the cytosol. It has been proposed that the enzymatically active part of the toxin disguise themselves as misfolded proteins to ensure that they enter the ER-associated protein degradation (ERAD) pathway [23]. The toxin enters the ERAD pathway by exposing hydrophobic regions upon dissociation of their α- and β-subunit, and as mentioned previously, defectively folded proteins are earmarked for degradation. However, the enzymantically active subunit of the toxin must evade degradation. The α-subunit of many αβ protein toxins have been found to possess few lysine residues within their sequence [24], and it is this that is believed to ensure the enzymatically active subunit escapes the ubiquitin-mediated protein degradation pathways during translocation from the ER into the cytosol. Moreover, this low lysine residue content of the α-subunit is necessary because ubiquitination of a defective protein requires lysine residues. Therefore, the camouflaged α-subunit is retrotranslocated from the ER into the cytosol using the host cell protein degradation transport machinery, where it can elicit its actions (Figure 5.6) [23].

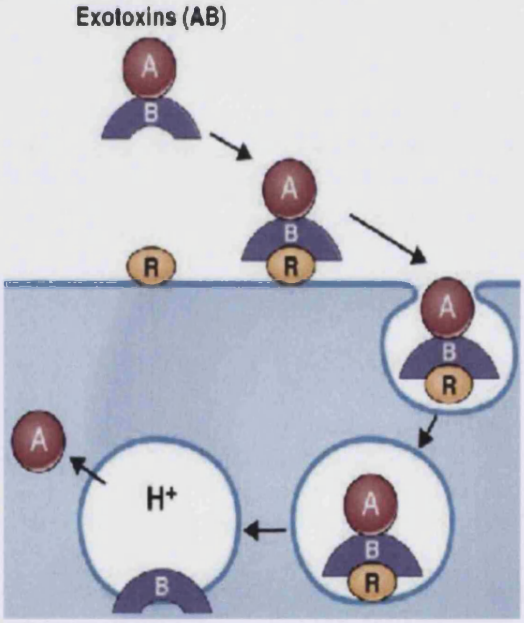

(Picture source:www.thepoint.lww.com)

Figure 5.6 Schematic of the transport of cholera toxin from the plasma membrane into the cytosol of the cell. The β-subunits bind to the GM1 receptor on the cell surface, causing the endocytosis of the whole Ctx. The toxin is translocated to the Golgi apparatus, where the αβ subunits dissociate. The β-subunits form a pore in the endosome for the translocation of the α-subunit, it is further transported to the endoplasmic reticulum and released into the cells cytoplasm. Within the cytosol, the α-subunit activates the G-protein to continually stimulate the production of cAMP. This causes the symptoms associated with cholera disease [25]. A is the α-subunit, B is the β-subunit and R is the GM1 receptor.

The α-subunit of the *Ctx* is composed of two polypeptide chains, A_1 and A_2. The enzymatic activation of the α-subunit requires the reduction of the disulfide bond which links the two subunits. The liberated A_1 polypeptide chain has been shown to exhibit both NAD^+-glycohydrolase and ADP-ribosyltransferase activities *in vitro* [26]. Cholera toxin exerts its effects on the small intestines through activation of adenylate cyclase, a transmembrane protein found on the inner surface of the cell membrane. The activation process is dependent on the presence of the α-subunit of the toxin, NAD^+, cellular cytosolic factors and ATP. The toxin causes the covalent modification of the GTP-binding protein [27], in the presence of NAD^+ as followed:

$$GTP-binding\ protein + NAD^+ \xleftrightarrow{choleratoxin} ADP-ribsoyl-GTP-binding\ protein \quad (5.1)$$

Cholera toxin catalyzes the transfer of ADP-ribose from NAD to a GTP-binding protein in the plasma membrane, which subsequently causes the activation of adenylate cyclase. GTP binds adenylate cyclase to catalyze the conversion of ATP to 3',5'-cylic AMP (cAMP). *Ctx*-induced cAMP causes the blockage of Na^+/H^+ and Cl^-/HCO_3^- exchanger ion channels. This leads to the cAMP-dependent net secretion of electrolytes and water from the cytoplasmic to the mucosal side of the epithelium. This is reliant on the active secretion of the chloride ions and the simultaneous inhibition of absorption of sodium and chloride ions in the epithelium [28]. This causes the efflux of water, increased chloride secretion and decreased sodium absorption, which affects the ion balance and osmolarity of the cells in the small intestine. The secretory transport processes are stimulated to such an extent that the reabsorptive capacity is exceeded [29]. This manifests itself as the characteristic symptoms of cholera, namely, rice water diarrhea and vomiting.

5.2 Preliminary Measurements of the Interaction between Tethered Vesicles and Cholera Toxin By Surface Plasmon Resonance

As demonstrated by the actions of lipolytic enzymes on tethered biomimetic membrane vesicles, it is possible to monitor the actions of a range of toxins that act at the membrane surface in real-time using SPR. This technique allows for the observable binding of the cholera toxin to the biomimetic model membrane surface and subsequently any changes in the membrane structure or integrity. Biomimetic membrane vesicles composing 67% DMPC, 1% biotin, 30% cholesterol, and 2% GM1 were prepared and tethered to the supramolecular surface. Cholera toxin was added to the system at the appropriate concentration.

It has previously been reported that cholera toxin is capable of inducing channels in lipid bilayers [30], and in doing so, causes the leakage of glucose entrapped within bilayer vesicles [31]. The toxin binds to and oligomerizes in target membranes generating small transmembrane pores. As demonstrated by osmotic protection experiments, pores formed in erythrocytes were approximately 0.7nm in size [32]. Therefore, any actions induced by the enterotoxin to the biomimetic membrane will be observed.

5.2.1 Monitoring the Interaction between Whole αβ-subunit Cholera Toxin and Biomimetic Membrane Vesicles

The biomimetic membrane vesicles used in chapter 4 were adapted to ensure *Ctx*-membrane interactions were observable. The inclusion of 2mol% GM1 ganglioside was incorporated into the bilayer of the biomimetic membrane vesicles. This ensured that the natural receptor of the *Ctx* was present within the model system. The addition of 0.6μmol.dm^{-3} whole *Ctx* to the tethered vesicle system (Figure 5.7) was followed as a change in reflectivity at the surface of the vesicles.

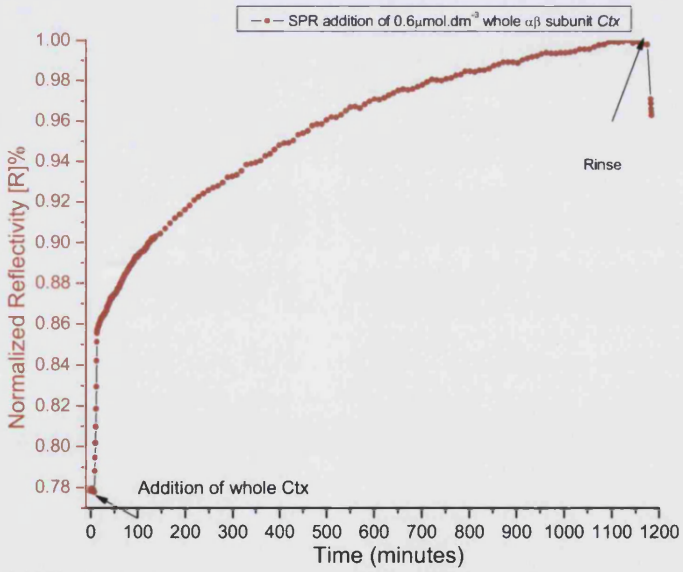

Figure 5.7 Measurement of change in mass density at the vesicle surface (SPR) over time upon the addition of whole Ctx.

The injection of the toxin into the tethered vesicle system showed an increase in reflectivity. The increase in mass density at the surface was the result of the β-subunits of the *Ctx* specifically binding to the GM1 receptors incorporated within the phospholipid

bilayer of the tethered vesicles. Maximal toxin binding was reached at around 1200 minutes. The initial binding of the toxin to the GM1 receptors was rapid, and was followed by a slower phase of toxin binding (time<20minutes). The slower phase of binding resulted from the decreased availability of the binding sites, therefore, toxin-receptor interactions decreased in frequency until equilibrium was reached. The approach of equilibrium at around 20hours coincides with the incubation period of the bacterium, therefore, this would suggest that cytotoxicity results as the analyte-ligand reaches equilibrium.

Analysis of the resonance angle scan curves before and after the addition of the whole *Ctx* (Figure 5.8), showed an increase in resonance minimum angle at the surface of 0.4°. This increase in reflectivity equated to the adsorption of 2.14ng.mm^{-2} mass at the tethered membrane surface, mediated by the GM1 receptors.

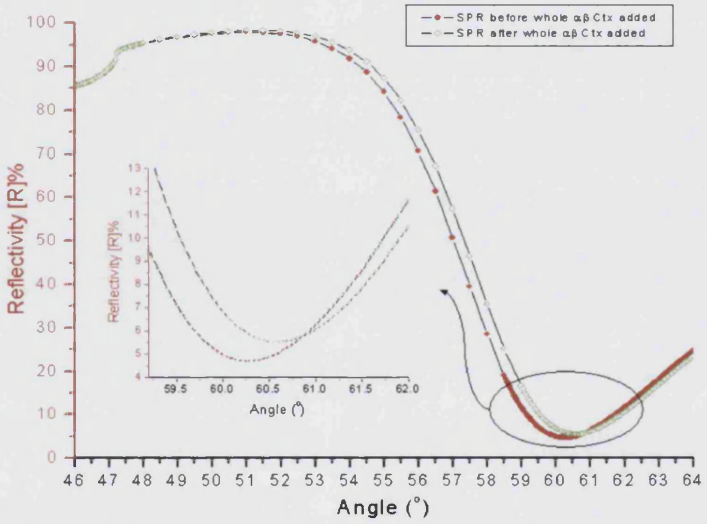

Figure 5.8 Resonance angle scan curves of the tethered vesicle system before and after the injection of 0.6μmol.dm^{-3} whole Ctx.

The initial results showed that the tethered biomimetic membrane system was a novel method for studying bacterial toxin-membrane interactions, and the measurement of change in reflectivity allowed for the quantitative analysis of adsorption of the protein toxin to the membrane surface. The incorporation of bacterial toxin receptors, such as GM1, allowed for the development of surfaces for the monitoring and analysis of specific interactions between bacterial toxins and cell surface receptors.

5.2.2 Monitoring the Interaction between β-subunit Cholera Toxin and Biomimetic Membrane Vesicles

The binding of the β-subunit of the cholera toxin to the GM1 receptors within the biomimetic membrane vesicles was monitored as a change in reflectivity (Figure 5.9).

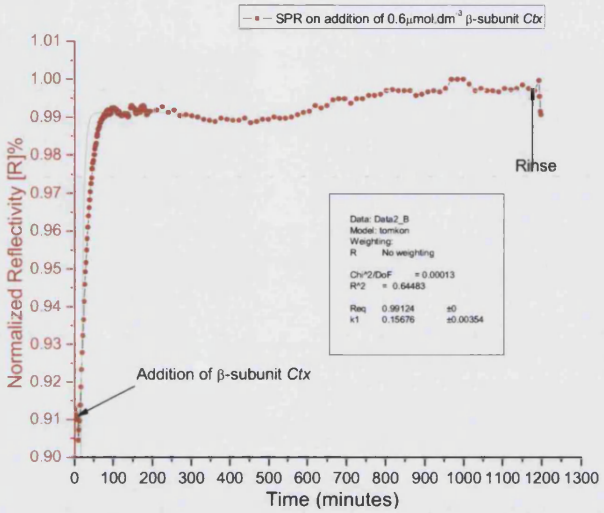

Figure 5.9 Measurement of change in mass density at the vesicle surface (SPR) over time upon the addition of β-subunit Ctx only.

The initial binding of the β-subunits of the *Ctx* was rapid, and reached an equilibrium faster than the whole toxin (Figure 5.8). There was no subsequent slower binding phase, as observed with the whole *Ctx*, suggesting that the α-subunit affects the binding kinetics. The kinetics plot derived from the interactions between the β-subunit and the GM1-containing membrane allowed for the determination of the equilibrium dissociation constant, which was determined to be $K_D = 7.2 \times 10^{-9} \text{mol.dm}^{-3}$. The K_D observed for the interaction between the β-subunit and the membrane was shown to be a high affinity interaction, this was because it was a receptor mediated interaction compared to a non-specific or non-receptor mediated interaction which tend to show lower affinity.

From the resonance scan curves, it can be shown that there was an increase in reflectivity upon addition of the β-subunit *Ctx* to the tethered vesicle system. A resonance minimum shift of 0.2^{o} was observed as a result of β-subunit *Ctx* adsorbing to the surface (Figure 5.10). The minimum shift equated to the adsorption of 1.07ng.mm^{-2} mass to the surface. This was a smaller adsorption of mass to the surface compared to the adsorption of whole toxin (2.14ng.mm^{-2} whole *Ctx* adsorption), because the molecular weight of the whole toxin was significantly greater than that of the β-subunits only.

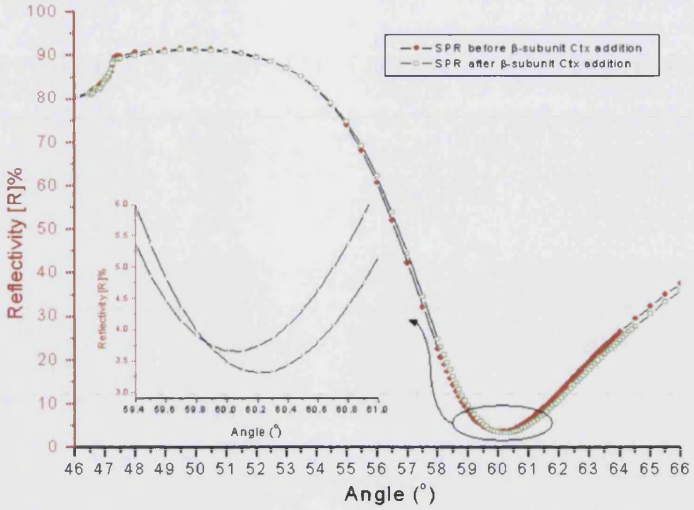

Figure 5.10 Resonance angle scan curves of the tethered vesicle system before and after the injection of 0.6μmol.dm^{-3} β-subunit Ctx only.

The use of the β-subunit in binding studies, gave the opportunity to determine affinity constants and binding not influenced by the α-subunit. Therefore, it gave a true equilibrium binding constant for the β-subunit and the GM1-containing membrane. It can be observed that the α-subunit does affect the binding between the toxin and the membrane surface, and that the binding of the whole toxin to the biomimetic membrane surface is reduced by the presence of the α-subunit.

5.2.3 Measurement of Dose-Response of Cholera Toxin on Biomimetic Membrane Vesicles

Cholera toxin has been shown to adsorb to the surface of biomimetic membrane vesicles (section 5.2.1 and 5.2.2). This adsorption was mediated by the protein-carbohydrate interaction between the β-subunits of the cholera toxin and the GM1 ganglioside present exclusively in mammalian cell membranes. This receptor-analyte interaction was concentration dependant, and varying the concentration of cholera toxin caused a dose dependant shift in the reflectivity (Figure 5.11).

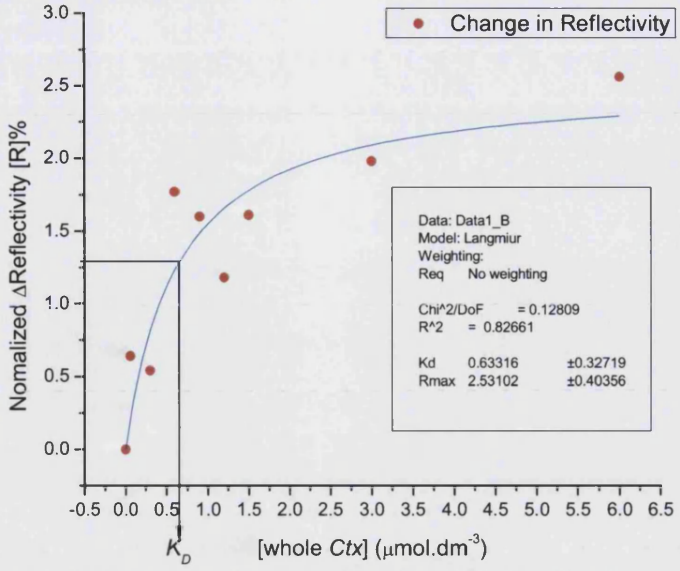

Figure 5.11 Langmuir isotherm for the normalized equilibrium for the resultant adsorption of mass from the surface as a function of cholera toxin concentration.

The multivalent interaction between the cholera toxin and the biomimetic membrane vesicles followed a standard Langmuir isotherm. From the Langmuir plot it was possible to determine the Langmuir equilibrium dissociation constant, K_D, for the adsorption of the cholera toxin to the biomimetic membrane vesicles. The K_D was determined directly from the plot at the point where $R_{eq}=R_{max}/2$ (Figure 5.11). The calculated K_D equilibrium dissociation constant for the interaction between the biomimetic membrane vesicles and cholera toxin was 6.3×10^{-7}mol.dm^{-3}, which was in good agreement with other reported K_D values [33].

The calculated dissociation equilibrium constant was of lower affinity compared to that determined between the β-subunit and the biomimetic membrane vesicles (7.2×10^{-9} mol.dm^{-3}), (Figure 5.9). The difference in affinity resulted from the influence of the α-subunit had on the interaction between the toxin and the membrane surface. Therefore, the whole toxin was used as the analyte to ensure a closer comparison to the real biological toxin system.

It is apparent that increasing the concentration of cholera toxin added to the tethered biomimetic membrane vesicles caused a concentration dependant interaction between the receptor and the analyte, and is summarized in Figure 5.12.

[cholera] ($\mu mol.dm^{-3}$)	Δ in resonance minimum (^{o})	Mass adsorption ($ng.mm^{-2}$)
0.06	0.12	0.64
0.3	0.1	0.54
0.6	0.33	1.77
0.9	0.35	1.6
1.2	0.22	1.18
1.5	0.3	1.61
3	0.37	1.98
6	0.48	2.56

Figure 5.12 Summary of the change in resonance minimum (^{o}) and the change in mass at the surface upon the addition of varying concentrations of cholera toxin to the biomimetic membrane vesicles.

Below a concentration of 0.6μmol.dm^{-3} the limit of detection for cholera toxin was approached, and at a concentration of 0.3μmol.dm^{-3} there was no observable change in reflectivity. From the resonance angle scans of the tethered biomimetic membrane vesicles before and after the addition of *Ctx* below 0.6μmol.dm^{-3}, there was no observable change in the resonance minima (Figure 5.13).

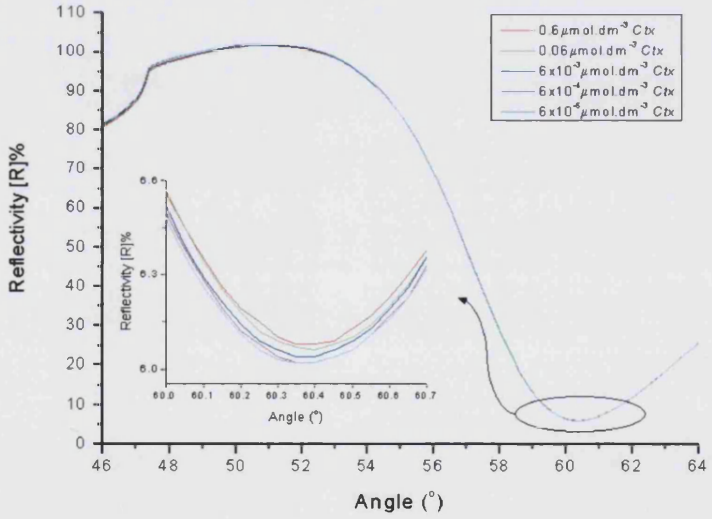

Figure 5.13 Resonance angle scans for the tethered biomimetic membrane vesicles before and after the addition of varying concentrations of cholera toxin (6 x 10^{-5} to 0.6μmol.dm^{-3}). No shift in the resonance minimum is observed.

Ctx concentrations below 0.06μmol.dm^{-3}, showed no change in the resonance minima. This would suggest that a too small change in reflectivity at the surface occurred or too few receptor-analyte interactions took place to see a change because the toxin was at a low

concentration. Therefore, the optimum concentration of cholera toxin to study receptor-analyte interactions is above 0.06μmol.dm^{-3}.

5.2.4 Monitoring the Interaction between Whole αβ-subunit Cholera Toxin and Biomimetic Membrane Vesicles Containing No GM1

Using immunohistochemical techniques, it has been determined that the tissue receptor for cholera toxin was the sialidase-resistant monosialosylganglioside [34]. The identity of the monosialosylganglioside was established to be GM1 [35]. It was shown to be an effective receptor for the bacterial toxin in final concentrations as low as 1ng.ml^{-1} [36]. Other gangliosides have been shown to bind the toxin with a lower capacity, including the disialoganglioside, GD_{1b}, which demonstrates a considerable binding capacity to cholera toxin [37]. The affinity of the β-subunit for the GM1 receptor on the cell surface is believed to be one of the highest affinity protein-carbohydrate interactions known, with an equilibrium dissociation constant of K_D = 4.3x10^{-8}mol.dm^{-3} [38], which is similar to the equilibrium dissociation constant determine in section 5.2.2. Therefore, it suggests that the interaction between β-subunit and the GM1 receptor has a higher affinity compared to the αβ-cholera toxin with the GM1 receptors. The high affinity binding is the result of a positive cooperativity between the toxin subunits [39] and through the multivalent interaction of the pentameric toxin with up to five GM1 receptors at the cell surface [40].

GM1 has now been well reported to have the highest affinity and capacity to bind cholera toxin. Using combined SPR and SPFS, the interaction of *Ctx* with tethered biomimetic membrane vesicles containing no GM1 ganglioside was monitored (Figure 5.14 Red and Blue plots), and was compared to the addition of *Ctx* to GM1-containing biomimetic vesicles (Figure 5.14 Fuchsia and Green plots).

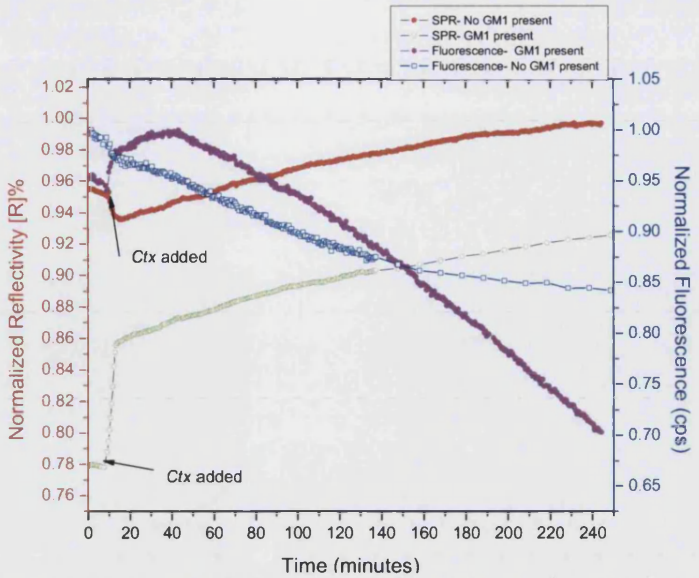

5.14 Simultaneous measurement of change in reflectivity at the vesicle surface (SPR) and change in florescence (SPFS) upon the addition of whole Ctx to biomimetic membrane vesicles containing no GM1 ganglioside(Red and Blue plot), compared to when GM1 is present within the vesicle bilayer (Green and Fuchsia plot)

The addition of 0.6μmol.dm^{-3} *Ctx* to the tethered vesicle system containing no GM1 showed a marked difference to that when GM1 ganglioside was present within the vesicle system. Upon the addition of the *Ctx* to the surface there was non-specific binding of the toxin to the membrane, therefore, *Ctx* has some intrinsic binding capacity to other membrane constituents. The non-specific binding may result from the presence of sterols in the vesicle bilayer, as cholesterol has been shown to be a target molecule for many bacterial pore-forming toxins. Therefore, the toxin may have a certain intrinsic binding capacity towards sterols or membrane phospholipids. It has been shown that pore-forming toxins, such as Streptolysin O from *Streptococcus pyogenes*, requires cholesterol for the initial events during membrane binding [41]. Cholesterol has been shown to be necessary for the oligomerization of the *Ctx* monomers [42, 43], therefore, there may be a certain degree of affinity between the *Ctx* and the GM1-deficient biomimetic vesicles as a result of cholesterol. This is supported by a report that suggests that in the absence of any ceramides or glycolipids, *Ctx* are still highly active when the concentration of the membrane cholesterol is raised above 35mol% [44]. The *Ctx* can be seen to be active within the membrane because there was a change in the fluorescence signal upon addition of the *Ctx* to the GM1-deficient vesicles (Figure 5.14 Blue plot). The diffusion of the dye encapsulated within the aqueous space of the tethered vesicle was increased, suggesting the toxin had oligomerized and formed pore-like structures within the phospholipid bilayer.

The pores subsequently provided an additional means of dye diffusion, causing an increased porosity of the membrane. The apparent dye diffusion coefficient for the leakage of BODIPY from GM1-deficient membrane vesicles was calculated to be $D^* = 5.8 \times 10^{-14} cm^2.s^{-1}$. However, the inclusion of GM1 in the vesicle bilayer allowed for specific toxin binding, and the calculated apparent dye diffusion coefficient was $D^* = 1.11 \times 10^{-13} cm^2.s^{-1}$. Therefore, the omission of the GM1 receptor from the biomimetic membrane vesicles caused a reduction in the diffusion of the encapsulated dye into the bulk solution compared to when GM1 was present within the bilayer.

The change in reflectivity was greater between *Ctx* and the membrane surface containing GM1 (Figure 5.15a) compared to *Ctx* and membranes deficient in GM1 (Figure 5.15b). There was a 0.35° shift in resonance minimum when GM1 was present within the vesicle bilayer upon addition of *Ctx*, which equated to the adsorption of $1.87 ng.mm^{-2}$ mass at the membrane surface. This was a significant increase in mass compared to when no GM1 was present, which exhibited a 0.05° shift in the resonance minimum. This equated to the adsorption of $0.268 ng.mm^{-2}$ mass at the membrane surface.

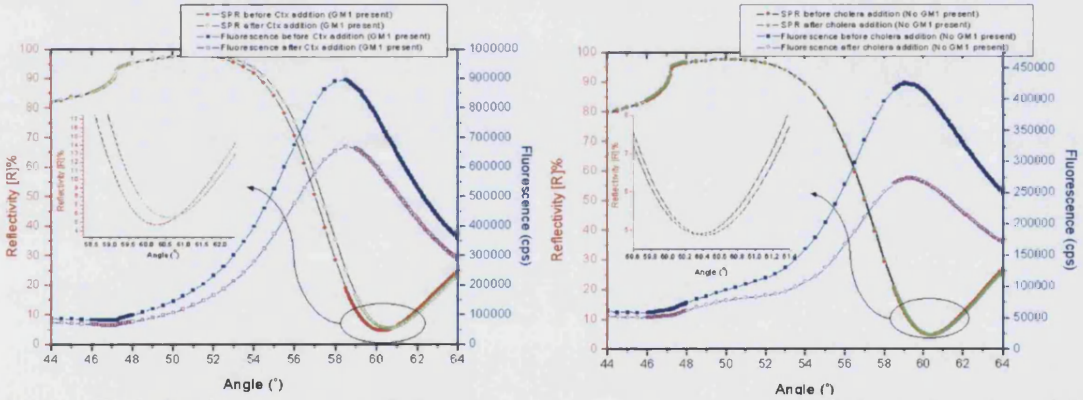

Figure 5.15 (a) Resonance and fluorescence angle scan curves of the tethered vesicle system before and after the injection of 0.6μmol.dm^{-3} Ctx to GM1-containing vesicles and (b) Scan curves before and after the injection of Ctx to GM1-deficient vesicles.

The inclusion of the GM1 glycoprotein mediated the attachment of cholera toxin to the biomimetic membrane surface. The ganglioside significantly increased the binding capacity of the toxin to the membranes. However, the toxins capacity to bind did occur via a non-specific interaction when the receptor was absent. This would suggest that the presence of a high sterol content within the tethered vesicle bilayer mediates non-specific toxin binding to the receptors. The omission of GM1 from the vesicle bilayers ensured a reduction in the permeability of the biomimetic membrane vesicles, as calculated from the

apparent dye diffusion coefficient. Therefore, the expression of GM1 within biological membranes ensures specific binding to *Ctx*, however, non-specific binding may also occur.

5.2.5 Monitoring the Interaction between Whole αβ-subunit Cholera Toxin and Biomimetic Membrane Vesicles Containing No Sterol

Sterols have been shown to affect the oligomerization of cholera toxin monomers [42, 45]. Cholesterol is inclined to form lipid rafts within biological membranes, and this acts to concentrate receptors and glycoproteins into the cholesterol domains. Therefore, cholesterol would tend to cause the concentration of the β-subunit monomers in the biomimetic membrane, which ensures oligomerization can take place. As mentioned in section 5.2.3, *Ctx* is highly active in membranes containing a high proportion of sterol, and *Ctx* tends to non-specifically adsorb to the vesicle surface when GM1 is absent.

Using combined SPR and SPFS, the interaction of *Ctx* with tethered biomimetic membrane vesicles containing no sterols was monitored (Figure 5.16).

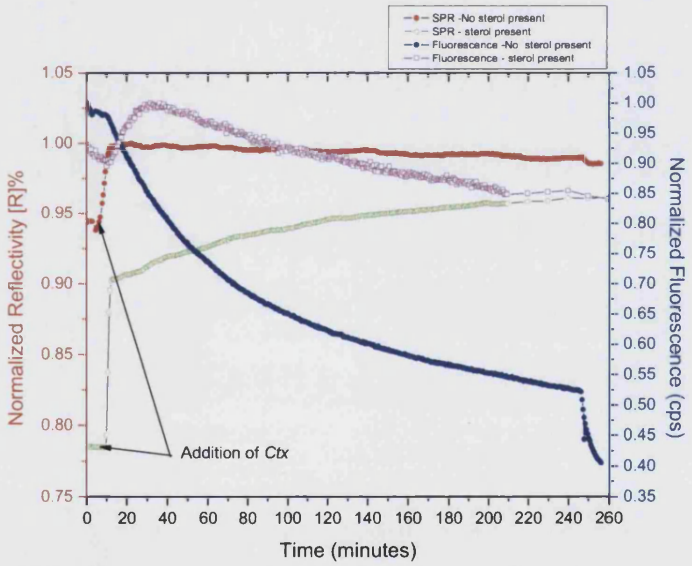

Figure 5.16 Simultaneous measurement of change in reflectivity at the vesicle surface (SPR) and change in florescence (SPFS) upon the addition of Ctx to biomimetic membrane vesicles containing no cholesterol (red and blue plot) compared to vesicles containing cholesterol (green and fuchsia plot).

Biomimetic membrane vesicles deficient in cholesterol showed a smaller change in reflectivity upon *Ctx* addition compared to cholesterol-containing vesicles. The smaller change in reflectivity suggests that cholesterol does affect *Ctx* binding, as well as affecting the oligomerization of the *Ctx* monomers. The change in fluorescence observed upon toxin

addition to the vesicles containing the sterol can not be readily compared to vesicles deficient in cholesterol, because sterols significantly alter the natural porosity and permeability of phospholipid bilayers (see section 4.7.3.1).

The omission of cholesterol from the biomimetic membrane vesicles showed reduced mass density adsorption to the surface (Figure 5.17). A resonance minimum shift of 0.15° was calculated from the resonance scans before and after the addition of *Ctx* to the cholesterol-free vesicles, which equated to the adsorption of 0.80ng.mm^{-2} of mass to the vesicle surface. This adsorption was significantly lower than that observed when tethered vesicles contained cholesterol (1.87ng.mm^{-2} mass adsorption calculated from Figure 5.15a). This suggests that cholesterol plays a dual role in *Ctx* pathogenicity, and causes toxin monomer oligomerization and also synergistically improves the capacity of the toxin to bind to biomimetic membranes.

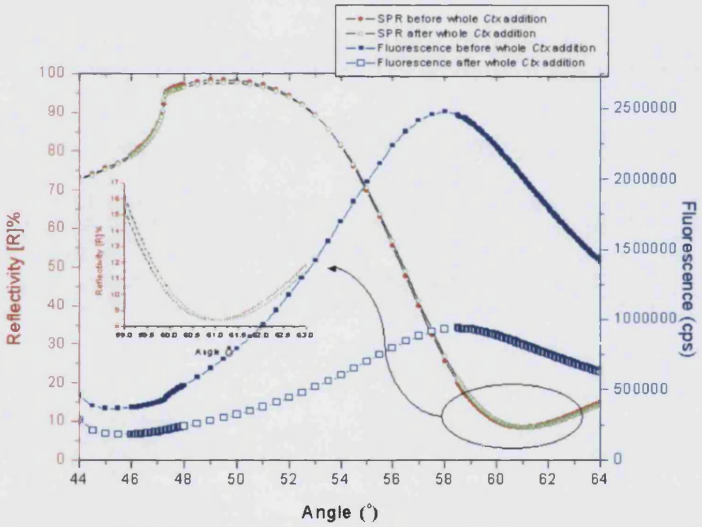

Figure 5.17 Resonance and fluorescence angle scan curves of the tethered vesicle system before and after the injection of 0.6μmol.dm^{-3} whole Ctx to cholesterol-deficient vesicles.

From the results present in this section, it is apparent that the tethered biomimetic membrane system provides a novel means of studying bacterial toxins. The combined SPR/SPFS technique provides a sensitive means of determining affinity constants and the change in mass density upon toxin addition. It is evident that toxin binding is mediated by the β-subunit and it shows high affinity towards the GM1 ganglioside, which is exclusively expressed in mammalian cells. Moreover, cholera toxin shows a non-specific affinity towards ganglioside-deficient membranes as a result of high sterol content. The expression of GM1 causes increased permeability of the membrane vesicles, as determined by the apparent dye diffusion coefficient, compared to vesicles not expressing the ganglioside

receptor. The omission of cholesterol causes a reduction in the binding capacity towards *Ctx*. Therefore, cholesterol has a dual role in *Ctx* pathogenicity, assisting toxin binding to the membrane and facilitating the oligomerization of the toxin monomers into a pentameric pore within the phospholipid bilayer.

5.3 Luminescence Spectrometry Analysis of Fluorescence Diffusion upon Cholera Toxin-Membrane Interactions

The BODIPY 650/665-X STP ester was used as the fluorescent dye in these experiments (Figure 5.18). It has been shown that BODIPY dyes have high photostability, narrow emission spectrum with large Stokes' shift and give less overlap with certain other fluorophores compared with other commercially available fluorescent dyes. These dyes tend to be relatively non-polar and the chromophore is electrically neutral. They have been favourably used because of their high extinction coefficients, good fluorescence quantum yields and relatively long excited-state lifetimes (>3nanoseconds) [46].

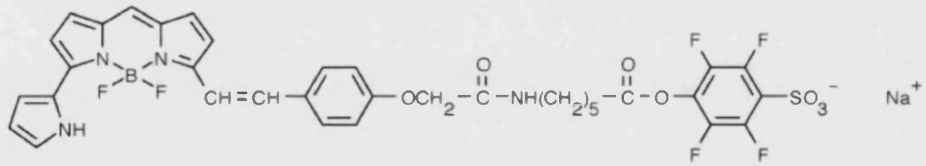

Figure 5.18 Chemical structure of 6-(((4,4-difluoro- 5-(2-pyrrolyl) -4-bora-3a,4a- diaza-s-indacene- 3-yl)styryloxy) acetyl) aminohexanoic acid, sulfotetrafluorophenyl ester, sodium salt, BODIPY dye molecule, which excites at 650nm and emits at 665nm.

The addition of whole- and β-subunit *Ctx* to tethered biomimetic membrane vesicles during kinetics experiments caused an unexpected phenomenon in the measured fluorescence response (as highlighted in Figure 5.19). Upon the addition of the *Ctx* to the biomimetic membrane surface there was an initial increase in the measured fluorescence signal, followed by the decrease in fluorescence as the encapsulated dye diffused through the permeated membrane. The increase in fluorescence signal has not been reported previously in literature.

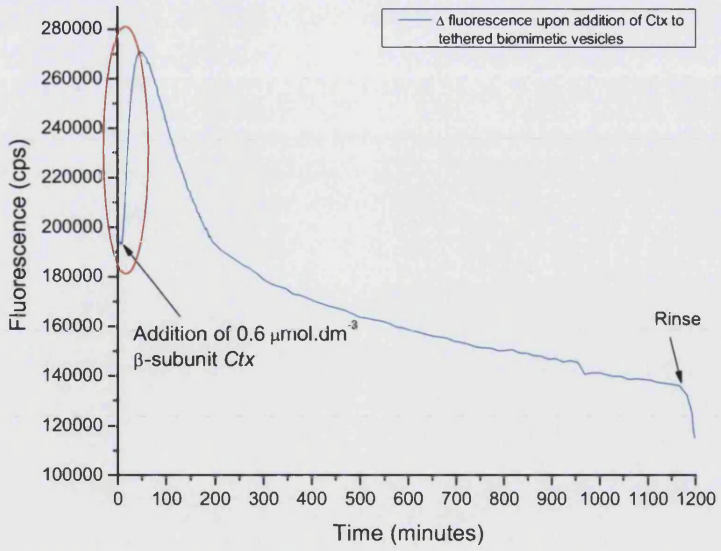

Figure 5.19 Monitoring the change in fluorescence as a result of biomimetic membrane permeation due to the addition of 0.6μmol.dm^{-3} β-subunit Ctx. Unreported increase in fluorescence upon toxin pore formation in the membrane vesicles is highlighted.

The increase in fluorescence observed upon *Ctx* addition could result from the encapsulated dye self-quenching (section 2.2.2). The encapsulation of the BODIPY dye within the aqueous space of the tethered vesicles concentrates the fluorophore, thereby increasing the potential for the dye molecules to come into contact with one another. This would cause the quenching of the dyes within the encapsulated space and therefore cause an underreporting in detected fluorescence. Quenching of fluorescent molecules requires molecular contact between the fluorescent molecule and the quencher, and encapsulation of the dye molecules increases the probability of molecular contact. The quencher may be another fluorescent molecule (self-quenching), therefore, the encapsulation of the dye within the vesicles could induce self-quenching. The oligomerization of the *Ctx* monomers into a transmembrane pore causes the permeation of the biomimetic membrane vesicles, and provides channels for the quenched fluorophores to diffuse through into the bulk solution. Diffusion of the BODIPY from the region of high fluorophore concentration to low fluorophore concentration in the bulk solution reduces the probability of molecular contact, and therefore reduces the probability of the BODIPY self-quenching. Diffusion of the supposed quenched BODIPY dye into the bulk solution removes the quenched state of the fluorophore and therefore could cause the increase in fluorescence signal until the fluorescent molecules are carried away into the bulk solution.

Using a luminescence spectrometer, the ability of BODIPY to self-quench was determined. BODIPY solutions ranging between 0.05-10μmol.dm^{-3} were prepared and analyzed in the spectrometer (Excitation = 633nm, Emission = 665nm, Scan speed = 200nm/minute). During SPFS kinetics experiments, the BODIPY dye is encapsulated at a 5μmol.dm^{-3} concentration within the aqueous space of the biomimetic membrane vesicles, therefore, BODIPY solutions within this range were analyzed. The maximum emission intensity was observed for all of the fluorophore concentrations analyzed, and plotted as a function of BODIPY concentration (Figure 5.20).

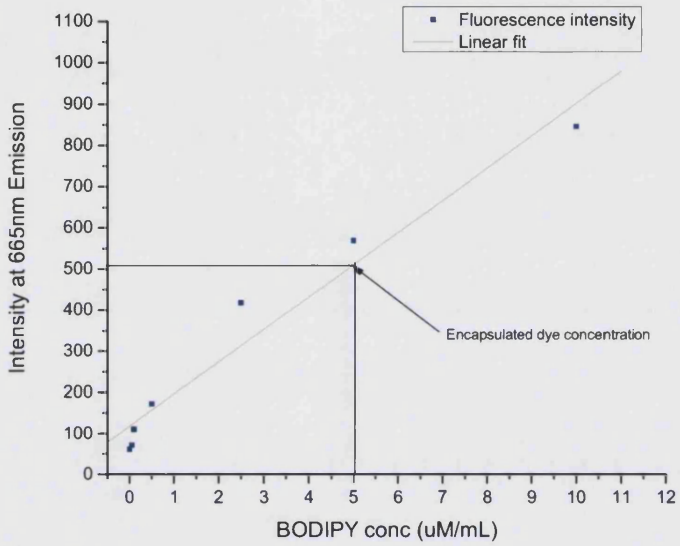

Figure 5.20 Luminescence spectrometry plot, with linear fit, of the fluorescence intensity of varying concentrations of BODIPY dye at emission at 665nm.

For each of the BODIPY concentrations tested, there was no evidence of fluorophore self-quenching, as intensity was directly proportional to dye concentration. Therefore, increasing the probability of molecular contact between BODIPY fluorophores, by encapsulating high concentrations of dye, did not cause quenching of the BODIPY. Above the working concentration (5μmol.dm^{-3}), the fluorescent dye did not self-quench and therefore, does not explain the increase in fluorescence seen upon addition of the *Ctx* pore-forming toxin to the biomimetic membranes (Figure 5.19).

The change in fluorescence intensity was not dependant on the age of the fluorophore solution or was not a result of fluorophore degradation (Figure 5.21). The intensity of the various dye concentrations taken over a seven day period showed no change in the linear fit. The linear fit for the dye concentrations taken on day one, day two and day seven were calculated to be 65.6, 53.7, and 59.9 respectively. Therefore, the fluorophore does not

degrade within the time scale tested and the increase in fluorescence was not a result of fluorophore by-products.

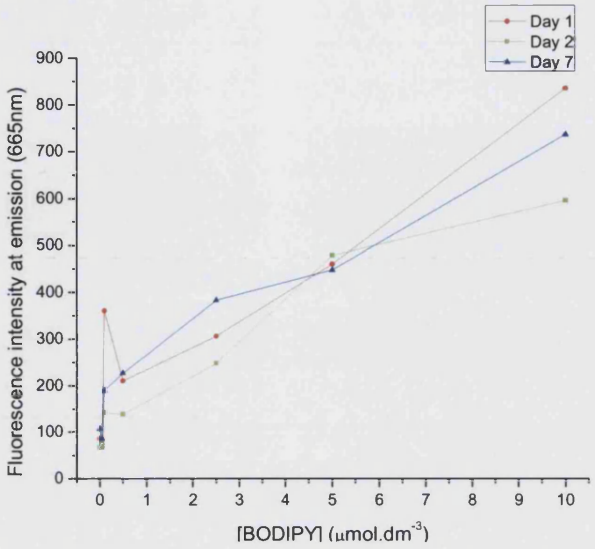

5.21 Luminescence spectrometry plot, with linear fit, of the fluorescence intensity of varying concentrations of BODIPY dye at emission at 665nm taken after 1 day, 2 days and 7 days.

A wide variety of substances act as quenchers, including amines, chloride and hydrogen peroxide. One of the most prominent quenchers is molecular oxygen, which quenches almost all known fluorophores. Oxygen quenches fluorescent molecules in a reversible manner, but the degree of quenching is dependant on the oxygen pressure and concentration [47]. The mechanism of quenching by oxygen is believed to be caused by the fluorophore undergoing an intersystem crossing into the triplet state, and the long-lived triplets are completely quenched, so fluorescence is not observed [48]. It has been reported that BODIPY is quenched by oxygen around 5% of the time [49]. Quenching by oxygen was minimized by removing dissolved oxygen in all buffers and samples by bubbling nitrogen through. However, this did not eliminate the increase in fluorescence observed upon toxin addition.

Another mechanism of quenching may arise from polarity effects. Charge effects are observed with quenchers including iodine and chloride. The charge of proteins and phospholipids can also have a marked effect of the intensity of fluorescence and changes in fluorescence can be seen during protein folding if a fluorophore moves from a hydrophobic to hydrophilic environment of vice versa. The BODIPY dye forms hydrogen bonds with water molecules when in solution, and the hydration of the dye may cause partial

quenching of the dye molecules, and the effect on the fluorescence signal may arise from this partial quenching caused by the hydration of the BODIPY. The effect of charge on fluorescence signal could be caused by the formation of the *Ctx* pore in the biomimetic phospholipid bilayer vesicles. As mentioned previously in this chapter, the β-subunits form a pentamer doughnut shape, with five monomers arranged symmetrically around the central axis, leaving a pore in the middle. It has been detailed that a very polar central pore is formed, and the many charged residues are located within this central pore, giving the pentamer a very unsymmetrical distribution of charges [50]. The β-subunits are stabilized when oligomarized by a variety of interactions, including hydrogen bonding between the β-subunits [51]. The charged pore and the hydrogen bonds involved in its stabilization could cause the phenomenon seen in the fluorescence signal. The pore formed by the *Ctx* provides a direct route for the encapsulated dye to diffuse into the bulk solution, but the charged residues may cause the water molecules surrounding the hydrated BODIPY dye to be stripped away temporarily while the dye traverses the *Ctx* pore. The temporary removal of the hydration state by the charged pore may cause the partial self-quenched dye to fluoresce more intensely while traversing the bacterial toxin pore. Upon emergence from the pore, the BODIPY becomes rehydrated and moves away into the bulk solution (Figure 5.22).

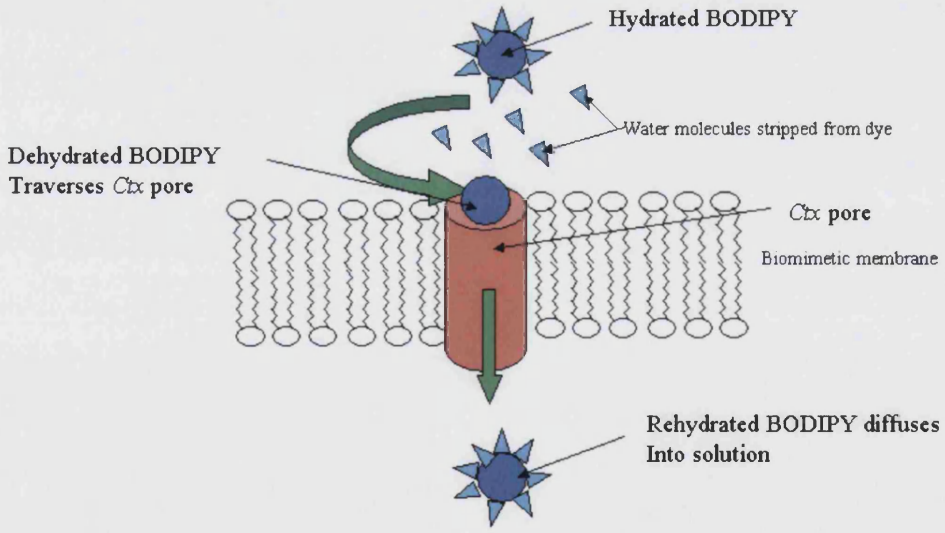

Figure 5.22 Schematic of the potential mechanism to explain the temporary increase in the fluorescence signal upon Ctx addition to biomimetic phospholipid vesicles. The hydrated BODIPY dye (partially quenched) diffuses towards the highly charged Ctx pore. The charged pore causes the water molecules hydrating the dye to be temporarily stripped, instigating the temporary un-quenching of the BODIPY as it traverses the Ctx pore. Upon emergence from the pore, the BODIPY dye becomes rehydrated, and therefore, returning it to its original partially quenched state.

Another proposed mechanism may be the influence of the substrate surface, as solid surfaces have been shown to cause distortions in the shape of tethered vesicles [52]. The solid surface may influence the vesicles by distorting the typically spherical vesicles and cause the compression of the biomimetic membrane vesicles. Therefore, this would bring the vesicles closer within the evanescent field, and subsequently cause an enhancement effect in the detected fluorescence, which may manifest as the rise in fluorescence upon pore formation. Therefore, β-subunit *Ctx* and whole *Ctx* were respectively added to the biomimetic membrane vesicles containing the encapsulated BODIPY in the bulk solution (vesicles were not tethered to the solid substrate), and the increase in fluorescence was subsequently observed (Figure 5.23).

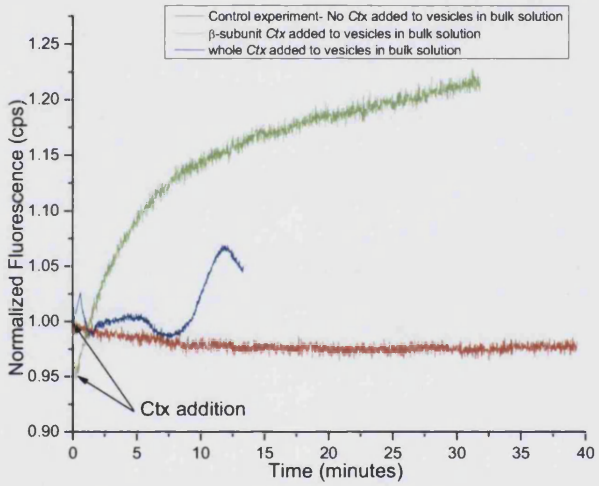

Figure 5.23 Observing the fluorescence upon addition of Ctx to biomimetic membrane vesicles free in the bulk solution (vesicles were not tethered to the surface). Initial increase in fluorescence still observed.

It can be observed that addition of the β-subunit or the whole *Ctx* to vesicles in solution causes the increase in fluorescence observed upon pore formation. This suggests that the solid surface does not affect the shape of the vesicles and is not caused by an enhancement effect in compressed vesicles. Therefore, biomimetic membrane vesicles in the bulk solution also show the increase in fluorescence observed upon toxin addition and is not caused by tethering to solid surfaces.

The initial increase in fluorescence signal observed upon addition of *Ctx* to biomimetic membrane vesicles was not a result of the encapsulated BODIPY dye self-quenching at high concentrations when confined to the aqueous space of the vesicles. The increase in

fluorescence was not an affect of the solid surface, as biomimetic vesicles in the bulk solution also showed this effect. The increase was best explained by the physical properties of the pentamer pore formed within the biomimetic membranes and the hydration of the BODIPY. The interior of the *Ctx* pores are highly charged, therefore, the charge may temporarily remove the bound water molecules from the dye causing the fluorophore to fluoresce more intensely while within the *Ctx* pore. Upon emergence from the charged pore, the dye rehydrates and this reinstates the partial self-quenched state. After the initial increased rate of diffusion caused at the time of pore formation, the rate of dye diffusion decreases and the fluorescence signal begins to fall as the BODIPY is free in the bulk solution.

5.4 Inhibition of Cholera Toxin-Membrane Interactions by Blocking the Membrane Receptors

Various drug molecules have been developed to target and relieve the symptoms associated with cholera disease as well as trying to prevent the actions of the toxins produced by pathogenic *Vibrio cholerae*. However, at present, the primary method for the treatment of patients suffering from cholera is to replace the electrolytes and water lost during episodes of diarrhoea and vomiting.

5.4.1 The Use of Oral Rehydration Therapy in the Treatment of Cholera

Oral rehydration therapy (ORT) is the main strategy recommended by the World Health Organization to achieve a reduction in diarrhoea-related mortality and malnutrition especially in children. Oral rehydration salts are balanced glucose-electrolyte mixtures first used in 1969 by UNICEF and WHO for clinical dehydration (Figure 5.24).

Oral Rehydration Salts	gram.litre^{-1}	%	Osmolarity composition	mmol.litre^{-1}
Sodium chloride	2.6	12.7	Sodium	75
Glucose	13.5	65.9	Chloride	65
Potassium chloride	1.5	7.3	Glucose	75
Trisodium citrate	2.9	14.1	Potassium	20
			Citrate	10
TOTAL	**20.5**	**100.00**	**Total Osmolarity**	**245**

Figure 5.24 The composition of the oral rehydration salts, which are dissolved in drinking water to the correct concentration, given to patients with acute diarrhoeal disease, including cholera [53].

It has been shown that glucose facilitates the adsorption of sodium and water in the small intestine, sodium and potassium are used to restore the essential ions lost during the purging, and citrate is included to correct the acidosis that occurs as a result of diarrhoea and dehydration, and also ensures the stability of the ORS mixture during storage [53].

Few pharmacological approaches to treat cholera have been developed, and the current treatment relies on the ORT. The provision of these oral rehydration fluids is a means of treating diarrhoeal diseases such as cholera, but does not prevent the actions of the cholera toxin either from binding to the cell membrane, being internalized into the cytosol or eliciting its actions on cAMP levels. Prevention of diarrhoea in cholera can be achieved by intervention at different stages of the mechanism by which the bacterium causes the imbalance in intestinal secretions.

5.4.2 The Use of Anti-Motility and Anti-Secretory Therapeutics in the Treatment of Cholera

Effective drug therapy against *Vibrio cholera* is pivotal for the prevention of outbreaks and for the rapid treatment during an outbreak. There are four major routes for cholera treatment, which include the supportive therapy using the oral rehydration salts. Anti-diarrhoeal drugs, which include the anti-motility and anti-secretory agents, were developed to reduce stool output and frequency. Anti-motility agents act by increasing the time taken for the occurrence of diarrhoea, thereby enhancing the potential for reabsorption of the fluids and electrolytes before excretion can occur. However, this class of therapeutic agent, which includes loperamide, has proven to be ineffective against cholera [54].

Anti-secretory agents, such as enkephalins, bind to the δ opioid peptide receptor, which causes the activation of inhibitory G proteins. This results in a reduction in the intracellular levels of cAMP, and subsequently results in the deactivation of the chloride and potassium ion channels which reduces the secretion of salts and fluid [55]. The anti-secretory agents directly inhibit the secretory processes by reducing stool volume in patients with high volume watery diarrhoea [56]. These drugs target intracellular signalling mechanisms, such as calcium binding proteins, helping to reduce stool weight and bowel frequency. However, these classes of therapeutic agent may have potential side effects including delayed onset of action and the interference of the absorption of other medications [57].

5.4.3 The Use of Anti-Microbials and the Cholera Vaccine in the Treatment of Cholera

Antimicrobial therapies has proven to be controversial, mainly due to the development of resistant strains of pathogens, especially in endemic areas [58]. However, anti-microbial agents have been shown to reduce the severity and duration of some *Vibrio* infections, such as multidose norfloxacin treatment, which significantly reduces stool output, duration of diarrhoea and fluid requirement compared with the other regimens [59].

Cholera vaccines were developed over 100 years ago, and various types have been developed, with varying efficiencies. The two major cholera vaccines developed are the oral killed whole cell-cholera toxin recombinant β-subunit vaccine and the oral live attenuated *Vibrio cholerae* vaccine. These oral vaccines have been shown to be well tolerated in field trials, and provide 80%-85% protection against *Vibrio cholerae* O1 for at least 6 months [60]. However, these vaccines can show high variability dependant upon the age of the patient [55].

5.4.4 Inhibition of Cholera Toxin-Receptor Binding in the Prevention and Treatment of Cholera

The rapid and high affinity binding between the cholera toxin and the GM1 receptor provides an attractive target for the prevention and treatment of cholera. The interaction between the bacterial toxin and the membrane receptor occurs almost instantaneously, is saturable and initially reversible [36, 61]. One strategy to prevent the analyte-receptor interaction between the cell membrane and the enterotoxin is to neutralize the toxin using a crude ganglioside mixture, because exogenous GM1 inactivates the cholera toxin in about

equimolar proportions. Administration of large amounts of GM1 or a structural analogue has been observed to prevent the binding of the toxin to the cell membrane receptors [14].

Another approach is to block the GM1 gangliosides with β-subunit cholera toxin. The β-subunit can not elicit toxicity towards cells itself, therefore the administration of the β-subunit could impede the interaction between the toxin secreted by the invading pathogen and the cell membrane. Therefore, blocking the binding sites prevents the microbial toxin from eliciting its toxic actions. *In vitro* studies have shown that pre-treatment of the gut of rabbits with $0.5\mu g.cm^{-1}$ β-subunit completely protects from experimental infection with high doses of active cholera toxin [62, 63].

Another approach to blocking the GM1 binding sites has been the development of small molecule antagonist to toxin-membrane binding. The benefit of developing these high affinity ligands that block the interaction between the bacterial toxin and the membrane receptors is that they do not have to pass any membranes to exert their effects, therefore they can potentially be any size and carry a charge [64]. Using competitive surface receptor binding assays, a series of bivalent ligands have been synthesized to inhibit the receptor binding processes of cholera toxin. Reports suggest that steric blocking at the receptor binding surface may account for the inhibitory properties of these synthetic bivalent ligands [64]. Multivalency allows strong interactions to occur from many intrinsically weak ligand-receptor pairings. The energetics needed for monovalent interactions compared to multivalency is different, and the enthalpy of binding is directly proportional to the number of binding epitopes [65]. This effect of multivalency causes an increase in the K_A values of the multivalent interactions relative to monovalent counterparts because there is a more positive entropy contribution to binding of a multivalent interaction [66]. These multiple interactions also show strong geometrically specific interactions, because the spatial ordering on one multivalent interactant can induce complementary ordering of the corresponding receptor sites on its partner [67]. These properties directly influence the design and application of therapeutic molecules that impede receptor-analyte binding.

Preventing toxin binding using small therapeutic molecules is an attractive approach to preventing cholera because the binding inhibitors can be administered prophylactically in high risk areas or as a therapy after an infection has begun. This method of preventing and

treating cholera is still in its infancy, because even though initial studies show promise, the compounds synthesized to date remain in development and have not be demonstrated to be effective *in vivo*.

The lanthanoid group of elements, which include lanthanum, cerium, europium and ytterbium, are chemically similar to each other and occur as stable trivalent cations in their natural state. Lanthanum and europium complexes have been shown to be effective at detecting neutral sugars, glycolipids and phospholipids. Europium complexes has been reported to detect sialic acid-containing gangliosides at physiological pH because there is a co-operative complexation of the oligosaccharide and sialic acid residues to the metal centre [68]. The presence of a sialic acid moiety confers a negative charge on a molecule, and this charge prompts a strong interaction with cations of biological relevance (Figure 5.25), such as calcium or lanthanides [69]. The sialic acid residues of the GM1 binds to the europium ions via multiple coordination sites with high affinity. Molecular recognition between GM1 and lanthanides has been exploited for the detection of cancer biomarkers. The development of lanthanide anticancer agents have initially demonstrated broader spectrum anti-tumour activity compared to classical platinum anti-tumour agents [70].

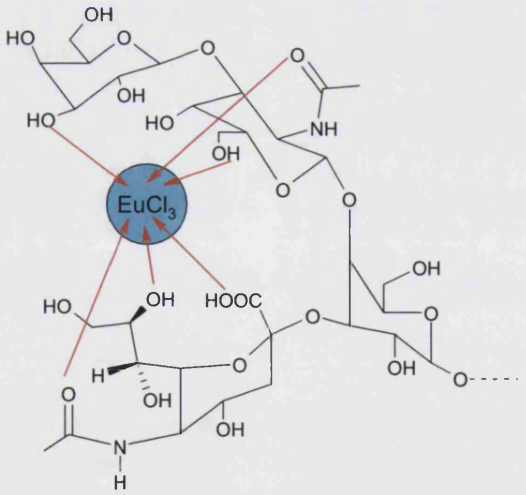

Figure 5.25 Schematic of the coordination of GM1 ganglioside to Europium III [68].

A novel use of lanthanide compounds as a toxin-receptor binding inhibitor is described, and its ability to bind to GM1 gangliosides reconstituted within tethered biomimetic membrane vesicles was observed.

5.4.4.1 Preliminary Measurements for the Effects on Europium III chloride on Biomimetic Membrane Vesicles

A 10μmol.dm^{-3} solution of Europium III (Eu^{3+}) was added to the biomimetic membrane vesicles after *Ctx* was added. Eu^{3+} did not displace bound cholera toxin (Figure 5.26) from GM1 receptors on biomimetic membrane vesicles.

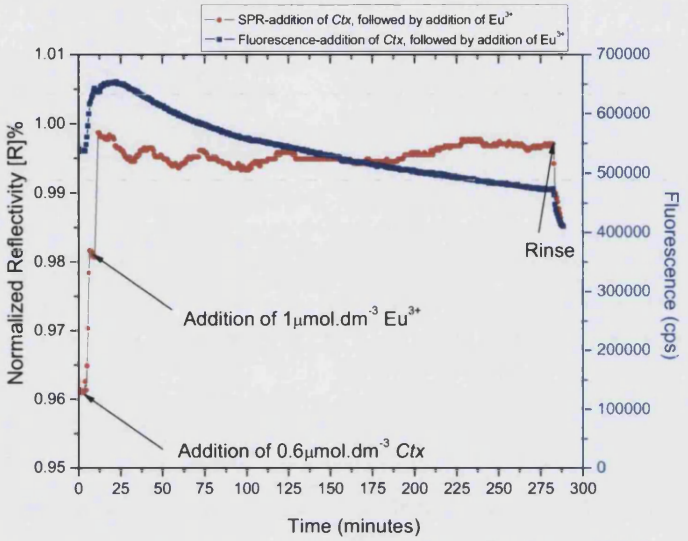

Figure 5.26 Simultaneous measurement of change in reflectivity (SPR) and Fluorescence (SPFS) upon addition of whole Ctx, followed by addition of Europium III during Ctx binding to membrane receptors.

The addition of cholera toxin to the tethered vesicle system caused the adsorption of the *Ctx* to the membrane surface, however, the subsequent addition of Eu^{3+} during the *Ctx* binding process did not prevent the bound toxin from eliciting its effects on the tethered vesicles. Therefore, Eu^{3+} did not prevent the oligomerization of the β-subunits and did not block the pore of the pentamer β-subunits.

Prior to the addition of cholera toxin, the injection of Eu^{3+} into the tethered biomimetic membrane system was followed by an increase in reflectivity. There was cooperative complexation between the europium chloride and the tethered vesicles. This was because there was an electrostatic interaction between the GM1 sialic acid carboxylate in the vesicle bilayer and the Eu^{3+}, and a secondary interaction with the oligosaccharide hydroxyls, resulted in a coordination shell [68]. The addition of the Eu^{3+} to the vesicle surface resulted in a 0.2° shift in the resonance minimum (result not shown), which equated to the adsorption of 1.07ng.mm^{-2} mass at the membrane surface. The coordination of Eu^{3+} to the GM1 receptors resulted in an increase in reflectivity at the membrane surface (Figure 5.27).

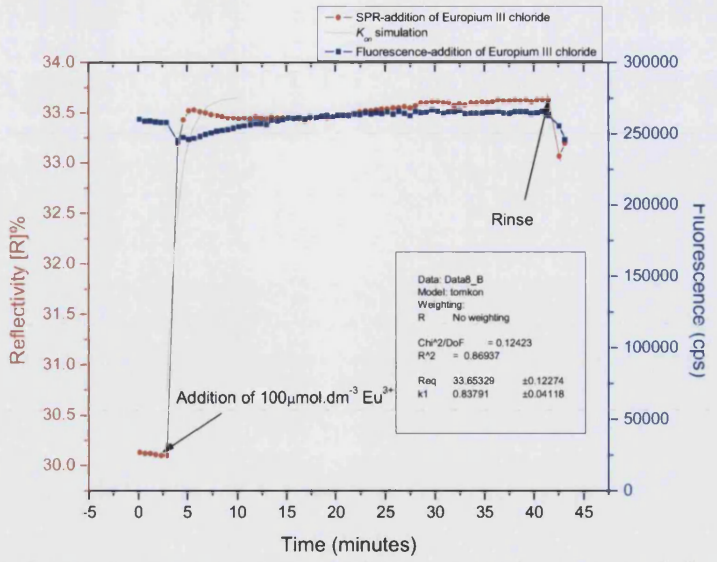

Figure 5.27 Simultaneous measurement of change in reflectivity and fluorescence upon addition of 100µmol.dm^{-3} Eu^{3+} to tethered biomimetic membrane vesicles containing GM1 ganglioside.

From the non-linear curve fitting, the association rate constant was determined to be k_{on} = 3379 mol^{-1}.Ls^{-1} while the dissociation rate constant was determined to be k_{off}= 0.5s^{-1}. From these rate constants the equilibrium dissociation constant was determined, K_D = 1.48x10^{-4} mol.dm^{-3}. The equilibrium dissociation constant was relatively weak compared to many biological interactions such as between streptavidin-biotin. This would support the notion that the sialic acid residues of GM1 bind Eu^{3+} via multiple coordination sites, and that each of the monovalent interactions are relatively weak [40], and collectively provide a stronger cooperative interaction. The affinity between the lanthanide metal and the ganglioside was relatively weak compared to that observed between *Ctx* and GM1, K_D =6.33x10^{-7}mol.dm^{-3}. The coordination of Eu^{3+} to the ganglioside does not show any adverse effects on the stability or viability of the tethered vesicles, as the fluorescence over time did not change significantly, suggesting the lanthanide did not cause a change in the membrane structure or alter the permeability barrier.

The addition of 0.6µmol.dm^{-3} *Ctx* to the Eu^{3+}-GM1 coordinated tethered vesicles (Figure 5.28a) did not follow the typical binding kinetics observed when the lanthanide was not bound to the GM1 receptors of the biomimetic membrane vesicles.

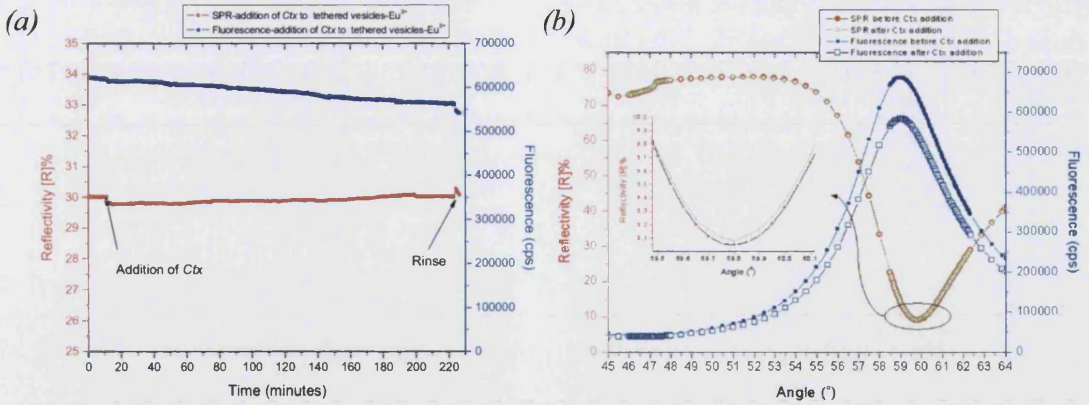

Figure 5.28 (a) Kinetics plot of the addition of 0.6μmol.dm^{-3} Ctx to Eu^{3+}-GM1 coordinated tethered biomimetic membrane vesicles. (b) Resonance angle scans before and after the addition of Ctx to the membrane surface.

There was little observable change in reflectivity upon addition of *Ctx* to the membrane surface coordinated with Eu^{3+}, which demonstrates the ability of Eu^{3+} to block the binding of *Ctx* to GM1, and subsequently prevent the oligomerization of the β-subunits into a pore and altering the permeability barrier. The calculated apparent dye diffusion coefficient for the leakage of the dye from Eu^{3+} coordinated vesicles was D* =2.75x10^{-15}cm^2.s^{-1}. This was a lower coefficient compared to the control vesicles with no lanthanide ions present (D* = 1.11x10^{-13}cm^2.s^{-1}), therefore, the europium significantly reduced the diffusion of the BODIPY and reduced the permeation of the biomimetic membrane vesicles. This was confirmed by the change in fluorescence upon addition of the bacterial toxin. The prevention of pore formation in the phospholipid membrane mediated by the interaction between Eu^{3+} and GM1 caused the membrane vesicles to maintain their integrity and no increase in the dye diffusion from the encapsulated aqueous space to the bulk solution was observed. This action of the lanthanide was verified by the resonance angle scans (Figure 5.28b), which demonstrated that there was no change in the resonance minimum before and after the addition of the toxin. Therefore, the lanthanide prevented the β-subunits from binding to the GM1 sites on the membranes.

5.4.4.2 Measurement of Dose-Response of Europium III chloride on Preventing Cholera Toxin Binding to Biomimetic Membrane Vesicles

Europium III chloride showed an inhibitory action on *Ctx* binding to GM1 receptors on biomimetic membrane vesicles, and this action was dependant upon the concentration of Eu^{3+} coordinated to the gangliosides (Figure 5.29). The binding of various concentrations of Eu^{3+} to the cell surface receptors followed a Langmuir isotherm binding kinetics.

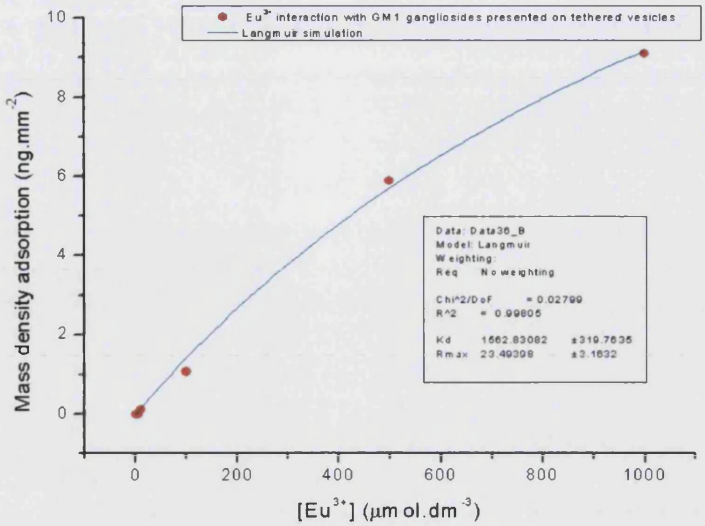

Figure 5.29 Langmuir simulation of the adsorption of Eu^{3+} to the GM1 gangliosides presented within the phospholipid bilayer of tethered biomimetic membrane vesicles.

The Eu^{3+} bound to the GM1 gangliosides in a concentration dependant manner, and the change in mass density at the surface of the membrane vesicles increased with higher concentrations of the lanthanide. However, because the metal ion has a small mass density, it was difficult to observe lower concentrations of Eu^{3+} binding to the GM1 receptors.

5.4.5 Inhibition of Cholera Toxin-Receptor Binding Using Other Lanthanide Complexes

There are fifteen metals comprising the lanthanide group, and all lanthanides closely resemble each other. The similar properties of lanthanides make the trivalent ions useful tools to study proteins and sugars. Lanthanide ions have been reported to activate a range of biological systems, and have been used in fluorescent studies to examine the biological function of phospholipase A_2 [71], α-amylase [72], the coagulant protein of Russell's viper venom [73] and staphylococcal nuclease [74]. Lanthanide ions show greater binding constants to biomolecules compared to calcium ions, therefore, lanthanides can act as substitutes for calcium activated enzymes, proteins and ion channels [75]. Therefore, the similarity in physical and chemical properties between the lanthanide group suggests they may also act as sialic acid binding ions, and thereby effectively blocking the specific binding and oligomerization of the *Ctx* β-subunits.

Five other trivalent lanthanide ions were compared to europium in their capacity to bind to GM1-containing tethered biomimetic membrane vesicles and their ability to inhibit the

formation of *Ctx* pores within the phospholipid bilayer. Lanthanum III nitrate, terbium III chloride, erbium III chloride, gadolinium III chloride and ytterbium III chloride were all coordinated to the GM1 gangliosides on tethered biomimetic membrane vesicles(all at 10μmol.dm^{-3}) and examined for their ability bind *Ctx* (Figure 5.30).

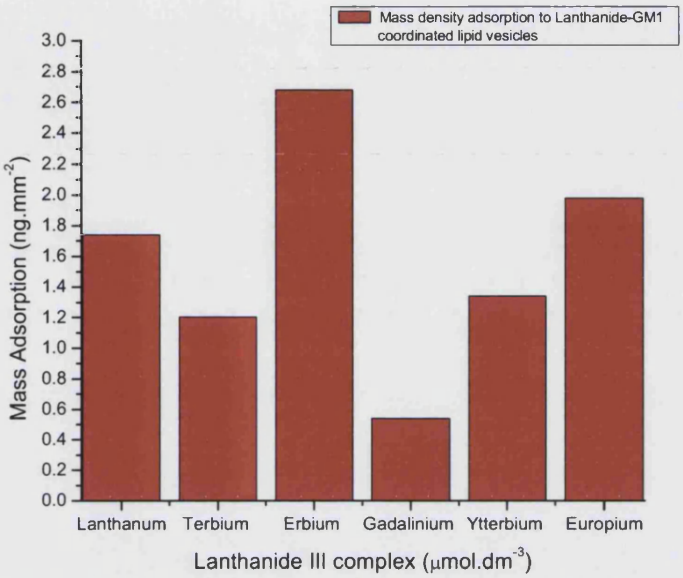

Figure 5.30 Comparison of the adsorption of Ctx to lanthanide-GM1 coordinated tethered biomimetic membrane vesicles compared to europium-GM1 vesicles.

Four of the five lanthanide ions tested showed improved resistance to *Ctx* binding compared to europium. Erbium III ions (Eb^{3+}) showed a reduction in the inhibitory action of preventing *Ctx* binding to the surface compared to Eu^{3+}. Gadolinium III (Gd^{3+}) showed the greatest inhibition in preventing the binding of the *Ctx* to the GM1 receptors on the vesicle surface, followed by terbium III (Tb^{3+}), ytterbium III (Yt^{3+}), then lanthanum III (La^{3+}). Therefore, all of the lanthanide trivalent ions tested coordinated to the sialic acid residue of GM1, which subsequently blocked the receptor from binding to other ligands. This blocking of the GM1 binding site thereby inhibited the oligomerization of the toxin monomers on the surface of biomimetic membranes.

The reduction in binding capacity conferred on the biomimetic membranes by the lanthanide trivalent ions was confirmed by calculating the apparent dye diffusion coefficient upon addition of the *Ctx* to the biomimetic membrane vesicles (Figure 5.31).

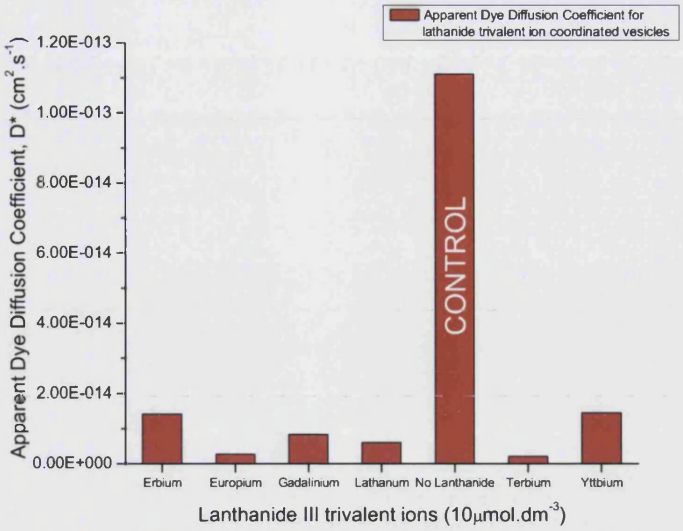

Figure 5.31 Comparison of the apparent dye diffusion coefficients ($cm^2.s^{-1}$) upon adsorption of Ctx to lanthanide-GM1 coordinated tethered biomimetic membrane vesicles compared to the control vesicles (No lanthanide trivalent ions present).

All lanthanide compounds tested, were shown to significantly inhibit the increased permeation of the tethered vesicles as a result of cholera toxin binding. Terbium III was shown to cause the greatest inhibition of cholera induced permeation, with an apparent dye diffusion coefficient of $D^* = 2.15 \times 10^{-15} cm^2.s^{-1}$. Moreover, the least inhibition to permeation was provided by Ytterbium III, with an apparent dye diffusion coefficient of $D^* = 1.45 \times 10^{-14} cm^2.s^{-1}$. A summary of the calculated dye diffusion coefficients are presented in Figure 5.32. Therefore, lanthanide trivalent ions significantly inhibit the binding of the cholera toxin to the GM1 receptors, and thereby inhibit the permeation of the biomimetic membranes.

Lanthanide Trivalent Ion Species	**Apparent Dye Diffusion Coefficient, D* ($cm^2.s^{-1}$)**
Control Test (No lanthanides)	1.11×10^{-13}
Lanthanum III	6.6×10^{-15}
Erbium III	1.42×10^{-14}
Europium III	2.75×10^{-15}
Ytterbium III	1.45×10^{-14}
Gadolinium III	8.37×10^{-15}
Terbium III	2.15×10^{-15}

Figure 5.32 Summary of the inhibitory effect on the permeation of biomimetic membrane vesicles, as calculated from the apparent dye diffusion coefficients for each of the lanthanide trivalent ions.

This novel application of lanthanide trivalent ions in preventing the binding and oligomerization of the β-subunits of *Ctx* could have a therapeutic application in treating

cholera. Lanthanides possess relatively low toxicity, particularly when complexed to ligands [76]. The toxicity of the lanthanides is dependant on the route of administration, their chemical form and the biological system to which they are administered. Intravenously and intraperitoneally administered lanthanide salts have a toxicity ranging between 50-500mg/kg bodyweight [77-79]. Toxicity is negligible when administered orally, because the lanthanides show very low absorption from the gastrointestinal tract [80]. Therefore, lanthanide salts, such as europium III chloride which has an LD_{50} of 5g/kg bodyweight [81], could be included in the recommended oral rehydration salt composition for administration during cholera outbreaks. The oral administration of a rehydration fluid containing a lanthanide salt would be tolerated by the body and would deliver the lanthanide trivalent ions directly to the gastrointestinal tract where it would bind to the GM1 receptors of the cells preventing further adsorption of the *Ctx* to the gastrointestinal cells. This novel application of lanthanides could potentially decrease the effects of the bacterial toxin and accelerate recovery.

5.5 Conclusions

The tethered biomimetic membrane system shows versatility for studying pore formation in biomimetic membranes. The tethered membrane system provides a simple and convenient method to study permeation processes and to determine the binding kinetics between the toxin and the receptor.

Cholera remains a prevalent disease, especially in areas with poor sanitation and where drinking water is contaminated, the disease is sporadic and accounts for many deaths each year especially among the vulnerable groups of the young, elderly and infirmed. The symptoms associated with the disease are the result of the enterotoxin produced by the pathogenic bacterium. The secreted toxin has been shown here to specifically bind to the GM1 ganglioside receptors expressed on the biomimetic membrane vesicles. However, sterols, such as cholesterol, also have an affect on the degree of toxin binding and the severity of the dye diffusion caused by the formation of pores in the biomimetic membrane vesicles. The toxin shows strong binding to the membrane receptors, and this was shown for both whole cholera toxin and the β-subunit toxin.

The blocking of the biomimetic cell surface receptors by trivalent lanthanide ions provides a means of inhibiting the interaction between the β-subunits of the cholera toxin monomers

and the GM1 ganglioside. This subsequently prevents the oligomerization of the toxin monomers from forming the cholera toxin pore in the membrane. Therefore, the permeability barrier of the biomimetic cells is maintained and the integrity of the biomimetic cell remains. This novel use of lanthanide ions could have an impact on the treatment of cholera disease. At present, the standard treatment of patients suffering from cholera is the administration of oral rehydration fluids to restore the electrolyte balance and replace the water lost during episodes of diarrhoea and vomiting. The inclusion of a trivalent lanthanide compound, such as europium III chloride, in the oral rehydration salt mixture could potentially advance the recovery of patient by preventing further toxin binding to the gut epithelial membranes. The administration of a trivalent lanthanide ion solution to patients not yet suffering from the disease in areas prone to or suffering an outbreak of cholera could minimize the probability of suffering toxin-associated symptoms.

This tethered biomimetic membrane system provides a means of evaluating potential therapeutic molecules which inhibit the interaction between the toxin and the cell surface receptors, and provides a good *in vitro* model to examine the interactions between the cholera toxin and cell surface, as well as between the huge range of pore forming and ion channel forming toxins and proteins.

5.6 Bibliography

1. Butterton, J., Calderwood, SB, *Vibrio cholerae O1*, in *Infections of the Gastrointestinal Tract*, M. Blaser, Smith, PD, Ravdin, Ll, Editor. 1995, Raven Press: New York. p. 649.
2. Bhattacharya, M.K., et al., *Efficacy of Oral Hyposmolar Glucose-based and Rice-based Oral Rehydration Salt Solutions in the Treatment of Cholera in Adults.* Scandinavian Journal of Gastroenterology, 1998. **33**(2): p. 159 - 163.
3. Fayad, I.M., et al., *Comparative efficacy of rice-based and glucose-based oral rehydration salts plus early reintroduction of food.* The Lancet, 1993. **342**(8874): p. 772-775.
4. Sack, D.A., et al., *Cholera.* Lancet, 2004. **363**(9404): p. 223-233.
5. Hirst, T.R. and J.M. D'Souza, *Vibrio cholerae and Escherichia coli thermolabile enterotoxin*, in *The Comprehensive Sourcebook of Bacterial Protein Toxins*, J.E. Alouf and M.R. Popoff, Editors. 2006, Elservier Ltd. p. 270-284.
6. Snow, J., ed. *On the Mode of Communication of Cholera.* 2nd Edition ed. 1855: London. 1-97.
7. Page, K.E., *Cholera: Mechanism of Infection, History and Treatment.* South Carolina Journal of Molecular Medicine, 2004. **5**: p. 26-29.
8. WHO, *Cholera Country Profile: Angola*, in *Global Task Force on Cholera Control.* 2007.
9. WHO, *Weekly epidemiological record.* World Health Organization, 2006. **81**: p. 297-308.
10. Waldor, M.K. and J.J. Mekalanos, *Lysogenic Conversion by a Filamentous Phage Encoding Cholera Toxin.* Science, 1996. **272**(5270): p. 1910-1914.
11. Karaolis, D.K.R., et al., *Comparison of Vibrio cholerae Pathogenicity Islands in Sixth and Seventh Pandemic Strains.* Infection & Immunity, 2001. **69**(3): p. 1947-1952.
12. Zhang, R.-G., et al., *The Three-dimensional Crystal Structure of Cholera Toxin.* Journal of Molecular Biology, 1995. **251**(4): p. 563-573.
13. Gill, D.M., *The arrangemnet of subunits in cholera toxin.* Biochemistry, 1976. **15**(6): p. 1242-1249.
14. Holmgren, J., *Actions of cholera toxin and the prevention and treatment of cholera.* 1981. **292**(5822): p. 413-417.
15. Hansson, H.A., J. Holmgren, and L. Svennerholm, *Ultrastructural localization of cell membrane G(M)1 ganglioside by cholera toxin.* Proceedings of the National Academy of Sciences of the United States of America, 1977. **74**(9): p. 3782-3786.
16. Orlandi, P.A. and P.H. Fishman, *Orientation of Cholera-Toxin Bound to Target-Cells.* Journal of Biological Chemistry, 1993. **268**(23): p. 17038-17044.
17. Tran, D., et al., *Ligands Internalized through Coated or Noncoated Invaginations Follow a Common Intracellular Pathway.* Proceedings of the National Academy of Sciences of the United States of America, 1987. **84**(22): p. 7957-7961.
18. Fishman, P.H., *ADP-ribosylating toxins and G proteins: insights into signal transduction*, ed. J. Moss and M. Vaughan. 1990, Washington D.C: American Society of Microbiology. 85-102.
19. Shinoda, S. and S.-i. Miyoshi, *Hemolysins of Vibrio cholerae and other vibrio species*, in *The Comprehensive Sourcebook of Bacterial Protein Toxins*, J.E. Alouf and M.R. Popoff, Editors. 2006, Elservier Ltd. p. 748-759.

20. Lencer, W.I. and B. Tsai, *The intracellular voyage of cholera toxin: going retro.* Trends in Biochemical Sciences, 2003. **28**(12): p. 639-645.
21. Feng, Y., et al., *Retrograde transport of cholera toxin from the plasma membrane to the endoplasmic reticulum requires the trans-Golgi network but not the Golgi apparatus in Exo2-treated cells.* Embo Reports, 2004. **5**(6): p. 596-601.
22. Fujinaga, Y., et al., *Gangliosides that associate with lipid rafts mediate transport of cholera and related toxins from the plasma membrane to endoplasmic reticulm.* Molecular Biology of the Cell, 2003. **14**(12): p. 4783-4793.
23. Hazes, B. and R.J. Read, *Accumulating evidence suggests that several AB-toxins subvert the endoplasmic reticulum-associated protein degradation pathway to enter target cells.* Biochemistry, 1997. **36**(37): p. 11051-11054.
24. London, E. and C.L. Luongo, *Domain-Specific Bias in Arginine Lysine Usage by Protein Toxins.* Biochemical and Biophysical Research Communications, 1989. **160**(1): p. 333-339.
25. Engelberg, N.C., V. DiRita, and T.S. Dermody, *Schaechter's Mechanisms of Microbial Disease.* Lippincott Williams & Wilkins, 2007. **4th Ed**.
26. Mekalanos, J.J., R.J. Collier, and W.R. Romig, *Enzymic Activity of Cholera Toxin .2. Relationships to Proteolytic Processing, Disulfide Bond Reduction, and Subunit Composition.* Journal of Biological Chemistry, 1979. **254**(13): p. 5855-5861.
27. Cassel, D. and T. Pfeuffer, *Mechanism of Cholera Toxin Action: Covalent Modification of the Guanyl Nucleotide-Binding Protein of the Adenylate Cyclase System.* PNAS, 1978. **75**(6): p. 2669-2673.
28. Flach, C.-F., E. Jennische, and I. Lonnroth, *Cholera toxin induces expression of ion channels and carriers in rat small intestinal mucosa.* FEBS Letters, 2004. **561**(1-3): p. 122-126.
29. Sharp, G.W.G. and S. Hynie, *Stimulation of Intestinal Adenyl Cyclase by Cholera Toxin.* 1971. **229**(5282): p. 266-269.
30. Ikigai, H., et al., *El Tor hemolysin of Vibrio cholerae O1 forms channels in planar lipid bilayer membranes.* Fems Microbiology Letters, 1997. **150**(2): p. 249-254.
31. Moss, J., et al., *Choleragen-Mediated Release of Trapped Glucose from Liposomes Containing Ganglioside Gm.* Proceedings of the National Academy of Sciences of the United States of America, 1976. **73**(10): p. 3480-3483.
32. Zitzer, A., et al., *Characterization of Vibrio-Cholerae El-Tor Cytolysin as an Oligomerizing Pore-Forming Toxin.* Medical Microbiology and Immunology, 1995. **184**(1): p. 37-44.
33. Townson, K., et al., *Solid phase immunoadsorption for therapeutic and analytical studies on neuropathy-associated anti-GM1 antibodies.* Glycobiology, 2007. **17**(3): p. 294-303.
34. Peterson, J.W., *Tissue-binding properties of the cholera toxin.* Infect Immun, 1974. **10**(1): p. 157-66.
35. Cuatrecasas, P., *Gangliosides and Membrane Receptors for Cholera Toxin.* Biochemistry, 1973. **12**(18): p. 3558-3566.
36. Cuatrecasas, P., *Interaction of Vibrio cholerae enterotoxin with cell membranes.* Biochemistry, 1973. **12**(18): p. 3547-3558.

37. Cumar, F.A., B. Maggio, and R. Caputto, *Ganglioside-Cholera Toxin Interactions - a Binding and Lipid Monolayer Study.* Molecular and Cellular Biochemistry, 1982. **46**(3): p. 155-160.
38. Arosio, D., et al., *Synthesis and cholera toxin binding properties of multivalent GM1 mimics.* Organic & Biomolecular Chemistry, 2004. **2**(14): p. 2113-2124.
39. Schon, A. and E. Freire, *Thermodynamics of Intersubunit Interactions in Cholera-Toxin Upon Binding to the Oligosaccharide Portion of Its Cell-Surface Receptor, Ganglioside-Gm1.* Biochemistry, 1989. **28**(12): p. 5019-5024.
40. Mammen, M., S.K. Choi, and G.M. Whitesides, *Polyvalent interactions in biological systems: Implications for design and use of multivalent ligands and inhibitors.* Angewandte Chemie-International Edition, 1998. **37**(20): p. 2755-2794.
41. Middlebrook, J.L. and L.D. Kohn, *Receptor-Mediated Binding and Internalization of Toxins and Hormones.* Academic Press, 1981.
42. Zitzer, A., et al., *Vibrio cholerae cytolysin: assembly and membrane insertion of the oligomeric pore are tightly linked and are not detectably restricted by membrane fluidity.* Biochimica Et Biophysica Acta-Biomembranes, 2000. **1509**(1-2): p. 264-274.
43. Zitzer, A., et al., *Mode of primary binding to target membranes and pore formation induced by Vibrio cholerae cytolysin (hemolysin).* European Journal of Biochemistry, 1997. **247**(1): p. 209-216.
44. Zitzer, A., et al., *Coupling of Cholesterol and Cone-shaped Lipids in Bilayers Augments Membrane Permeabilization by the Cholesterol-specific Toxins Streptolysin O and Vibrio cholerae Cytolysin.* J. Biol. Chem., 2001. **276**(18): p. 14628-14633.
45. Zitzer, A., et al., *Oligomerization of Vibrio cholerae cytolysin yields a pentameric pore and has a dual specificity for cholesterol and sphingolipids in the target membrane.* Journal of Biological Chemistry, 1999. **274**(3): p. 1375-1380.
46. Mason, W.T., *Fluorescent and luminescent probes for biological activity: A practical guide to technology for quantatative Real-Time analysis.* Academic Press, 1999(2nd Edition).
47. Kautsky, H., *QUENCHING OF LUMINESCENCE BY OXYGEN.* Transactions of the Faraday Society, 1938. **35**: p. 216-219.
48. Lakowicz, J.R., *Principles of Fluorescence Spectroscopy.* Kluwer Academic, 1999(2nd Edition).
49. Karolin, J., et al., *Fluorescence and absorption spectroscopic properties of dipyrromethene boron difluoride (BODIPY) derivatives in liquids, lipid membranes, and proteins.* Journal of the American Chemical Society, 1994. **116**(17): p. 7801-7806.
50. McCann, J.A., et al., *Conformational changes in cholera toxin B subunit ganglioside GM1 complexes are elicited by environmental pH and evoke changes in membrane structure.* Biochemistry, 1997. **36**(30): p. 9169-9178.
51. Sixma, T.K., et al., *Refined structure of Escherichia coli heat-labile enterotoxin, a close relative of cholera toxin.* Journal of Molecular Biology, 1993. **230**(3): p. 890-918.
52. Seifert, U., *Adhesion of Vesicles in 2 Dimensions.* Physical Review A, 1991. **43**(12): p. 6803-6814.
53. WHO, *Oral Rehydration Salts: Production of the new ORS*, in *Division of Child and Adolescent Health and Development.* 1998: Geneva.

54. Bowie, M., D., I. Hill, D., and M. Mann, D., *Loperamide for treatment of acute diarrhoea in infants and young children. A double-blind placebo-controlled trial.* South African Medical Journal, 1995. **85**(9): p. 885-7.
55. Thiagarajah, J.R. and A.S. Verkman, *New drug targets for cholera therapy.* Trends in Pharmacological Sciences, 2005. **26**(4): p. 172-175.
56. Farthing, M.J.G., A. Casburn-Jones, and M.R. Banks, *Getting control of intestinal secretion: thoughts for 2003.* Digestive and Liver Disease, 2003. **35**(6): p. 378-385.
57. Casburn-Jones, A.C. and M.J.G. Farthing, *Management of infectious diarrhoea.* Gut, 2004. **53**(2): p. 296-305.
58. Garg, P., et al., *Expanding multiple antibiotic resistance among clinical strains of Vibrio cholerae isolated from 1992-7 in Calcutta, India.* Epidemiology and Infection, 2000. **124**(3): p. 393-399.
59. Dutta, D., et al., *Efficacy of norfloxacin and doxycycline for treatment of Vibrio cholerae O139 infection.* Journal of Antimicrobical Chemotherapy, 1996. **37**(3): p. 575-581.
60. Ryan, E.T. and S.B. Calderwood, *Cholera vaccines.* Clinical Infectious Diseases, 2000. **31**(2): p. 561-565.
61. Holmgren, J., L. Lindholm, and I. Lonnroth, *INTERACTION OF CHOLERA TOXIN AND TOXIN DERIVATIVES WITH LYMPHOCYTES: I. BINDING PROPERTIES AND INTERFERENCE WITH LECTIN-INDUCED CELLULAR STIMULATION.* Journal of Experimental Medicine, 1974. **139**(4): p. 801-819.
62. Holmgren, J., *Comparison of the tissue receptors for Vibrio cholerae and Escherichia coli enterotoxins by means of gangliosides and natural cholera toxoid.* Infection and Immunity, 1973. **8**(6): p. 851-859.
63. Holmgren, J., et al., *Interaction of cholera toxin and membrane Gm1 ganglioside of small intestine.* Proceedings of the National Academy of Sciences of the United States of America, 1975. **72**(7): p. 2520-2524.
64. Pickens, J.C., et al., *Nonspanning bivalent ligands as improved surface receptor binding inhibitors of the cholera toxin B pentamer.* Chemistry & Biology, 2004. **11**(9): p. 1205-1215.
65. Fan, E. and E.A. Merritt, *Combating infectious disease through multivalent design.* Current Drug Targets - Infectious Disorders, 2002. **2**(2): p. 161-167.
66. Dam, T.K., et al., *Binding of multivalent carbohydrates to concanavalin A and Dioclea grandiflora lectin - Thermodynamic analysis of the "multivalency effect".* Journal of Biological Chemistry, 2000. **275**(19): p. 14223-14230.
67. Kiessling, L.L., J.E. Gestwicki, and L.E. Strong, *Synthetic multivalent ligands in the exploration of cell-surface interactions.* Current Opinion in Chemical Biology, 2000. **4**(6): p. 696-703.
68. Alpturk, O., et al., *Lanthanide complexes as fluorescent indicators for neutral sugars and cancer biomarkers.* Proceedings of the National Academy of Sciences of the United States of America, 2006. **103**(26): p. 9756-9760.
69. Sillerud, L.O., et al., *Assignment of C-13 Nuclear Magnetic-Resonance Spectrum of Aqueous Ganglioside Gm1 Micelles.* Biochemistry, 1978. **17**(13): p. 2619-2628.
70. Kostova, I., *Lanthanides as Anticancer Agents.* Current Medicinal Chemistry - Anti-Cancer Agents, 2005. **5**: p. 591-602.
71. Hershberg, R.D., et al., *Phospholipase-A2 Complexes with Gadolinium(Iii) and Interaction of Enzyme-Metal Ion Complex with Monomeric and Micellar*

Alkylphosphorylcholines - Water Proton Nuclear Magnetic-Relaxation Studies. Biochemistry, 1976. **15**(11): p. 2268-2274.
72. Darnall, D.W. and E.R. Birnbaum, *Lanthanide Ions Activate Alpha-Amylase.* Biochemistry, 1973. **12**(18): p. 3489-3491.
73. Furie, B.C. and B. Furie, *Interaction of Lanthanide Ions with Bovine Factor-X and Their Use in Affinity Chromatography of Venom Coagulant Protein of Vipera-Russelli.* Journal of Biological Chemistry, 1975. **250**(2): p. 601-608.
74. Furie, B., et al., *Interaction of Lanthanide Ions with Staphylococcal Nuclease.* Journal of Biological Chemistry, 1973. **248**(16): p. 5821-5825.
75. Horrocks, W.D. and D.R. Sudnick, *Lanthanide Ion Luminescence Probes of the Structure of Biological Macromolecules.* Accounts of Chemical Research, 1981. **14**(12): p. 384-392.
76. Thunus, L. and R. Lejeune, *Overview of transition metal and lanthanide complexes as diagnostic tools.* Coordination Chemistry Reviews, 1999. **184**: p. 125-155.
77. Haley, T.J., *Pharmacology and toxicology of the rare earth elements.* Journal of Pharmaceutical Sciences, 1965. **54**(5): p. 663-670.
78. Haley, T.J., et al., *Pharmacology and toxicology of dysprosium, holmium, and erbium chlorides.* Toxicology and Applied Pharmacology, 1966. **8**(1): p. 37-43.
79. Haley, T.J., et al., *Pharmacology and toxicology of terbium, thulium, and ytterbium chlorides,.* Toxicology and Applied Pharmacology, 1963. **5**(4): p. 427-436.
80. Zielhuis, S.W., et al., *Lanthanide bearing microparticulate systems for multi-modality imaging and targeted therapy of cancer.* 2006, Utrecht University: Utrecht, Netherlands.
81. Haley, T.J., et al., *Pharmacology and toxicology of europium chloride.* Journal of Pharmaceutical Sciences, 1965. **54**(4): p. 643-645.

6.0 Solid Supported Lipid Bilayer Vesicles: Method to Study Amyloidosis

Tethered biomimetic membrane vesicles have also found a novel application in studying the effects of protein aggregation as a result of insoluble proteins and/or peptides. The accumulation of insoluble peptides tends to cause detrimental effects to a biological system, therefore, they are naturally kept soluble or are degraded quickly. In this chapter, the affect of β-amyloid peptide aggregation is described in relation to their effects towards biomimetic membranes.

Chapter Synopsis

The formation of insoluble aggregate proteins, in particular β-amyloid, and their involvement in amyloidosis disorders will be reviews with a focus on Alzheimer's disease. Preliminary measurements concerning the interaction between the β-amyloid peptide and simple DMPC-GM1-cholesterol vesicles will then be detailed. The influence of GM1 and cholesterol on β-amyloid binding will also be discussed. Additional measurements showing the interaction between a more complex vesicle system (multiple phospholipid species-GM1-cholesterol) will be detailed and binding constants determined. The potential neurotoxicity mechanisms will be reviewed, and using kinetics data, a proposed hypothesis will be developed. Finally, a novel therapeutic for the inhibition of β-amyloid binding to biomimetic membrane vesicles will be detailed, with potential applications of the compound.

6.1 Amyloidosis and their Related Diseases

Amyloidosis is a disorder initiated by the formation of an insoluble form of a protein or peptide, which is caused by the alteration in the peptides secondary structure. The formation of these β-pleated sheet amyloids causes their deposition within the structure of an organ or a tissue. Amyloidosis disorders can either be systemic, whereby they affect many different organ systems, or localized whereby they are organ specific. The causes of amyloidosis are highly variable, and may result from an inherited mutation in the precursor protein, the abnormal production of a protein or result from physical or chemical damage.

Despite the heterogeneity of the precursor proteins which form amyloid deposits, they all share a common core structure, consisting an anti-parallel β-strand lying perpendicular to the long axis of the fibril [1] (Figure 6.1). The highly ordered core and conformation confers the distinctive physiochemical properties of amyloid fibrils, including their relative

stability and resistance to proteolysis [2]. The amyloid deposits contain several common non-fibrillar components, including apolipoprotein E, type IV collagen and the normal plasma glycoprotein serum amyloid P component (SAP). The SAP component within the amyloid deposit confers the uncharacterized specific binding to its cellular ligand [3].

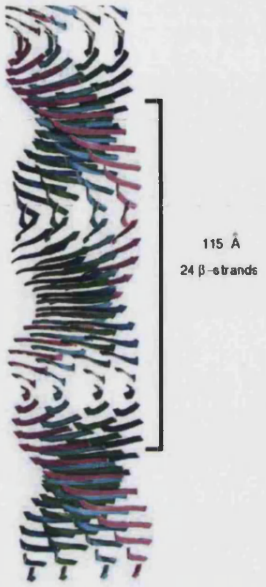

Figure 6.1 Molecular model of the generic common core of an amyloid fibril. β-sheets (four illustrated here) form the protofilament structure, with the sheets running parallel to the axis of the protofilament, with their component β-strands perpendicular to the fibril axis. The β-sheets twist around a common helical axis that coincides with the axis of the protofilament, giving a helical repeat containing 24 β-strands (the repeated unit is indicated by the boxed region) [1].

6.1.1 Systemic Amyloidosis

Systemic amyloidoses disorders are either acquired or inherited, and tend to be rare. There are at least twenty known different proteins that form amyloid fibrils *in vivo*. Inherited systemic amyloidosis disorders are typically due to the inheritance of a point mutation in the precursor protein, whose structure makes them amyloidogenic. The rare hereditary systemic amyloidoses are very difficult to treat and are usually fatal. The extracellular deposits can be present in any or all of the connective tissues, intestines, and blood vessel walls. Mutations can occur in a variety of genes, with the most common cause being a mutation in the TTR gene. This gene encodes the transthyretin blood protein, which normally transports thyroid hormone and vitamin A to the body tissues. The abnormal form of transthyretin tends to accumulate in tissues such as the heart, kidneys, nerves, and intestine. Its presence interferes with the normal functions of the organ, and as the deposits enlarge, more tissue damage occurs and the disease progresses [4]. Other amyloid fibril

proteins that cause hereditary amyloidosis include apolipoproteins AI and AII, fibrinogen A α-chain, and lysozyme [5].

6.1.2 Organ-specific Amyloidosis

The formation of amyloid deposits are a pathological hallmark of amyloidoses disorders, and these deposits occur in a range of specific organs and give rise to various common medical disorders. These conditions begin as asymptomatic diseases, because their progression tends to be slow, gradual and typically age related. Subsequently, they lead to the development of degenerative diseases. The disease becomes clinically significant when it affects organ function by replacing the normal cell structure.

Type II non-insulin dependant diabetes mellitus (NIDDM) is a metabolic disorder which affects more than 160 million individuals worldwide [6]. The disorder results from the body's ineffective use of insulin, and is largely the result of excess body weight and physical inactivity. Over time, type II diabetes causes damage to the heart, blood vessels, eyes, kidneys and nerves. The overall risk of dying among people with this form of diabetes is at least double the risk of individuals without it [6]. A pathological hallmark of this disease is the presence of amyloid deposits in the islets of Langerhans. These deposits are composed of islet amyloid polypeptide (IAPP), which is a hormone stored with insulin in vesicles and secreted by the islet β-cells. The disorder manifests itself as a reduction in the mass of insulin-producing β-cells [7], because of the formation of cytotoxic fibre intermediates, which have been shown *in vitro* to lead to β-cell failure [8].

The infiltration of amyloid fibrils into the heart often results in restrictive cardiomyopathy. This tends to manifest as heart failure and conduction abnormalities [9]. Increased thickness of the myocardial wall, caused by increased amyloidal deposition, leads to systolic and diastolic dysfunction, and cardiac arrhythmias [10]. Currently, cardiac ultrasound is considered the non-invasive test of choice to diagnose cardiac amyloidosis, because cardiac biopsy is hindered by procedural risks and uncertainties concerning sampling errors [11]. The therapeutic strategy depends on the characterization of the type of amyloid protein and extent of disease. Treatment may include chemotherapy, stem cell transplantation, and liver transplantation. Heart transplantation is controversial and is rarely performed.

Neurological amyloidoses result in the manifestation of a range of diseases, including the dementia disorders such as Parkinson's disease, Huntington's disease and the transmissible spongiform encephalopathies. Of these neurological amyloidoses, only prion diseases are transmissible. Prion diseases cause fatal neurodegenerative disorders related to a conformational change in the cellular prion protein into a misfolded protein capable of aggregation [12]. The prion proteins self-associate into ordered, stable supramolecular structures composed of the misfolded proteins. Human forms of the prions, such as those which cause Creutzfeldt-Jakob disease (CJD), are misfolded self-replicating proteins which are infectious and neurotoxic [13]. The protein responsible for CJD is a glycosylphosphatidylinositol-anchored protein, which during post-translation, becomes misfolded into the β-sheet conformation. Conversion to the misfolded protein results in an increased exposure of hydrophobic residues, which leads to the aggregation of the protein molecules into aggregates, protofibrils, ordered rigid amyloid fibrils and plaques [14].

Parkinson's disease is the second most common neurodegenerative disease, and is characterized by the progressive loss of dopamine neurons and the accumulation of Lewy bodies. The α-synuclein, a protein found in mammalian brain tissue and enriched in presynaptic nerve terminals, has been identified as a fibril forming protein in individuals suffering from Parkinson's disease [15]. The N-terminus of the α-synuclein forms an amphipathic *a*-helical domain that specifically associates with lipid rafts. This has been implicated in the regulation of dopamine transmission and synaptic vesicle. Mutations in the genes encoding the α-synuclein, have been reported to cause the formation of amyloid fibrils via a gain-of-function mechanism causing its deposition in Lewy Bodies [16]. The mutant protein has also been reported to display an increased tendency to self-aggregate *in vitro* compared to the wild-type α-synuclein [17].

The standard procedure for diagnosing amyloidoses is by histological examination of autopsied tissue. The highly ordered amyloid fibrils stain with Congo red, and are observed as an apple-green birefringence (double refraction) under polarized light. Immunoelectron microscopy is used to characterize the amyloid deposits, and is preferred to light microscopy immunohistochemical analysis, which can be misleading due to the low specificity of the technique [18, 19].

The prevailing therapeutic approach towards amyloidoses is based on reducing the concentration of the amyloidogenic precursor. For amyloid A amyloidosis (a disorder initiated by chronic inflammatory diseases), hereditary periodic fevers and certain neoplasms, treatment of the underlying disorder is encouraged, which aims to suppress the inflammatory activities and thereby suppressing the circulating levels of the serum precursor protein. No specific drug treatment is presently available for hereditary amyloidosis, but one recommended strategy is a liver transplant, because the liver is the main organ synthesizing most of the amyloidogenic precursor proteins [19]. The fibrils cause functional and structural damage to organs and tissues in the body, and this causes huge therapeutic problems and massive economic burdens in research and treatment of the associated diseases.

6.2 Alzheimer's disease

Dementia is generally defined as the "loss of intellectual abilities of sufficient severity to interfere with social or occupational functioning" [20], and involves the loss of functions such as memory, calculation, speech, and problem solving. According to the World Health Organization, there are around 100 known causes of dementia, which include multiple strokes, infections of the brain, severe thyroid deficiency and severe brain injury. However, the most common cause of dementia is Alzheimer's disease, which accounts for between 50-70% of all dementias worldwide. The disorder was first reported in 1906 by Dr Alois Alzheimer, who described a patient who had died of an unusual mental illness. The disease generally has three kinds of symptoms; impaired daily living, abnormal behaviour and loss of cognitive functions.

In the early stages of the disease, the most complicated functions, such as those learnt in a professional capacity, are the first lost. However, basic functions, such as toilet habits and recognition of immediate family members, are preserved. As the disease progresses, additional functions are lost (Figure 6.2). In the more advanced stages, the patient becomes almost completely dependent on others in terms of being fed, bathed, dressed and exercised. The rapid progression of this disease leads to premature death, often due to food going into the lungs or fracture due to a fall. Patients can, however, survive up to 15-20 years after the onset of illness.

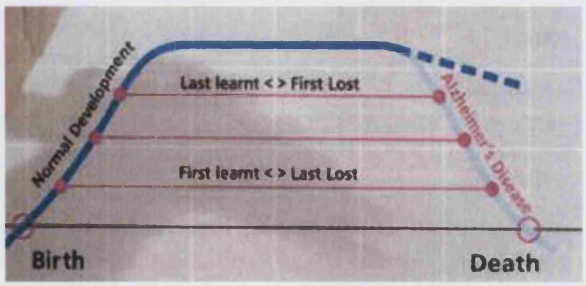

Figure 6.2 Development cycle from birth to death, demonstrating the gradual decline in cognitive function of a typically aging individual (-----) compared to a patient suffering from Alzheimer's disease (—).

Alzheimer's disease can affect people of all ages, however, the prevalence of the disease significantly increases with age. Around 5% of individuals aged 65-74 suffer from Alzheimer's disease, and the incidence exponentially increases to around 50% in individuals aged over 85 [21]. It is generally reported that Alzheimer's disease does not discriminate on basis of gender, soci-economic status or lifestyle. It is believed that men and women are equally at risk from developing the disorder, but in developed countries, it is more commonly observed in women because this is a reflection on the increased longevity of women compared to men.

The early diagnosis of Alzheimer's disease is pivotal to ensure the correct provision of care and to minimize the impact the disorder forces upon the individual sufferer and those close to them. At present, the only definitive way to diagnose Alzheimer's disease is to study the brain tissue for hallmarks of neuronal loss and β-amyloid deposits within the tissue. However, this can only be done at the time of autopsy, therefore, it is only possible to speculate from behavioural changes that an individual is suffering from Alzheimer's disease while the person is still alive. Neuroimaging techniques are looking into detecting neuronal damage in areas of the brain involved in memory before disease associated symptoms occur [22, 23]. The progression of the disorder varies from person to person, and typically, an individual may live with Alzheimer's disease for up to 8 to 10 years, though some may live with the disease for up to 20 years. At present there is no cure for Alzheimer's disease, and therapeutic intervention is possible but is highly dependant on the advancement of the disease. Some drugs, such as tacrine and galantamine, help to alleviate some symptoms in sufferers with early and mild Alzheimer's for a limited time. These drugs act as cholinesterase inhibitors, thereby preventing the breakdown of acetylcholine, which is important for memory and thinking [24, 25]. Limited treatment is available for

severe/advanced Alzheimer's disease, and tends to be an N-*methyl D-aspartate* antagonist, which regulates glutamate that leads to brain cell death when produced in excess [26].

6.3 β-amyloid, Amyloid Precursor Protein and the Neurological Hallmarks of Alzheimer's Disease

The brains of Alzheimer's disease sufferers have been shown to contain an abundance of β-amyloid plaques and neurofibrillary tangles. Neuropathological changes include neuronal loss (Figure 6.3), whereby the cortex of the brain shrinks and causes damage to areas involved in thinking, planning and memory. Shrinkage of the hippocampus is also observed in people suffering from Alzheimer's disease, causing the loss of key areas involved in the formation of new memories. The mechanisms causing neurodegeneration are uncertain, but reports show evidence that mutations in the amyloid precursor protein (APP) occur. The APP is an integral membrane protein concentrated in the synapses of neurons, and its primary function has not been definitively elucidated. However, the APP has been implicated to act in regulating synapse formation. Using cultured hippocampal neurons lacking APP, it has been shown that excitatory synaptic transmission is enhanced [27]. APP knock-out mice show enhanced neuritic outgrowth and increased number of synapses, which is subsequently believed to lead to enhanced glutamate toxicity in the knock-out mice [28]. APP has also been implicated in cell adhesion and motility, because the integral membrane protein possesses several domains that promote binding to specific substrates such as heparin and collagen. Exposure of experimental animals to an enriched environment which stimulates learning, has demonstrated that there is an up-regulation of APP production [29], suggesting that APP may have a role in memory and learning.

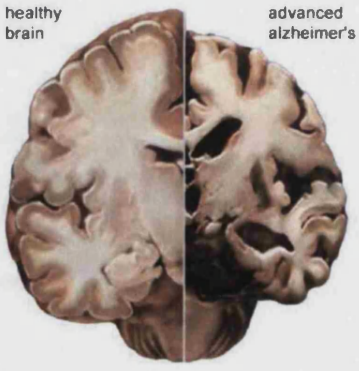

(Picture source http://www.alz.org)

Figure 6.3 Crosswise section through the middle of the brain between the ears, comparing a brain section of a healthy individual (left section) and an advanced Alzheimer's sufferer (right section).

Normally, APP is processed to form a soluble amyloid precursor protein (sAPP), whereby it is cleaved by α-secretase. The enzyme causes the integral membrane protein to be 'shedded' from its membrane location to form a soluble form of the APP. α-secretase cleaves the integral membrane APP close to the membrane spanning domain (Figure 6.4), to form a soluble APP 612 amino acids in length. The sAPP is believed to be a growth regulatory molecule and provides neuroprotection. *In vitro* studies have shown that sAPP confers increased resistance to excitotoxicity and glucose deprivation-induced injury on neurons [30]. In support of these studies, it has been demonstrated that sAPP protects neurons against β-amyloid toxicity and other oxidative stresses [31]. It is believed that the sAPP protective mechanism is based on its rapid effects on ion channel function. sAPP causes the activation of potassium channels and suppresses the agonist NMDA neurotransmitter mimic [32], therefore reducing excitability and preventing injury caused by over excitation. The soluble protein has also demonstrated neuro-protectivity *in vivo*, where post-ischemic administration of the sAPP protects neurons in the rat hippocampus against ischemic injury. Treatment with sAPP resulted in increased neuronal survival, and the surviving cells show a continued ability to synthesize protein [33].

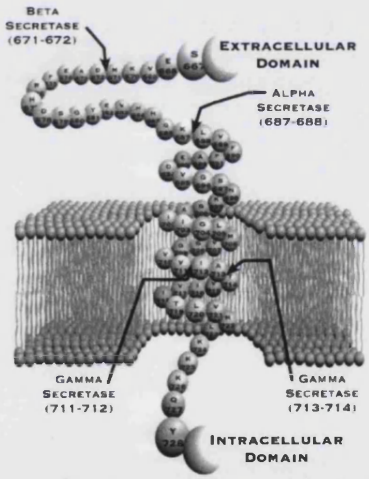

Figure 6.4 Schematic of the membrane spanning and cleavage sites of APP_{770}. Soluble APP is generated from the cleavage of the protein by α-secretase. The $A\beta_{1-40}$ fragment, generated by β and γ cleavage, comprises residues 672–711 of APP_{770} while the amyloid-β_{1-42} fragment spans residues 672–713 [29].

The integral APP may also be cleaved by β- and γ-secretase to produce the 40 or 42 amino acid amyloid β1-40 or amyloid β1-42 (Figure 6.4). Cleavage by these enzymes generates the β-amyloid associated with the formation of aggregate amyloids, which subsequently leads to the formation of senile plaques. The processing of the APP led to the development

of the amyloid cascade (Figure 6.5). The amyloid cascade describes the processing of the APP via two pathways, either cleavage to produce a soluble APP, which provides the neuroprotective protein, or the production of the insoluble amyloid-β protein, which oligomerizes to form aggregates and shows neurotoxicity [34, 35]. Various factors influence whether α- or β-secretase cleavage of the integral membrane APP occurs. Conditions that promote β-secretase cleavage include glucose deprivation, increased Ca^{2+} levels and traumatic head injury [30]. Environmental factors may also contribute to β-amyloid deposition, such as acidic conditions and the presence of an oxidizing environment [36]. The presence of various metal ions, including iron, zinc and aluminium can also promote aggregation of β-amyloid [30]. However, β-amyloid has been shown to be a normal product during cell metabolism, and that low concentrations (pico- to nano-molar) of the peptide confer increased neuronal survival of hippocampal cells in culture [37]. Moreover, other reports have demonstrated that low concentrations of β-amyloid modulates a variety of cellular responses relevant to neuronal plasticity and survival [38, 39]. Therefore, the induction of neurotoxicity by β-amyloid appears to be concentration dependant.

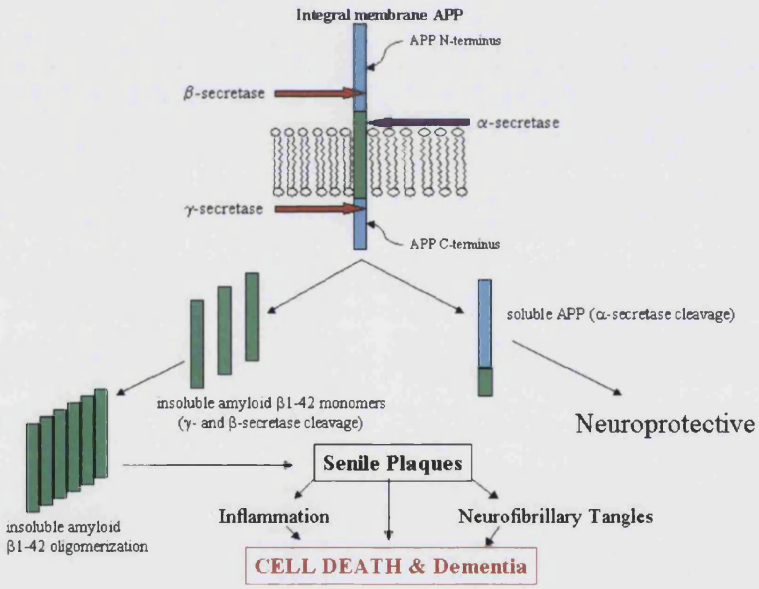

Figure 6.5 The amyloid cascade, whereby the processing of the integral membrane amyloid precursor protein (APP) may occur via two pathways: (i) Cleavage within the transmembrane region by α-secretase generates a soluble APP that provides neuroprotection against excitotoxicity or (ii) cleavage of the extracellular- and intracellular- domains of the APP, resulting in the formation of amyloid-β that precipitates to forms the insoluble β-amyloid, and in turn causes cell death.

As the precipitated β-amyloid peptide ages, it self-assembles into higher-ordered structures, and *in vitro* studies have shown that after several days the β-amyloid peptide forms insoluble aggregates [40]. It is the aggregated β-amyloid that induces toxicity [40, 41]. The aggregated β-amyloid peptide forms fibrils, which subsequently form senile plaques. These plaques are dense deposits of the β-amyloid peptide and cellular material on the extracellular face of neurons (Figure 6.6). The hydrophobic terminus of the β-amyloid 1-42 peptide is believed to influence the solubility and state of aggregation of the peptide. High molecular weight β-amyloid peptide 1-42 shows reduced solubility compared to the β-amyloid peptides 1-39 and 1-40, therefore, the hydrophobic C-terminus appears to be the critical determinant of solubility [42, 43]. The aggregation of the β-amyloid on the cellular membrane acts as a seed and thereby initiates the aggregation of β-amyloid [44]. The binding of the β-amyloid to the cell membrane has not been definitely described, and contradictory reports have suggested that the interaction between the peptide and the membrane may be mediated by a cell surface receptor or may aggregate via a non-specific association with the cell membranes [45].

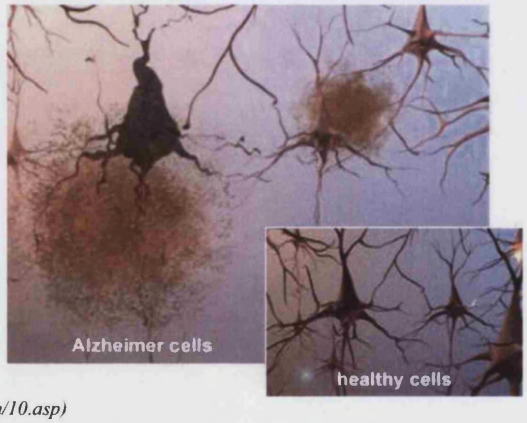

(Picture source: www.alz.org/brain/10.asp)

Figure 6.6 Comparison of healthy neurons and neurons containing the β-amyloid plaques.

The formation of the amyloid plaques is believed to occur via a two step mechanism, whereby the initial formation of a seeding aggregate is followed by the long term deposition of the β-amyloid peptide [46, 47].

6.4 The Mechanism of Toxicity

The mechanism with which β-amyloid induces neurotoxicity is not definitive. However, it has been suggested that damage is caused by the disruption of cellular Ca^{2+} homeostasis [48, 49], and that the β-amyloid peptide causes the influx of Ca^{2+} ions. However, this mechanism has now been modified because it appears that ion homeostasis is disrupted as a result of β-amyloid's involvement in inducing cellular oxidative stress and the formation of ion-conducting pores in the membrane [30]. The mechanism that β-amyloid causes oxidative stress is unclear, however, two hypotheses have been suggested. One possibility is that β-amyloid forms free radical moieties on certain amino acids that then propagate to the cell membrane [50], or β-amyloid binds to a specific cell surface receptor that subsequently induces oxidant stress [51]. β-amyloid has been shown to induce the accumulation of reactive oxygen species and hydrogen peroxide in neurons *in vitro*, and causes membrane lipid peroxidation in cultured neurons [52].

The neurotoxicity induced by β-amyloid has been reported to result from the indirect promotion of the inflammatory cascade. It has been suggested that inflammatory reactions occur in association with the amyloid plaques in Alzheimer's disease and that inflammation contributes to neurodegeneration, because plaques contain a variety of cytokines and other inflammatory mediators [53, 54].

The self-assembly of the β-amyloid peptide into plaques has been observed to induce programmed cell death, and this may drive neuronal degeneration in individuals suffering from Alzheimer's disease. The hallmarks of programmed cell death in non-demented cells include morphological and biochemical changes such as membrane blebbing, compaction of nuclear chromatin and intra-nucleosomal DNA fragmentation. Moreover, cultured neurons treated with β-amyloid trigger degeneration through activation of programmed cell death [55], as observed by the characteristics mentioned above.

However, it is still unclear whether β-amyloid aggregation is the cause of Alzheimer's disease or a consequence of some other underlying mechanism. This is because it has also been shown that substantial numbers of amyloid plaques were found in the brains of non-demented individuals [56], suggesting that β-amyloid deposition does not necessarily lead to Alzheimer's disease.

6.5 Preliminary Measurements of the Interaction between Tethered Biomimetic Membrane Vesicles and β-amyloid 1-42

The tethered biomimetic membrane vesicles have also found a novel application as a model membrane mimic to monitor the interaction between insoluble β-amyloid neurodegenerative peptides, as found in Alzheimer's sufferers, and the cell membrane. The simultaneous measurements of change in reflectivity and fluorescence allowed for the sensitive detection of analyte-ligand events and the determination of binding constants between the interactants. The interaction between β-amyloid 1-42 and DMPC-GM1-cholesterol vesicles was observed and compared to the interaction between β-amyloid 1-42 and negatively charged phospholipid-GM1-cholesterol vesicles. The influence GM1 and cholesterol offers to β-amyloid binding was subsequently established.

6.5.1 The Interaction Between DMPC-GM1-cholesterol Membrane Vesicles and β-amyloid 1-42

The initial biomimetic membrane model was composed of 1% biotin, 2% GM1, 30% cholesterol and 67% DMPC attached to the solid substrate via biotin-streptavidin coupling (as detailed in section 3.3.4). The biomimetic membrane vesicles used were to determine the proof-of-principle that it was possible to monitor the interaction between β-amyloid 1-42 and a simple single phospholipid species membrane mimic. A 10μmol.dm^{-3} solution of β-amyloid 1-42 was prepared and injected into the tethered vesicle system, and a change in reflectivity was observed (Figure 6.7).

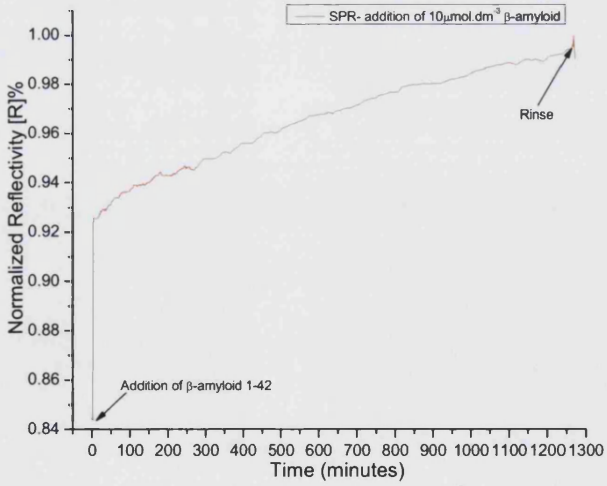

Figure 6.7 Kinetics plot for the addition of 10μmol.dm^{-3} β-amyloid 1-42 peptide to the biomimetic membrane vesicle surface composed of DMPC phospholipids.

From the kinetics plot (Figure 6.7), the interaction between the biomimetic membrane and the β-amyloid peptide was observed in real-time. Therefore, the biomimetic membrane system provided a novel method to study protein aggregation and amyloidosis *in vitro*. The addition of the peptide to the system was observed as a change in the reflectivity. The adsorption of the peptide occurred via a two step mechanisms. The amyloid bound to the surface and followed a typical Langmuir interaction between 0 minutes and ~200 minutes. At the initial stage, the amyloid peptide specifically bound to the membrane surface and seeded. However, following the first step, the amyloid began to non-specifically adsorb to the membrane surface, suggesting that the amyloid peptide binds to a specific receptor and/or receptors, which seeds the peptide to the membrane surface, and further peptide binding occurs via non-receptor specific attachment.

The adsorption of the amyloid peptide to the DMPC-GM1-cholesterol membrane surface was simultaneously monitored as a change in fluorescence (Figure 6.8). The addition of the peptide caused a change in the properties of the simple biomimetic membrane, and therefore caused a change in fluorescence.

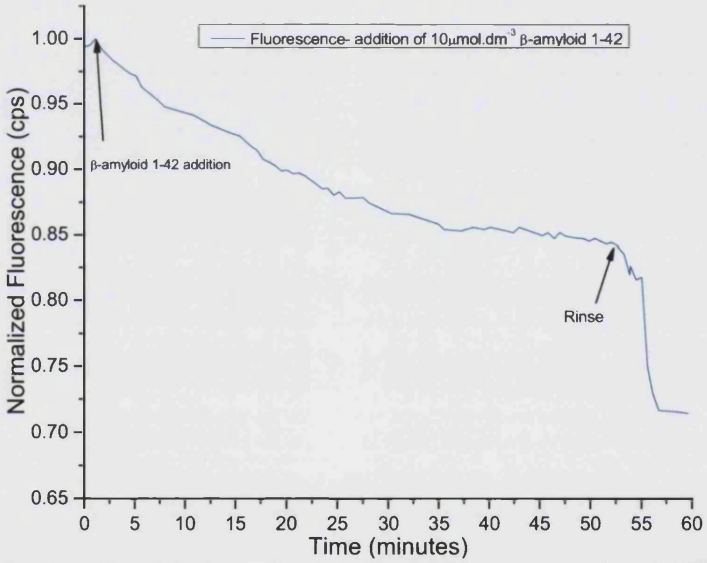

Figure 6.8 Monitoring the change in fluorescence of the encapsulated BODIPY dye within the tethered biomimetic DMPC-GM1-cholesterol membrane vesicles upon addition of 10μmol.dm^{-3} β-amyloid.

Using the simple DMPC biomimetic model, it was possible to observe a change in fluorescence upon addition of the β-amyloid peptide. Addition of the Alzheimer's peptide caused an increase in the BODIPY dye diffusion from the encapsulated space of the tethered phospholipid vesicles, through the lipid bilayer and into the bulk solution.

Therefore, the tethered biomimetic membrane system provided an attractive model to study the affects of amyloidosis and the associated peptide.

The adsorption of the amyloid peptide to the biomimetic membrane surface was confirmed by observing the change in the angle at which resonance occurred (Figure 6.9).

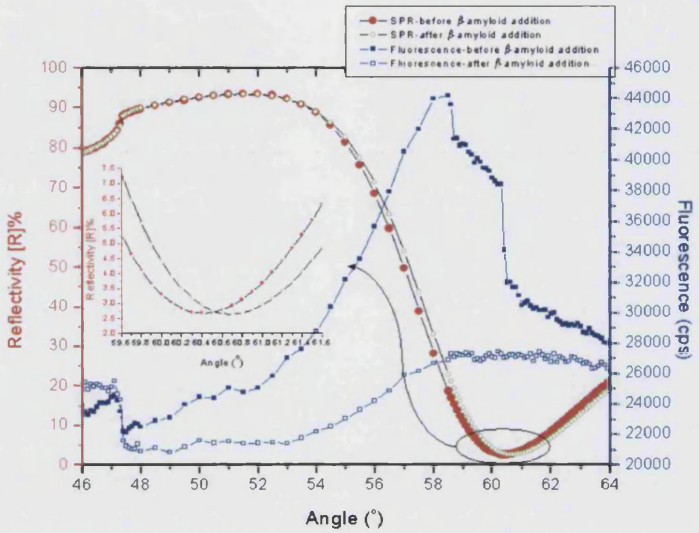

Figure 6.9 Resonance angle scan for the addition of β-amyloid 1-42 to the DMPC-GM1-cholesterol model membrane system. The adsorption of the peptide to the surface resulted in a resonance minimum shift of 0.3°.

The addition of the β-amyloid 1-42 peptide to the tethered biomimetic membrane vesicle system resulted in a 0.3° shift in the resonance minimum. This shift equated to a 1.61ng.mm^{-2} increase in mass density at the surface, therefore the tethered membrane system allowed for the quantitative determination of the adsorption of the neurodegenerative peptide to the biomimetic membrane surface.

6.5.2 The Interaction Between GM1-deficient DMPC Membrane Vesicles and β-amyloid 1-42

Biomimetic membrane vesicles containing 1% biotin, 30% cholesterol and 69% DMPC were prepared and tethered to the solid support. The GM1 ganglioside was excluded from the vesicle bilayer.

The membrane receptor for the adsorption of β-amyloid has not been definitively determined, and various receptors have been reported to specifically associated with β-amyloid. These include NK-1 tachykinin receptor [57] and a range of membrane phospholipids [58], such as phosphatidylinositol which was shown to be the most efficient

inducer of β-amyloid aggregation [59]. However, the GM1 ganglioside predominates in reports to mediate the fibrillogenesis of the β-amyloid on membrane surfaces. It has been shown that the β-amyloid peptide binds to membranes containing GM1 and upon binding undergoes a conformational transition from a random coil to an ordered structure rich in β-sheets [60]. Therefore, the GM1 ganglioside would appear to be the membrane receptor for β-amyloid and its subsequent aggregation.

Biomimetic membranes deficient in GM1 were tethered to the solid substrate and 10μmol.dm^{-3} β-amyloid 1-42 was injected into the system to observe any interaction between the analyte and membrane (Figure 6.10).

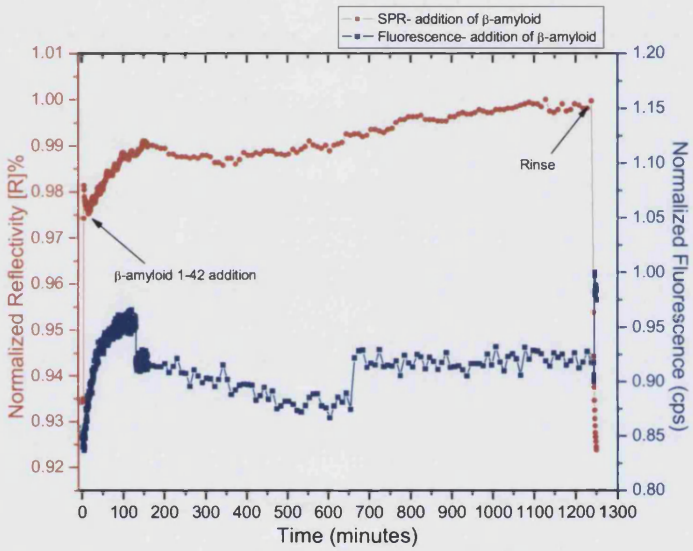

Figure 6.10 Kinetics plot for the addition of 10μmol.dm^{-3} β-amyloid 1-42 peptide to the GM1-deficient DMPC biomimetic membrane vesicles.

The addition of the β-amyloid to the GM1-deficient membrane system showed weak non-specific attachment to the surface. The β-amyloid was allowed to associate with the biomimetic membranes for 20 hours, and a change in reflectivity was observed. However, upon rinsing of the system, the reflectivity returned to its initial value, suggesting that the peptide was very loosely and/or non-specifically associated to the DMPC-cholesterol vesicles and was not mediated by a specific receptor. Therefore, it would suggest that GM1 is a receptor for β-amyloid binding. The change in fluorescence observed upon β-amyloid addition did not show the expected increase in dye diffusion from the encapsulated vesicle space to the bulk solution as monitored when GM1 was present in the vesicle bilayer (Figure 6.8). Therefore, it appears that GM1 is the specific membrane receptor for β-amyloid 1-42 neuropeptide, and that membranes deficient in the ganglioside do not

mediate specific binding, but show a weak attraction maybe between the phospholipid head group or sterol with the β-amyloid peptide. This observation suggests that the interaction between β-amyloid and GM1 was ganglioside-specific, as it has been shown that β-amyloid (1-40) does not change conformation in the presence of various phospholipid species, but does change conformation upon GM1-βamyloid interaction [60]. The moiety responsible for binding β-amyloid is believed to be the sialic acid group, which in turn is stabilized by the terminal galactose residue of the GM1 [61].

The confirmation that GM1 acts as the membrane receptor for β-amyloid was verified by monitoring the shift in resonance minimum upon β-amyloid addition to GM1-deficient vesicles (Figure 6.11).

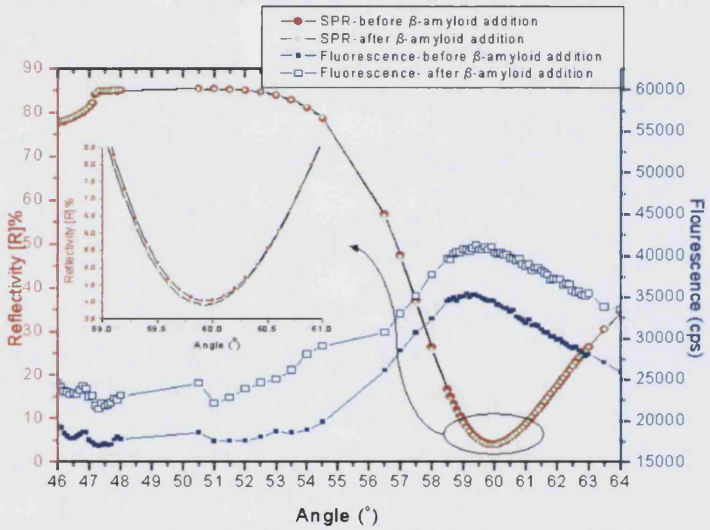

Figure 6.11 Resonance angle scan for the GM1-deficient DMPC tethered biomimetic membrane vesicles before and after the addition of 10μmol.dm^{-3} β-amyloid. No shift in resonance minimum was observed (see inlaid graph).

The addition of the β-amyloid to the GM1-deficient biomimetic membrane vesicles resulted in no shift in the resonance minimum. Therefore, no adsorption of the peptide to the membrane surface was observed. Moreover, this suggests that GM1 is a membrane receptor for the β-amyloid peptide. GM1 would provide a reliable receptor for ligand binding because gangliosides show an almost constant concentration between 20 and 70 years of age [62], therefore, its continual expression in neuronal membranes provides an attractive receptor for any analyte to bind. The GM1 receptor is ubiquitously found in the eukaryotes, and acts as a natural receptor for many analytes including some bacterial toxins (section 5.1.2).

6.5.3 The Interaction Between Multi-Species Phospholipid Biomimetic Membrane Vesicles and β-amyloid 1-42

Tethered biomimetic membranes containing a mixture of phospholipid species were prepared to included 1% biotin, 2% GM1, 30% cholesterol, 50% DMPC, 13.5% 1,2-Dimyristoyl-*sn*-Glycero-3-Phosphoethanolamine (DMPE), 1.75% 1,2-Dimyristoyl-sn-Glycero-3-[Phospho-L-Serine] (DMPS) and 1.75% 1,2-Dimyristoyl-*sn*-Glycero-3-[Phospho-*rac*-(1-glycerol)] (DMPG), and were subsequently attached to the solid substrate using biotin-streptavidin coupling. The mixed DMPC, DMPE, DMPS and DMPG vesicles will be called mixed-vesicles.

The composition of biological membranes varies significantly depending on its cellular location, the functions the membrane performs and its age. The macromolecular composition of neuronal membranes are considerably different to other membranes such as those composing the epithelia. The phospholipid content of neuronal membranes have been shown to contain a higher proportion of negatively charged phospholipids and also contains a very high proportion of long-chained polyunsaturated fatty acids [63, 64]. Therefore, the chemical composition of the tethered biomimetic membrane vesicles was altered to reflect the negative charge associated with neuronal membranes.

The addition of 10μmol.dm^{-3} β-amyloid to the tethered mixed-vesicles was followed by simultaneous measurements of change in reflectivity and fluorescence (Figure 6.12).

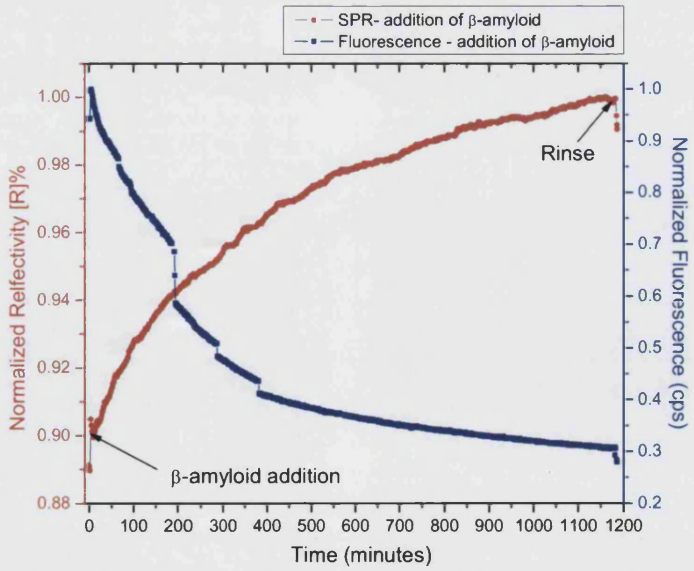

Figure 6.12 Kinetics plot following the adsorption of 10μmol.dm^{-3} β-amyloid to mixed phospholipid-GM1-cholesterol biomimetic membrane vesicles.

The increase in reflectivity observed upon addition of β-amyloid 1-42 to the mixed-vesicle surface equated to the adsorption of the neuro-peptide to the membrane surface. The adsorption of the analyte to its respective receptors followed a slow association binding, whereby the change in reflectivity showed a gradual increase over time, until equilibrium was reached at around 1100 minutes. The slow binding of the peptide to the surface would reflect the slow progressive accumulation of the β-amyloid peptide characteristic of Alzheimer's and other amyloidosis disorders.

The addition of the neuro-peptide to the mixed-vesicle surface resulted in a shift in the angle at which resonance was achieved. The change in reflectivity and fluorescence as a function of resonance angle was shown in Figure 6.13.

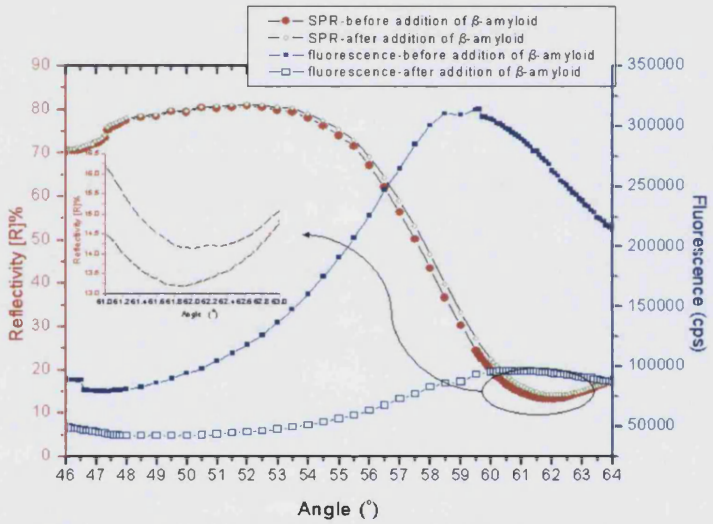

Figure 6.13 Resonance angle scan for the addition of β-amyloid 1-42 neurodegenerative peptide to the mixed-vesicle biomimetic model membrane system. The adsorption of the peptide to the surface results in a resonance minimum shift of 0.5°.

The addition of the β-amyloid 1-42 peptide to the mixed-vesicle biomimetic membrane surface resulted in a 0.5° resonance shift, which equated to the adsorption of 2.68ng.mm^{-2} of the peptide to the vesicle membrane. The analyte-ligand interaction resulted in a 40% increase in mass adsorption compared to the DMPC tethered vesicles (Figure 6.9). The increase in binding capacity observed for the mixed-vesicle system probably reflects the influence of the negative charge conferred on the mixed-vesicle surface by the inclusion of negatively charged phospholipid species in the membrane bilayer. The negative charge on the surface would result in an electrostatic interaction between the membrane and the insoluble β-amyloid peptide. This electrostatic interaction has been observed to occur

between the C-terminus of the β-amyloid peptide and the negatively charged phospholipid. Using circular dichroism and electron paramagnetic resonance, it has been reported that electrostatic and hydrophobic interactions contribute to peptide-receptor binding [65]. These additional non-specific forces resulted in an interaction between the basic peptide residues and the negatively charged lipids in the membrane, which works in synergy with the specific binding between the β-amyloid peptide and the GM1 ganglioside receptors present on the biomimetic membrane surface. The electrostatic and hydrophobic interactions have not been reported to occur between the β-amyloid peptide and neutral biomimetic membrane vesicles [66], such as membranes composed of DMPC. Therefore, increased binding was observed between the negatively charged surface and the amyloid compared to the neutral surface and the peptide.

6.5.4 The Interaction Between GM1-Deficient Multi-Species Phospholipid Biomimetic Membrane Vesicles and β-amyloid 1-42

Mixed-vesicles were prepared (as discussed in section 3.3.5) with the exclusion of GM1 from the bilayer vesicles. The GM1-deficient mixed-vesicles were tethered to the solid support and monitored for their interaction with β-amyloid 1-42.

The influence of electrostatic and hydrophobic forces on the adsorption of β-amyloid to biomimetic membrane vesicles was investigated using tethered mixed-vesicles deficient in the GM1 receptor. The exclusion of the ganglioside from the vesicle bilayer resulted in the removal of the membrane receptor, therefore blocking the potential for specific receptor-analyte interactions. Therefore, any adsorption of β-amyloid to the membrane surface would be the result of non-specific binding. The addition of the β-amyloid 1-42 peptide to the GM1-deficient mixed-vesicles was monitored simultaneously as a result of change in reflectivity and fluorescence (Figure 6.14a) and compared to GM1-containing mixed-vesicles (Figure 6.14b).

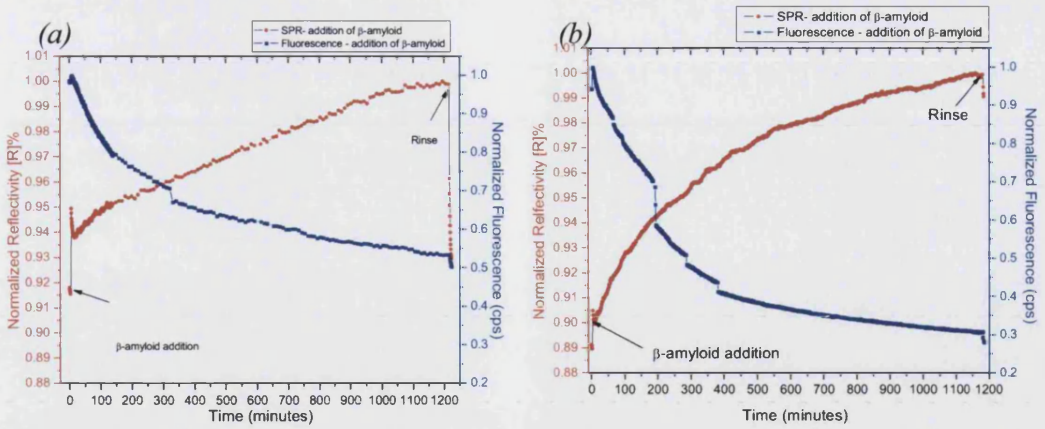

Figure 6.14(a) Kinetics plot monitoring the addition of 10μmol.dm^{-3} β-amyloid to GM1-deficient biomimetic mixed-vesicles, and, (b) the addition of 10μmol.dm^{-3} β-amyloid to GM1-containing biomimetic mixed-vesicles.

The addition of the β-amyloid to the GM1-deficient mixed-vesicles (Figure 6.14a) resulted in a change in reflectivity until equilibrium was reached. The increase in reflectivity equated to the interaction between the peptide and the membrane surface. However, because the GM1 membrane receptor was absent from the tethered biomimetic membranes, the peptide-membrane interaction was not the result of specific analyte-receptor interactions. Therefore, the increase in reflectivity was the result of an electrostatic and/or hydrophobic association. The rinsing of the tethered membrane system resulted in the dissociation of the β-amyloid ligand from the membrane surface. Moreover, this dissociation suggests that the interaction was relatively weak and not a specific interaction resulting from the binding of the neuro-peptide to its specific GM1 receptor (Figure 6.14b).

The weak association observed between the negatively charged GM1-deficient mixed-vesicle surface and the β-amyloid was confirmed by monitoring the shift in resonance minimum upon addition of the peptide (Figure 6.15).

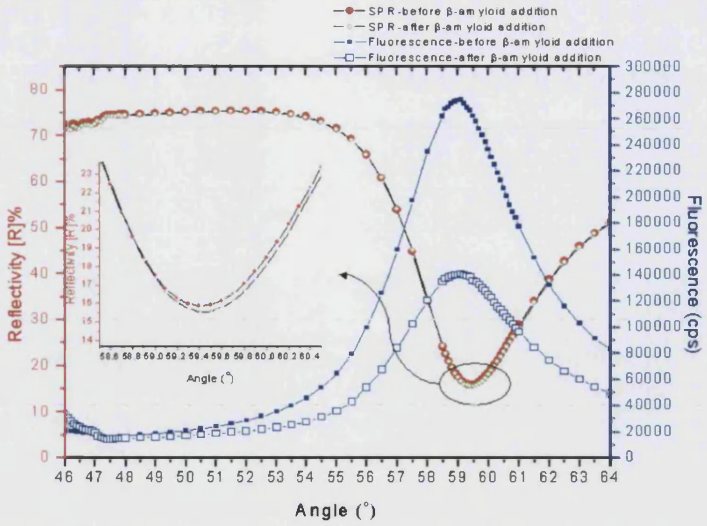

Figure 6.15 Resonance angle scans for the addition of 10μmol.dm^{-3} β-amyloid 1-42 to the biomimetic GM1-deficient mixed-vesicle system. The addition of the peptide resulted in no overall shift in the resonance minimum.

The addition of the peptide to the GM1-deficient mixed-vesicle surface resulted in a 0° shift in the resonance minimum. Therefore, this equated to no adsorption of the β-amyloid peptide to the surface lacking the membrane receptors, compared to the adsorption of 2.68ng.mm^{-2} β-amyloid to GM1-containing mixed-vesicles (Figure 6.13). This suggests that additional forces play a significant role in the binding between the β-amyloid peptide and the membrane surface, and that these hydrophobic and electrostatic forces act to stabilize the β-amyloid peptide on the surface. Therefore, the specific binding resulting from the interaction between GM1 and the neuro-peptide acts to anchor the β-amyloid to the membrane surface and the negatively charged phospholipids and sterols act to stabilize the structure. The interaction between the GM1 and the β-amyloid resulted in the formation of an amyloid 'seed', whereby the GM1-bound amyloid accelerates fibrillogenesis in a first-order kinetics model [67]. The pathway from the 'seeding' of the peptide is believed to occur via:

1) The rapid commitment to form either stable monomer/dimer or an unstable intermediate.
2) The cooperative association of intermediates into a multimeric 'seed'.
3) The elongation of the 'seed' into filaments via addition of other amyloid intermediates.
4) The lateral aggregation of filaments into fibrils, and
5) Fibril elongation via end-to-end association [68].

6.5.5 The Interaction Between Cholesterol-Deficient Multi-Species Phospholipid Biomimetic Membrane Vesicles and β-amyloid 1-42

Mixed-vesicles were prepared (as discussed in section 3.3.5) with the exclusion of cholesterol from the bilayer vesicles. The cholesterol-deficient mixed-vesicles were tethered to the solid support and monitored for their interaction with β-amyloid 1-42.

Sterols, such as cholesterol, typically play a significant role in biological membrane dynamics. They are key in influencing the permeability and compartmentalization of the membranes, and their abundance within eukaryotic membranes have made them attractive targets for certain bacterial toxins and toxic analytes to circumvent the membrane barrier. The brain contains the highest cholesterol content of all the organs, and contains around 20% of the total body cholesterol [69]. Cholesterol has been reported to alter the affinity of the β-amyloid for phospholipid membranes, and both *in vitro* and *in vivo* studies have shown that inhibition of cholesterol biosynthesis leads to a reduction in β-amyloid aggregation [70]. Therefore, biomimetic membrane mixed-vesicles deficient in cholesterol were prepared and tethered to the solid substrate. The biomimetic membranes were monitored for any change in reflectivity and/or fluorescence upon β-amyloid addition to the system (Figure 6.16a) and compared to cholesterol-containing mixed-vesicles (Figure 6.14b).

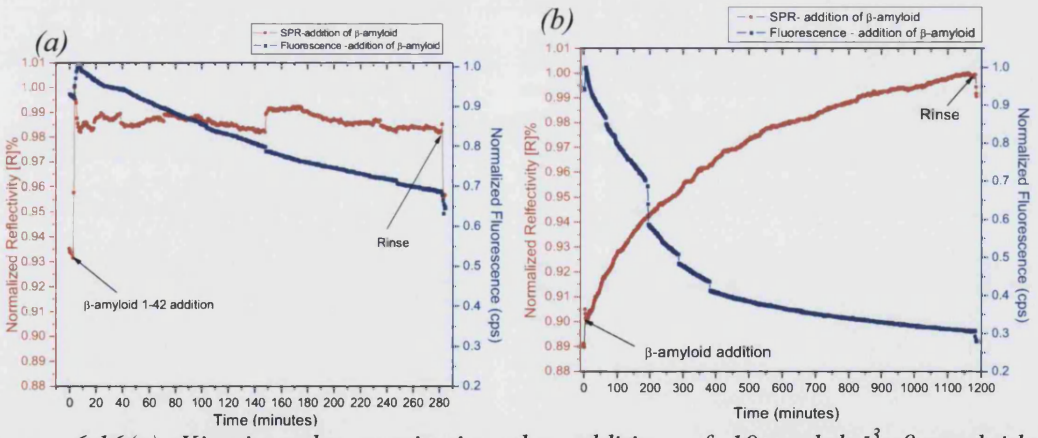

Figure 6.16(a) Kinetics plot monitoring the addition of 10μmol.dm^{-3} β-amyloid to cholesterol-deficient biomimetic mixed-vesicles, and, (b) the addition of 10μmol.dm^{-3} β-amyloid to cholesterol-containing biomimetic mixed-vesicles.

The addition of β-amyloid 1-42 to the cholesterol-deficient mixed-vesicles resulted in an increase in reflectivity, until an equilibrium value was reached. Non-specifically bound peptide was subsequently removed by rinsing the system with fresh buffer. The

cholesterol-deficient mixed-vesicles maintained an affinity towards the β-amyloid because the GM1 receptor was present within the vesicle bilayer. However, the non-specific binding associated with the electrostatic and hydrophobic interactions was reduced. Therefore, this suggests that the cholesterol influenced the non-specific binding of the β-amyloid to the membrane surface. The binding between the cholesterol-deficient vesicles (Figure 6.16a) followed a different kinetics path compared to cholesterol-containing vesicles (Figure 6.16b). It has been reported that the membrane cholesterol to phospholipid ratio directly influences the extent of high-affinity lipid binding, and that pure phospholipid biomimetic membranes show reduced binding compared to cholesterol containing vesicles [71]. The influence of sterols on the binding capacity of the β-amyloid towards biomimetic membranes suggests that cholesterol affects the charge of the membrane, thereby influencing the non-specific association between the membrane and the neuro-peptide, and causes the concentration of GM1 receptors into lipid domains. Therefore, receptor clustering into lipid domains facilitates amyloid aggregation. Cholesterol also affects the diffusion of the encapsulated BODIPY, and dye diffusion was significantly reduced upon the adsorption of the β-amyloid to the cholesterol-deficient mixed-vesicles (Figure 6.16a) compared to the adsorption of β-amyloid to the cholesterol-containing mixed-vesicles (Figure 6.16b).

Cholesterol may also act to influence β-amyloid binding to biological membranes by altering the fluidity of the phospholipid bilayers. *In vivo* studies have shown that the fluidity and lipid composition of the membranes changes with increasing age, and that aged membranes show reduced fluidity compared with the membranes of younger eukaryotes [72]. All regions of the human brain are rich in cholesterol, but alterations in the amount of the sterol are highly variable during aging, ranging from no change to a 40% decrease [73, 74]. β-amyloid and the APP have been shown to be located in membrane domains enriched in cholesterol [75], and that β-amyloid perturbs biological membranes, and this action is believed to be dependant on the cholesterol content of the membrane [76]. Reducing membrane cholesterol below normal membrane levels results in an increased sensitivity of the cells to β-amyloid toxicity [77]. Therefore, the depletion of membrane cholesterol may possibly stimulate β-amyloid cytotoxicity.

The binding effects of the β-amyloid 1-42 towards cholesterol-deficient biomimetic membranes was confirmed by observing the change in resonance shift upon addition of the neuro-peptide to the membrane surface (Figure 6.17).

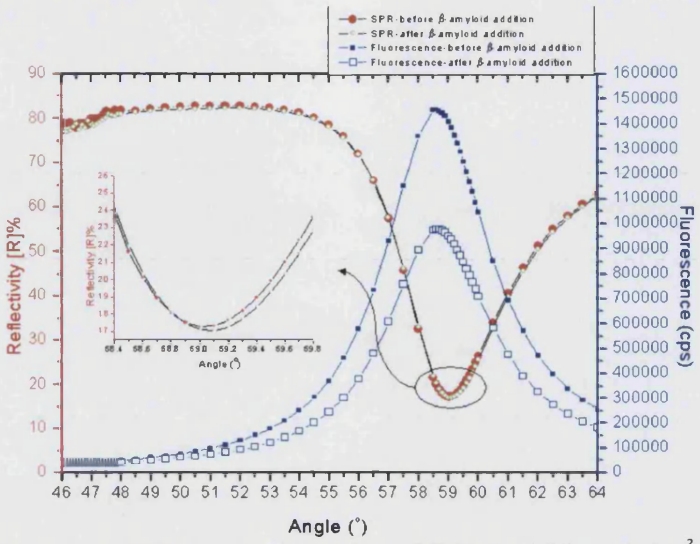

Figure 6.17 Resonance angle scans form the addition of 10μmol.dm^{-3} β-amyloid 1-42 neuro-peptide to the biomimetic cholesterol-deficient mixed-vesicle system. The addition of the peptide resulted in a 0.1° shift in the resonance minimum.

The addition of the β-amyloid 1-42 peptide to the cholesterol-deficient mixed-vesicles resulted in a 0.1° shift in the resonance minimum, which equated to a 0.54ng.mm^{-2} increase in mass at the membrane surface, compared to the 2.68ng.mm^{-2} adsorbed to cholesterol-containing vesicles (Figure 6.13). Therefore, cholesterol significantly affected the binding capacity of the biomimetic membranes towards β-amyloid.

There is a synergistic relationship between the membrane phospholipid species, cholesterol content and the presence of GM1 receptors within the biomimetic membrane vesicles which regulates the degree of β-amyloid binding. Phospholipids which confer an overall negative charge on the extracellular face of the biomimetic membranes showed an increased capacity to bind β-amyloid 1-42 peptides compared to phospholipids which conferred a neutral charge. The presence of GM1 within the phospholipid bilayer acted as a membrane surface receptor for the neuro-peptide, and the elimination of the ganglioside from the vesicle composition removed the capacity to bind β-amyloid in a specific interaction. However, biomimetic membrane vesicles deficient in GM1 did show a capacity to non-specifically associate with the β-amyloid via electrostatic attraction and hydrophobic forces, but this association was weak and was disrupted easily. Sterols also regulated the interaction between the biomimetic membrane vesicles and the β-amyloid 1-

42 peptide. Removal of the cholesterol from the biomimetic membrane bilayer caused a significant reduction in the binding between the analyte and receptors on the membrane surface. This phenomenon is believed to result from either a change in the overall surface charge of the vesicles or a change in the fluidity of the membranes as a result of altered membrane-associated cholesterol content. Therefore, the sterol content, phospholipid species and ganglioside content of neuronal membranes significantly affects the binding of the β-amyloid.

6.6 Dose Response of β-amyloid 1-42 Towards Biomimetic Membrane Vesicles

Amyloid fibrils are produced upon the formation of β-sheet proteins which have a high propensity to aggregate and fibrillize. Oligomeric β-sheet intermediates form before the appearance of fibrils, and disappear upon fibril formation [78]. It is the fibrils which show the greatest stability compared to the oligomeric intermediates and the monomeric β-amyloid peptides [79]. The conversion of the β-amyloid peptides from the protofibril intermediates to the β-amyloid fibrils is concentration dependant, and upon reaching the critical concentration of the chain-like intermediates, they are rapidly converted into the amyloid fibrils. Moreover, the number and size of the plaques/fibrils formed does not correlate with the severity of the disease at the time of death [80, 81]. However, the protofibrils and intermediate aggregated β-amyloid have been implicated in the alteration of membrane permeability and with the pathogenicity of Alzheimer's disease [82].

Various concentrations, ranging between 0.1-10μmol.dm^{-3}, were added to the tethered mixed-vesicle biomimetic membrane system (GM1-mixed phospholipids-cholesterol), and monitored for changes in reflectivity and fluorescence (Figure 6.18).

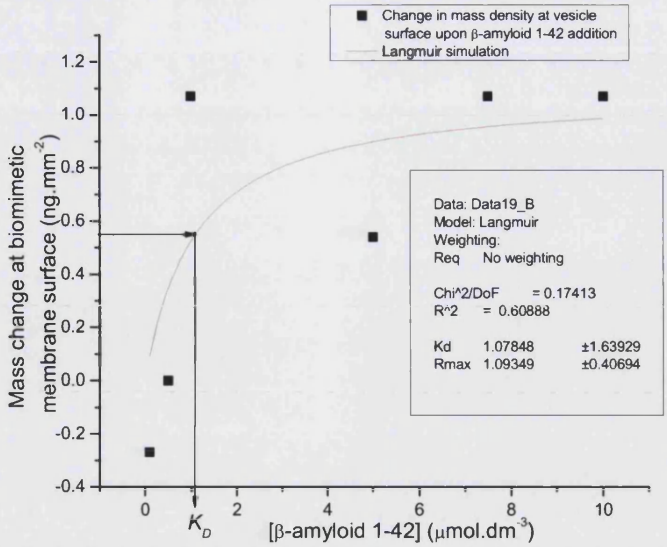

Figure 6.18 Langmuir simulation for change in mass at the biomimetic membrane surface upon addition of β-amyloid peptide. The equilibrium dissociation constant, K_D, is marked.

The addition of the β-amyloid 1-42 to the biomimetic membrane surface followed a concentration dependant Langmuir isotherm and allowed for the determination of the affinity constants. The equilibrium dissociation constant for β-amyloid 1-42 and the biomimetic membrane vesicles was determined to be, $K_D = 1.09 \times 10^{-6} mol.dm^{-3}$, which was in good agreement with other reported values of $1.4 \times 10^{-6} mol.dm^{-3}$ [61, 83]. The affinity between the β-amyloid and the membrane surface was mediated by the specific interaction between the GM1 ganglioside receptor on the membrane surface and the C-terminus of the β-amyloid peptide.

The addition of β-amyloid 1-42 to the biomimetic membrane surface also showed a concentration dependant effect on the permeation of the vesicle bilayer (Figure 6.19).

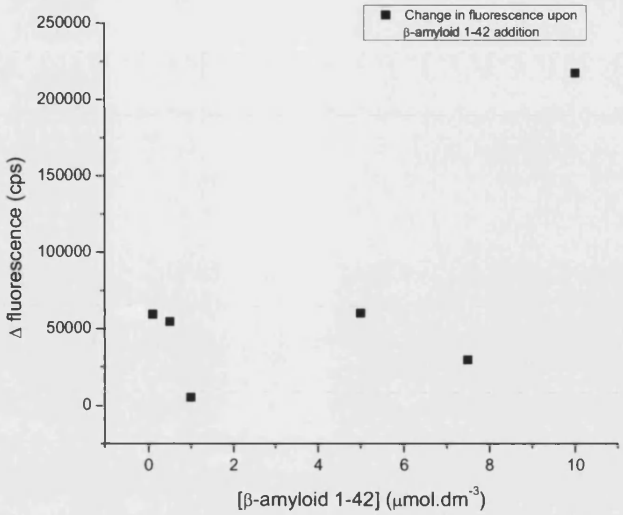

Figure 6.19 Plot of the change in fluorescence upon β-amyloid addition to the biomimetic membrane surface.

At lower concentrations of β-amyloid (0.1-7.5μmol.dm^{-3}), the diffusion of the BODIPY dye from the aqueous vesicle space to the bulk solution was relatively constant, and similar changes in fluorescence were observed upon β-amyloid peptide addition. However, at the higher peptide concentration (10μmol.dm^{-3}), an greater change in fluorescence was observed. This suggests that β-amyloid caused a concentration dependant change in the permeability of the biomimetic membrane vesicles.

The addition of varying concentration of β-amyloid caused a concentration dependant effect on the tethered biomimetic membrane vesicles. The adsorption of the peptide to the membrane surface occurred via a dose-dependant mechanism, and followed a Langmuir isotherm. The concentration dependence of the peptide allowed for the determination of the equilibrium dissociation constant, which was found to be in agreement with other reported values. The alteration in membrane permeability in the biomimetic membranes showed little variation in the change in fluorescence at lower concentration of the β-amyloid 1-42 peptide, however, at the highest concentration tested, a greater change in fluorescence was observed. Therefore, it would suggest β-amyloid permeation of the membrane was concentration dependant and relies on the accumulation of the amyloid peptides on the membrane surface, until a critical concentration is achieved, whereby they cause a change in the membrane structure. This progressive accumulation of the neurodegenerative peptide is expressed *in vivo* as the characteristic slow progression of Alzheimer's disease.

6.7 Comparison Between Juvenile β-amyloid 1-42 and Aged β-amyloid 1-42 and Their Effects Towards Biomimetic Membrane Vesicles

The conformation and state of aggregation of the β-amyloid is of importance to the degree of interaction with the tethered biomimetic membrane vesicles, and therefore, with the interaction with biological membranes. It has been readily observed that monomeric β-amyloid adsorbs to biomimetic lipid vesicles less readily compared to the aggregated intermediate fibril β-amyloid [84]. The self-assembly of aggregated amyloid intermediates causes hydrophobic domains to become exposed, and these domains have not been detected in the monomeric β-amyloid peptides or the mature fibrils. Therefore, the formation of intermediate fibrils allows for the aggregates to interact with the biomimetic membranes via hydrophobic forces, aiding the stabilization of the aggregate to the membrane. The loss of these hydrophobic domains in the mature fibrils causes a decrease in the binding capacity and stabilization of the fibrils compared to the intermediate fibril aggregates [85]. In another study, it was shown that biomimetic lipid vesicles became disrupted to a lesser extent as a result of aged β-amyloid fibrils compared to the monomeric peptide and the intermediate β-amyloid fibrils [86]. Therefore, tethered biomimetic membrane vesicles were used to compare the extent of binding to the membrane surface using juvenile β-amyloid and aged β-amyloid (Figure 6.20). Aged β-amyloid was formed from juvenile β-amyloid 1-42 which was vortexed slowly (500 RPM) for 7 days to ensure mature fibril formation.

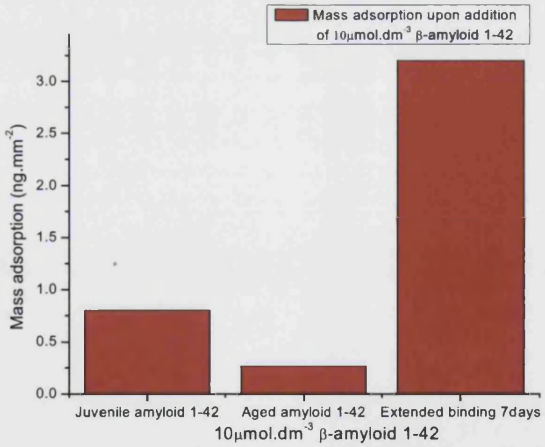

Figure 6.20 Comparison of the mass adsorption of juvenile β-amyloid (day 0) and aged β-amyloid (day 7) on the tethered biomimetic membrane vesicles, and the overall mass adsorption observed when the juvenile β-amyloid 'seeds' and binding occurs over a 7 day period.

The extent of juvenile β-amyloid adsorption (0.8ng.mm^{-2} over 20 hours) was significantly higher than that of the aged β-amyloid (0.27ng.mm^{-2} over 20 hours). This suggested that aged β-amyloid has a lower binding capacity to the biomimetic membranes because the mature fibrils have fewer exposed binding sites, and the loss of the hydrophobic domains contribute to the decreased mass adsorption compared to the juvenile β-amyloid. It has been reported that on incubation in solution, all β-amyloid peptides initially undergo a transformation from mixtures of β-sheet, α-helix, and random coil conformations to eventually adopt to a complete β-sheet structure [86], therefore, the intermediate β-amyloid fibrils show a greater degree of association with the biomimetic membranes. The report also demonstrated that the ability of β-amyloid to induce aggregation decays progressively, and they loose the capacity to aggregate after 24 hours of incubation. Therefore, the aged β-amyloid would show a reduction in adsorption to the biomimetic membranes compared to the juvenile peptide. The binding of the juvenile β-amyloid peptide was followed for an extended period of time (over 7 days), and showed that β-amyloid adsorbs significantly more to the surface (3.2ng.mm^{-2} over 168 hours). Therefore, the bound juvenile peptide acts as a 'seed' for subsequent binding of the peptide to the surface.

The extent of β-amyloid aggregation significantly affects the adsorption of the peptide to the biomimetic membrane surface. Juvenile amyloid showed more binding to the membrane surface because it transitions from the mixed conformations to an all β-sheet conformation. Therefore, the juvenile β-amyloid transitions through the conformations to the intermediate fibril formation, which have more exposed hydrophobic domains. The transition from the intermediate β-amyloid fibrils to the mature fibrils, which occurs within 24 hours, caused a loss in the capacity to aggregate and thereby caused a reduction in the adsorption to the membrane surface. The addition of the mature fibrils to the tethered membrane system could not aggregate because they tend to loose the hydrophobic domains, which reduced the non-specific electrostatic and hydrophobic forces between the mature fibrils and the membrane surface. Therefore, mature amyloid fibrils can not adsorb to the membrane surface to an extent observed with juvenile β-amyloid peptides and intermediate aggregates. Therefore, the 'seeding' of the amyloid produces the characteristic slow progression of Alzheimer's disease *in vivo*.

6.8 Discussion Concerning the Mechanism of β-amyloid Neurotoxicity Towards Biomimetic Membrane Vesicles

The means with which β-amyloid causes the cytotoxic effects on neurons has not been definitively identified because it is not possible to directly observe the pathogenic events, and various models have been proposed as to how β-amyloid causes Alzheimer's disease. It is assumed that the amyloid results in a gain-of-function which induces pathophysiological cellular responses by altering the cell membrane composition and destabilizing the cellular homeostasis.

The original assumption made about the toxicity caused by β-amyloid was that the deposition of the amyloid was necessary for cell death to occur in Alzheimer's disease. However, it is still presently unknown whether it is the deposited β-amyloid that causes neuronal death or whether it is an intermediate β-amyloid peptide that causes toxicity. Therefore, much research has focused on whether β-amyloid fibrillization is the cause of neuronal death or a result of another upstream process.

One of the theories presented for β-amyloid toxicity is that the neuro-peptide causes membrane poration followed by non-specific membrane leakage or specific ionic transport through ion channels. The formation of channels in the neuronal membrane would subsequently lead to the destruction of the ionic gradients and membrane potential of the neurons which maintains this balance in order to function correctly for their signalling role. *In vitro* studies have shown that β-amyloid peptides form cation selective channels within planar lipid bilayers [87]. It has been proposed that non-fibrillar β-amyloid peptides form calcium-permeable ion channels in the cell membranes, allowing excessive calcium influx which disrupts the ionic gradients of the neurons. The disruption of neuronal homeostasis in cultured cells by nanomolar concentrations of β-amyloid, show morphological changes, such as beading, granulation and swelling of neuronal bodies [88]. The transmembrane region of the β-amyloid peptide has been reported to increase the permeability of neurons to Ca^{2+}, Na^{+}, and K^{+} [89], and reduce the fluidity of murine brain homogenate preparations [76]. Atomic force microscopic examination of β-amyloid peptides reconstituted in membrane bilayers have been shown to form 'disc-like' shapes, with an outer diameter of 8-12nm and a central pore-like cavity with a diameter of 1-2nm [90].

The presence of 'pore-like' structures in neuronal membranes would therefore provide a realistic hypothesis for a contributing mechanism in neuronal degradation in Alzheimer's

disease. The formation of pores within membranes *in vitro* and *in vivo* would cause the disruption of the permeability barrier and result in the flux of ions and solutes. The tethered biomimetic membrane system and the dye diffusion model, therefore, provides a means to study any changes in the porosity of the membrane caused by β-amyloid. Various tethered membrane systems comprising different membrane components were monitored for changes in fluorescence upon addition of 10μmol.dm^{-3} β-amyloid 1-42. DMPC-GM1-cholesterol biomimetic membrane vesicles (red fluorophore leakage), mixed phospholipid-GM1-cholesterol biomimetic membrane vesicles (green fluorophore leakage), Cholesterol-deficient mixed phospholipid-GM1 biomimetic membrane vesicles (blue fluorophore leakage), and GM1-deficient mixed phospholipid-cholesterol biomimetic membrane vesicles (fuchsia fluorophore leakage) were produced (Figure 6.21).

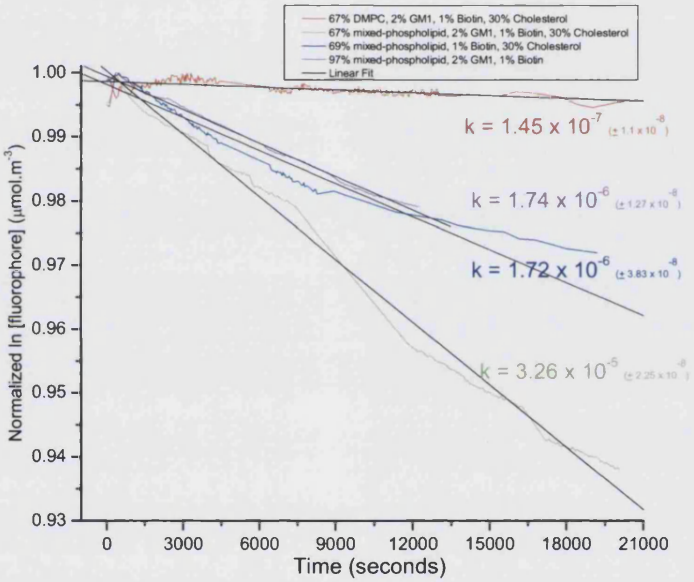

Figure 6.21 Plot of the normalized ln fluorescence concentration (μmol.m^{-3}) as a function of time (seconds), with linear fit data, for the four vesicle systems; 1) pure DMPC biomimetic membrane vesicles, 2) mixed-vesicles, 3) GM1-deficient mixed-vesicles, and 4) cholesterol-deficient mixed-vesicles upon addition of 10μmol.dm^{-3} β-amyloid 1-42.

Monitoring the leakage of the encapsulated BODIPY within the tethered biomimetic membrane vesicles, as a result of β-amyloid permeation, allowed for the determination of the apparent dye diffusion coefficient for each of the systems. The pure DMPC vesicles containing cholesterol and GM1 showed the slowest diffusion of the BODIPY dye from the encapsulated space to the bulk solution, with a calculated apparent dye diffusion coefficient of $D^* = 1.08 \times 10^{-17} cm^2.s^{-1}$. The addition of β-amyloid to cholesterol-deficient mixed-vesicles showed an apparent dye diffusion coefficient of $D^* = 1.30 \times 10^{-16} cm^2.s^{-1}$, whereas the addition of β-amyloid to GM1-deficient mixed-vesicles showed an apparent

dye diffusion coefficient of $D^* = 1.29 \times 10^{-16} cm^2.s^{-1}$. The greatest diffusion of BODIPY dye was observed in the mixed-vesicle system, with a calculated apparent dye diffusion coefficient of $D^* = 2.44 \times 10^{-15} cm^2.s^{-1}$. Therefore, biomimetic membrane vesicles comprising the GM1 ganglioside receptor, cholesterol, and a negatively charged surface provided the lowest barrier against dye diffusion as a result of β-amyloid addition. This suggests that the β-amyloid peptide causes a change in the porosity of the tethered biomimetic membrane vesicles, and the pores formed in the bilayer provide non-specific channels for the flux of the encapsulated molecules within the aqueous space of the vesicles.

The DMPC vesicles offered the highest barrier against β-amyloid permeation because β-amyloid showed a preference for negatively charge lipids, therefore, the β-amyloid did not readily form the channels through the phospholipid bilayer. Moreover, the omission of cholesterol from the vesicles showed an improved barrier against β-amyloid porosity because sterols form domains in membranes, and cause the concentration of membrane surface receptors within these domains. Therefore, exclusion of cholesterol from the vesicle bilayer prevented the concentration of the GM1 receptors within domains and thereby caused a reduction in fibrillization of the bound monomeric and dimeric β-amyloid peptides. This reduction in aggregation and fibrillization would cause a decrease in the formation of the 'pore-like' structures, and therefore show reduced porosity compared to the GM1-deficient and mixed-vesicle systems.

The omission of GM1 from the mixed-vesicles showed decreased dye diffusion compared to the mixed-vesicle system, because there was no receptor for β-amyloid adsorption. The exclusion of the GM1 from the vesicle bilayer prevented the specific adsorption of the β-amyloid to the membrane surface, however, the β-amyloid still associated with the biomimetic membrane via non-specific hydrophobic and electrostatic forces, and were free to laterally diffuse and self-assemble.

The mixed-vesicle system, comprising the GM1 receptors, cholesterol and the negatively charged phospholipids conferred the lowest resistance to β-amyloid induced porosity. The increased permeation resulted from the inclusion of the membrane receptor, which allowed for specific adsorption of the β-amyloid to the surface, and the inclusion of the sterol, which acted to concentrate the GM1 receptors into lipid domains and provided a greater opportunity for the β-amyloid peptides to aggregate. The mixed phospholipid species also

enhanced the porosity of the vesicles by providing a negative charge on the biomimetic membrane surface. This ensured the non-specific association of the peptide and the membrane. A summary of the results are presented in Figure 6.22.

Vesicle System	First order rate constant k (sec^{-1})	Apparent dye diffusion coefficient D* ($m^2.sec^{-1}$)
DMPC vesicles (67% DMPC, 2% GM1, 30% cholesterol, 1% Biotin)	1.45×10^{-7} ($\pm 1.1 \times 10^{-8}$)	1.08×10^{-17}
Sterol-deficient mixed vesicles (97% DMPC, 2% GM1, 1% Biotin)	1.74×10^{-6} ($\pm 1.27 \times 10^{-8}$)	1.30×10^{-16}
GM1-deficient mixed vesicles (69% mixed phospholipids, 30% cholesterol, 1% Biotin)	1.72×10^{-6} ($\pm 3.83 \times 10^{-8}$)	1.29×10^{-16}
Mixed vesicles (67% mixed phospholipids, 2% GM1, 30% cholesterol, 1% Biotin)	3.26×10^{-5} ($\pm 2.25 \times 10^{-8}$)	2.44×10^{-15}

Figure 6.22 Summary of the resistance of the various biomimetic membrane systems to β-amyloid induced porosity as a result of β-amyloid fibrillization and channel formation, and calculated from the apparent dye diffusion coefficient to quantify the diffusion of encapsulated BODIPY from the entrapped vesicle aqueous space to the bulk solution.

The proposed mechanism of toxicity induced by β-amyloid is as a result of increased permeation of the biomimetic membranes. The addition of the β-amyloid peptide to the membrane systems allowed for the quantification of the apparent dye diffusion coefficient, which describes the rate at which encapsulated fluorescent dye molecules diffused from the entrapped aqueous vesicle space and into the bulk solution. The β-amyloid caused an increase in the diffusion of the dye, therefore, it would suggest that the projected channel formation hypothesis would satisfy the observations made here. Therefore, from the increased apparent dye diffusion coefficient data it would seem that β-amyloid caused pores in the phospholipid bilayer, which subsequently allowed the non-specific flux of the ions/solute. The increase in permeability of the biomimetic membrane vesicles would reflect the *in vivo* hypothesis of neurotoxicity, whereby the increased flux causes neuronal damage, and subsequently neuronal death.

6.9 Blocking the GM1 receptor with Lanthanide Trivalent Ions and its Effects on β-amyloid Binding

The therapeutic pathways which have been explored for the control or cure of Alzheimer's disease are varied, and include drugs that reduce the production of the insoluble amyloid protein, drugs that increase the rate of clearance of the misfolded/aggregated proteins, and those that increase the native-state stability or increase the kinetic barrier to misfolding aggregation [91]. *In vivo*, proteins are assisted with their folding by the chaperone system. It also facilitates the refolding or retrotranslocation of misfolded proteins back into the cytoplasm, where they are degraded by the proteasomes [92]. Small molecule ligands which bind to the native state of the mutated and/or misfolded proteins have been investigated. These ligands can stabilize the mutated native state proteins to compensate for the influence of the misfolded protein [91]. Chemical chaperones are small molecules that bind to a protein, stabilize the folded peptide and thereby reduce protein misfolding. It has been reported that osmolytes, such a trimethylamine *N*-oxide and glycerol, mimic the effect of naturally occurring chaperone molecules, and correct folding defects by preferentially hydrating partially denatured proteins and stabilize the native conformation [93]. These chemical chaperones were found to force the β-amyloid peptide into transition from the intermediate fibrils to the mature fibrils, thereby preventing the accumulation of the toxic intermediate β-amyloid fibrils. However, no *in vivo* studies or clinical trials using chemical chaperones have been performed, therefore, their actual therapeutic benefit to Alzheimer's sufferers has not been established.

As mentioned in chapter 5, lanthanide complexes have been used to label GM1 gangliosides for fluorescent studies [94], and it was also shown (section 5.6.4) that trivalent lanthanide ions prevent the actions of cholera toxin by blocking the GM1 receptor, and thereby preventing toxin binding to the cell surface. Therefore, it was hypothesized that the coordination of trivalent ions to GM1 receptors within the biomimetic membrane mixed-vesicles would block the specific binding of the β-amyloid to the membrane surface, and thereby preventing aggregation and the subsequent cytotoxicity. Mixed phospholipid vesicles containing 2% GM1, 1% biotin, 30% cholesterol and 67% mixed phospholipids were tethered to the solid support. Trivalent lanthanide ions were coordinated to the GM1 receptors of the biomimetic membrane vesicles, and was subsequently followed by the addition of 10μmol.dm^{-3} β-amyloid 1-42 (Figure 6.23).

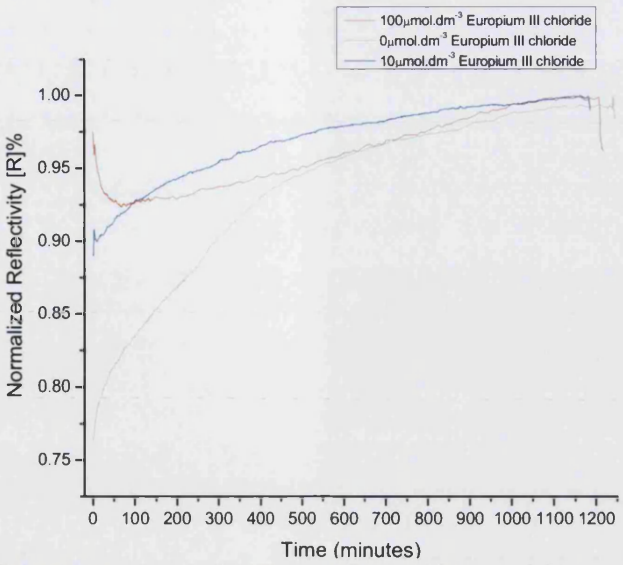

Figure 6.23 Plot of the change in reflectivity upon addition of 10μmol.dm^{-3} β-amyloid to Europium III chloride-labelled GM1 biomimetic membrane mixed-vesicles, at three concentrations of the lanthanide compound (0, 10 and 100 μmol.dm^{-3}).

The addition of varying concentrations of europium III chloride caused an increase in reflectivity (Figure 6.23), which was dependent on the concentration of the lanthanide ions. The addition of 10μmol.dm^{-3} and 100μmol.dm^{-3} europium caused a shift in the resonance angle scan that equated to the adsorption of 2.68ng.mm^{-2} and 6.96ng.mm^{-2} europium to the GM1 receptors respectively. The subsequent addition of 10μmol.dm^{-3} β-amyloid 1-42 to the europium coordinated mixed-vesicle system caused a europium concentration dependant change in the reflectivity. In the control experiment, where no europium was adsorbed to the GM1 receptors, there was a significantly greater shift in the resonance minimum that equated to the adsorption of 2.68ng.mm^{-2} β-amyloid. However, the GM1 receptors coordinated to 10μmol.dm^{-3} europium showed a smaller shift in the resonance minimum upon β-amyloid addition (2.14ng.mm^{-2}). This suggests that the europium reduced the binding capacity of the β-amyloid to the biomimetic membrane vesicles because the GM1 receptors were blocked by the europium. At the higher europium concentration of 100μmol.dm^{-3}, there was no change in the resonance minimum upon addition of β-amyloid to the system. Therefore, at the higher concentration of europium, β-amyloid adsorption to the GM1 receptors was inhibited. A summary of the results are presented in Figure 6.24.

[Europium] ($\mu mol.dm^{-3}$)	Europium adsorption ($ng.mm^{-2}$)	β-amyloid 1-42 adsorption ($ng.mm^{-2}$)
0	-	$2.68ng.mm^{-2}$
10	$2.68ng.mm^{-2}$	$2.14ng.mm^{-2}$
100	$6.96ng.mm^{-2}$	$0ng.mm^{-2}$

Figure 6.24 Comparison of the adsorption of the three concentrations of trivalent lanthanide ions, and the subsequent adsorption of β-amyloid (10μmol.dm-3) to the coordinated GM1:lanthanide biomimetic membrane mixed-vesicles.

The change in fluorescence upon $10\mu mol.dm^{-3}$ β-amyloid addition to the europium coordinated mixed vesicles showed that the lanthanide altered the porosity and dye diffusion of the tethered biomimetic membrane vesicles (Figure 6.25).

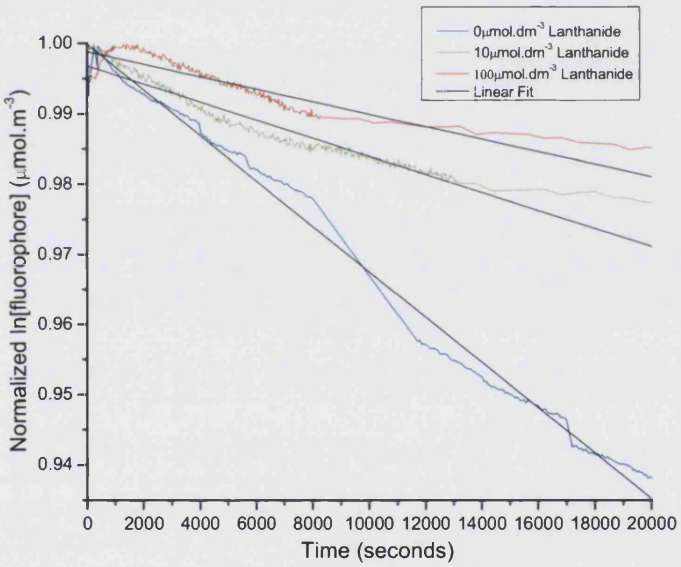

Figure 6.25 Plot of the normalized ln fluorophore concentration ($\mu mol.m^{-3}$) as a function of time (seconds), with linear fit data, for the porosity of mixed-vesicles upon addition of $10\mu mol.dm^{-3}$ β-amyloid to the three lanthanide concentrations co-ordinated to the GM1 receptors; 1) No lanthanide, control, 2) $10\mu mol.dm^{-3}$ europium III chloride, 3) $100\mu mol.dm^{-3}$ europium III chloride.

The coordination of the lanthanide compounds to the GM1 receptors altered the permeation of the biomimetic membrane vesicles caused by β-amyloid. It has been reported in this chapter that β-amyloid causes the formation of channels in the biomimetic membrane bilayer, and the channels allow the diffusion of encapsulated BODIPY dye from the aqueous entrapped space to the bulk solution. The change in fluorescence as a result of β-amyloid permeation allowed for the quantification of the apparent dye diffusion

coefficient for each of the vesicle systems. The control system, where no lanthanide compounds were present, showed the highest porosity, with a calculated apparent dye diffusion coefficient of, $D^* = 2.41 \times 10^{-16} cm^2.s^{-1}$. The addition of $10 \mu mol.dm^{-3}$ europium III chloride prior to the addition of β-amyloid to the system, resulted in a decrease in the porosity of the tethered biomimetic membrane vesicles. The apparent dye diffusion coefficient for the $10 \mu mol.dm^{-3}$ europium coordinated biomimetic membrane vesicles was $D^* = 9.57 \times 10^{-17} cm^2.s^{-1}$. The $100 \mu mol.dm^{-3}$ europium coordinated vesicles resulted in a greater coefficient, and was calculated to be, $D^* = 6.61 \times 10^{-17} cm^2.s^{-1}$. Therefore, the addition of europium caused the inhibition of β-amyloid binding to the membrane surface by blocking the GM1 surface receptors. This subsequently prevented the oligomerization of the β-amyloid peptides and the formation of the 'pore-like' channels in the biomimetic membranes. Therefore, the adsorption of europium reduced the diffusion of the entrapped BODIPY dye within the vesicle aqueous space to the bulk solution.

As described in chapter 5, europium could be a potential therapeutic candidate because it is tolerated well in the body and can be administered orally without toxicity problems. Therefore, the administration of a therapeutic drug containing a trivalent lanthanide compound, such as europium, could be administered to Alzheimer's disease sufferers to prevent the binding of the β-amyloid to the neuronal surface and reduce the aggregation of the β-amyloid peptide, thereby inhibiting channel formation which leads to neuronal death. The compound must cross the blood-brain barrier to bind the GM1 receptors of the neurons, therefore, it could be encapsulated into liposomes targeted to the neurons. Europium compounds administered to Alzheimer's disease patients could potentially reduce neuronal loss and subsequently slow down the progression of the amyloidosis disorder.

6.10 Conclusions

The tethered biomimetic membrane vesicles provide a novel method to study amyloidosis disorders. The system provides a technique to follow the kinetic events associated with the formation of aggregated peptides in real-time. The tethered biomimetic membrane system provides a reliable method to determine the equilibrium association and dissociation constants, which have been shown to correlate well with other reported values.

Alzheimer's disease is a very distressing disorder for the sufferers and those close to them. The disorder is typically an age related disease, and the prevalence increases significantly over the age of 65 years old. The life expectancy of a person suffering from the disease can be variable, however, the disorder may progress very quickly. Alzheimer's disease also attaches huge financial pressures to governments and individuals for the prevision of an appropriate standard of care, therefore, inexpensive and reliable treatments are continually being sourced. The hallmarks of the disease include the formation of β-amyloid aggregates, plaque and tangle formation and neuronal loss. The aggregation of the insoluble β-amyloid peptide produces what is believed to be toxic intermediates, which subsequently mature into fibrils and plaques. The adsorption of β-amyloid to membranes shows a capacity to bind the GM1 receptors, however, the β-amyloid aggregates may associate with membrane sterols and negatively charged phospholipids. The stabilized adsorbed amyloids act as a seed to allow the accumulation of the peptide to the membrane surface.

The cause of neuronal loss has not been definitively determined, however, a potential mechanism is believed to involve the formation of β-amyloid 'pore-like' structures in the membranes, which causes increased permeation of the membranes. The increased porosity of biomimetic membrane vesicles was shown here, and it is believed that the flux of cations causes neuronal damage and their subsequent death. The increased porosity observed upon addition of the β-amyloid peptide to the biomimetic membrane surface can be inhibited by the coordination of lanthanide trivalent ions to the GM1 receptors. The adsorption of europium to the GM1 blocks the receptors, effectively inhibiting the binding of the β-amyloid to the membrane surface, and thereby preventing the formation of the channels and reducing the associated permeation. Europium could have a potential novel application in the treatment of people suffering from Alzheimer's disease by slowing the progression of the disorder and extending the life expectancy of the patients.

The tethered biomimetic membrane system provides a novel means of determining affinity constants, which are reliable and comparable to other methods to determine the constants. It has also been demonstrated that the system may be used to evaluate potential therapeutic drug candidates, such as the lanthanide trivalent compounds. The system provides a good *in vitro* model of neuronal membranes, which can be easily modified to precise experimental specifications to create a firmer understanding of the underlying mechanisms involved behind the initiation, progression and prevention of the deliberating disorder.

6.11 Bibliography

1. Sunde, M., et al., *Common Core Structure of Amyloid Fibrils by Synchrotron X-ray Diffraction.* Journal of Molecular Biology, 1997. **273**: p. 729-739.
2. Lachmann, H.J. and P.N. Hawkins, *Systemic amyloidosis.* Current Opinion in Pharmacology, 2006. **6**(2): p. 214-220.
3. Pepys, M.B., et al., *Amyloid P component. A critical review. Amyloid-.* International Journal of Experimental and Clinical Investigation, 1997. **4**: p. 274-295.
4. Benson, M.D. and T. Uemichi, *Transthyretin amyloidosis.* Amyloid, 1996. **3**(1): p. 44-56.
5. Pepys, M.B., *Amyloidosis.* Annual Review of Medicine, 2006. **57**(1): p. 223-241.
6. WHO, *Diabetes.* 2006, World Health Organization: Geneva.
7. Kahn, S., E., S. Andrikopoulos, and C. Verchere, B., *Islet amyloid: a long-recognized but underappreciated pathological feature of type 2 diabetes.* Diabetes, 1999. **48**(2): p. 241-53.
8. Janson, J., et al., *The mechanism of islet amyloid polypeptide toxicity is membrane disruption by intermediate-sized toxic amyloid particles.* Diabetes, 1999. **48**(3): p. 491-8.
9. Shah, K.B., Y. Inoue, and M.R. Mehra, *Amyloidosis and the Heart: A Comprehensive Review.* Archives of Internal Medicine, 2006. **166**(17): p. 1805-1813.
10. Van Geluwe, F., et al., *Amyloidosis of the heart and respiratory system.* European Radiology, 2006. **16**(10): p. 2358-2365.
11. Kwong, R.Y. and R.H. Falk, *Cardiovascular Magnetic Resonance in Cardiac Amyloidosis.* Circulation, 2005. **111**(2): p. 122-124.
12. Martins, S.M., et al., *Formation of Soluble Oligomers and Amyloid Fibrils with Physical Properties of the Scrapie Isoform of the Prion Protein from the C-terminal Domain of Recombinant Murine Prion Protein mPrP-(121-231).* Journal of Biological Chemistry, 2006. **281**(36): p. 26121-26128.
13. Zanusso, G. and S. Monaco, *Molecular mechanisms of human prion diseases.* Drug Discovery Today: Disease Mechanisms, 2005. **2**(4): p. 511-518.
14. Soto, C., *Unfolding the role of protein misfolding in neurodegenerative diseases.* Nature Reviews Neuroscience, 2003. **4**(1): p. 49-60.
15. Tan, E.-K. and L.M. Skipper, *Pathogenic mutations in Parkinson disease.* Human Mutation, 2007. **28**(7): p. 641-653.
16. Spillantini, M.G., et al., *alpha -Synuclein in filamentous inclusions of Lewy bodies from Parkinson's disease and dementia with Lewy bodies.* Proceedings of the National Academy of Sciences of the United States of America, 1998. **95**(11): p. 6469-6473.
17. Conway, K.A., J.D. Harper, and P.T. Lansbury, *Accelerated in vitro fibril formation by a mutant [alpha]-synuclein linked to early-onset Parkinson disease.* 1998. **4**(11): p. 1318-1320.
18. Rocken, C., et al., *The classification of amyloid deposits in clinicopathological practice.* Histopathology, 1996. **29**(4): p. 325-35.
19. Obici, L., et al., *Clinical aspects of systemic amyloid diseases.* Biochimica et Biophysica Acta (BBA) - Proteins & Proteomics, 2005. **1753**(1): p. 11-22.
20. APA, *Diagnostic and Statistical Manual of Mental Disorders DSM-IV-TR.* 4th Edition ed. American Psychiatric Association, ed. Brandon/Hil. 1994: American Psychiatric Publishing, Inc.
21. ADEAR, *Alzheimer's Disease Fact Sheet*, N.I.o. Aging, Editor. 2006: Silver Spring, Maryland.

22. Merrill, M., *First MRI/PET tool for Alzheimer's detection developed*, in *Healthcare I.T. News EU.* 2007.
23. Bartlett, S., *MRI for in vivo detection of amyloid plaques.* The Lancet Neurology, 2005. **4**(5): p. 276.
24. vandenBerg, C.M., Y. Kazmi, and M.W. Jann, *Cholinesterase Inhibitors for the Treatment of Alzheimers Disease in the Elderly.* Drugs & Aging, 2000. **16**: p. 123-138.
25. Kaduszkiewicz, H., et al., *Cholinesterase inhibitors for patients with Alzheimer's disease: systematic review of randomised clinical trials.* British Medical Journal, 2005. **331**(7512): p. 321-327.
26. ADEAR, *Alzheimer's Disease Medications Fact Sheet*, N.I.o. Aging, Editor. 2005: Silver Spring, Maryland.
27. Priller, C., et al., *Synapse Formation and Function Is Modulated by the Amyloid Precursor Protein.* Journal of Neuroscience, 2006. **26**(27): p. 7212-7221.
28. Steinbach, J.P., et al., *Hypersensitivity to seizures in beta-amyloid precursor protein deficient mice.* Cell Death and Differentiation, 1998. **5**(10): p. 858-866.
29. Turner, P.R., et al., *Roles of amyloid precursor protein and its fragments in regulating neural activity, plasticity and memory.* Progress in Neurobiology, 2003. **70**(1): p. 1-32.
30. Mattson, M.P., *Cellular actions of beta-amyloid precursor protein and its soluble and fibrillogenic derivatives.* Physiological Reviews, 1997. **77**(4): p. 1081-1132.
31. Goodman, Y. and M.P. Mattson, *Secreted Forms of Beta-Amyloid Precursor Protein Protect Hippocampal-Neurons against Amyloid Beta-Peptide-Induced Oxidative Injury.* Experimental Neurology, 1994. **128**(1): p. 1-12.
32. Furukawa, K., et al., *Activation of K+ channels and suppression of neuronal activity by secreted beta-amyloid-precursor protein.* Nature, 1996. **379**(6560): p. 74-78.
33. Smith-Swintosky, V.L., et al., *Secreted Forms of Beta-Amyloid Precursor Protein Protect against Ischemic Brain Injury.* Journal of Neurochemistry, 1994. **63**(2): p. 781-784.
34. Hardy, J.A. and G.A. Higgins, *Alzheimers-Disease - the Amyloid Cascade Hypothesis.* Science, 1992. **256**(5054): p. 184-185.
35. Hardy, J. and D.J. Selkoe, *The amyloid hypothesis of Alzheimer's disease: Progress and problems on the road to therapeutics.* Science, 2002. **297**(5580): p. 353-356.
36. Dyrks, T., et al., *Amyloidogenicity of Beta-A4 and Beta-A4-Bearing Amyloid Protein-Precursor Fragments by Metal-Catalyzed Oxidation.* Journal of Biological Chemistry, 1992. **267**(25): p. 18210-18217.
37. Whitson, J.S., D.J. Selkoe, and C.W. Cotman, *Amyloid-Beta Protein Enhances the Survival of Hippocampal-Neurons Invitro.* Science, 1989. **243**(4897): p. 1488-1490.
38. Pedersen, W.A., M.A. Kloczewiak, and J.K. Blusztajn, *Amyloid beta-protein reduces acetylcholine synthesis in a cell line derived from cholinergic neurons of the basal forebrain.* Proceedings of the National Academy of Sciences of the United States of America, 1996. **93**(15): p. 8068-8071.
39. Zhang, C., et al., *Focal Adhesion Kinase Expressed by Nerve-Cell Lines Shows Increased Tyrosine Phosphorylation in Response to Alzheimers a-Beta Peptide.* Journal of Biological Chemistry, 1994. **269**(41): p. 25247-25250.
40. Pike, C.J., et al., *Invitro Aging of Beta-Amyloid Protein Causes Peptide Aggregation and Neurotoxicity.* Brain Research, 1991. **563**(1-2): p. 311-314.
41. Pike, C.J., B.J. Cummings, and C.W. Cotman, *Beta-Amyloid Induces Neuritic Dystrophy Invitro - Similarities with Alzheimer Pathology.* Neuroreport, 1992. **3**(9): p. 769-772.

42. Jarrett, J.T., E.P. Berger, and P.T. Lansbury, *The Carboxy Terminus of the Beta-Amyloid Protein Is Critical for the Seeding of Amyloid Formation - Implications for the Pathogenesis of Alzheimers-Disease.* Biochemistry, 1993. **32**(18): p. 4693-4697.
43. Jarrett, J.T., E.P. Berger, and P.T. Lansbury, *The C-Terminus of the Beta-Protein Is Critical in Amyloidogenesis*, in *Alzheimers Disease: Amyloid Precusor Proteins, Signal Transduction, and Neuronal Transplantation.* 1993. p. 144-148.
44. Hayashi, H., et al., *A seed for Alzheimer amyloid in the brain.* Journal of Neuroscience, 2004. **24**(20): p. 4894-4902.
45. Kremer, J.J., et al., *Correlation of beta-amyloid aggregate size and hydrophobicity with decreased bilayer fluidity of model membranes.* Biochemistry, 2000. **39**(33): p. 10309-10318.
46. Maggio, J.E., et al., *Reversible Invitro Growth of Alzheimer-Disease Beta-Amyloid Plaques by Deposition of Labeled Amyloid Peptide.* Proceedings of the National Academy of Sciences of the United States of America, 1992. **89**(12): p. 5462-5466.
47. Jarrett, J.T. and P.T. Lansbury, *Seeding One-Dimensional Crystallization of Amyloid - a Pathogenic Mechanism in Alzheimers-Disease and Scrapie.* Cell, 1993. **73**(6): p. 1055-1058.
48. Mattson, M.P., et al., *Beta-Amyloid Precursor Protein Metabolites and Loss of Neuronal Ca2+ Homeostasis in Alzheimers-Disease.* Trends in Neurosciences, 1993. **16**(10): p. 409-414.
49. Barger, S.W., et al., *Beta-Amyloid Precursor Protein Mismetabolism and Loss of Calcium Homeostasis in Alzheimers-Disease*, in *Alzheimers Disease: Amyloid Precusor Proteins, Signal Transduction, and Neuronal Transplantation.* 1993. p. 158-164.
50. Hensley, K., et al., *A Model for Beta-Amyloid Aggregation and Neurotoxicity Based on Free-Radical Generation by the Peptide - Relevance to Alzheimer-Disease.* Proceedings of the National Academy of Sciences of the United States of America, 1994. **91**(8): p. 3270-3274.
51. Yan, S.D., et al., *RAGE and amyloid-[beta] peptide neurotoxicity in Alzheimer's disease.* 1996. **382**(6593): p. 685-691.
52. Behl, C., et al., *Hydrogen-Peroxide Mediates Amyloid-Beta Protein Toxicity.* Cell, 1994. **77**(6): p. 817-827.
53. Breitner, M.D. and C.S. John, *THE ROLE OF ANTI-INFLAMMATORY DRUGS IN THE PREVENTION AND TREATMENT OF ALZHEIMER'S DISEASE.* Annual Review of Medicine, 1996. **47**(1): p. 401-411.
54. Breitner, J.C.S., et al., *Inverse Association of Antiinflammatory Treatments and Alzheimers-Disease - Initial Results of a Cotwin Control Study.* Neurology, 1994. **44**(2): p. 227-232.
55. Cotman, C.W., *The beta-amyloid peptide, peptide self-assembly, and the emergence of biological activities: A new principle in peptide function and the induction of neuropathology.* Annals of the New York Academy of Sciences, 1997. **814**: p. 1-16.
56. Katzman, R., et al., *Clinical, Pathological, and Neurochemical Changes in Dementia - a Subgroup with Preserved Mental Status and Numerous Neocortical Plaques.* Annals of Neurology, 1988. **23**(2): p. 138-144.
57. Terzi, E., G. Holzemann, and J. Seelig, *Interaction of Alzheimer beta-amyloid peptide(1-40) with lipid membranes.* Biochemistry, 1997. **36**(48): p. 14845-14852.
58. Chi, E.Y., S.L. Frey, and K.Y.C. Lee, *Ganglioside GM1-Mediated Amyloid-beta Fibrillogenesis and Membrane Disruption.* Biochemistry, 2007. **46**(7): p. 1913-1924.

59. McLaurin, J. and A. Chakrabartty, *Characterization of the interactions of Alzheimer beta-amyloid peptides with phospholipid membranes.* European Journal of Biochemistry, 1997. **245**(2): p. 355-363.
60. Choo-Smith, L.P. and W.K. Surewicz, *The interaction between Alzheimer amyloid beta(1-40) peptide and ganglioside G(M1)-containing membranes.* Febs Letters, 1997. **402**(2-3): p. 95-98.
61. Choo-Smith, L.-P., et al., *Acceleration of Amyloid Fibril Formation by Specific Binding of Abeta -(1-40) Peptide to Ganglioside-containing Membrane Vesicles.* Journal of Biological Chemistry, 1997. **272**(37): p. 22987-22990.
62. Svennerholm, L., et al., *Membrane-Lipids of Adult Human Brain - Lipid-Composition of Frontal and Temporal-Lobe in Subjects of Age 20 to 100 Years.* Journal of Neurochemistry, 1994. **63**(5): p. 1802-1811.
63. Murphy, E.J., D.K. Anderson, and L.A. Horrocks, *Phospholipid and phospholipid fatty acid composition of mixed murine spinal cord neuronal cultures.* Journal of Neuroscience Research, 1993. **34**(4): p. 472-477.
64. Carrie, I., et al., *Specific phospholipid fatty acid composition of brain regions in mice: effects of n;-3 polyunsaturated fatty acid deficiency and phospholipid supplementation.* J. Lipid Res., 2000. **41**(3): p. 465-472.
65. Esposito, C., et al., *Exploring interaction of beta-amyloid segment (25-35) with membrane models through paramagnetic probes.* Journal of Peptide Science, 2006. **12**(12): p. 766-774.
66. Lindstrom, F., et al., *Association of amyloid-beta peptide with membrane surfaces monitored by solid state NMR.* Physical Chemsitry & Chemical Physics, 2002. **4**: p. 5524-5530.
67. Naiki, H. and K. Nakakuki, *First-order kinetic model of Alzheimer's beta-amyloid fibril extension in vitro.* Laboratory Investigation, 1996. **74**(2): p. 374-383.
68. Pallitto, M.M. and R.M. Murphy, *A mathematical model of the kinetics of beta-amyloid fibril growth from the denatured state.* Biophysical Journal, 2001. **81**(3): p. 1805-22.
69. Puglielli, L., R.E. Tanzi, and D.M. Kovacs, *Alzheimer's disease: the cholesterol connection.* 2003. **6**(4): p. 345-351.
70. Wang, S.S.-S., D.L. Rymer, and T.A. Good, *Reduction in Cholesterol and Sialic Acid Content Protects Cells from the Toxic Effects of ?-Amyloid Peptides.* Journal of Biological Chemistry, 2001. **276**(45): p. 42027-42034.
71. Subasinghe, S., et al., *Cholesterol is necessary both for the toxic effect of A? peptides on vascular smooth muscle cells and for A? binding to vascular smooth muscle cell membranes.* Journal of Neurochemistry, 2003. **84**(3): p. 471-479.
72. Igbavboa, U., et al., *Increasing Age Alters Transbilayer Fluidity and Cholesterol Asymmetry in Synaptic Plasma Membranes of Mice.* Journal of Neurochemistry, 1996. **66**(4): p. 1717-1725.
73. Soderberg, M., et al., *Lipid Compositions of Different Regions of the Human-Brain During Aging.* Journal of Neurochemistry, 1990. **54**(2): p. 415-423.
74. Avdulov, N.A., et al., *Lipid binding to amyloid beta-peptide aggregates: Preferential binding of cholesterol as compared with phosphatidylcholine and fatty acids.* Journal of Neurochemistry, 1997. **69**(4): p. 1746-1752.
75. Chochina, S.V., et al., *Amyloid beta-peptide(1-40) increases neuronal membrane fluidity: role of cholesterol and brain region.* Journal of Lipid Research, 2001. **42**(8): p. 1292-1297.
76. Muller, W.E., et al., *Beta-Amyloid Peptide Decreases Membrane Fluidity.* Brain Research, 1995. **674**(1): p. 133-136.

77. Arispe, N. and M. Doh, *Plasma membrane cholesterol controls the cytotoxicity of Alzheimer's disease A?P (1-40) and (1-42) peptides.* FASEB Journal, 2002. **16**(12): p. 1526-1536.
78. Harper, J.D., C.M. Lieber, and P.T. Lansbury, *Atomic force microscopic imaging of seeded fibril formation and fibril branching by the Alzheimer's disease amyloid-beta protein.* Chemistry & Biology, 1997. **4**(12): p. 951-959.
79. Walsh, D.M., et al., *Amyloid beta-protein fibrillogenesis - Detection of a protofibrillar intermediate.* Journal of Biological Chemistry, 1997. **272**(35): p. 22364-22372.
80. Lemere, C.A., et al., *Sequence of deposition of heterogeneous amyloid beta-peptides and APO E in Down syndrome: Implications for initial events in amyloid plaque formation.* Neurobiology of Disease, 1996. **3**(1): p. 16-32.
81. Terry, R.D., et al., *Physical Basis of Cognitive Alterations in Alzheimers-Disease - Synapse Loss Is the Major Correlate of Cognitive Impairment.* Annals of Neurology, 1991. **30**(4): p. 572-580.
82. Lashuel, H.A. and P.T. Lansbury Jr., *Are amyloid diseases caused by protein aggregates that mimic bacterial pore-forming toxins?* Quarterly Reviews of Biophysics, 2006. **39**(2): p. 167-201.
83. Valdes-Gonzalez, T., J. Inagawa, and T. Ido, *Neuropeptides interact with glycolipid receptors A surface plasmon resonance study.* Peptides, 2001. **22**(7): p. 1099-1106.
84. Good, T.A. and R.M. Murphy, *Aggregation State-Dependent Binding of Beta-Amyloid Peptide to Protein and Lipid Components of Rat Cortical Homogenates.* Biochemical and Biophysical Research Communications, 1995. **207**(1): p. 209-215.
85. Murphy, R.M., *Kinetics of amyloid formation and membrane interaction with amyloidogenic proteins.* Biochimica et Biophysica Acta (BBA) - Biomembranes, 2007. **1768**(8): p. 1923-1934.
86. Kurganov, B., M. Doh, and N. Arispe, *Aggregation of liposomes induced by the toxic peptides Alzheimer's A beta s, human amylin and prion (106-126): facilitation by membrane-bound G(M1) ganglioside.* Peptides, 2004. **25**(2): p. 217-232.
87. Arispe, N., H.B. Pollard, and E. Rojas, *Beta-amyloid Ca2+-channel hypothesis for neuronal death in Alzheimer Disease.* Molecular and Cellular Biochemistry, 1994. **140**(2): p. 119-125.
88. Lin, H., R. Bhatia, and R. Lal, *Amyloid beta protein forms ion channels: implications for Alzheimer's disease pathophysiology.* Faseb Journal, 2001. **15**(13): p. 2433-2444.
89. Avdulov, N.A., et al., *Amyloid beta-Peptides Increase Annular and Bulk Fluidity and Induce Lipid Peroxidation in Brain Synaptic Plasma Membranes.* Journal of Neurochemistry, 1997. **68**(5): p. 2086-2091.
90. Quist, A., et al., *Amyloid ion channels: A common structural link for protein-misfolding disease.* Proceedings of the National Academy of Sciences of the United States of America, 2005. **102**(30): p. 10427-10432.
91. Cohen, F.E. and J.W. Kelly, *Therapeutic approaches to protein-misfolding diseases.* 2003. **426**(6968): p. 905-909.
92. Hershko, A. and A. Ciechanover, *THE UBIQUITIN SYSTEM.* Annual Review of Biochemistry, 1998. **67**(1): p. 425-479.
93. Yang, D.-S., et al., *Manipulating the Amyloid-beta Aggregation Pathway with Chemical Chaperones.* J. Biol. Chem., 1999. **274**(46): p. 32970-32974.
94. Alpturk, O., et al., *Lanthanide complexes as fluorescent indicators for neutral sugars and cancer biomarkers.* Proceedings of the National Academy of Sciences of the United States of America, 2006. **103**(26): p. 9756-9760.